Can SUMOylation of the Beta-2-Adrenergic receptor influence cell signalling and cardiac myocyte physiology?

Jiayue Ling

MSc, BSc (Hons)

This thesis submitted in fulfilment of requirements for the Degree of Doctor of Philosophy (Ph.D.)

November 2021

Institute of Cardiovascular and Medical Sciences

College of Medical, Veterinary and Life Sciences

University Of Glasgow

University of Glasgow

Abstract

The beta 2 adrenergic receptor (β_2AR) is a transmembrane, G protein-coupled receptor that can be modified post-translationally by phosphorylation, ubiquitination, palmitoylation and glycosylation. These modifications regulate β_2AR signalling and desensitisation. SUMOylation is a post-translational modification that is related to ubiquitin, hence the name "SUMO" (small ubiquitin-like modifier). SUMO is a small protein which is covalently attached to substrate proteins on lysine residues following activation of specific SUMO enzyme cascades. Following the discovery that the cardiac signalling protein sarcoplasmic Reticulum Ca^{2+} ATPase 2a (SERCA2a) could be modified by SUMO and since there are more than 1000 SUMO substrates in nature (Hay, 2013), it is possible that SERCAR2a may not be the only cardiac protein that could be SUMOylated. The Baillie group has used peptide array technology to identify putative SUMOylation sites by inducing in vitro SUMOylation of 15 mer peptides which contained potential SUMO conjugation motifs (Frank, 2002). Baillie group has confirmed putative SUMOylation sites on multiple cardiac specific proteins such as ryanodine receptor (RyR), L-type Ca^{2+} channel (LTCC), myosin binding protein C, cardiac troponin I (cTnI) and β_2AR via the consensus motif ψKxE/D. Therefore, I hypothesised that the β_2AR could also be SUMOylated and that this action is a novel point of regulation for β_2AR receptor signalling.

In my thesis,

1. I confirm that β_2AR is a substrate for SUMOylation and that β_2AR SUMOylation can be promoted by the SUMO E3 ligase PIASγ.
2. I show that enhanced SUMOylation driven by PIASγ overexpression rapidly declined after agonist treatment suggesting that SUMOylation is involved in early signalling events.
3. I compare the physiological responses of WT and SUMOylation-null mutants of β_2AR in NRVMs using adenoviral gene transfer. Following transfection of the receptors to NRVMs I evaluated five different parameters of contractility using the CellOPTIQ® platform. Using these techniques, I report that untransfected NRVMs displayed expected short-term

enhancements in the contractile response to isoproterenol. However, NRVMs transfected with WT and mutant β_2AR did not respond as expected. Counter-intuitive data resulting from excessive levels of over-expression of WT and a SUMOylation-null mutant of β_2AR was recorded.

Conclusively, I report the novel finding that β_2AR is a substrate of SUMOylation and β_2AR SUMOylation can be promoted by the SUMO E3 ligase PIASγ. A first-in-class SUMO-β_2 antibody was tested in my work in different cells and tissues confirming that SUMOylation is ubiquitous. I also reported that SUMOylation is engaged in early β_2AR signalling events. However, using a variety of different model systems and techniques I was unable to definitively characterise the function of this modification. Functional studies via adenovirus vector in animal models to study the role of β_2AR SUMOylation in heart failure are the future direction to this project.

Table of Contents

List of Tables

List of Figure

Acknowledgement

Firstly, I would like to express my biggest gratitude to my supervisor, Professor George S. Baillie. I would never have finished this PhD journey without George's trust and encouragement over the past 4 years. George, you have been the best supervisor, boss, and mentor to me. I will always be so grateful for your encouragement, advise, support and the opportunities you offered me to work in your lab. I feel really lucky to be one of your students, and to have had my PhD experience in Baillie lab. Del, as my second supervisor, although I did not spend a lot of time with you, you helped me through difficult times and whenever I needed your help, especially when I needed advice on my writing. Thank you to the Chinese Scholarship council and Chinese government for the generous funding throughout my PhD.

I would like to thank all the members in Baillie lab that gave me help and supports along this journey. It has been an honour and a pleasure to work with you all. Angie, Gonzalo, Bracy, Alice, Connor, Gillian, Tara, Lauren, Chloe, Emma, Ellie, and Tom, you have provided me with your technical advice, emotional supports and lot of laughs that will always be appreciated and never forgotten. You guys are not just lab mates but also great friends to me. A special thank you to Angie, you have been one of the biggest supporters in my PhD life, not just as a role model, but also as a big sister to me. You took care of me so good at work and in life with delicious food, I am very lucky to know you. A big thank you to the Freeman lab members, Fiona, Jack, Oom and Dilys, your thoughtful encouragement alongside in Lab 535 have helped me go through tough times.

I have been very lucky to have benefited from various collaborations alongside this project. To Professor Godfrey Smith and his group, Ana and Aileen, thank you Aileen for providing me with the rabbit cardiomyocytes, big thanks to Ana for teaching me CellOPTIQ® and helping me with all the analysis and emotional support during the long experiment days. To Professor Will Fuller and his lab for all the daily support through my project especially after the fire accident in our lab. Special thanks to Sharon and Xing, Sharon thank you for being an excellent teacher on generating virus and walking me through the whole process when I was

frustrated. Xing thank you for not just being a colleague but also a good friend along all these years. To Professor Stuart Nicklin and his lab, Nic and Arun, thank you for assisting me with PIASγ viral preparations and helping to troubleshoot the β_2AR virus generation, with continuous professional suggestions and encouragement. To Dr. Niall MacQuaide and Dr. Ken Campbell from University of Kentucky for providing the human heart used in this project which makes a big contribution in this thesis.

Finally, I would like to thank my family and friends who supported me along these 4 years, here in Glasgow and far away in China. I would never be who I am now without my parents and family's unconditionally love, trust~~s~~ in my choices, and support for me to study abroad. To all my wonderful friends Eva, Rashida and Blessy, thank you for all the fun you bring to me. To my flatmate and friend, Yu, you have been with me along all my PhD life, thanks for listening and comforting me when I go through difficulties in life. To Hossam, thank you for always making me laugh and always standing next to me and have my back, thank you for brightening my life. To all the lovely people I met in Glasgow in the past 5 years, it is my pleasure to know you all.❤️

Author’s Declaration

I declare this work presented in this thesis were carried out by myself, except where otherwise cited or acknowledged. This work has not been submitted previously for any other higher degree and was supervised by Professor George S. Baillie and Dr Delyth Graham.

Jiayue Ling

Nov.2021

Definitions/Abbreviations

%	Percent
°C	Degrees Celsius
3D	Three dimensional
5×	5 times
AAV	Adeno-associated virus
AC	Adenylyl cyclase
ACCF	American College of Cardiology Foundation
ACE	Angiotensin converting enzyme
AD	Adenovirus
Ad5	Adenovirus serotype 5
ADP	Adenosine diphosphate
Adr	Adrenaline
AHA	American Heart Association
AMP	Adenosine monophosphate
ANOVA	Analysis of variance
AP	Action potential
AP-2	Adaptor protein 2
AR	Adrenergic receptor
ARBs	Angiotensin II receptor blockers
ARVM	Adult rabbit ventricular myocyte
ATP	Adenosine triphosphate
BNP	B-type natriuretic peptide
bp	Base pair
BSA	Bovine serum albumin
Ca^{2+}	Calcium ions
cAMP	Cyclic adenosine monophosphate
$CaCl_2$	Calcium chloride
Capns2	Calpain small subunit2
CAR	Coxsackievirus and adenovirus receptor
CAST	Calpastatin
CD50	Time from 50% contraction to 50% relaxation

CHAPS	3-((3-cholamidopropyl) dimethylammonio)-1-propanesulfonate
CHD	Coronary heart disease
CHX	Cycloheximide
CI	Cell index
CICR	Ca^{2+}-induced Ca^{2+} release
cm	Centimeters
CO_2	Carbon dioxide
COS-7 cells	Cells that are derived from the cells being CV-1 in origin and carrying the SV40 genetic material
CPE	Cytopathic effect
CRP	C-reactive protein
CsCl	Caesium Chloride
cTnI	Cardiac troponin I
Cys	Cysteine
DAPI	4',6-diamidine-2-phenylindole
dH_2O	Distilled water
DMEM	Dulbecco's modified eagle's medium
DMSO	Dimethyl sulfoxide
DNA	Deoxyribonucleic acid
DN90	Time from peak to 90% relaxation
Drp1	Dynamin related protein
E.coli	Escherichia coli
E1	SUMO activating enzyme
E1 (chapter 4)	Early region 1
E2	SUMO conjugating enzyme
E3	SUMO ligase
E3 (chapter 4)	Early region 3
EC	Excitation contraction
EC_{50}	Drug that causes 50% of the maximal response
ECG	Electrocardiograph
ECL	Enhanced chemiluminescence
EDTA	Ethylenediaminetetraacetic acid
eEF2	Eukaryotic elongation factor 2

EGTA	Ethylene glycol-bis(ß-aminoethyl ether)-N,N,N′,N′-tetra acetic acid
Endo	Endocardium
EPAC	Exchange protein activated by cAMP
Epi	Epicardium
ERK	Extracellular signal regulated kinase
EtOH	Ethanol
FBC	Full blood count
FBS	Fetal bovine serum
g	Grams
G418	Geneticin
GAPDH	Glyceraldehyde 3-phophate dehydrogenase
GDP	Guanine diphosphate
GFP	Green fluorescent protein
Gly	Glycine
GPCRs	G protein-coupled receptors
GRKs	G protein receptor kinases
G_s protein	G stimulatory
$G_{\alpha s}$	Gα subunit of the Gs protein
GTP	Guanine triphosphate
H^+	Hydrogen ions
HA	Hemagglutinin
HCl	Hydrochloride
HDAC	Histone deacetylase
HEK 293	Human embryonic kidney 293
HEK 293 AD	Human embryonic kidney 293 adherence
HEPES	4-(2-hydroxyethyl)-1-piperazineethanesulfonic acid
HF	Heart failure
HFpEF	Heart failure with preserved ejection fraction
HFrEF	Heart failure with reduced ejection fraction
His	Histidine
hr	Hour
H/R injury	Hypoxia/reoxygenation injury
HRP	Horseradish peroxidase

HS	Horse serum
IC_{50}	Drug that causes 50% inhibition of competitor binding
IGF1	Insulin-like growth factors 1
IgG	Immunoglobulin G
IL-6	Interleukin 6
IP_3	Inositol 1,4,5-triphosphate
I/R injury	Ischemia/reperfusion injury
ITRs	Inverted terminal repeats
ISO	Isoprenaline/Isopropanol
K^+	Potassium ions
KCl	Potassium chloride
KCNA5	Potassium voltage-gated channel subfamily A member 5
KCNQ	Potassium voltage-gated channel subfamily Q member
kDa	Kilodaltons
kg	Kilogram
LB	Lysogeny broth
LFTs	Liver function tests
LG	L-glutamine
LOE	Level of evidence
Log	Logarithm
LRH-1	Live receptor homolog 1
LSM	Laser-scanning confocal microscope
LTCC	L-type-Ca^{2+}-channels
LV	Left ventricle
M	Molar
M1	NRVM day 1 medium
M199	Medium 199
M1 mAChR	M1 muscarinic acetylcholine receptor
M2	NRVM day 2 medium
MAPK	Mitogen-activated protein kinase
MCS	Mechanical circulator support
MEM	Minimum essential medium
mer	Amino acid peptide
Mg	Magnesium

mg	Milligram
MG-132	Carbobenzoxy-Leu-Leu-lucinal
$MgCl_2$	Magnesium chloride
MI	Myocardial infarction
min	Minutes
ml	Milliliter
mM	Millimolar
mm	Millimeter
MOI	Multiplicity of infection
MUT	Mutant
N106	N-(4-methoxybenzo[d]thiazol-2-yl)-5-(4-methoxyphenyl)-1,3,4-oxadiazol-2-amine
$Na_4P_2O_7$	Tetrasodium pyrophosphate
Na^+	Sodium ions
NaCl	Sodium chloride
NaF	Sodium fluoride
$NaHPO_4$	Monosodium phosphate
NaOH	Sodium hydroxide
NCS	Neonatal calf serum
NCX	Na^+/Ca^{2+} exchanger
NEM	N-ethylmaleimide
NICE	National Institute for Health and Clinical Excellence
ng	Nanogram
nM	Nanomolar
nm	Nanometers
NR4A	Nuclear receptor 4A
NRVM	Neonatal rat ventricular myocyte
NSAIDs	Nonsteroidal anti-inflammatory drugs
NTproBNP	N terminal pro-BNP
NYHA	New York Heart Association
P	Phosphate group
PBS	Phosphate buffered saline
PCR	Polymerase chain reaction
PDE	Phosphodiesterase

PFA	Paraformaldehyde
PFU	Plaque forming units
PhosERK	Phosphorylated ERK
PhosPKA substrate	Phosphorylated PKA substrate
Phos$ß_2$	Phosphorylated $ß_2$AR
PIAS	Protein inhibitor activated STAT
PKA	Protein kinase A
PKC	Protein kinase C
PLA	Proximity ligation assay
PLB	Phospholamban
PLC	Phosphatidylinositol
PLC-γ1	Phospholipase C-γ1
POPDC	Popeye domain-containing proteins
PPAR	Peroxisome proliferator-activator receptors
P/S	Penicillin/streptomycin
PTM	Post-translational modification
Rac	Ras related small GTPase protein
RANGAP1	RAN GTPase activating protein 1
RCA	Rolling-circle amplification
Rho	Ras homolog family
RIPA	Radioimmunoprecipitation assay
RNA	Ribonucleic acid
ROS	Reactive oxygen species
rpm	Rotations per minute
RyR	Ryanodine receptor
s	Second
SAE1	SUMO-activating enzyme subunits 1
SAE2	SUMO-activating enzyme subunit 2
SDS-PAGE	Sodium dodecyl sulphate polyacrylamide gel electrophoresis
SEM	Standard error of the mean
SENPs	Sentrin specific proteases
SERCA2a	Sarcoplasmic reticulum Ca^{2+} ATPase
SIM	SUMO interacting motif

SL	Sarcolemma
SM	SUMO mutant
SNP	Single nucleotide polymorphism
SUMO	Small ubiquitin-like modifier
SR	Sarcoplasmic reticulum
TBS	Tris buffered saline
TBS-T	Tris-buffered saline-tween 20
TCR	T cell antigen receptor
TFTs	Thyroid function tests
TNF	Tumor necrosis factor
TnI	Troponin I
TR	Thyroid hormone nuclear receptor
Tris HCl	Tris hydrochloride
U&Es	Urea and electrolytes
UBC9	Ubiquitin carrier protein 9
UP90	Time from baseline to 90% contraction
V	Volts
VP	Viral particle
v/v	Volume/volume
w/v	weight/volume
WGA	Wheat germ agglutinin
WT	Wild type
YFP	Yellow fluorescent protein
α	Alpha
α_{1A}AR	Alpha 1A adrenergic receptor
α-Syn	α-Synuclein
ß	Beta
ßARK	ß-adrenergic receptor kinase
B-AR	Beta adrenergic receptor
B_1AR	Beta 1 adrenergic receptor
B_2AR	Beta 2 adrenergic receptor
B^3AR	Beta 3 adrenergic receptor
B_3AR	Beta 4 adrenergic receptor
ε	Epsilon

γ	Gamma
μg	Microgram
μl	Microliter
μm	Micrometer
μM	Micromolar
λ_{ex}	Fluorescence excitation wavelengths
λ_{em}	Fluorescence emission wavelengths

Chapter1. Introduction

1.1 The Cardiovascular System

The cardiovascular system, also called as circulatory system, continually circulates oxygen to human body, removes carbon dioxide and provide cells and organs with nutrients and energy. The cardiovascular system is also a control system for the human body. It carries hormones to different tissues and organs to regulate the body's biological activities (Herring and Paterson, 2018).

1.1.1 The Anatomy of the Heart

The human heart consists of four chambers with hollow muscles, is roughly conical in shape, and measures approximately 12cm long × 9cm wide (**Figure 1.1**). The human heart is located obliquely across the midline of the chest with the cardiac apex behind the fifth left intercostal space (Herring and Paterson, 2018). The four chambers of the heart are built on annulus fibrosus which is a ring of fibrous fatty tissue. The atrioventricular surface appears at the base of heart, and it moves towards the cardiac apex during contraction. Other structural features include the endocardium which lines up the cardiac chambers and is a thin sheet of flattened endothelial cells over connective tissue and smooth muscle cells. In addition, the valve surfaces and all blood vessels are connected by the endocardium. The epicardium on the other hand covers the outer surface of the heart, which is a thin layer of flattened mesothelial cells over connective tissue. The whole heart is covered by pericardium. Pericardial fluid occupies the narrow mesothelium lined space between the epicardium and pericardium. Pericardial fluid protects the heart by lubricating the cardiac surfaces.

The four chambers consist of the right atrium, right ventricle, left atrium and left ventricle. The right atrium is a muscular chamber with a thin wall. The right atrium receives the venous blood retuning from the two venae cavae and the coronary sinus. The right ventricle is the chamber with a free wall that is around 0.5cm thick. It resembles a pocket surrounding the interventricular septum. The left atrium is the chamber that receives blood from the four pulmonary veins and then transfers it into the left ventricle through the bicuspid valve. The wall of left

ventricle is around three times thicker than the right ventricle wall since the left side must generate higher arterial pressures.

The tricuspid valve is a valve with three cusps and connects the right atrium to the right ventricle. Each of the cusps is thin, about 0.1mm thick, assembled of connective tissue and covered by endothelium. The pulmonary valve has three equally sized and cusps as it guides the blood from the ventricle into the pulmonary artery. The bicuspid valve that guides the blood through from left ventricle is the mitral valve. The cusp margins are tightened by chordae tendineae to two papillary muscles in the left ventricle and that prevents eversion. The aortic valve also consists of three cusp valves (Herring and Paterson, 2018).

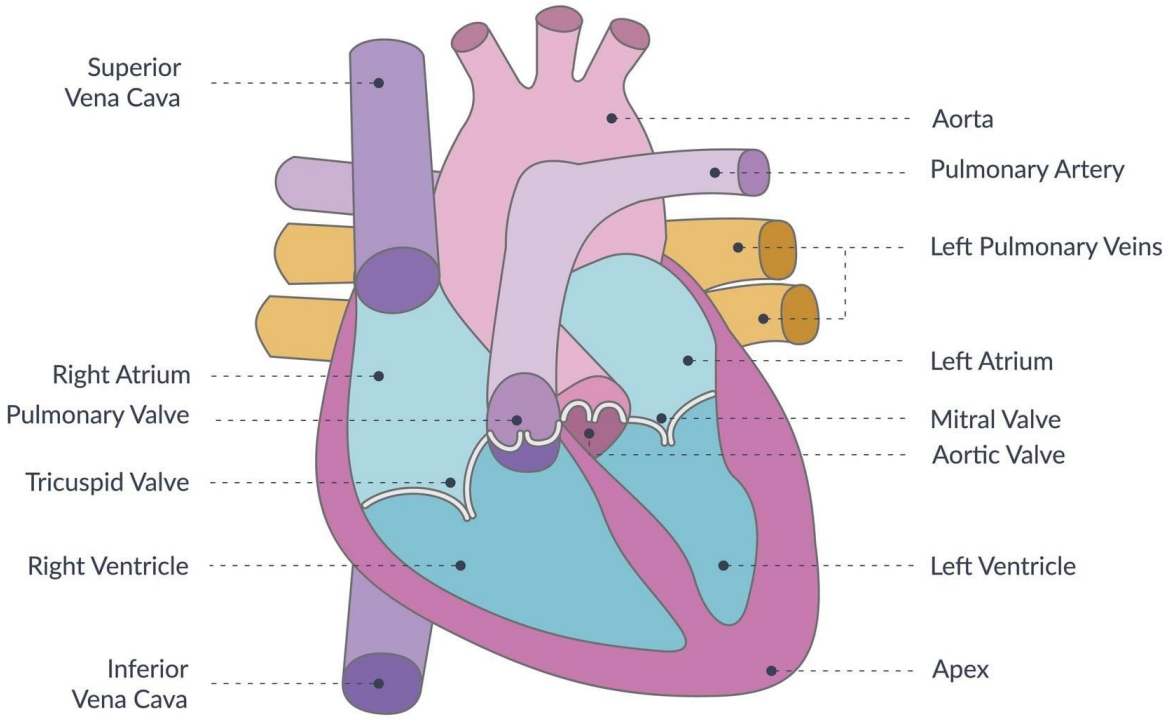

Figure 1.1 Anatomy of Heart. (Hackensack Meridian Health website) (https://www.hackensackmeridianhealth.org/HealthU/2019/02/04/know-your-heart-anatomy-101/).

1.1.2 Cardiac myocyte contraction.

Human cardiac myocytes are highly developed muscle cells that have a cylindrical shape. They are normally 10-20μm wide and 50-100μm long (Herring and Paterson, 2018). The main function of cardiac myocytes is to contract. The mechanism of contraction is underpinned by movement of thin actin filaments that slide into the spaces between thick myosin filaments (Squire, 2016). The thin and thick filaments are propelled past each other by formation, rotation and breaking the biochemical bonds or crossbridges on repeat. The crossbridge was first observed under the electron microscope by Hugh Huxley in 1957 (Squire, 2016). The crossbridge under the microscope looks like it is the head of myosin molecules outstanding from the side of the thick filament. Each of the crossbridges acts like single, independent force generators, and substantial force are generated because the swivelling action of hundreds of myosin heads per filament (Squire, 2016). The isoform of the myosin decides the speed of crossbridge cycling, and therefore the filament sliding (**Figure 1.2**). It shown that an adult human ventricle contains 97% slow-sliding β-myosin and 3% fast-sliding α-myosin (Herring and Paterson, 2018). The contractile force is determined by the numbers of crossbridges.

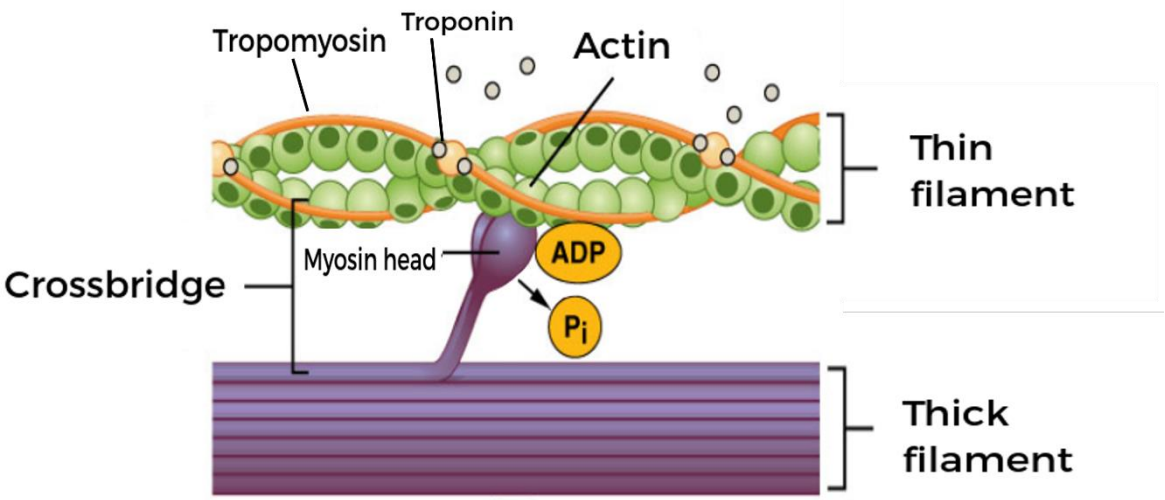

Figure 1.2 Cardiac myocytes sliding filament mechanism. The myosin heads bind to the actin protein binding site to form a crossbridge. Adapted from (https://theory.labster.com/sliding-filament-theory/). Legends added to the original figure.

1.1.3 Cardiac Cycle

The cardiac cycle is the cycle of atrial and ventricular contraction. Based on the positions of the inlet and outlet valves, the ventricular cycle is divided into four phases, they are ventricular filling, isovolumetric contraction, ejection, and isovolumetric relaxation (Herring and Paterson, 2018). One complete ventricular cycle lasts about 0.9s. **Table 1.1** shows the duration and the states of inlet and outlet valves of each phrase in ventricular cycle. **Figure 1.3** illustrates the changes in valves during the cardiac cycle (Herring and Paterson, 2018).

	Ventricular filling	**Isovolumetric Contraction**	**Ejection**	**Isovolumetric Relaxation**
Duration (s)	0.5	0.05	0.3	0.08
Inlet Valves	Open	Closed	Closed	Closed
Outlet Valves	Closed	Closed	Open	Closed

Table 1.1 The ventricular cycle phrases duration time and outlet and inlet valves states.

Ventricular diastole is the period of time that the two ventricles are relaxing from contraction. Ventricular diastole takes almost two thirds of the cardiac cycle in a resting heartbeat, and this high percentage of the time provides enough time to fill the ventricles. At the beginning of cardiac cycle, the atria are also in diastole, therefore, blood flows from the superior and inferior vena cava through the relaxed atria and opened atrioventricular valves into the ventricles. The filling process is a rapid process, and the ventricles fill within 0.15s. In the last third period of filling time, extra blood is pumped out by atrial contraction into the ventricle. After ventricular systole, atrial systole starts and lasts 0.35s. Atrial

systole is the contracting of cardiac muscle cells of both atria after electrical stimulation and conduction of electrical currents through the atrial chambers (Shiels, 2011). The atrial systole is divided into the isovolumetric phase and ejection phase. Once the ventricular pressure breaches the level of atrial pressure, the atrioventricular valves are closed by the reversed pressure gradient. Because vortices are formed close to the valve cusps during the late filling phase, the backflow during the closing atrioventricular valves is minimal. Ejection begins when ventricular pressure reaches arterial pressure, and the outflow valves are pushed open. The rapid ejection phase takes only the first half of the ejection phase, but three quarters of the stroke volume is ejected in this time. The rapid ejection phase only lasts 0.15s. During the ejection phase, the cusps of the open aortic valve lie close to the entrances to the coronary arteries but do not block them, since vortices behind the cusps cause to floating between midstream and the aorta wall. Each ventricle becomes a closed chamber after the aortic and pulmonary valves close (Herring and Paterson, 2018). The relaxing myocardium makes the ventricular blood pressure drop rapidly. The pressure difference forces the atrioventricular valves to open, which terminates the isovolumetric relaxation phase only when ventricular blood pressure drops below atrial pressure. The next event in the sequence is blood flooding from the atria which have been filling up during ventricular systole and the next ventricular cycle begins (Herring and Paterson, 2018).

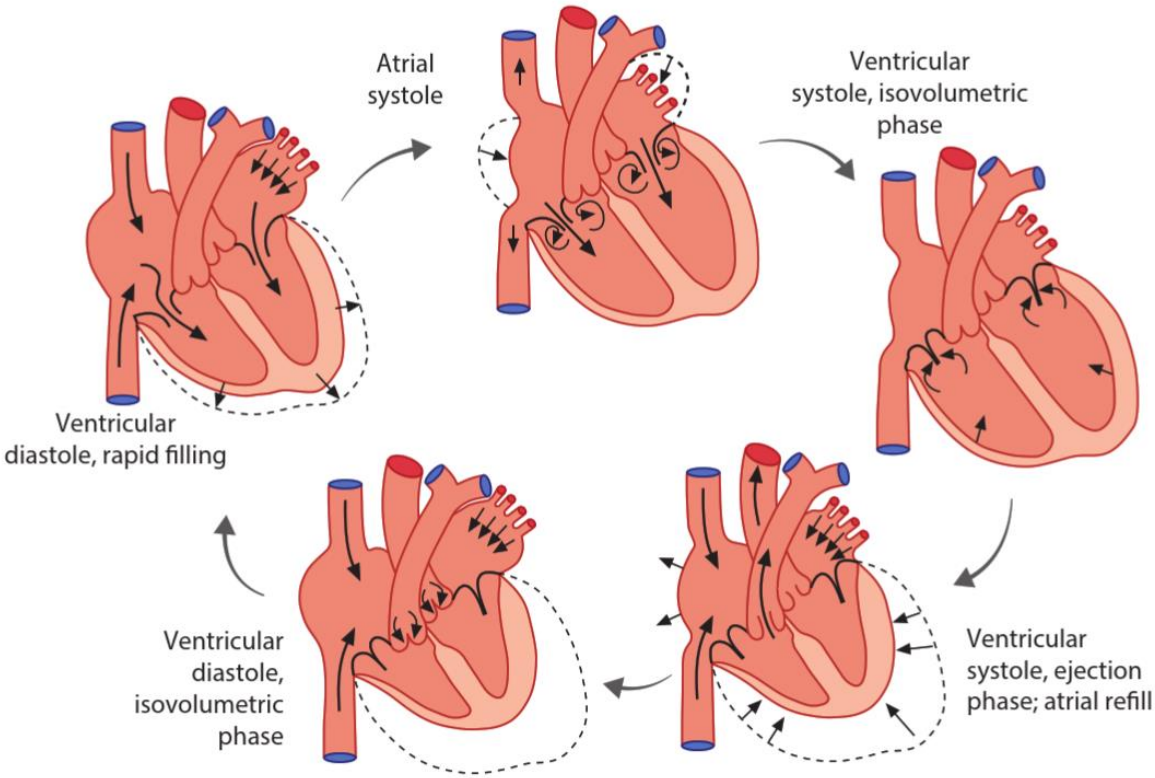

Figure 1.3 Changes in valves, atrial and ventricular volumes during the cardiac cycle. (Herring and Paterson, 2018).

1.1.4 Excitation Contraction (EC) Coupling

Excitation contraction (EC) coupling is the process that coordinates the cellular mechanisms that produce heartbeats. Electrical excitation of the cardiomyocytes is referred to as EC coupling (**Figure 1.4**). This involves both activation of the myofilaments and the scarcolemmal action potential (AP) trigger. Scarcolemma is the plasma membrane of the muscle cells The increase of intracellular calcium ion concentration plays a key role in the linkage between excitation and contraction (Schlüter, 2016). Scarcolemmal Ca^{2+} influx causes the Ca^{2+} increase, during the time that AP triggers ensuing Ca^{2+} release from the sarcoplasmic reticulum (SR), where the intracellular Ca^{2+} is stored. Sarcolemmal Ca^{2+} transfers predominantly through L-type Ca^{2+} channels (LTCC), and SR Ca^{2+} release mainly through ryanodine receptors (Schlüter, 2016). This Ca^{2+} release process is a characteristic function of cardiomyocytes and called Ca^{2+}-induced Ca^{2+} release (CICR)(Fabjato & Fabjato, 1975). After the termination of SR Ca^{2+} release, the Ca^{2+}

concentration starts to reduce. The reduction of Ca^{2+} concentration is regulated by several pathways. The two most important of them involve the SR Ca^{2+} -ATPase (SERCA)/phospholamban (PLB) complex and the Na^{+} -Ca^{2+} exchanger (NCX). Firstly, the Ca^{2+} reuptake is regulated by SERCA, which is regulated by PLB, while Ca^{2+} extrusion from the cells is regulated by sarcolemmal NCX. The increase in Ca^{2+} concentration driven by CICR elicits contraction via Ca^{2+} binding to filament protein troponin C. Troponin C induces an actin-myosin interaction, and as a consequence causes release of Ca^{2+} from troponin C and induces relaxation (Schlüter, 2016).

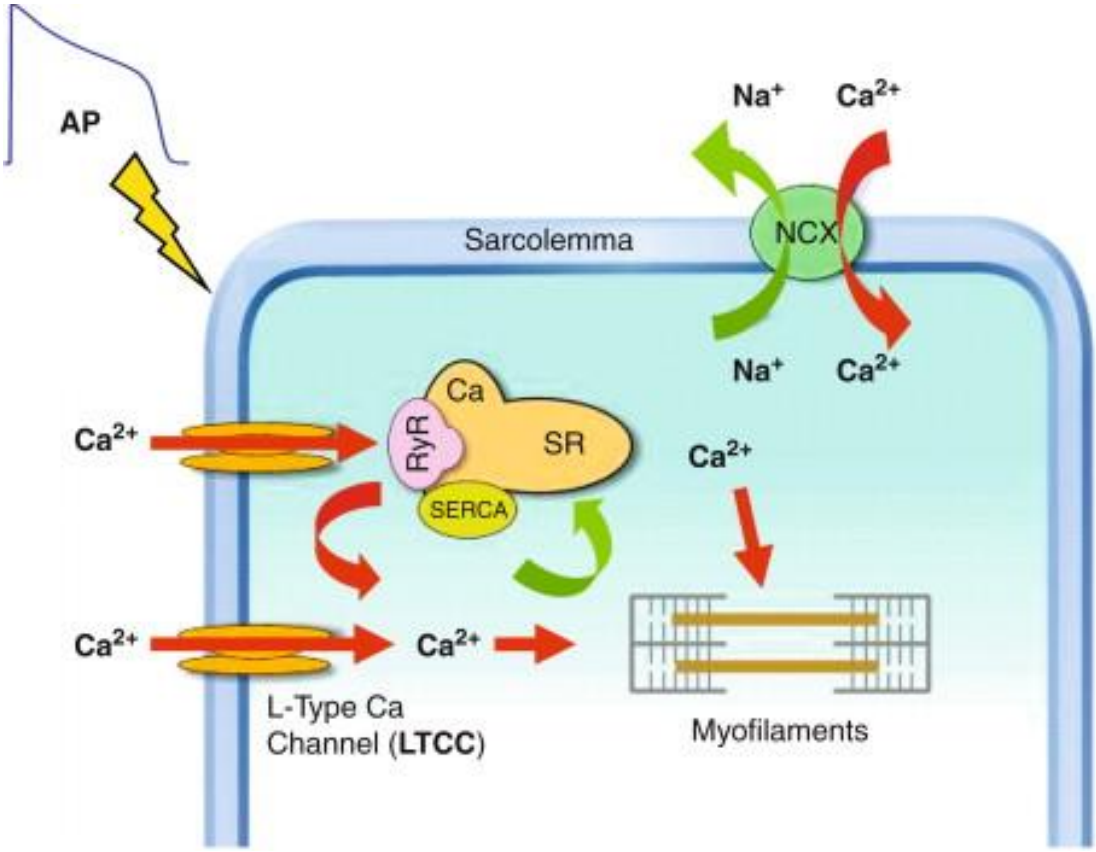

Figure 1.4 Excitation-Contraction (EC) coupling diagram. The diagram shows the EC coupling pathway in cardiomyocytes. The cell membrane sarcolemma (SL) separates the intra- and extracellular space. The figure shows the SL being excited by an action potential (AP) which opens L-type Ca^{2+} channels (LTCC) in the cell membrane allowing Ca^{2+} influx (shown by red arrows) down its concentration gradient into the cell. Ca^{2+} can also enter the cell via reverse-mode Na+– Ca^{2+} exchange (NCX). Ca^{2+} influx can trigger Ca^{2+} release from the sarcoplasmic reticulum (SR) through ryanodine receptors (RyR). Together, these Ca^{2+} influxes cause a transient rise in Ca^{2+}that initiates contraction at the myofilaments. Relaxation occurs when Ca^{2+} is removed from the cytosol (green arrows) either back across the SL via forward-mode NCX or back into the SR via the SR Ca^{2+}-pump (SERCA)(Shiels, 2011).

1.2 Heart Failure (HF)

Heart failure is a serious condition and has become a severe global disease threating an estimated 26 million people worldwide and causing more than 1 million hospitalizations annually in both Europe and United States (Liu, 2018).

1.2.1 Definition of HF

Heart failure is defined as the inadequacy of cardiac output to meet the metabolism demands of functional organs and tissues. When a patient has a heart failure condition, his/her blood flow out of the heart slows and blood returning to the heart through the veins store up, causing congestion in the body's tissue and organs (Yancy et al., 2013).

1.2.2 Symptoms, Diagnosis and Classification of HF Stages

Patients that suffer from heart failure usually seek medical advice because they feel unwell, and it influences their daily life. The symptoms are various, **Table 1.2** presents a range of possible symptoms that a heart failure patient may develop as the disease progresses. Since most of the symptoms are not identical or exclusive to heart failure, it is extremely vital for the clinical cardiologist to diagnose heart failure with appropriate tests.

Symptoms of Heart Failure
Fatigue
Shortness of breath at rest or during exercise
Discomfort while breathing (dyspnea)
Rapid breathing (tachypea)
Difficulty in breathing while bending (bendopnea)
Orthopnea
Paroxysmal nocturnal dyspnea
Cough
Wheeze
Diminished exercise capacity
Nocturia
Weight gain/loss
Abdominal pain (particularly confined to the right upper quadrant)
Loss of appetite or early satiety
Increasing abdominal girth or bloating
Edema (of the extremities, scrotum, or elsewhere)
Palpitations
Syncope
History of Cheyne-Stokes respirations during sleep (often reported by the family rather than by the patient)
Somnolence, confusion or diminished mental acuity
Depression

Table 1.2 List of symptoms of heart failure. Symptoms that commonly happened to HF patients are listed. (Greenberg et al., 2020).

The diagnosis of heart failure is extremely important for clinical evaluation, but there is no single symptom, physical finding, or test that can facilitate acute diagnosis. An electrocardiograph (ECG) and/or B-type natriuretic peptide (BNP) assay are recommended by the National Institute for Health and Clinical Excellence (NICE) guidelines on chronic heart failure primary and secondary care in England (Hobbs et al., 2010). If both results are in the normal range, then heart failure is unlikely, and an alternative diagnosis should be considered to explain the symptoms. If either of the tests is abnormal, then an echocardiogram or other imaging test would be advised to confirm underlying cardiac dysfunction. The diagnostic workflow of heart failure in primary care is shown below suggested by NICE in England (**Figure 1.5**).

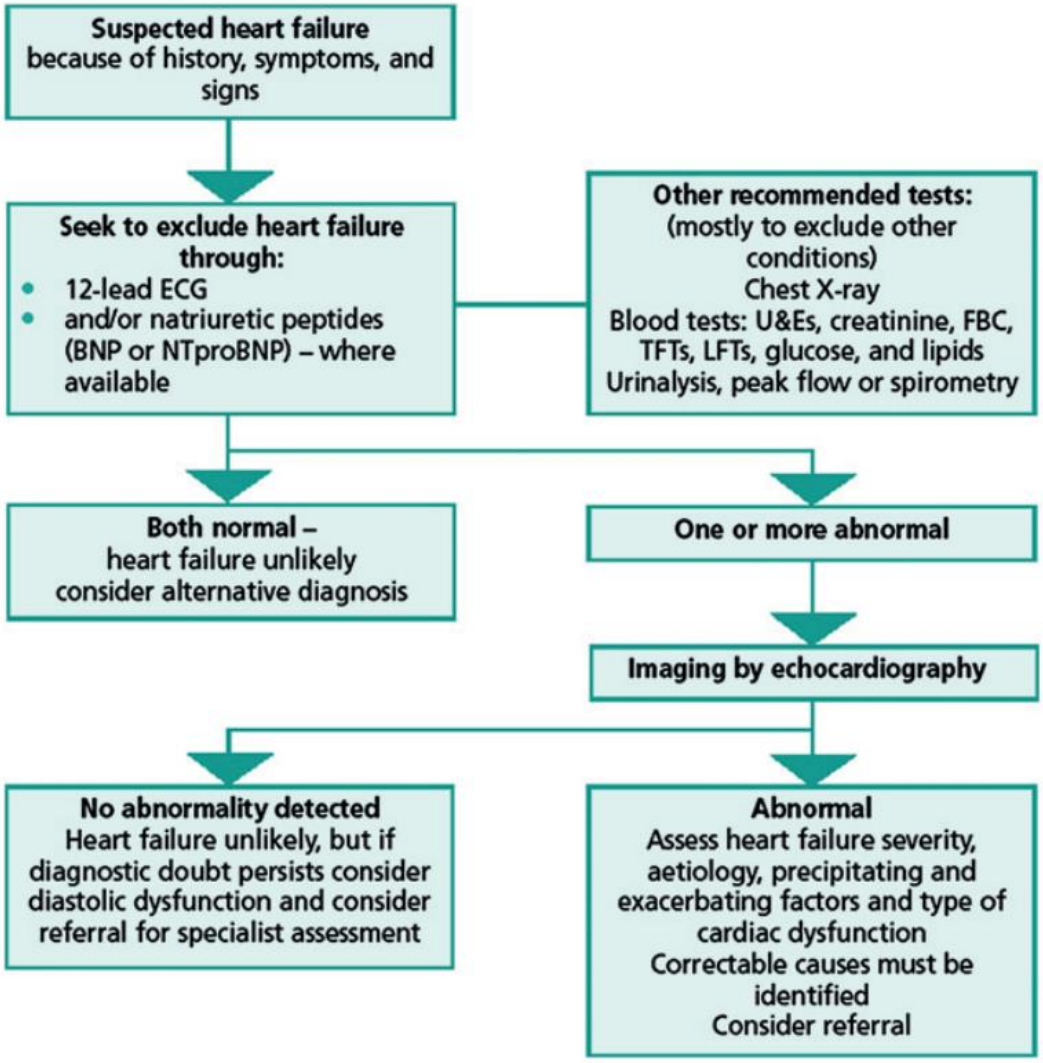

Figure 1.5 The diagnosis workflow of chronic heart failure for use in primary care by the National Institute for Health and Clinical Excellence in England (Hobbs et al., 2010)). BNP, B-type natriuretic peptide; FBC, full blood count; LFTs, liver function tests; NTproBNP, N terminal pro-BNP; TFTs, thyroid function tests; U&Es, urea and electrolytes.

In 2001, the New York Heart Association (NYHA) defined a clear way of classifying the extent of heart failure by functional limitation. The method catalogues the patients into one of four categories based on how much they are limited during physical activity. The limitations and symptoms apply to normal breathing and different degrees of breath shortness and/or angina (Liu, 2018).

Class I: Cardiac disease, but no symptoms and no limitation in ordinary physical activity, e.g., no shortness of breath when walking and climbing stairs.

Class II: Mild symptoms (mild shortness of breath and/or angina) and slight limitation during ordinary activity.

Class III: Marked limitation in activity due to symptoms, even during less-than-ordinary activity, e.g., walking short distances (20-100m) and/or being comfortable only at rest.

Class IV: Severe limitations. Experiences symptoms even while at rest and/or mostly bedbound patients.

The American College of Cardiology Foundation (ACCF) and American Heart Association (AHA) have also catalogued the development and progression of heart failure stages and their descriptions can be used to describe individuals and populations. **Figure 1.6** illustrates stage A to D of heart failure based on the state of individual patients.

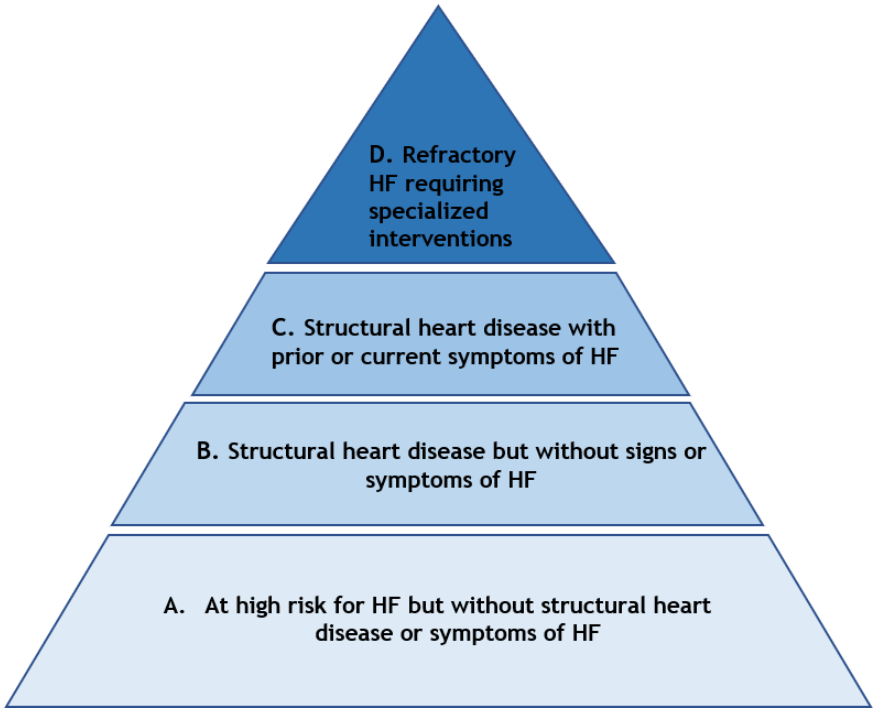

Figure 1.6 ACCF/AHA stages of Heart failure. (Yancy et al., 2013).

1.2.3 The Cause of HF

Heart failure is a syndrome developed during a disease progress rather than a primary diagnosis. There are multiple factors that that contribute to heart failure development. The most common cause of heart failure is coronary heart disease where plaques start to grow. This action decreases cardiac blood supply, which may result in asymptomatic left ventricular dysfunction or the progression of chronic heart failure (Diwan & Hill, 2020). There are several risk factors suggested to have a causal role in the development of heart failure. Having an unhealthy lifestyle is one of the risk factors and includes smoking, being overweight and having a high fat, cholesterol-rich diet, and physical inactivity. Different heart diseases are also a major cause of heart failure. These conditions include coronary heart disease (CHD), myocardial infarction, high blood pressure, abnormal heart valves, congenital heart disease, severe lung disease, diabetes, obesity, and low red blood cell count etc.

Eight groups of risk factors for heart failure are defined by Bui and Schocken et al., it established a foundation that supports the current knowledge of the risk factors (Bui et al., 2011)(Schocken et al., 2008).

1. Major clinical risk factors: aging, males, hypertension, LV hypertrophy, myocardial infarction, valvular heart disease, obesity and diabetes.
2. Minor clinical risk factors: smoking, dyslipidemia, chronic kidney disease, albuminuria, sleep-disordered breathing, anemia, increased heart rate, dietary risk factors, sedentary lifestyle, low socioeconomic status, and psychologic stress.
3. Immune-mediated risk factors: Peripartum cardiomyopathy and hypersensitivity.
4. Infections: Viral, parasitic (Chagas disease), and bacterial.
5. Toxic risk precipitants: Chemotherapy (anthracyclines, cyclophosphamide, 5-fluorouracil), targeted cancer therapy (trastuzumab, tyrosine kinase inhibitors), cocaine, nonsteroidal anti-inflammatory drugs (NSAIDs), thiazolidinediones, doxazosin, and alcohol consumption.
6. Genetic risk predictors: single nucleotide polymorphism (SNP) (e.g., α2CDel322-325, β1Arg389), family history, and history of congenital heart disease.
7. Morphologic risk predictors: Increased LV internal dimension, mass, and asymptomatic LV dysfunction.
8. Biomarker risk predictors: Immune activation (e.g., insulin-like growth factors 1 [IGF1], tumor necrosis factor [TNF], interleukin 6 [IL-6], C-reactive protein [CRP]), natriuretic peptides (e.g., brain natriuretic peptide [BNP] and n-terminal [NT]-BNP)), and high- sensitivity cardiac troponin.

1.2.4 Pathophysiologic models of HF

Heart failure is a disorder that involves abnormal functioning of multi-systems mainly caused by abnormalities of cardiac function. It characterized by dysfunction of skeletal muscle, renal function, and stimulation of the sympathetic nervous system. In the past decades of heart failure research, three possible

pathophysiologic models have gained attention. The first is the cardiorenal model where heart failure is considered as an issue of excessive salt and water retention that is caused by abnormalities of renal blood flow. The second model is called cardiocirculatory, or the hemodynamic model. In this model, heart failure is reviewed as a result of abnormalities in the pumping capacity of the heart and excessive peripheral vasoconstriction. The last theory is the neurohormonal model. Overexpression of biologically active molecules that are capable of exerting toxic effects on the heart and circulation is suggested to drive heart failure progression (Liu, 2018) (Mann & Bristow, 2005) (Batlle et al., 2007).

1.2.5 Management of HF

There are various options to manage heart failure, including 1. Pharmacological management with antagonists of the renin-angiotensin-aldosterone and sympathetic nervous systems, 2. device therapy 3. cardiac surgery 4. gene therapy in targeting the molecular mechanisms implicated in heart failure, and finally 5. non-pharmacological management such as changing of lifestyle, such as the cessation of smoking and reduction of alcohol consumption (Gardner, 2007; Hulot, Isgikawa, and Hajjar, 2016).

The ACCF/AHA guideline for the management of heart failure has suggested principals for the management of heart failure based on different stages.

At stage A of heart failure, there is no obvious evidence of heart failure, but bad lifestyle and high-risk factors that can lead to heart failure were observed with the patients. The key point to manage at stage A is to recognize and control the risk factors that may lead heart failure. Hypertension is one of the major risk factors for the development of heart failure. Long-term treatment of both systolic and diastolic hypertension has been shown to reduce the risk of incident heart failure by about 50% (Kostis et al., 1997). Diabetes mellitus and being overweight have become linked to heart failure as risk factors (Yancy et al., 2013). Obesity presumably increases the heart burden to increase the risk of heart failure. To control being overweight, it is important to have a healthy lifestyle and good diet. Standard therapies for diabetes mellitus such as Angiotensin-converting enzyme

(ACE) inhibitors or angiotensin II receptor blockers (ARBs) can prevent the development of diabetes and prevent heart failure. Another risk factor for heart failure is smoking. Patients should be advised strongly to be aware of the hazards and try to quit smoking.

Patients that have been diagnosed with stage B heart failure, in general are suggested to follow the medical advice made to stage A patients. Blood pressure management is particularly important in patients with LV hypertrophy (Yancy et al., 2013). ACE inhibitors and beta-blockers have been shown to impede maladaptive LV remodelling in patients with stage B heart failure as a prevention of heart failure (Yancy et al., 2013). Also, diuretic-based antihypertensive therapy has been shown to prevent stage B heart failure in a wide range of patients (Group et al., 2002).

Patients at stage C have a more complicated situation than stage A and B. Patients should be advised how to monitor their symptoms and weight control, restrict their sodium intake, take the prescriptions, and stay physically active. Their health and physical situation should be under close observation. Sodium restriction is reasonable for patients with symptomatic heart failure to reduce congestive symptoms. As a result of depressed breathing, sleep disorders are common in patients with symptomatic heart failure. Another effective way of managing the patients is exercise training. Studies have shown that exercise training reduces mortality and hospitalizations for heart failure patients (Correction Piepoli et al., 2004). The medication decision process is shown below (**Figure 1.7**) (Yancy et al., 2013).

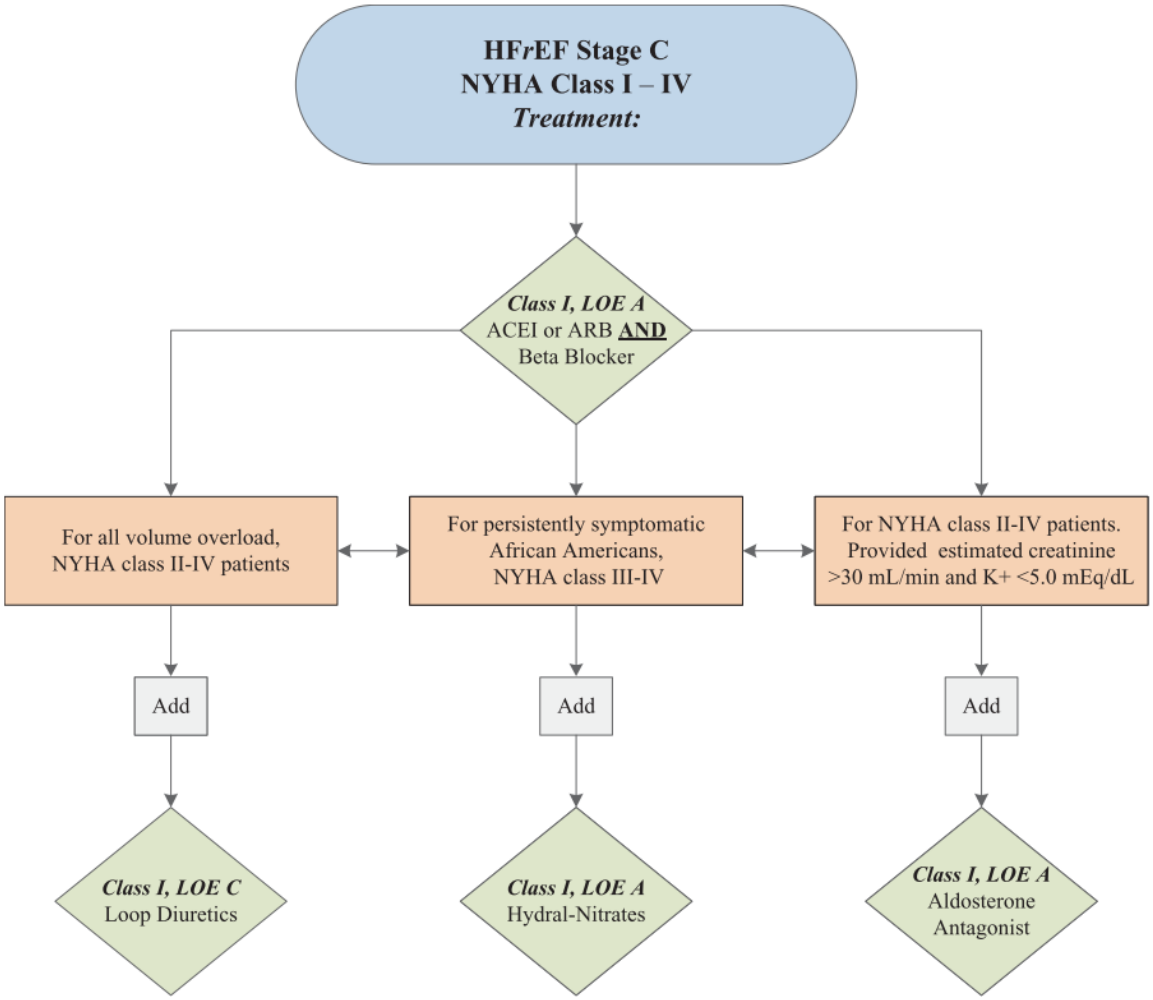

Figure 1.7 Stage C heart failure patient guideline of medical therapy. (Yancy et al., 2013) ACEI, angiotensin-converting enzyme inhibitor; ARB, angiotensin-receptor blocker; HFrEF, heart failure with reduced ejection fraction; Hydral-Nitrates, hydralazine, and isosorbide dinitrate; LOE, level of evidence; NYHA, New York Heart Association.

Stage D heart failure, which is also known as advanced heart failure or end-stage heart failure, refers to continually developing severe symptoms. Water retention is a serious problem for patients at this stage, sodium and fluid balance are best implemented in the context of weight and symptom monitoring programs. As the European Society of Cardiology describes, patients with truly refractory heart failure will be eligible for specialized, advanced treatment strategies, such as mechanical circulator support (MCS), procedures to facilitate fluid removal, continuous inotropic infusions, or cardiac transplantation or other innovative or experimental surgical procedures, or for end-of-life care, such as hospice (Kushner et al., 2009).

1.2.6 Molecular mechanisms underpinning Heart failure

As the prognosis of heart failure is not favourable, fundamental research has focused on the molecular mechanisms at play in heart failure disease development. Post-translational modifications are vital to maintain coordinated protein function in the cardiovascular system. SUMOylation is a post-translational modification that has recently been highlighted as being involved in multiple cardiovascular processes and it's dysregulation results in heart disease and ultimately in heart failure (Maejima, 2020). SERCA2a is one of the most prominent substrates for SUMOylation which is involved in heart failure disease development (Le et al., 2017). More on information on SUMOylation and heart disease is provided later in this Chapter and in Chapter 5.

1.3 The β_2 Adrenergic Receptor (β_2AR)

The Beta 2 adrenergic receptor (β_2AR) is a transmembrane receptor that belong to the superfamily of membrane proteins known as G-protein-coupled receptors (GPCRs) (Madamanchi, 2007a). There are four subtypes of β-ARs, β_1AR, β_2AR, β_3AR and β_4AR (Madamanchi, 2007b). The β_1-AR is found primarily in the heart, and it comprises 75-80% of the total β-ARs in the heart. The β_2AR is expressed in the lung and kidney and blood vessels as well as the heart and equates to 20-25% of cardiac βARs. The β_3AR is found primarily in the adipose tissue, and minimally in the heart. The β_4AR is now thought as a low affinity state of β_1AR.

1.3.1 The concept of Adrenergic Receptors

All adrenergic receptors (ARs) belong to the large G protein-coupled receptor superfamily. There are two main groups of adrenergic receptors, α and β with 9 subtypes in total. The α-ARs are divided into α_1AR as a G_q coupled receptor and α_2AR as a G_i coupled receptor. α_1AR has 3 subtypes $\alpha_{1A,}$ α_{1B} and α_{1D} and α2AR also has 3 subtypes $\alpha_{2A,}$ α_{2B} and α_{2c}. As mentioned above, β-AR has 4 subtypes and all of them are coupled to G_s proteins, while β_2-AR and β_3-AR also coupled to G_i (Fay,

1967). ARs can interact directly with heterotrimeric G proteins and a variety of kinases and phosphatases that result in reversible phosphorylation of the receptors on specific serine, threonine, or tyrosine residues (Fay, 1967).

1.3.2 Crystal Structure of the β_2AR

The B_2AR belongs to the GPCR family that has a structure containing an extracellular amino terminus, intracellular carboxyl terminus and seven transmembrane α-helices, which are all connected by three intracellular and three extracellular loops (Madamanchi, 2007) (**Figure 1.8**).

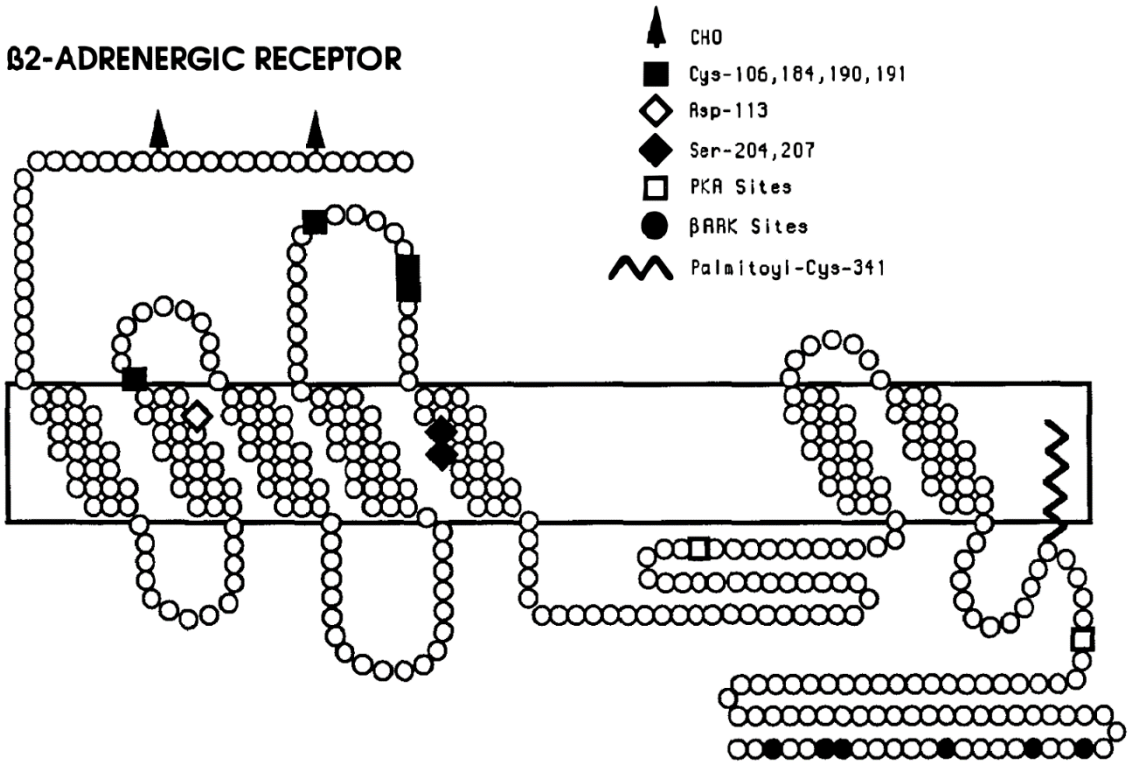

Figure 1.8 Schematic primary structure diagram of the β_2AR. (Dohlman et al., 1991). Important amino acids are indicated and as discussed below. CHO, N-linked oligosaccharide; PKA, cAMP-dependent protein kinase; ßARK, ß-adrenergic receptor kinase.

The primary structure provides limited information for the research into functional aspects of the B_2AR. The Human B_2AR protein and sequence was first recognized in the 1990s, but the structure of B_2AR study was not well established until 2007 (Noble & Smith, 2015). The challenge was that the conformational

instability of B_2AR in its agonist independent basal form made it difficult to crystalise. The three-dimensional crystal (3D) structure provided a way to visualise the spatial characteristics of each individual amino acid of B_2AR, which in turn allowed prediction of various protein-protein interaction sites and assessment of ligand binding pockets for pharmacological intervention (Maeda & Schertler, 2013). Rhodopsin was the first GPCR that been crystallised (Palczewski et al., 2000). Since then, rhodopsin has been used as a template to predict other GPCRs' crystal structure like the B_2AR. Helix 8 is known as one of the two addition helical segments along the B_2AR structure and has been shown to interact with transmembrane domain 1. Helix 8 has been shown to play a role in B_2AR homodimer formation and in the delivery of functional B_2AR complexes to the plasma membrane (Parmar et al., 2017). The crystal structure also indicated that there is disorder among the N-terminus (residues 1-28), the majority of the C-terminus (residues 343-365) and a stretch of 26 amino acids in the third intracellular loop (Rasmussen, et al., 2011) (Cherevoz, et al., 2007). One possible insight into the disordered parts might be that they are stabilised following post translational modification or when the receptor interacts with other proteins (Wright &Dyson, 2015). Studies have shown that the changes between a carazolol bound inactive structure and an agonist bound active structure are little and only occur on the extracellular side of the receptor. Carazolol is a fluorescent antagonist that was used to study binding domain of the B_2AR (Tota & Strader, 1990).The biggest change between inactive and active structure of B_2AR is the onward movement of TM6 on the cytoplasmic side of B_2AR (Noble & Smith, 2015). **Figure 1.9** indicates the structure changes between inactive and active B_2AR.

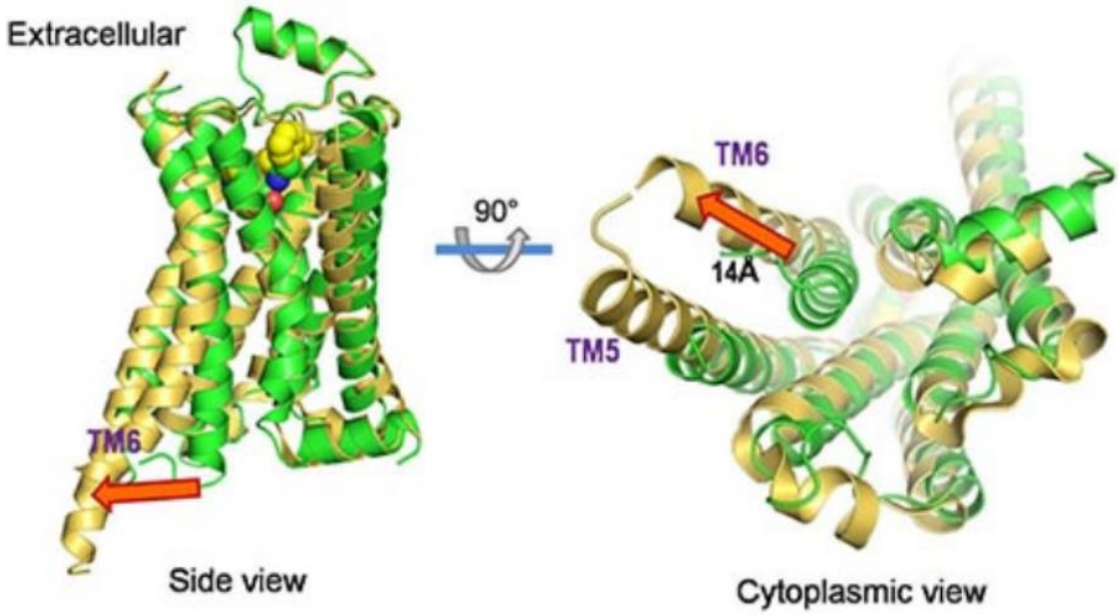

Figure 1.9 Comparison between inactive and active structures of $ß_2$AR. (Noble & Smith, 2015). The active conformation of $ß_2$AR from $ß_2$AR-Gs complex is coloured in gold and the carazolol bound inactive structure is shown in green.

1.3.3 G-Protein-Coupled Receptor (GPCR) Signal Transduction

G proteins can bind to the nucleotides guanosine-5'-triphosphatye (GTP) and guanosine diphosphate (GDP), and act as molecular switches in the transduction of intracellular signalling. In the active conformation, G proteins are bound to GTP, and when bound to GDP, they are switched to inactive state (J. Wang et al., 2018). Heterotrimeric G proteins consist of α, ß and γ subunits. When an external activator binds to a GPCR, it triggers the receptor's conformational change and the recruitment of a G protein that is located on the plasma membrane in order to switch GDP for GTP on the subunit Gα, so that it will lead to its activation. The dissociation of two subunits of GTP-bound Gα and dimeric Gßγ complex subunit are led by GDP-GTP exchange of the heterotrimeric G protein. Both of these subunits can transduce signals by a variety of signalling routes, with the best-known being enzymes that produce second messengers that induce physiological change. Conversely, the catalytic Gα subunit can also hydrolyse the bound GTP back to GDP, resulting it's reassociation with the Gßγ complex subunit and

termination of the G protein activation cycle (J. Wang et al., 2018). There are 21 Gα subunits, 6 Gß subunits and 12 Gγ subunits discovered until now (J. Wang et al., 2018). The diversity of G protein subunits allows a range of different functions in signalling transduction including different enzyme effectors. The $G\alpha_s$ stimulates the enzyme adenylyl cyclase (AC), which produces the second messenger cyclic adenosine monophosphate (cAMP) from ATP. cAMP then activates protein kinase A (PKA) and initiates the phosphorylation of a wide range of intracellular proteins which regulate cellular processes (Cao, 2019). On the other hand, $G\alpha_i$ inhibits AC, and therefore, inactivates cAMP-driven signalling events. $G\alpha_q$ can activate phospholipase C (PLC) that in turn leads to the cleavage of the membrane-bound phosphatidylinositol 4,5-bisphosphate to the second messenger inositol 1,4,5-triphosphate (IP_3). IP_3 promotes Ca^{2+} release from the endoplasmic reticulum. Intracellular Ca^{2+} release and diacylglycerol diffused from the plasma membrane then activates protein kinase C (PKC), which triggers specific cellular signalling events (J. Wang et al., 2018). **Figure 1.10** shows the GPCR signal pathway diagram (Lynch & Wang, 2016).

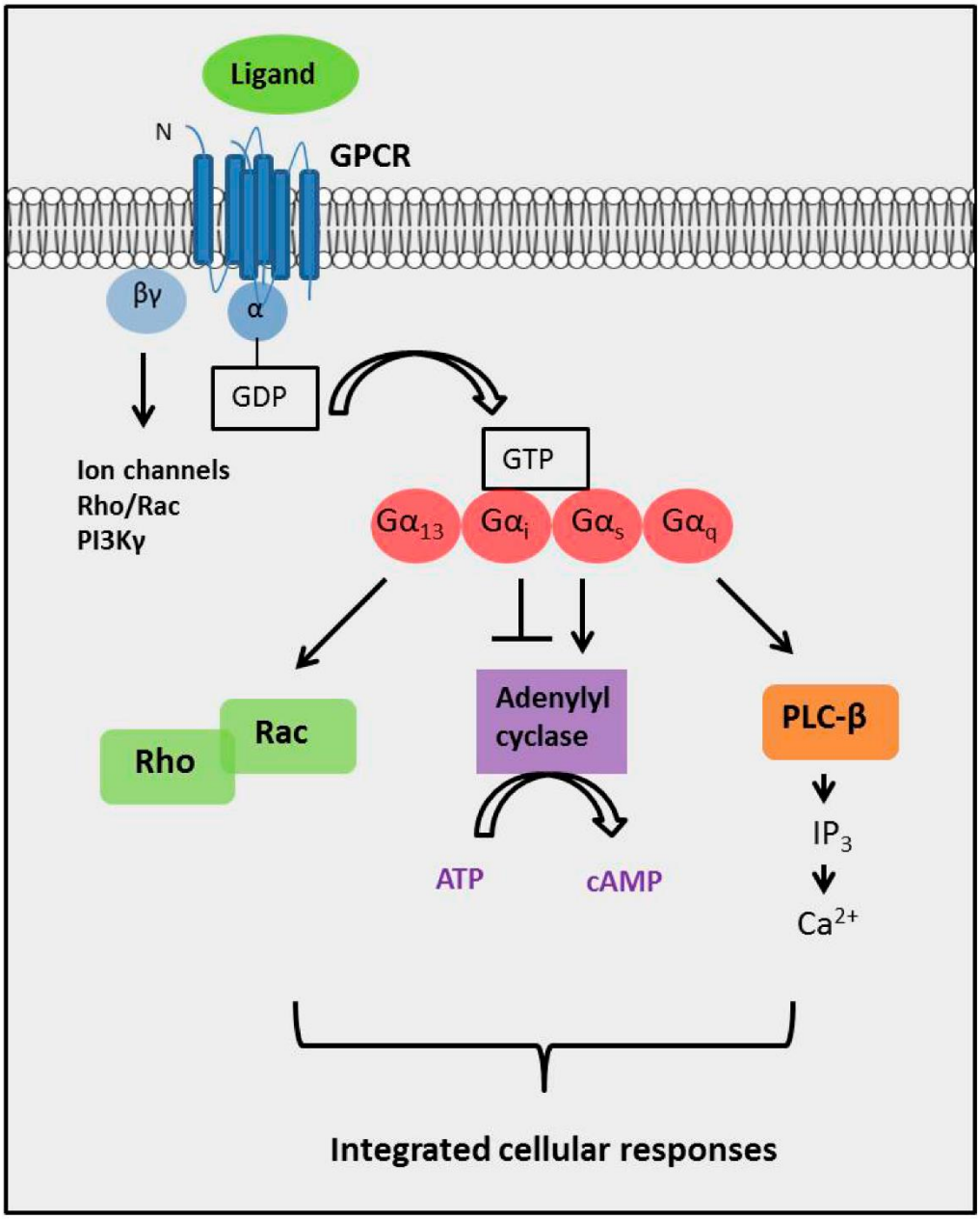

Figure 1.10 GPCR signal pathway through heterotrimeric G proteins. (Lynch & Wang, 2016). GPCRs transfer extracellular signals through plasma membrane to intracellular and regulate cellular processes by heterotrimeric G proteins. GDP, guanosine diphosphate; GTP, guanosine triphosphate; cAMP, cyclic adenosine monophosphate; Rho, Ras homolog family; Rac, Ras related small GTPase protein; IP3, inositol triphosphate; ↓: Signaling activation; ⊥: signalling inhibition.

1.3.4 β_2AR Signalling and Regulation (Desensitization)

When stimulated, cardiac β_2ARs activate associated G stimulatory (Gs) protein. Adenylyl cyclase (AC) is then activated by the Gα subunit of the Gs protein ($G\alpha_s$), which generates the second messenger cyclic adenosine monophosphate (cAMP) that in turn activates cAMP-dependent protein kinase A (PKA) (Madamanchi, 2007). Other cAMP effectors are exchange protein activated by cAMP (EPAC), cyclic-nucleotide gated ion channels and Popeye- domain containing proteins (Jes´ et al., 2009) (Talke et al., 2003). In a cardiac setting, activated PKA phosphorylates troponin I, the L-type Ca^{2+} channel and phospholamban (PLB), to enhance contractility (Freedman & Lefkowitz, 2004). Notably, during heart failure, β_2-adrenoceptors are downregulated and desensitized while other remaining receptors are uncoupled from Gs. The expression of the $G\alpha_i$ subunit also increases and acts to further antagonize β-adrenergic signalling. β-receptor antagonists are regarded as a standard treatment in heart failure (Feldman et al., 1988) (Neumann et al., 1988) (Bohm et al., 1990) (**Figure 1.11**).

Agonists like isoprenaline bind to β_2AR which triggers phosphorylation of the receptor by PKA at serines in the third intracellular loop and the proximal cytoplasmic tail (McGraw & Liggett, 2005). This phosphorylation event decreases the coupling of the receptor to the Gs subunit, and this is one of the mechanisms of β_2AR desensitization. G-protein-coupled receptor kinases (GRKs) are a family of enzymes that phosphorylate the β_2AR at different serines and threonines in the cytoplasmic tail. The multi-functional scaffold protein β-arrestin binds to the GRK phosphorylated β_2AR , to disassociate the receptor from Gs and as a result desensitize β_2AR function (McGraw & Liggett, 2005). The uncoupling between receptor and Gs also promotes β-arrestin-dependent receptor internalization. The scaffolding action of β-arrestin also brings other proteins into the β_2AR microdomain. An example of which is E3 ubiquitin ligases which tags the β_2AR with ubiquitin to promote receptor degradation (Shenoy et al., 2001). Another example is phosphodiesterase enzymes which are recruited to the vicinity of the β_2AR by β-arrestin to degrade cAMP as part of the desensitization mechanism (Baillie et al., 2002).

Desensitization is the process that limits function of the β_2AR after prolonged agonist activation (McGraw & Liggett, 2005). Desensitization is critical for the cells to integrate the myriad signals that are received, and to adapt the changes between physiologic and pathologic states. Studies have shown that long-term desensitization of β_2AR is the consequence of a series of processes, which includes short-term cellular events like GRK and PKA phosphorylation, Gi coupling, and PDE4 recruitment and long- term events that result in decreased receptor expression which known as receptor "downregulation". Downregulation is driven by transcriptional and protein degradation mechanisms (McGraw & Liggett, 2005). Research has shown that when cells are treated with isoproterenol/isoprenaline (ISO) as an agonist of β_2AR, β_2AR receptors are phosphorylated rapidly by GRKs, which leads to β-arrestin binding and rapid desensitization and internalization of β_2AR (Carr et al., 2016)(Benovic, 2002). A comparison was made between the ubiquitination of wild type β_2AR and phosphorylation defective β_2AR, in which all GRK and PKA sites were mutated to alanine. ISO which is an agonist stimulation caused ubiquitination of the WT β_2AR but not in the mutant β_2AR in COS-7 cells (Shenoy et al., 2001). Also, by using co-immunoprecipitation it was shown that the mutant β_2AR did not undergo internalization or β-arrestin binding after ISO treatment (Shenoy et al., 2001).

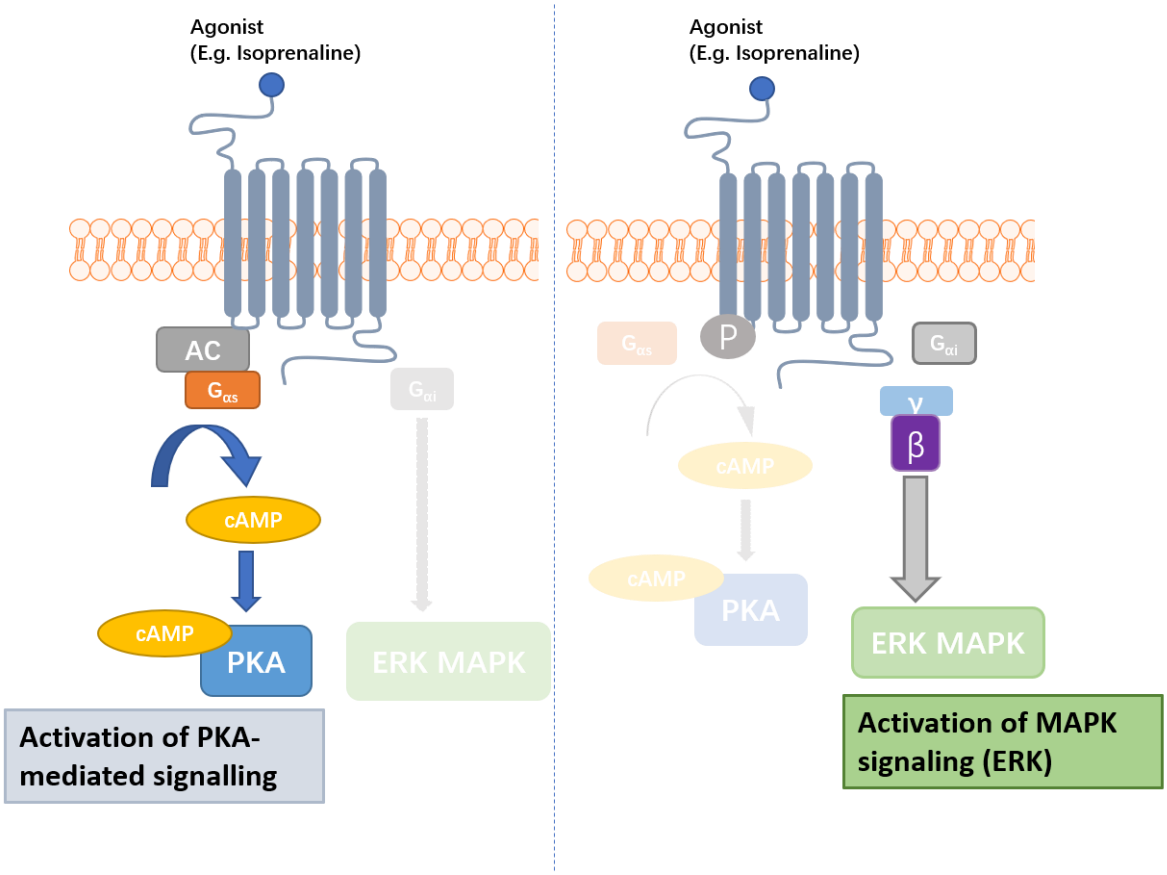

Figure 1.11 Agonist binding ß$_2$AR signalling pathway. Upon agonist binding the ß$_2$AR activates AC via the Gs protein. AC initiates the conversion of ATP to cAMP. cAMP is the intracellular second messenger who can go on to activate multiple targets, one of which is PKA. The ß$_2$AR is a target for PKA. This PTM of the ß$_2$AR results in reduced coupling between the ß$_2$AR and Gs and switches it to Gi. In the active state, the Gα-GTP subunit of Gi dissociates from the Gß Gγ subunits. Gα mediates inhibition of AC and the free Gß Gγ subunits mediate activation of the MAPK signalling pathway such as ERK. AC, adenylyl cyclase; ATP, adenosine triphosphate; cAMP, cyclic adenosine monophosphate; PKA, protein kinase A; PTM, post-translational modification; MAPK, mitogen-activated protein kinase; ERK, extracellular-signal-regulated kinase.

1.3.5 Internalization of β_2AR

As previously noted, receptor desensitization is a common feature of GPCR-based signalling systems. Receptor internalization, is now known to be the main route to desensitization in a number of scenarios (Fisher et al., 2010). Many GPCR internalization events depend on GPCR-kinase (GRK), which phosphorylates the amino acids in the C-terminal tail of the receptor. After the receptor becomes phosphorylated, β-arrestin recruitment initialises internalization of the GPCR into clathrin pits, which eventually take the receptor into membrane bound vesicles by endocytosis. The internalization is a fast process that happens within about three minutes after agonist stimulation (Morrison et al., 1996). After the receptor becomes internalized, it moves away from the cell surface to endosomal compartments (Kallal et al., 1998). When β-arrestin binds to the receptor as the outcome of agonist stimulation, it binds with high affinity directly and stoichiometrically to clathrin which is the major structural protein of the coated pits (Goodman et al., 1996). Then the receptor-arrestin complex binds to the adaptor protein 2 (AP-2) to trigger clathrin coated endosome formation (Laporte et al., 2000). Ubiquitination of β-arrestin also contributes to β_2AR internalization. (Shenoy et al., 2001). β-arrestin2 has interactions with two different E3 ubiquitination ligases, NEDD4 and Mdm2. NEDD4,an E3 ubiquitin protein ligase of ubiquitination, mediates agonist-dependent ubiquitination, lysosomal targeting and degradation of the β_2AR (Sudha K. Shenoy et al., 2008). NEDD4 recruitment is also promoted by β-arrestin-β_2AR interaction (Han et al., 2013). β-arrestin2-mediated recruitment of NEDD4 to the activated receptor and NEDD4-mediated ubiquitination regulate the internalization of β_2AR in the lysosomal compartments (Sudha K. Shenoy et al., 2008). Shenoy et al. found out a dominant negative NEDD4 selectively inhibited ISO-mediated ubiquitination and degradation of β_2AR in HEK293 cells. The same study showed that siRNA against the other ligase Mdm2 has a prolonged effect on β_2AR internalization. Cells transfected with Mdm2 siRNA had a slower rate of receptor internalization but with a minor effect on the slower process of receptor degradation compared to the non-transfected one (Sudha K. Shenoy et al., 2007).

1.3.6 Post-Translational Modification (PTMs) of the β_2AR

A post-translational modification (PTM) is a modification of a protein as a result of the covalent attachment of functional group or small proteins. PTMs have been confirmed as playing a vital role in the function of the β_2AR. For example, phosphorylation by PKA can initiate a switch from Gs to inhibitory Gi, signalling whereas phosphorylation by GRK is the trigger to recruit β-arrestin binding and ubiquitination of the receptor that is vital for receptor down-regulation (Shenoy et al., 2006). All of these steps are essential for receptor desensitization. There are also other PTMs of β_2AR that play important roles in cell signalling regulation. The β_2AR has been confirmed to undergo both N-and O- linked glycosylation, a PTM in which a carbohydrate group is attached to a hydroxyl or another functional group on a protein (Rands, et al., 1990)(Benya et al., 2000) (Sadeghi & Birnbaumer, 1999). β_2AR has also been shown to be palmitoylated, which is the addition of a fatty acid such as palmitic acid, at cysteine 341 (Ovchinnikov et al., 1988). When this cysteine residue is mutated to serine, attenuation of the ability of the β_2AR to stimulate adenylyl cyclase (AC) in an agonist-dependent manner is observed, which suggests that palmitoylation at this site may be required for adequate Gs-β_2AR coupling.

Post translational modification has been regarded as one of the mechanisms, which can compensate for the loss of functionality during heart failure. Proteins could be modified at any point of their life cycle, ranging from directly after ribosomal translation until the proteins are relocated to a specific cellular compartment or tissue. PTM control of heart rate is probably the best example of the importance of this process. β_2AR activation by catecholamines promotes phosphorylation of both troponin I and phospholamban. Troponin I phosphorylation causes desensitization of troponin I to Ca^{2+} ions (Bodor et al., 1997), and phospholamban phosphorylation reduces the inhibitory action of phospholamban on SERCA2a (MacLennan and Kranias, 2003). The combination of these actions improves cardiac relaxation, therefore, lead to related to heart failure. Thus, catecholamine levels are increased in heart failure to promote optimal function

(Kaumann et al., 1999). Other more recent discoveries include post translational modifications such as ubiquitin (Pagan et al., 2013), ISG15 (Voigt & Antje, 2014), and SUMOylation (Kho et al., 2011), which also appear to play an important regulatory role in cardiac function.

1.4 SUMOylation

A large number of proteins are modified post-translationally by the ubiquitin-like protein SUMO (small ubiquitin-like modifier) which is covalently attached to substrate proteins on lysine residues following activation of specific enzyme cascades known as SUMOylation (Watts, 2013)(Kho et al., 2015)(Geiss-Friedlander & Melchior, 2007).

1.4.1 The SUMO Paralogues

SUMO proteins are about 10kDa in size and similar to the three-dimensional structure of ubiquitin (Geiss-Friedlander & Melchior, 2007). SUMO proteins are widely expressed in the eukaryotic kingdom. The human genome of SUMO encodes four SUMO subtypes: SUMO-1, SUMO-2, SUMO-3, and SUMO-4. Apart from SUMO-4, the SUMO 1-3 proteins are ubiquitously expressed, and SUMO-2 and SUMO-3 are 97% identical, but only share 50% sequence identity with SUMO-1 (Watts, 2013). SUMO-4 is mainly expressed in kidney, lymph node and spleen (Liberati et al., 2018). SUMO-1 and SUMO-2/3 have distinct functions as they are conjugated to different target proteins. SUMO-4 shares about 86% identity with SUMO-2 and SUMO-3, but the role of SUMO-4 remains unclear. It is not known whether this isoform can be processed to its mature conjugation-competent form in vivo (Geiss-Friedlander & Melchior, 2007).

1.4.2 The SUMOylation Cascade

SUMOylation is a vital process in most organisms (Geiss-Friedlander & Melchior, 2007). Similar to ubiquitylation, SUMOylation is a reversible process that starts with the formation of an isopeptide bond between the C-terminal Gly residue of the modifier protein and the ε-amino group of a Lys residue on the surface of the

substrate protein (Watts, 2013). An enzymatic cascade is involved in both ubiquitylation and SUMOylation. The outline of the reversible SUMOylation cascade is presented in **Figure 1.12** (Wilkinson & Henley, 2010). The immature SUMO protein was first activated by the SUMO-specific E1 activating enzyme heterodimer AOS1-UBA2. A thioester bond between the active-site cysteine residue of SUMO-activating enzyme subunit 2 (SAE2) and the C-terminal glycine residue of SUMO is formed in this step. This activation step requires ATP. Following this, SUMO is transferred to the active site cysteine of the SUMO E2 enzyme ubiquitin-conjugating 9 (UBC9) forming a thioester linkage between the catalytic Cys residue of UBC9 and C-terminal carboxy group of SUMO protein (Wilkinson & Henley, 2010). UBC9 is the only discovered SUMO-conjugating enzyme at present. UBC9 directly binds to the consensus SUMOylation motif on substrate protein. Finally, SUMO protein is transferred to substrate protein by UBC9 (Mendler et al., 2016a). In this step, an isopeptide bond is formed between the C-terminal Gly residue of SUMO and a Lys side chain of the substrate protein. E3 ligases facilitate the ligation step of SUMOylation, which helps catalyse the transfer of SUMO from UBC9 to a substrate protein (Gareau & Lima, 2010). This lysine is part of a SUMO conjugation motif – ψKxE/D (where γ is a large hydrophobic residue, K is the lysine SUMO acceptor and x is any residue (Li et al., 2010)(Hay, 2005).

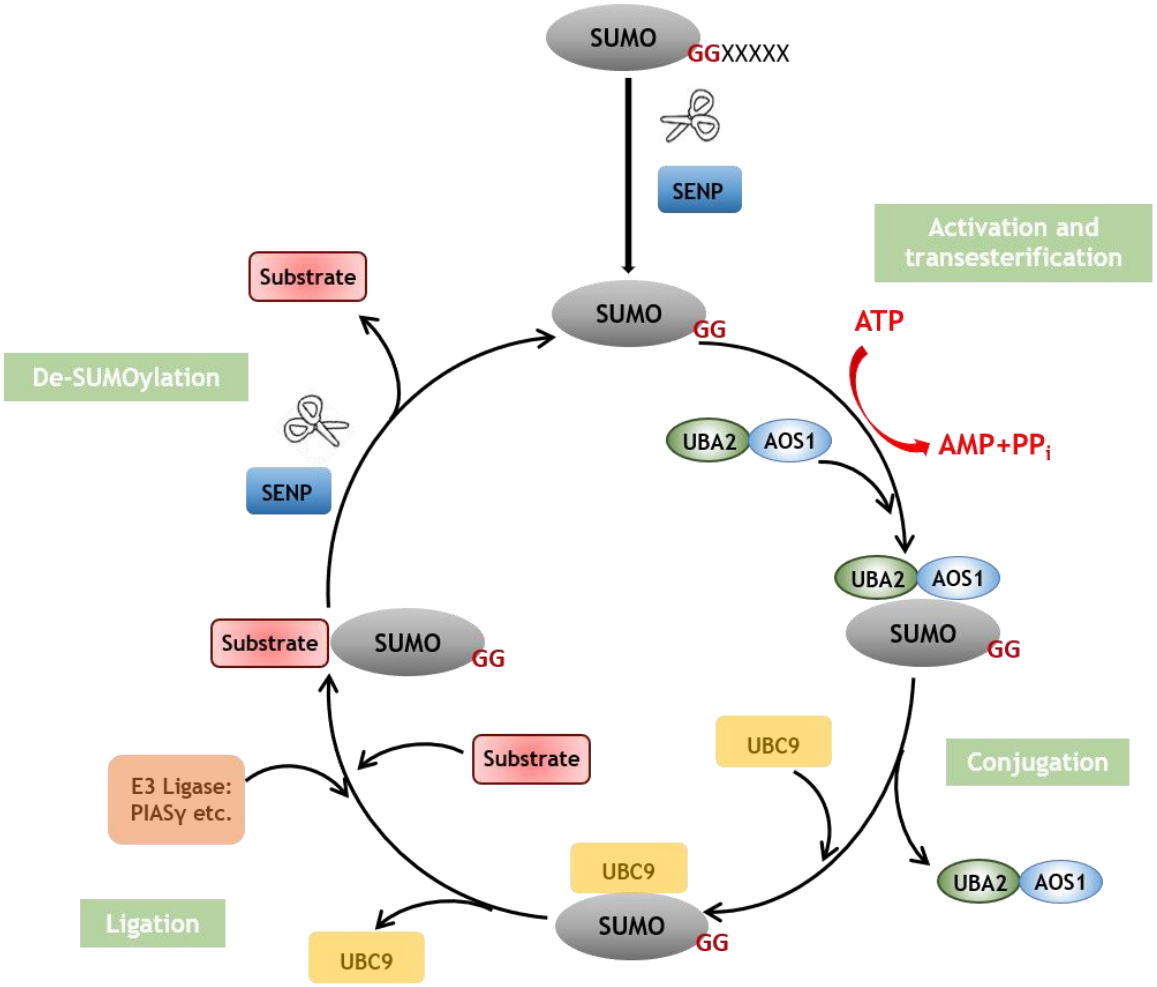

Figure 1.12 The mechanism of reversible SUMOylation cascade. Nascent SUMO (small ubiquitin-related modifier) reveals its C-terminal Gly-Gly motif accomplished by SUMO-specific isopeptide (sentrin-specific proteases; SENPs), which remove 4 C-terminal amino acids from SUMO. Mature SUMO is activated by the E1 heterodimer AOS1-UBA2 with the ATP support, which leads to a thioester bond between the C-terminal Gly residue and C173 in UBA2. Then SUMO is transferred to the catalytic Cys residue of the E2 enzyme UBC9. At last, an isopeptide bond is formed between the C-terminal Gly residue of SUMO and a Lys residue in the substrate SUMO, small ubiquitin-like modifier. UBC9, ubiquitin-conjugating 9.

1.4.3 The SUMO Consensus Motif

Most SUMO-modified proteins contain an acceptor Lys within a ψKXE motif. These consensus motifs play a vital role in stabilizing the interactions between the E2 enzyme and the substrate proteins since it directly interacts with the SUMO E2 enzyme UBC9 (Sampson et al., 2001). Substrate recognition is helped by the electrostatic interaction and the hydrogen bonds between E2 and the residues close to the lysine of this motif (Shetty et al., 2020).

1.4.4 The Role of SUMOylation

Since SUMO was first found and studied in the 1990s, SUMOylation has attracted much attention as it is involved in various cellular events and the regulation of a range cellular processes. At the protein level, SUMOylation can influence protein stability, cellular location, enzyme activity and ability to form protein-protein interactions (Hay, 2005). In the cardiac setting, it has been shown that SUMOylation is involved in heart development, cardiac function, and disease progression.

1.4.4.1 SUMOylation in Cancer and Parkinson Diseases Progresses

As SUMOylation is a ubiquitous process in many cell types and tissues, aberrant SUMOylation can lead to many diseases. For example, Dong et al. found that SUMOylation deficiency of ß-arrestin-2 resulted in slower migration of breast cancer cells (Dong et al., 2020). The data indicated that SUMOylation of ß-arrestin-2 might be a regulatory point for breast tumour treatment.

The PTMs phosphorylation, SUMOylation and ubiquitination have also been shown to affect proteins that influence Parkinson's disease. α-Synuclein (α-Syn) is a key protein in Parkinson's disease pathogenesis in familial and sporadic forms. SUMOylation has been shown to play a role in α-Syn's aggregation, exocytosis, and degradation. Specifically, SUMOylation can inhibit α-Syn aggregation (Junqueira

et al., 2019) following SUMOylation at Lys-102. DJ-1 is another Parkinson's disease related protein that can be SUMOylated to reduce its degradation and contribute to the elimination of reactive oxidative species. Finally, Dynamin related protein (Drp1), another protein implicated in Parkinson's disease progression can be modified by SUMO-1 to enhances its mitochondrial recruitment and promote fragmentation of mitochondria and cellular apoptosis. Conversely, SUMO-2/3 modification can lower mitochondrial localization of Drp1 and prevent cell death (Junqueira et al., 2019).

1.4.4.2 SUMOylation in Cardiovascular System

SUMOylation is one of the key PTMs that can also regulate cardiac proteasome function and change cardiac protein homeostasis. In recent times, there has been much research focusing on the role of SUMOylation in different cardiovascular diseases.

1.4.4.2.1 SUMOylation in Myocardial Ischemia and Reperfusion (MI/R) Injury

SERCA2a SUMOylation is also known to result in reduced MI/R injury and this process can be regulated by luteolin (Chen et al., 2019). Histone deacetylase (HDAC) induces deacetylation, chromatin condensation and transcriptional suppression (Chen et al., 2019). One of the isoforms of HDAC, HDAC4, is degraded following SUMOylation to reduce the generation of reactive oxygen species (ROS). HDAC4 SUMOylation plays a vital role in protecting the myocardium during hypoxia/reoxygenation (H/R) injury (Granger et al., 2008). Apoptosis is a basic but also an important mechanism in cell death during MI/R injury. Eukaryotic elongation factor 2 (eEF2) is one of the proteins that is involved in polypeptide chain elongation in protein translation (Chen et al., 2019). Also, eEF2 is one of the substate proteins for SUMOylation. Research has shown that phosphorylation of eEF2 increased eEF2 proteolytic cleavage and translocation to the nucleus via a SUMOylation-dependent process (Q. Yao et al., 2014). Phosphorylated eEF2 that

was SUMOylated induced cardiomyocyte apoptosis (Q. Yao et al., 2014). These data confirm a role for SUMOylation in human MI/R injury mechanisms.

1.4.4.2.2 SUMOylation in Heart Failure

Kho et al. first discovered that increased levels of SUMO-1 was protective against heart failure in mouse and that this was related to the SUMOylation of SERCA2a. They found that SUMO-1 adeno-associated virus-mediated gene transfer helped to improve heart function in heart failure mouse models as this action maintained the quantity of SERCA2a proteins in the heart (Kho et al., 2011) (Kho et al., 2015a). SUMOylation of SERCA improved its stability even in a disease context and this helped resist deleterious functions associated with HF. This concept has also been confirmed in a large swine model of heart failure (Tilemann et al., 2013). The group also discovered that SUMO-1 overexpression in isolated cardiomyocytes increased the contractility and accelerated Ca^{2+} decay (Tilemann et al., 2013).

The calpain-calpastatin pathway is an apoptotic pathway and proteins that are involved in it were found to be associated with SUMO-2. In contradiction to the protective action of SUMO described above, studies have shown that mice which overexpress SUMO-2 developed cardiomyopathy symptoms. The conjugation between SUMO-2 and the calpain small subunit2 (Capns2) inhibitor calpastatin (CAST) results in a reduced inhibition therefore an increase in the enzymatic activity of Capns2. This SUMOylation event has been proved to be detrimental in cardiomyopathy and subsequent heart failure (E. Y. Kim et al., 2015).

1.4.4.2.3 SUMOylation of Sarcoplasmic Reticulum Ca^{2+} ATPase 2a (SERCA2a)

As it mentioned above, several studies have shown that protein SUMOylation is associated with critical cellular pathways, many of which ultimately affect cardiac function and development, which suggests that SUMOylation could be regarded as a promising target for the treatment of cardiovascular diseases. Kho. et al discovered that SERCA2a gets modified by SUMO-1 and that SUMOylation of

SERCA2a is reduced in animal models of heart failure in comparison to normal hearts. The group also showed SUMOylation is a critical post-translational modification that regulates SERCA2a function and also represents an avenue for the design of novel therapeutic strategies for heart failure. Additionally, SUMO-1 levels are also shown to be reduced during disease. Interestingly, Hajjar and colleagues managed to prove that restoring SUMO-1 expression by gene transfer increased SUMO-1 in the myocardium of heart failure and subsequently increased left-ventricular function. There are several possible reasons for the positive effects: one of these could be that the overexpression of SUMO-1 causes an increase in SUMOylation of the transcription factor SP1, which plays an essential role in regulation of SERCA2a in both healthy and diseased hearts. As a result, SUMOylation has been thought to cause increased transcription of SERCA2a (Kho et al., 2011).More recently, Hajjar et al identified and characterized a small molecule named N106, which increases SUMOylation of SERCA2a by directly activating the SUMO-activating enzyme (E1 ligase) and trigger intrinsic SUMOylation of SERCA2a (Kho et al., 2015a).

Since there are more than 1000 SUMO substrates in nature (Hay, 2013), it is possible that SERCA2a may not be the only cardiac protein that could be SUMOylated. The Baillie group has used peptide array technology to identify putative SUMOylation sites on cardiac signalling proteins by in vitro SUMOylation of immobilised 15 mer peptide array libraries (Frank, 2002) which contained potential SUMO conjugation motifs found on proteins such as troponin I, Myosin binding protein C, L-type calcium channel and the β_2AR.

1.4.4.2.4 Other SUMOylation Susceptible Cardiac Proteins

There are more than 1000 proteins known as SUMO substrate in the nature (Hay, 2013). Therefore, SERCA2a may not be the only cardiac protein that can be SUMOylated. Sp2.0 SUMOylation site identification software (GPS-SUMO, Guangzhou, China) was used by Baillie group (unpublished data) to identify putative SUMOylation sites on β_2AR, RyR, LTCC, cTNI and myosin binding protein C. The software examined lysines residues and the surrounding amino acids to identify the possible SUMOylation motifs on the cardiac proteins. To validate the

results from sp2.0, peptide arrays with 15 mer peptides which contains the possible SUMOylation sites that in the results were designed and then the arrays were SUMOylated using an *in vitro* assay (described in Chapter 2-General Materials and Methods) (

Figure 1.13). The peptide arrays confirmed that there is more than one possible cardiac protein that can be SUMOylation substrate. From the arrays, the following cardiac proteins are tested as potential SUMOylation substrates: RyR (positions 833,841,1572,3413,4385,4265,4601), β_2AR (positions 60,227 and 235), LTCC (position 1621), myosin binding protein C (position 543 and 1816), and cTNI (position 177 and 178) (**Figure 1.13**).

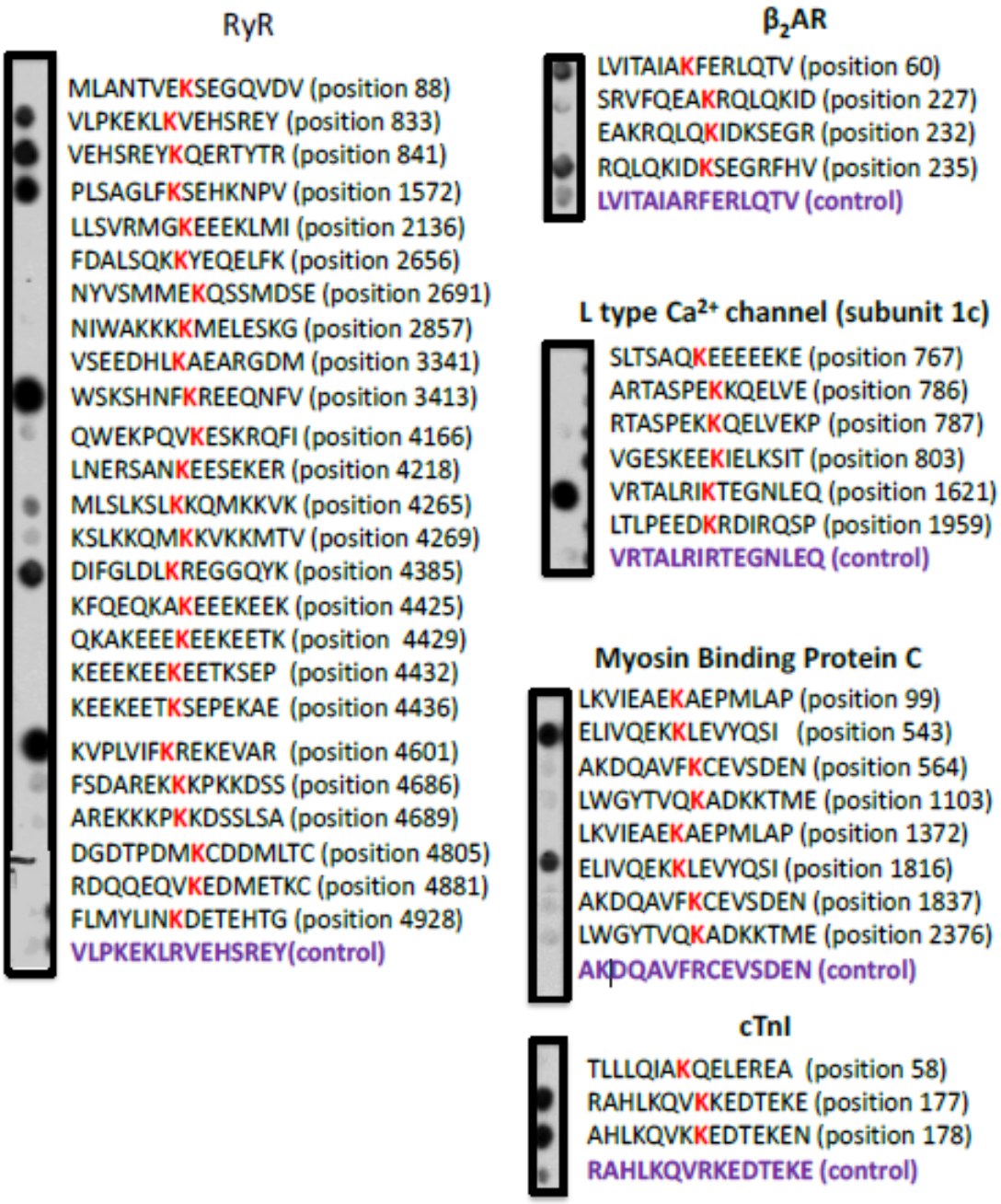

Figure 1.13 SUMOylation sites of cardiac protein confirmation via peptide array. Baillie group used sequence analysis to identify putative SUMOylation sites on the RyR, LTCC, cTNI, β_2AR and myosin binding protein C. To validate the analysis results, 15 mer peptide arrays which contained potential SUMOylation binding motifs were synthesized (Frank, 2002). The arrays were SUMOylated by an *in vitro* assay (described in **Chapter 2. General Materials and Methods**). RyR, ryanodine receptor, LTCC, L-type Ca^{2+} channel, cTNI, cardiac troponin I, β_2AR, beta 2 adrenergic receptor. Amino acid abbreviations in appendix.

Following the finding of the potential lysine residues on β_2AR (position 60,227 and 235), the conservation of the lysine residues on these positions' cross different species were studied using UniProt Sequence Analysis (www.uniprot.org). These identified sites (60, 227 and 235) were examined in the following species: human, rat, mouse, bovine, dog, cat, guinea pig, rhesus monkey, golden hamster, and pig. Most of these potential lysine residues are highly conserved except dog and cat at position 60; dog, cat and pig at position 227; dog and guinea pig at position 235. There are few possible reasons for highly conservation in these potential key residues for SUMOylation: 1). Position 227 and 235 are located in the third intracellular loop of the receptor where most of the PTM binding sites located (Hilger, 2021). The sequence of the key amino acids residues are often highly conserved along different animal species. 2). It could relate to the exon high conservation in the GPCR protein sequences. There are evidence showing the exon that encodes a 14 amino acid sequence that forms the distal part of 7th transmembrane helix, which are highly conserved among most secretin GPCRs (Markovic & Grammatopoulos, 2009).

Position 60

Human	NVLVITAIAKFERLQTVTNY
Rat	NVLVITAIAKFERLQTVTNY
Mouse	NVLVITAIAKFERLQTVTNY
Bovine	NVLVITAIAKFERLQTVTNY
Dog	NVLVITAIARFERLQTVTNY
Cat	NVLVITAIARFERLQTVTNY
Guinea pig	NVLVITAIAKFERLQTVTNY
Rhesus monkey	NVLVITAIAKFERLQTVTNY
Golden hamster	NVLVITAIAKFERLQTVTNY
Pig	NVLVITAIAKFERLQTVTNY

Position 235

Human	RVFQEAKRQLQKIDKSEGRF
Rat	RVFQVAKRQLQKIDKSEGRF
Mouse	RVFQVAKRQLQKIDKSEGRF
Bovine	RVFQVAKRQLQKIDKSEGRF
Dog	RVFQVAQRQLQKIDRSEGRF
Cat	RVFQVAQRQLQKIDKSEGRF
Guinea pig	RVFQVAKKQLQKIDRSEGRF
Rhesus monkey	RVFQEAKRQLQKIDKSEGRF
Golden hamster	RVFQVAKRQLQKIDKSEGRF
Pig	RVFQVARRQLQKIDKSEGRF

Position 227

Human	PLVIMVFVYS RVFQEAKRQL QKIDKSEGRF
Rat	PLVVMVFVYSRVFQVAKRQLQKIDKSEGRF
Mouse	PLVVMVFVYSRVFQVAKRQLQKIDKSEGRF
Bovine	PLVVMVFVYSRVFQVAKRQLQKIDKSEGRF
Dog	PLVVMVFVYSRVFQVAQRQLQKIDRSEGRF
Cat	PLVVMVFVYSRVFQVAQRQLQKIDKSEGRF
Guinea pig	PLVVMVFVYSRVFQVAKKQLQKIDRSEGRF
Rhesus monkey	PLVIMVFVYSRVFQEAKRQLQKIDKSEGRF
Golden hamster	PLVVMVFVYSRVFQVAKRQLQKIDKSEGRF
Pig	PLVVMVFVYSRVFQVARRQLQKIDKSEGRF

Figure 1.14 Conservation of SUMOylation of β_2AR potential sites among different species. Potential β_2AR SUMOylation sites lysine 60, 227 and 235 conservations throughout different animal species. Amino acid abbreviations in appendix.

1.5 Aims and Hypothesis

1.5.1 Hypothesis

I hypothesize that SUMOylation of β_2AR at lysine 235 in the human β_2AR is a critical regulatory mechanism of heart failure that will be upregulated in the heart failure cardiomyocytes.

1.5.2 Aims

My general aim is to determine the functional relevance of SUMOylation on the β_2AR, at site lysine 235 which is based on human β_2AR sequence. Previous work using techniques such as invitro SUMOylation of peptide array has confirmed the possibility that the β_2AR may be SUMOylated within a regular SUMO consensus motif. Also, a SUMO-site specific antibody was designed and produced to recognize only the SUMOylated form of the β_2AR in both cell and tissue lysate. To test my hypothesis, I plan to examine the SUMOylation of the β_2AR in a number of experimental contexts including human embryonic kidney (HEK) cells, primary cultures of cardiac myocytes and tissues from small rodent models of heart failure. Specifically, my aims are as follows:

1. To demonstrate whether the β_2 adrenergic receptor is a substrate for SUMOylation under *in vitro* conditions.
2. To produce wild type β_2AR and SUMO mutant K232R-K235R β_2AR adenovirus and assess virus purity and function via determination of plaque forming units (PFU)/ml, total viral particle (vp)/ml.
3. To compare adrenergic signalling in primary cardiac myocytes infected with wild type β_2AR and SUMO mutant K232R-K235R β_2AR adenovirus.
4. To determine the influence of SUMOylation of the β_2AR on cardiomyocyte contractility using CellOPTIQ® technology.
5. To assess changes in SUMOylation of in heart tissue derived from human heart failure patient and healthy heart donor.

Chapter2. General Materials and Methods

2.1 General Laboratory Practice and Materials

All laboratory chemicals were supplied by Sigma-Aldrich (Dorset, UK) unless otherwise stated. Any hazardous reagents were handled and disposed of according to relevant Control of Substances Hazardous to Health regulations. Personal protective equipment including laboratory coats and gloves were worn during all procedures.

Glassware was washed using Decon 75 detergent (Decon Laboratories Ltd, East Sussex, UK), rinsed with distilled water and then dried at 37℃ prior to use. The water used in all experiments was purified by a water purification system with automatic sanitization module (Millipore, France). Sterile disposable plastic containers and dispensers were used including microcentrifuge tubes (Grenier Bio-one, Stonehouse, UK), universals (Corning, Birmingham, UK) stripettes (Corning, Birmingham, UK) and pipette tips (Rainin, California, USA). To sterilize, all required reagents, laboratory items and liquids were autoclaved in a Prestige Medical autoclave (Prestige Medical, Blackburn, UK). To prepare buffers, solutions and media, all solid chemicals were weighed out using a Mettler Toledo balance (sensitive to 0.01g) (Mettler Toledo, Ohio, USA), or a Sartorius CP124S balance (sensitive to 0.0001g) (Sartorius, Bradford, UK). Solutions were prepared using distilled water unless otherwise stated. The pH of these solutions was measured using a Mettler Toledo Seven Easy digital pH meter (Mettler Toledo, Ohio, USA) and adjusted using concentrated HCl or NaOH. Volumes were dispensed using a Gilson battery powered pipetting aid (1-25ml) and Gilson pipettes (0.5-1000µl; Gilson Medical Instruments, Staffordshire, UK). Centrifugation was carried out in either a temperature-controlled Sigma-Aldrich 1-14k rpm tabletop microcentrifuge (Sigma-Aldrich, Dorset, UK), a ThermoFisher Scientific Cl31 multispeed centrifuge (ThermoFisher Scientific, Paisley, UK), or a Beckman Coulter Optima L-80 XP ultracentrifuge (Beckman Coulter, High Wycombe, UK) depending on the sample volumes, the size of sample containers and speed requirements. Temperature sensitive incubations were completed using a Grant OLS200 water bath (Grant Instruments, Cambridge shire, UK) or a Techne Dir-Block DB2A heat block (Teche, Stafford shire, UK).

2.2 Mammalian Cell Culture

All cell culture procedures were undertaken in Class II flow hoods (ThermoFisher Scientific, Paisley, UK). Standard aseptic techniques were used, and all solutions and instruments were autoclaved and kept in sterile conditions. Media and reagents were purchased from Gibco (ThermoFisher Scientific, Paisley, UK) unless stated otherwise. The tissue culture flasks, plates, dishes, and other consumables were supplied from Corning (Sigma Aldrich, Dorset, UK). All cultured cells were regularly checked under a phase contrast inverted microscope (Leitz Diavert, Berlin, Germany).

2.2.1 HEK293 Cells

HEK293 cells were originally derived from human embryonic kidneys (HEK). HEK293 cells were widely used because of their reliable fast growth and propensity for transfection. HEK293 cells were cultured in growth medium containing Dulbecco's Modified Eagle's Medium (DMEM) supplemented with 10% fetal bovine serum (FBS), 1% L-glutamine (LG) and 1% penicillin/streptomycin (P/S), remained in incubators with humidified air at 37℃ and 5% CO_2.

2.2.2 HEKβ_2Cells

HEKβ_2 cells are a stable HEK293 cell line which overexpresses the GFP/Flag tagged form of the β_2AR (McLean & Milligan, 2000). Cells were cultured in growth medium consisting of Dulbecco's Modified Eagle's Medium (DMEM) supplemented with 10% New-born Calf Serum (NCS), 1% penicillin/streptomycin (P/S), 1% L-glutamine (LG) and minimum essential medium (MEM) at 37 ºC in humidified air with CO_2. HEKβ_2 cells contain an extra component of geneticin G418 in the growth medium at 1mg/ml. This antibiotic prevents growth of HEK293 cells, which do not express the GFP/Flag-tagged β_2AR. Cells were passaged at approximately 85-90% confluency.

2.2.3 Neonatal Rat Ventricular Myocytes

Neonatal rat ventricular myocytes (NRVM) are a widely used model to study cardiac biochemical mechanisms because of the similarities to adult ventricular myocytes and ease to isolation and culture (Golden et al., 2012).

2.2.3.1 Isolation of Neonatal Rat Ventricular Myocytes

Hearts were removed from 1-2-day old Sprague-Dawley rats following sacrifice by anaesthesia overdose via intraperitoneal injection of Euthatal. Animals were maintained in accordance with the UK animals (Scientific Procedures) Act of 1986. The hearts were placed into a 10cm petri dish containing ice-cold ADS buffer (120 mM NaCl, 20 mM HEPES, 1 mM Na_2PO_4, 5 mM glucose, 5.4 mM KCl, 1.8 mM $MgSO_4$, pH 7.4) and dissected to remove remaining atrial and aortic tissue. Then the hearts were squeezed gently with forceps to remove the residual blood in the ventricles and transferred into a new 10cm dish with fresh ice-cold ADS buffer. Then the hearts were cut into $1mm^3$ pieces and placed into 50ml falcon tube. The minced hearts were left to settle down at the bottom of the tube and the ADS buffer was removed. Collagenase buffer (0.06% (w/v) pancreatin, 0.03% (w/v) collagenase) was used for serial enzymatic digestions. The collagenase buffer was added and then incubated at 37 ^oC in a shaking water bath. The first digestion was to remove pericardial collagen. The supernatant was removed and 4.5ml fresh collagenase buffer was added and incubated for 20 minutes. After the digestion, the tissues were allowed to settle, and supernatant was transferred to a 15 ml Falcon tube containing 0.5 ml neonatal calf serum (NCS) to end the digestion. The complex was centrifuged at 1250rpm for 5 minutes and pellets were resuspended in 2 ml NCS and incubated at 37 ^oC until all the digestions were completed. The digestions were repeated for 5 times. After the last digestion, cells were collected and centrifuged as before and resuspended in 10 ml of Day 1 Medium (M1) (4:1 ration of DMEM/Medium 199 (M199) supplemented with 10% horse serum (HS), 5% NCS, 1% L-glutamine and 1% penicillin/streptomycin). At this stage, the cells are mainly fibroblasts and NRVM. To remove the fibroblasts, a pre-plating step was required. 10 ml of cells were plated in a 10 cm dishes and incubated at 37 ^oC for

2 hours. During the pre-plating, the fibroblasts were stuck down to the surface of the dish and NRVM remained in the medium. The NRVM were collected with the medium in a new 50ml Falcon tube, an extra 5 ml of M1 medium was used to wash the dish and the wash was added into the tube. The cells were centrifuged as before, and the pellet was resuspended in 10 ml of M1. After the cells were counted on a standard hemocytometer, the cells were seeded in coated 6/12 well plates at requiring cell density. For biochemical experiments, plates were coated with 1% (w/v) bovine gelatin (Sigma), and cells were seeded at $8x10^6$ cells per well. For microscopical analysis, coverslips were sterilized in 70% ethanol, and air dried before coating $1\mu g/cm^2$ mouse laminin (Corning). Cells were seeded at $4x10^6$ cells per well. Cells were incubated in humidified incubator with 5% CO_2 at 37 ºC.

2.2.3.2 Maintenance of Neonatal Rat Ventricular Myocytes

After 24 hours of culture in M1, the medium was replaced with Day 2 Medium (1:4 ratio of DMEM/M199 supplemented with 5% HS, 0.5%NCS, 1% L-glutamine and 1% penicillin/streptomycin).

2.2.4 Adult Rabbit Ventricular Myocytes

Adult rabbit cardiac myocytes were isolated by Aileen Rankin (Professor Godfrey Smith's group). Animals were maintained in accordance with the UK animals (Scientific Procedures) Act of 1986. New Zealand White rabbits (2–2.5 kg) were sacrificed by intravenous injection of 500U heparin together with an overdose of sodium pentobarbitone (100 mg kg^{-1}). The heart was removed, cannulated onto a Langendorff perfusion column via the aorta. Then heart was perfused retrogradely at a perfusion rate of 25 ml min−1 at 37 ºC, initially with Krebs-Henseliet solution for 3 minutes, and then with a calcium-free Krebs-Henseliet solution (Sigma Aldrich, K3753) containing 0.1 mM EGTA (ethylene glycol-bis(ß-aminoethyl ether)-N,N,N′,N′-tetra acetic acid) chelating agent for a further 4 min. Hearts were then perfused with Krebs-Henseliet solution supplemented with 0.75 mg ml−1 collagenase (type 1, Worthington Chemical), 0.05 mg ml^{-1} protease (type XIV,

Sigma Aldrich) and 140 μM $CaCl_2$ for 12 minutes. These enzymes aided the digestion of the heart with proteases breaking the peptide bonds in proteins and collagenase breaking peptide bonds in collagen. The ventricle was perfused for approximately 12 minutes before being removed and placed in a culture flask with 10mls of a high potassium KB solution (70 mM KO, 40mM KCl, 50mM glutamic acid, 20mM taurine, 20mM KH_2PO_4, 3mM $MgCl_2$, 10mM glucose, 1mM EGTA, 10mM HEPES to pH 7.4) containing 0.1g BSA. Flasks were shaken for 15 minutes with regular checking under the microscope for the presence of cells. Cells were filtered and centrifuged for 1min at 5g, and the supernatant was replaced with 10ml of KB and centrifuged fora second time replacing the supernatant with KB once more. After 30 minutes, the KB was replaced with Krebs-Henseliet solution containing 100μM $CaCl_2$ solution and the cells were allowed to settle. The supernatant removed and a solution Krebs solution containing 200μM $CaCl_2$ was added. A further 2 repeats of settling cells and removing supernatant were undertaken before replacing the supernatant with Krebs containing 500μM and 1mM $CaCl_2$, after which, the cells were ready for use.

2.2.5 Cell Subculture

When the cells reached approximately 85-90% confluency, they were passaged. To passage the cells, growth media was removed, and the cells were washed with sterile phosphate buffered (PBS) to remove the remaining media. The PBS was then removed, and the cells were detached with 5ml trypsin-EDTA solution per 150cm^2 culture flasks of cells incubated at 37 ^oC for 5 minutes. Fresh growth media was added to neutralize the trypsin-EDTA solution with the ratio of trypsin-EDTA: Fresh growth media being 1 in 3. Then the complex was transferred to a new falcon tube and subject to centrifugation at 7,000rpm for 4 minutes at room temperature to separate the cell pellet and media. The supernatant was subsequently removed, and cell pellet was resuspended in fresh growth media and re-plated in new flasks in different ratio according to the requirement.

2.2.6 Cell Counting

Cells were counted using a Bright Line Hemocytometer (Sigma-Aldrich, Dorset, UK). 10µl of a cell suspension was added under a cover slip onto the hemocytometer grid. Using a light microscope, the number of viable cells in each 1mm corner square was counted and averaged. Only cells crossing the top or left-hand edge of any square were counted. The average number of cells in each 1mm square was derived and multiplied by 10^4 to get the number of cells per ml in the suspension. The subsequent concentration of cells per ml could be calculated using the following equation:

Cell number/ml = Average cell count per square x 10^4 x original volume

The calculated cell concentration (cells/ml) was used for seeding cells at the required density.

2.2.7 Cryopreservation

To cryopreserve the cells, the cell pellet was prepared in the same manner as when it was sub cultured. The pellet was then resuspended in 7.5% dimethyl sulfoxide (DMSO) and 20% FBS in growth medium. DMSO is a cryoprotectant which protects the cells from damage during the freezing procedure. The cell and media complex were aliquoted into cryovials, small tubes designed for cryopreservation, then set into a freezing container filled with 100% isopropanol and placed into -80 freezer for 24 hours. This process allowed cells to freeze slowly. After 24 hours, the frozen cells were transferred to liquid nitrogen tanks for long term storage.

2.3 Isolation of Plasmid DNA and Transient Transfection

Transient transfection is a method that introduces foreign genes to increase cell expression of a particular protein. Transient transfection will not incorporate the foreign gene into a cell's genome permanently. The transfected cells expressed the transfected gene for several days, but after that the foreign gene is lost in cell division. To confirm that the transfection has been successfully expressed in

the cell, normally a reporter gene is included in the transfection plasmids, reporter genes indicate the presence of the gene of interest within the cells. Transient transfection could be assisted by the use of chemical reagents, one of those have been used in this thesis is Lipofectamine LTX (ThermoFisher Scientific, Paisley, UK). Lipofectamine LTX is a liposome transfection reagent based on lipofection method. Negatively charged DNA of the gene of interest is trapped in a cationic lipid vacuole, and the liposome is formed by the reagent. The formed liposome containing the gene of interest fuses with the target cell membrane and then release the intertest of genome into the cell (Sandbichler, Aschberger and Pelster, 2013)

Cells transfected with wild type β_2AR YFP-tagged, K232-235 SUMO site null β_2AR YFP-tagged and PIASγ HA-tagged DNA were used in this thesis. Wild type β_2AR YFP-tagged and K232-235 SUMO site null β_2AR YFP-tagged DNA were transiently transfected in HEK293 cells to study the mechanistic function of SUMOylation on β_2AR. Specifically, I was interested in how the β_2AR signalling pathway is affected when the β_2AR is modified by SUMO. HA-tagged SUMO DNA was used to promote SUMOylation of the β_2AR when the experimental design required it. Negative controls used here were a set of cells that were transfected with empty transfection reagent and called “mock” transfected cells.

2.3.1 Isolation of Plasmid DNA From *E. coli*

Yellow fluorescent protein (YFP) is a genetic mutant form of green fluorescent protein (GFP), originally derived from the jellyfish *Aequorea Victoria*. YFP’s excitation peak is 514nm and its emission peak is 527nm (Nagai *et al.*, 2002), so the transfection efficacy can be checked via fluorescence microscopy or immunoblotting for the YFP tag. The hemagglutinin (HA) tag is derived from the human influenza virus HA protein (ThermoFisher Scientific, 2017). The HA tag can also be used to determine transfection success by immunoblotting.

A scraping of *E.coli* bacterial glycerol stock that expresses the plasmid vector containing the gene of interest was taken using a sterile pipette and inserted into a sterile falcon tube with 10ml of sterile lysogeny broth (LB) buffer (1% (w/v)

bacto-tryptone, 0.5% (w/v) bacto-yeasst extract and 170 mM NaCl containing appropriate antibiotic at 37 °C for 3 hours with shaking before the overnight incubation. Next, the resulting bacterial culture was transferred to 2L flasks, filled with 500ml LB buffer containing 100µg/ml appropriate antibiotic and further incubated at 37 °C overnight in an orbital shaker (Cole Parmer, London, UK). The antibiotic for wild type β_2AR YFP-tagged, K232-235 SUMO site null β_2AR YFP-tagged plasmid DNA was kanamycin 100µg/ml and the antibiotic for PIASγ HA was ampicillin 500µg/ml. The resistance gene for the correct antibiotic is encoded within the plasmid vector to ensure that only bacterial cells exogenously expressing the protein of interest grow.

The overnight bacterial culture mixture was transferred into plastic centrifugation vessels and spun down at 6000rpm using a Beckman Coulter Optima L-80 XP ultracentrifuge (Beckman Coulter, High Wycombe, UK) at 4 °C. Supernatant was discarded and the pellet was used to isolate and purify the plasmid DNA using the Invitrogen PureLink™ HiPure Plasmid Maxiprep Kit (ThermoFisher Scientific, Paisley, UK). The procedure was performed followed manufacturer's instructions. The purified DNA was eluted with filter sterilized TE buffer which can help to stabilize the structure of plasmid DNA. The resulting DNA preparations were maintained at -20 °C for long term storage.

2.3.2 Storage of Plasmid DNA as Glycerol Stocks

To store the plasmid DNA, 900µl of overnight cell culture of bacteria containing the plasmid of interest was mixed with 900µl of 40% glycerol solution, to reach a final glycerol concentration of 20%. The glycerol was sterilized by autoclaving prior to use. The glycerol stock was snap frozen using dry ice and stored at -80 °C. Glycerol stocks were always kept on dry ice when removed from the -80 °C freezer.

2.3.3 Quantification of DNA Concentration

The concentration and purity of purified DNA was determined using a Nanodrop 200 spectrophotometer (ThermoFisher Scientific, Paisley, UK). Absorbance at

260nm was used to measure the concentration and the A_{260}/A_{280} ratio was used for assessment of purity.

2.3.4 Transient Transfection of Plasmid DNA

The HEK293 cells were seeded on the appropriate size of plates or dishes depends on the specific experiment 16 hours before transient transfection. The cell confluency was 60-80% on the day of transfection. Plasmid DNA was transiently transfected into cells using Lipofectamine LTX according to manufacturer's instructions. The plasmid complex and LTX reagent complex were prepared with OPTIMEM (ThermoFisher Scientific, Paisley, UK). OPTIMEM is a reduced serum media since the serum will reduce transfection efficiency. Cells were incubated for a minimum of 24 hours to allow sufficient protein expression. As a negative control, mock transfected cells were transfected with empty transfection reagent.

2.4 Preparation of Cell Lysate

Cells were lysed to access the cellular proteins. The procedure was performed with all reagents and tubes on ice to limit protein degradation. The culture media was removed and washed with cold PBS twice, then appropriate amount of 3T3 lysis buffer (25 mM HEPES, 50mM NaCl, 50mM NaF, 30mM $Na_4P_2O_7$, 5mM EDTA, 10% glycerol, 1% triton, pH=7.5) was added to the dishes depending on the size of the dish, cell confluency on the day and protein concentration required for experiments. The cells were scraped using a sterile scraper and the lysate was collected into an Eppendorf tube, which were rotated on a wheel at 4 ^{o}C for 30 minutes. The lysate was then centrifuged at 14,000 rpm for 10 minutes at 4 ^{o}C. The supernatant was collected and stored at -80°C. The 3T3 lysis buffer contained triton, which disrupts the cell membranes to release proteins. The buffer was supplemented with protease cocktail inhibitor tablets (Roche, West Sussex, UK), Phos-stop tablets (Roche, West Sussex, UK) and 25mM NEM (N-ethylmaleimide) (Sigma-Aldrich, Dorset, UK). The protease cocktail inhibitor tablets inhibit a broad spectrum of proteases which lyse proteins. Phos-stop tablets inhibit phosphatases

which helps maintain phosphorylation levels of proteins. The NEM inhibits enzymes which promote de-SUMOylation.

2.5 Protein Quantification by the Bradford Assay

Protein concentrations in cell lysates was determined using the Bradford assay (Bradford, 1976) The assay measures protein concentration by detecting the absorbance shift of the dye Coomassie Brilliant Blue G-250. The assay was performed in a clear 96 well plate. A standard curve was obtained using a series of different concentrations of bovine serum albumin (BSA) from 0-5µg. Each well contained 50µl of a 1:50 -1:200 dilution of samples of unknown concentration and 200µl of Bradford Reagent (Bio-Rad, Hertfordshire, UK) diluted 1:5 with distilled water. All standard BSA and samples were measured in triplicate. The plate was measured at 595nm using an Anthos 2010 plate reader with a 595nm filter and analysed using ADAP software. The unknown protein concentrations are derived by comparison to the BSA standard curve.

2.6 Western Immunoblotting

Western immunoblotting is a method used to detect specific target proteins using antibody-based probes. This method can be used to determine the identity, quantity, molecular weight, and post-translational modifications of proteins that exist within the thousands of proteins in cellular lysates (Najafov and Hoxhaj, 2017a). Protein mixtures in cell lysates were separated by molecular weight using an electric field and a porous acrylamide-based matrix. Determination of molecular weight was estimated via comparison against molecular weight markers of known mass. Proteins on gels can then be electro-transferred onto a nitrocellulose membrane to increase the portability and robustness of protein capture. Specific proteins of intertest were identified by the primary antibody which can be applied directly to the membrane. The method works efficiently as the primary antibody was designed and raised to recognize the desired target protein. A secondary antibody conjugated to an enzyme such as horseradish peroxidase (HRP) or a fluorescent probe (which can be detected by various

visualization methods) allows for the identification and quantification of the protein of interest.

2.6.1 Sample Preparation

Following the determination of protein concentration, samples were normalized to the same concentration at 1.5ug/µl using 3T3 lysis buffer and diluted in 5x laemlli protein sample buffer (10mM Tris-Cl, pH 6.8, 10% glycerol, 5% ß-mercaptoethanol, 2% SDS, 0.01% bromophenol blue) to break the protein structure. SDS is an anionic detergent that binds uniformly to proteins giving them a net negative charge and it also has the ability to disrupt the secondary and tertiary structure of the proteins into linear molecules (Najafov and Hoxhaj, 2017b). Bromophenol blue was used to allow visualization of the samples passing through the gel. Samples in laemlli sample buffer were heated for 5 minutes at 95 ^{o}C to denature the protein. The high temperature breaks the higher structure of proteins including hydrogen boding, three-dimensional shapes, and protein subunit arrangement (Mahmood and Yang, 2012).

2.6.2 SDS-PAGE (Sodium Dodecyl Sulphate Polyacrylamide Gel Electrophoresis)

Before running the gels, the combs were carefully removed from the well, 15-30µg of denatured protein per well was loaded directly onto SDS-PAGE precast gel (NuPAGE 4-12% Bis-Tris Gel, ThermoFisher Scientific, Paisley, UK). 2µl of Precision Plus Protein Standard (Bio-Rad, Hertfordshire, UK) was added to the first well of each gel. The molecular weight markers provide a way of estimating the molecular weight of proteins of interest. Gels were immersed in NuPAGE® MES (for protein size <50kDa) or MOPs (for protein size >50kDa) SDS Running Buffer (ThermoFisher Scientific, Paisley, UK) in the Xcell® SureLock MiniCell system (ThermoFisher Scientific, Paisley, UK). Gels ran at 180V until the samples travelled into the gel after which the gel was run at 200V until bromophenol blue dye was observed to run off the bottom of the gel. Gels could be run longer if a more extensive separation of proteins was required. The proteins moved through the

polyacrylamide gel matrix toward the positive anode, smaller proteins migrating faster than larger proteins (Najafov and Hoxhaj, 2017b).

2.6.3 Protein Transfer to nitrocellulose

After the electrophoresis finished, gels were transferred to nitrocellulose membranes (ThermoFisher Scientific, Paisley, UK). Transfer buffer was prepared by diluting 5% of 20x from NuPAGE® Transfer Buffer (ThermoFisher Scientific, Paisley, UK) in 20% (v/v) methanol in distilled water. The procedure was performed in transfer buffer to minimize any bubbles between the gels and membranes that would hinder a complete transfer. The membrane, filter papers and sponges were soaked in the transfer buffer. The gel was removed from electrophoresis cassette, and a sponge-paper-gel-membrane-paper-sponge transfer sandwich was assembled. A roller was used to roll out the air bubbles between gel and membrane. Then the transfer sandwich was closed and clamped tightly into an Xcell® II Blot Module (ThermoFisher Scientific, Paisley, UK), the blot module was filled up with transfer buffer. Since the proteins were negatively charged, proteins travelled from negatively charged cathode toward positively charged anode. Thus, the membrane was facing anode when the blot module was placed in the system. Usually, 30V of current was applied for 90 minutes, however, if smaller molecular weight proteins were of interest, current was applied at 20V for 90 minutes.

2.6.4 Detection of proteins of interest

After the transfer was complete, the membranes were blocked in either 5% Marvel or 5% BSA or 5% phosphoblocker (Cambridge Bioscience, Cambridge, UK) /TBST (marvel milk powder in 1xTBS-T, 20mM Tris-HCl, 150mM NaCl, 0.1% Tween20, pH 7.6) for 1 hour with gentle shaking to block unspecific antibody binding. When a phospho-antibody was used as the primary antibody, the membranes were blocked in 5% BSA or 5% phosphoblocker in TBST because milk contains phosphor-casein which might interfere with certain phosphor-specific antibodies and increase the background or decrease the signals (Najafov and Hoxhaj, 2017b). Following the blocking, the membrane was incubated with appropriate primary antibody **Table**

2.1 at the appropriate dilution prepared in blocking buffer at 4 ºC overnight. The next day membranes were washed with 1x TBS-T 3 times for 5 minutes. Appropriate Licor Alexa-Fluor conjugated secondary antibodies (Licor Odyssey, Nebraska, USA) or HRP conjugated secondary antibodies were prepared in blocking buffer with 1:5000 dilution **Table 2.2**. The membranes were incubated with the secondary antibodies which recognize the primary antibodies. Secondary antibody incubation was for 1 hour under constant agitation at room temperature in the dark, as the Alexa-Fluor fluorescent conjugated secondary antibodies are light sensitive. Membranes were washed three times for 5 minutes with 1x TBS-T before visualization.

Table 2.1 Primary antibodies. (WB-western blotting; IF-immunofluorescence, PLA-proximity ligation assay; PA-peptide array)

Primary Antibody	Host Species	Dilution	Supplier Catalogue Number	Application
β_2AR	Rabbit	1:1000	Abcam ab137494	WB
β_2AR	Rabbit	1:1000	Thermo-Fisher PA5-12977	WB
β_2AR (E-3)	Mouse	1:100-1:1000	Santa Cruz; Sc-271322	WB, IF, PLA
Phospho-β2AR (pSer345/pSer346)	Rabbit	1:1000	Sigma; SAB4301467	WB
GAPDH	Mouse	1:5000	Thermo-Fisher PA1-987	WB
HA Tag	Mouse	1:1000	Cell Signaling; 2367S	WB
P44/42 MARK (Erk1/2)	Mouse	1:1000	Cell Signaling; 4696S	WB
P-p44/42 MARK (p-Erk1/2)	Rabbit	1:1000	Cell Signaling; 9101S	WB
PIASγ	Mouse	1:1000	Abnova; H00051588-B01P	WB
Phospho-(Ser/Thr) PKA Substrate	Rabbit	1:1000	Cell Signaling; 9621S	WB
SUMO 1 (C-terminal)	Rabbit	1:1000	Enzo; BMLPW9460-0025	WB; PA
SUMO2/3 (N-terminal)	Rabbit	1:1000	Enzo; BMLPW9465-0025	WB
SUMO-β_2	Rabbit	1:100-1:1000	Custom made with Badrilla	WB, IF, PLA,
UBC9	Mouse	1:1000	Santa Cruz; sc-271057	WB
YFP Tag	Mouse	1:100-1:1000	Gentaur.LTD MBS330115	WB, IF, PLA

Table 2.2 Secondary antibodies. HRP-Horseradish Peroxidase.

Primary Antibody	Host Species	Dilution	Supplier; Catalogue Number
Donkey anti-Rabbit	Rabbit	1:5000	Licor; 925-68073
Donkey anti-Mouse	Mouse	1:5000	Licor; 925-68072
Anti-Rabbit HRP	Rabbit	1:5000	Sigma; A6154
Anti-Mouse HRP	Mouse	1:5000	Sigma; NXA931

For the membranes incubated with Licor Alexa-Fluor conjugated secondary antibodies, membranes were scanned using a Licor Odyssey scanner (Licor Odyssey, Nebraska, USA). The scanner can read 700nm and 800nm wavelengths allowing the detection of different species of 2nd antibodies. Digital images were collected and analysed using Licor Odyssey software (Licor Odyssey, Nebraska, USA).

Membranes that were incubated with HRP-conjugated secondary antibodies were visualized using enhanced chemiluminescence (ECL) method. The membranes were incubated with Pierce® ECL western blotting substrate (ThermoFisher Scientific, Paisley, UK) for 4 minutes and then placed in a developing cassette with appropriate light sensitive film (Kodak, London, UK) for appropriate amounts of time. Films were then developed in the dark room using an X-OMAT (Kodak, London, UK).

The results of western blots with respect to intensity of the bands of proteins of interest were normalized to the "housekeeping protein" glyceraldehyde-3-phosphate dehydrogenase (GAPDH) as a loading control. All images were analysed and quantified by Image J software (NIH, Maryland, USA).

2.7 *In Vitro* SUMOylation Assay

In vitro SUMOylation assays were done by using the SUMOylation kit (Enzo Life Science, Exeter UK). The SUMOylation kit was designed around the SUMOylation conjugation cycle. The kit contains purified human SUMO-1, SUMO-2, and SUMO-3

proteins, activating E1 enzyme, E2 enzyme, and ATP (required co factor for SUMO conjugation). This kit provides a means of generating SUMOylated proteins in *vitro*, by covalent linkage of the carboxy-terminal of SUMO-1, -2 and -3 to specific lysine residues on the target protein via isopeptide bonds. HEK$ß_2$ cell lysate, which stably expressed the $ß_2$-adrenergic receptor ($ß_2$AR) and HEK293 cells transfected with wild type $ß_2$AR and SUMO mutant $ß_2$AR plasmid DNA were used in SUMOylation assays. 20µg lysate protein was used for each assay. The assay mix containing all the components listed above was prepared and dH_2O was adjusted to make the 20µl of final volume in each reaction. The reaction complex was incubated at 30 ^oC for 30 minutes. The assays were quenched by addition of 5 µl 5× sample buffer followed by heating to 95°C and western blotting was used to detect the protein modification by SUMO. A negative control was processed in the same manner with the Mg-ATP omitted. The Ran GTPase-activating protein RanGAP1, a key regulator of the Ran GTP/GDP cycle required for the bi-directional transport of proteins and ribonucleoproteins across the nuclear pore complex, was the first protein shown to be post translationally modified by SUMO (Matunis, Coutavas and Blobel, 1996). RanGAP1 was included as positive control in the SUMOylation kit.

2.8 Analysis of Protein-Protein interactions

The confirmation and analysis of the protein-protein interactions was vital to this study. To that end, a range of different techniques was performed to evaluate protein-protein interactions.

2.8.1 Solid Phase Peptide Array

To investigate the SUMO motifs on of the $ß_2$AR, peptide array membranes with full length $ß_2$AR sequence were created utilizing 25-mer overlapping peptides with a 5-amino acid shift between spots. Membranes were wet in TBS-T and blocked in TBS-T containing 5% BSA for 4 hours with constant agitation. $ß_2$AR membrane were rinsed in TBS-T and were overlaid with SUMO assay mix to promote SUMOylation. Arrays and SUMO assay mix were incubated at 37^oC for 4 hours with constant shaking. After that membrane were washed 3 times for 10 minutes in TBS-T and were incubated with SUMO-1 rabbit primary antibody diluted in 1:1000 in TBS-T

with 1% BSA for 2 hours with constant agitation at room temperature. Membranes were washed in TBA-T 3 times for 10 minutes and incubated with Anti-Rabbit IgG secondary antibody diluted in 1:5000 in TBS-T with 1% BSA for 1 hour at room temperature before visualizing with ECL reagent. As a control, β_2AR membrane not overlaid with any SUMO kit reagent were also incubated with the same primary and secondary antibodies as the experiment group.

2.9 Cell-Based Assays

2.9.1 Real-time xCELLigence Measurements

The xCELLigence real-time cell assay is a cell-based assay which uses a 96-well plate (E-plate) with integral sensor electrode arrays that allow the cell impedance to be measured and assayed in real time. The changes in cell impedance correlate with cell shape changes including the attachment ability in short term and cell growth in long term (Atienza *et al.*, 2006; Yu *et al.*, 2006).

A set of E 96-well plate (Roche, USA) was used with HEK293 cells transiently expressing wild type β_2AR or SUMO mutant β_2AR or untransfected HEK293 cells. Cells were seeded in the plate the day before treatment at 10,000/well seeding density, in triplicates, after background measurements were taken. The cells were incubated in the hood for 30 minutes before placing back to the station to make sure all the cells have attached to the bottom of the well and are touching the sensor. The cells were treated with a series of different concentrations of prototypical β_2AR-selective agonist isoprenaline (ISO) 16 hours after seeding. Controls with vehicle (DMSO only) were also performed. The cells were continuously monitored for up to 2 hours and the impedance as reflected by cell index (CI) values were set to record every 30 second. The xCELLigence data were analysed using the RTCA software (ACEA Biosciences®, USA). The results from various treatments were compared to baseline normalized Cell Index CI, which was normalized by the timepoint of the stimulation of ISO and baseline corrected using vehicle treated cell index values.

2.10 Microscopic Analysis

2.10.1 Immunostaining and Confocal Microscopy

HEKß$_2$ cells were plated on a coverslip in 6 well plates (Corning, USA). PIASγ plasmid DNA was transfected in HEKß$_2$ cells to promote SUMOylation, isoprenaline was added to activate the ß$_2$AR signalling pathway. Cells were stimulated with 10μM ISO for 10 minutes before fixation. After ISO stimulation, culture medium was removed to stop the treatment and cells were fixed with 4% paraformaldehyde at room temperature for 10 minutes and permeabilized in 0.1% triton X-100 in PBS for 4 minutes. After 3 times wash with Tris-buffered saline (TBS), the cells were blocked with 10% goat serum and 2% BSA (w/v) in TBS for 1 hour followed by three washes with TBS. The primary antibodies used were diluted in required concentration in blocking buffer diluted 1:100 with TBS and added to cells incubated at 4 ^{o}C overnight. After 3 washes with TBS, the coverslips were incubated with 1:500 diluted secondary antibodies Alexa Fluor 594 Goat anti-rabbit IgG for 1 hour in dark. Following several extensive washes with TBS, the coverslips were dehydrated and mounted on slides with ProLong Gold anti-Fade reagent with 4', 6-diamidino-2-phenylindole (DAPI) nuclear stain. The immunostaining was visualized using a Zeiss Pascal laser-scanning confocal microscope with oil immersion objective (63×/1.4 NA plan apochromat lens). Images were captured and processed on Zeiss LSM Image microscope with a 63x water immersion objective (Carl Zeiss, UK) and analysed using the ImageJ. Pearson's coefficient and Manders' coefficient were calculated by ImageJ.

2.10.2 Duolink^{TM} Proximity Ligation Assay (PLA)

In situ proximity ligation assay is a method that detects protein interactions using two recognition events. The mechanism of PLA allows improvement of detection of protein-protein interactions, by using antibodies with attached DNA strands that participate in ligation, replication, and sequence decoding reactions (Söderberg *et al.*, 2008)(**Figure 2.1**). A proper detection complex formation is used to initiate a localized rolling-circle amplification (RCA) reaction, generating a long-single-stranded DNA molecule, rolled-up in a ball that can be detected by

hybridizing fluorescence-labelled probes. The hybridization reaction only happens when two target proteins are in less than 40nm proximity, but not if they are further apart (Söderberg *et al.*, 2006). This assay was used to confirm whether the SUMOylation of the β_2AR occurs in HEK293 cells and also in rabbit adult cardiomyocytes. The assay is also useful to evaluate how the location of the β_2AR changes under different experimental conditions following SUMOylation.

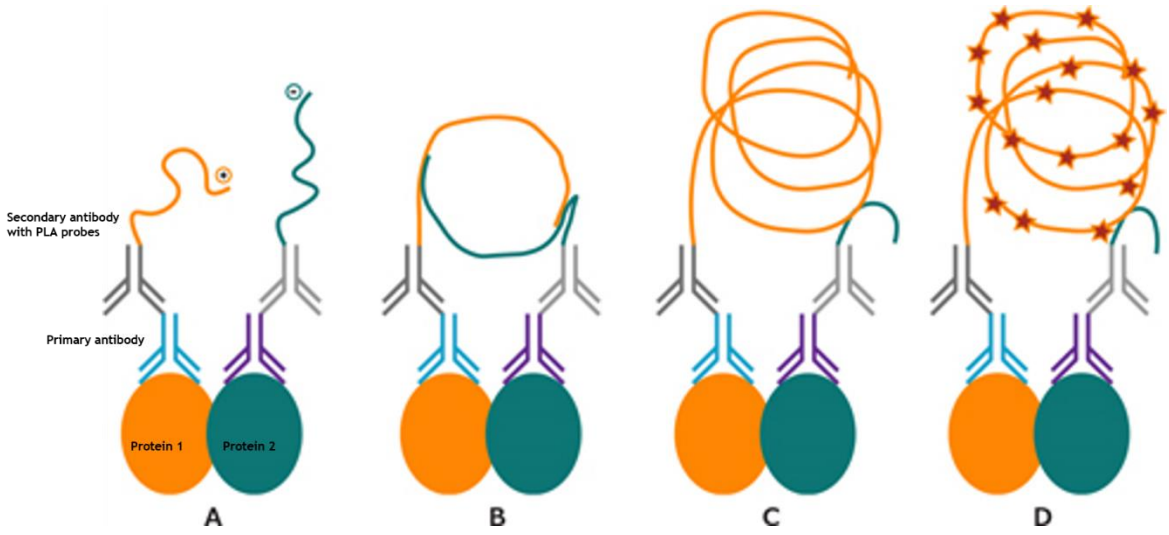

Figure 2.1 Schematic diagram of in situ PLA. (A) Cells were incubated with primary antibodies specific to the target proteins raised in two different species. A pair of PLA probes (PLUS and MINUS) was bonded to the primary antibodies respectively with unique DNA strand attached. (B) The two DNA strands interact through circle-forming DNA oligonucleotides and use ligase to complete the DNA circle. (C) Rolling-circle amplification (RCA) occurred by polymerase. (D) Fluorescent probes are hybridized to the synthesized DNA strand allowing the PLA signals to be visualized. (Adapted from https://www.sigmaaldrich.com/), legends added to the original figure.

HEK293 cells transiently expressing wild type β_2AR or SUMO mutant β_2AR and untransfected HEK293 cells were seeded on 13nm coverslip the day before the treatment. The coverslips were blocked in 4% paraformaldehyde (PFA) at room temperature for 15 minutes. The coverslips were rinsed three times with PBS for 10 minutes with gentle shaking to remove fixation solutions. The cell membranes were then labelled with 5µg/ml Wheat Germ Agglutinin (WGA) (ThermoFisher Scientific, Paisley, UK) / filter sterilized PBS in dark for 20 minutes. After two washes with PBS, the coverslips were permeabilized in 0.1% Triton X-100/ filter sterilized PBS for 10 minutes. Then the coverslips were incubated following the manufacturer's instructions. The coverslips were washed with 1x wash buffer A (0.01M Tris, 0.15M NaCl, 0.05% Tween-20, pH 7.4) once for 10 minutes. The

coverslips were then incubated with Duolink® blocking buffer at 37℃ for 1 hour. Primary antibodies raised in two different animal species, SUMO-β_2 (Rabbit) and β_2AR (Mouse) were diluted in Duolink® antibody diluent 1:50 and incubated in a humidity chamber overnight at 4 ºC. The cells were incubated with two corresponding PLA probes diluted in 1:5 in the antibody diluent at 37 ºC for 1 hour. The anti-Mouse PLUS and anti-Rabbit MINUS PLA probes are special secondary antibodies that were oligonucleotide-labelled and recognize primary antibodies, where hybridization between oligos occurs if probes are less than 40nm apart. The cells were allowed to through ligation (Ligase diluted 1:40 in ligation buffer) and amplification (Polymerase diluted 1:80 in amplification buffer) to complete the circularization of oligos. The coverslips were washed with 1x wash buffer A twice for 5 minutes between each reaction. The coverslips were washed with 1x wash buffer B (0.2M Tris, 0.1M NaCl, pH 7.5) after amplification twice for 10 minutes and followed by 1-minute wash with 0.01x wash buffer B. Finally, the coverslips were mounted on slides with Duolink® Mounting Medium with 4', 6-diamidino-2-phenylindole (DAPI) nuclear stain. Hybridization of amplified oligos with complementary fluorescently labelled oligos (594 λ_{ex} / 624 λ_{em}) allowed visualization of the localization of the PLA signals shown as red spots. All the incubation steps after cells were labelled with WGA were performed in dark. The PLA signals were detected using a Zeiss LSM 520 confocal microscope with a 63x oil immersion objective (Carl Zeiss, Cambridge, UK). Quantification of PLA was done by recording the red spots with Image J and GraphPad Prism 6.0.

2.11 Tissue Homogenization

Tissue homogenization is necessary to break down tissue and release cellular contents.

2.11.1 Human Heart Tissue Preparation

A group of human heart tissue samples isolated from patients with different heart conditions were kindly provided by Dr. Ken Campbell, from University of Kentucky. All the steps were carried out on ice to minimize protein degradation. Tissue was

weighted out without allowing to thaw and transferred to a universal. 5ml chilled CHAPS lysis buffer (50mM HEPES pH7.4, 100mM NaCl, 1% CHAPS, 1mM EDTA, 1% glycerol) supplied with protease inhibitors and phosphatase inhibitors 2 and 3 was added into the universal. Tissues were chopped into small pieces using clean small-bladed scissors. Then then complex was homogenized for four cycles of 10 seconds chilling on ice between each cycle. After the last homogenization, the mixture was rotated for 1 hour at 4ºC. Supernatant was collected by centrifuging for 30 minutes at 14,000 rpm at 4 ºC. The supernatant was aliquoted in 100µl and stored at -80ºC. Protein concentration was assessed by Bradford assay (described in section **2.5 Protein Quantification by the Bradford Assay**). Samples were assessed using immunoblotting (described in section **2.6 Immunoblotting**).

2.12 Statistical Analysis

Statistical Analysis was performed using GraphPad Prism Version 6 (GraphPad Prism, California, USA). All data values in this thesis are presented as mean ± standard error of the mean (SEM) from at least three independent experimental replicates unless otherwise stated. Levels of statistical significance was evaluated by *p*-value, calculated using paired or unpaired Student's *t*-tests, one-way or two-way analysis of variance (ANOVA) depending on the different types of the data. A *p*-value of <0.05 (*) was considered significant, *p*-value of <0.01 (**) was considered highly significant, *p*-value of <0.001 (***) was considered extremely significant.

Chapter3. *In Vitro* SUMOylation of the β_2AR

3.1 Introduction

3.1.1 SUMOylation of the β_2AR and Cardiac Signalling Proteins

There are more than 1000 SUMO substrates in nature (Hay, 2013) and although most of the SUMO substrates are located in the nucleus, SUMOylation is not a PTM limited to nuclear proteins but is also seen in the cytoplasm and plasma membrane (Le et al., 2017a). For example, potassium channel activities are regulated by SENP1 and 2 as part of the SUMOylation process. Potassium voltage-gated channel subfamily Q member (KCNQ) and potassium voltage-gated channel subfamily A member 5 (KCNA5) are prime examples. Potassium channels are involved in regulating vascular tone and the sinus rhythm (Le et al., 2017b). SERCA2a is another membrane protein that was found to be a SUMOylation substrate by Hajjar's group (Kho et al., 2011). SERCA2a SUMOylation has been shown to improve cardiac function by up regulating its activity and expression. Another cardiac protein called protein kinase Cα (PKC) has also been shown to have SUMOylation sites and be a substrate of SUMOylation (Sun et al., 2014). PKCα plays a negative role in cardiomyocyte contraction and SUMOylation has been indicated to have an inhibitory role in PKCα kinase function (Sun et al., 2014). Overall, data suggests that inhibition of PKCα kinase activity by SUMOylation can be cardio protective. The above evidence shows that both cytoplasmic and membrane bound proteins can act as SUMO substrates in the cardiac setting.

3.1.2 Post-Translational Modification (PTMs) of β_2AR and Antibodies

A post-translational modification (PTM) is a modification of a protein as a result of the covalent attachment of functional group or smaller proteins. PTMs have been confirmed as playing a vital role in the function of the β_2AR. PTMs can happen at any time during the life cycle of a protein ranging from directly after ribosomal translation up until the protein has been relocated to a specific cellular function. PTMs can alter the target protein's conformation, activity, localization and

protein-protein interactions (R. A. Bradshaw et al., 2010). Developing a specific antibody that can robustly recognize the modified form of the substrate without picking up the non-modified residue is a challenging task (Arur & Schedl, 2014). The most developed and well-studied PTM using a site-specific antibody use is phosphorylation, which is a PTM where a phosphate group is attached to either a serine, threonine or tyrosine residue by a kinase (Grisan et al., 2020). Previous members in Baillie lab have collaborated with cardiovascular life science company Badrilla® (Badrilla, Leeds, UK) to develop a SUMOylation site-specific β_2AR antibody which had been validated by peptide array and biochemical analysis.

3.1.3 Production of the SUMO-β_2AR Specific Polyclonal Antibody

A specific antibody was designed to recognise an epitope representing the SUMOylated β_2AR (**Figure 3.1**). Previous data in Baillie lab had shown that lysines 60 and 235 to be the dominant SUMOylation sites, however, as the lysine at 60 emerges from the membrane into the first intra-cellular loop, this may not reflect real life due to the proximity of this lysine to the cell membrane. Further analysis utilising alanine scanning revealed that both lysines at positions 232 and 235 are susceptible to SUMOylation. The SUMO-β_2 antibody was designed based on lysine 235 modification (Wills, 2017). The antibody was designed to detect the antigen that is a combination of SUMO and β_2AR but not SUMO or β_2AR alone. The antibody was designed by Lauren Wills who worked as a PhD student in Baillie lab and was produced in rabbits by a commercial collaborator, Badrilla.

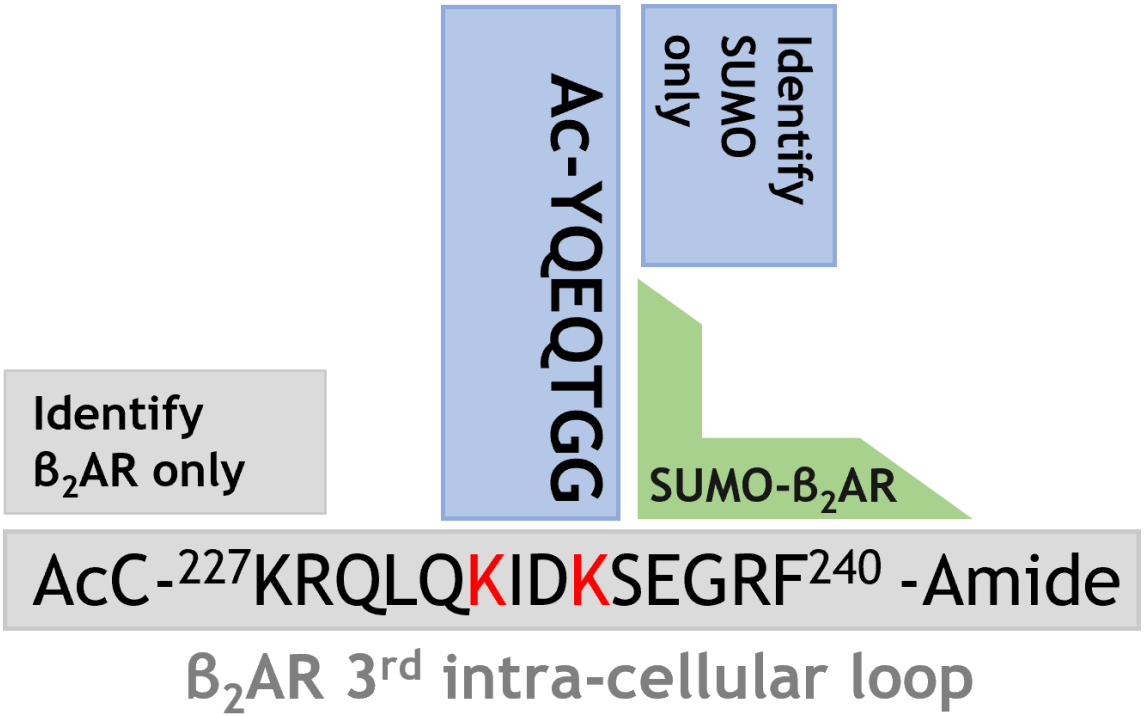

Figure 3.1 SUMO-β_2 antibody epitope design schematic. Custom SUMO-β_2 antibody was raised against partial sequence of β_2AR KRQLQKIDKSEGRF with addition of partial sequence of SUMO QTGG. Amino acid abbreviations in appendix.

3.2 Hypothesis and Aims

Preliminary data has shown that the β_2AR can be SUMOylated in order to modulate receptor signalling and stability in model cell lines. Also, the potential SUMOylation sites have been identified by previous member in Baillie lab. However, the function of SUMOylation using SUMO-null mutations in the β_2AR receptor has not been determined. The main aim of the experimental work in this chapter is to determine whether the ablation of β_2AR SUMOylation resulted in detectable changes in receptor signalling. More specifically, the aims are listed as followed:

1) To construct a SUMOylation-null β_2AR in a HEK293 cell line to allow a model in which to investigate the effect of SUMOylation on receptor signalling.
2) To determine the influence of β_2AR SUMOylation on receptor signalling in the above model using a variety of *in vitro* signalling assays.

3.3 Results

3.3.1 Confirmation of β_2AR SUMOylation *in vitro*

3.3.1.1 *In Vitro* SUMOylation Assay

An *in vitro* SUMOylation assay mix was incubated with cell lysates isolated from WT β_2AR stably transfected HEK cells. RanGap1 was used as a positive control to show the efficiency of the SUMOylation assay (**Figure 3.2A**) and SUMOylated RanGap1 was detected in +ve control lane 1 (ATP present) indicating that the SUMOylation assay mix was active. Lysates from HEK293 cells transiently expressing WT β_2AR were also incubated with SUMOylation kit assay mix. A band for SUMOylated β_2AR was detected by western blotting in lane 2 at 75kDa with a custom antibody which was developed against SUMOylated β_2AR having lysine 235 modification (**Figure 3.2B&C**). No bands were detected in negative controls missing either SUMO assay components (lane 1) or ATP (lane 3). This data suggests that the custom antibody can detect SUMOylated β_2AR in a cellular context.

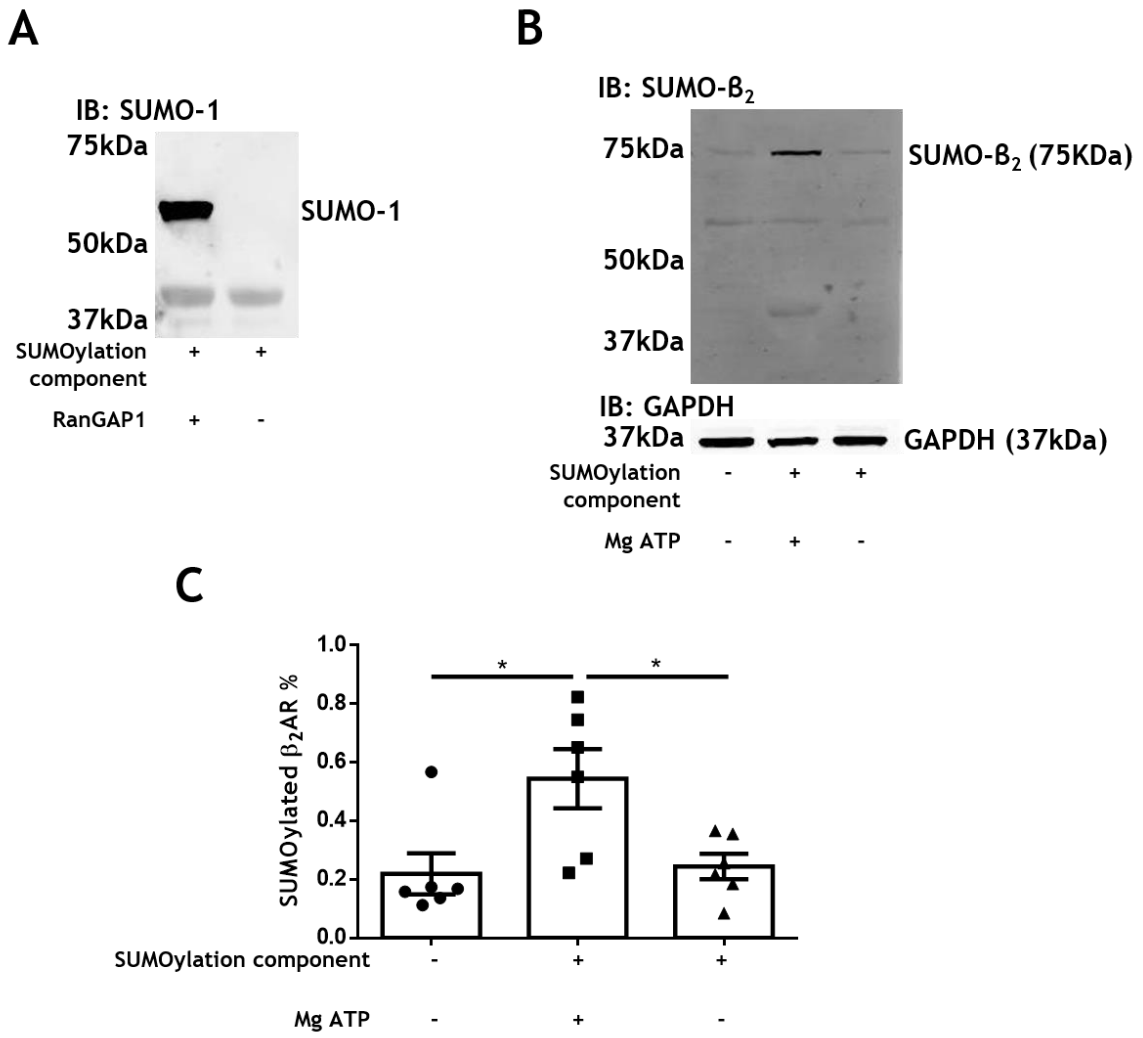

Figure 3.2 Confirmation of in vitro SUMOylation in β_2AR. Lysates from HEK293 stably expressing β_2AR used to perform a SUMOylation assay followed by western blotting. (A) RanGAP1 was SUMOylated via SUMOylation kit as a positive control, SUMOylated RanGAP1 was detected with ATP present. (B&C) SUMOylated β_2AR was detected by SUMO- β_2 antibody at 75kDa (n=6, *$p<0.05$).

3.3.1.2 Over-expression of PIASγ in HEKβ$_2$ cells promotes β$_2$AR SUMOylation

The stable HEKβ$_2$ cell line has been selected to investigate the influence of SUMOylation on β$_2$AR as it is a well-established model for examining signal transduction driven by of β$_2$AR activation (Bolger et al., 2006) (Bolger et al., 2003) (Perry et al., 2002). PIASγ is a SUMO E3 ligase that has been shown to add fidelity to substrate SUMOylation. To determine if PIASγ can promote SUMOylation of the β$_2$AR, 4, 6 and 8μg PIASγ-HA was transfected into HEKβ$_2$ cells (**THIS WORK DONE BY Dr. LAUREN WILLS**)(S.-Y. Sohn & Hearing, 2012)(Wills, 2017). Successful transfection was shown by immunoblotting for the presence of PIASγ at 57kDa (**Figure 3.3A, upper blot**). A band was not seen in the mock transfected control (lane 1). Lastly, the blot was probed with the SUMO-β$_2$ site-specific custom antibody that only recognizes SUMOylated β$_2$AR. A band was detected at ~75kDa which increased in intensity as the amount of transfected PIASγ increased to a maximum of 8ug. This data indicates that increased PIASγ expression promotes SUMOylation of β$_2$AR (**Figure 3.3B&C**).

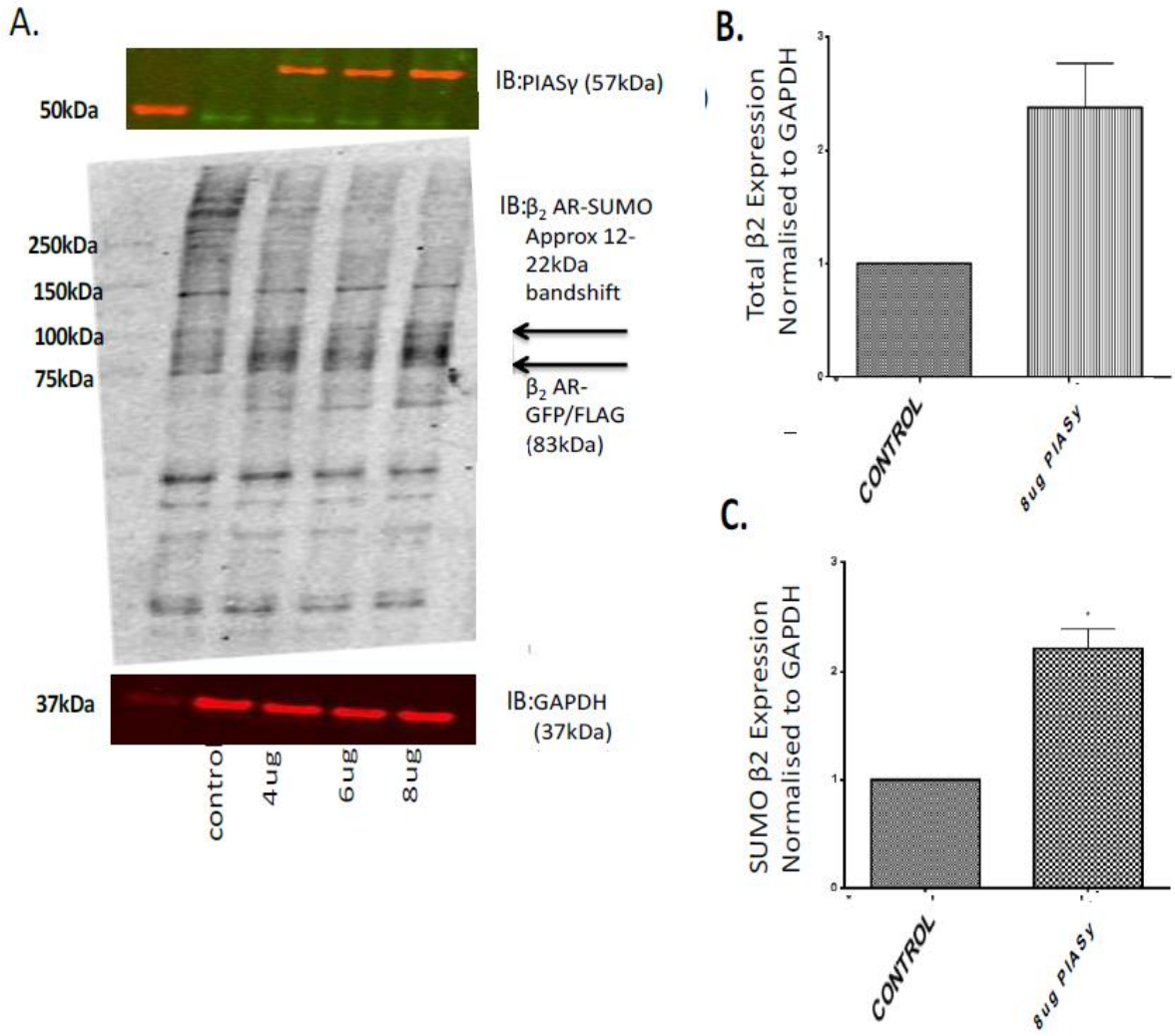

Figure 3.3 Transfection of PIASγ in HEKβ$_2$ cells promotes β$_2$AR SUMOylation. HEKβ$_2$ cells were transfected with 4ug, 6ug or 8ug of PIASγ plasmid DNA and immunoblotted for total β$_2$AR, SUMO-β$_2$ and GAPDH as a loading control shown in A, statistical analysis is shown B&C (n=3). Adapted from Dr. Lauren Wills thesis (Wills, 2017).

3.3.1.3 Over-expression of PIASγ in HEKβ$_2$ cells with Isoprenaline time course promotes β$_2$AR SUMOylation

PIASγ with a HA tag was transfected in HEKβ$_2$ cells to promote β$_2$AR SUMOylation as shown before for other proteins (Li et al., 2010). Again, successful transfection was observed following a western blot (**Figure 3.4A, upper panel**). Analysis by densitometry revealed statistically significant transfection of HA-PIASγ (**Figure** 3.4**B**).

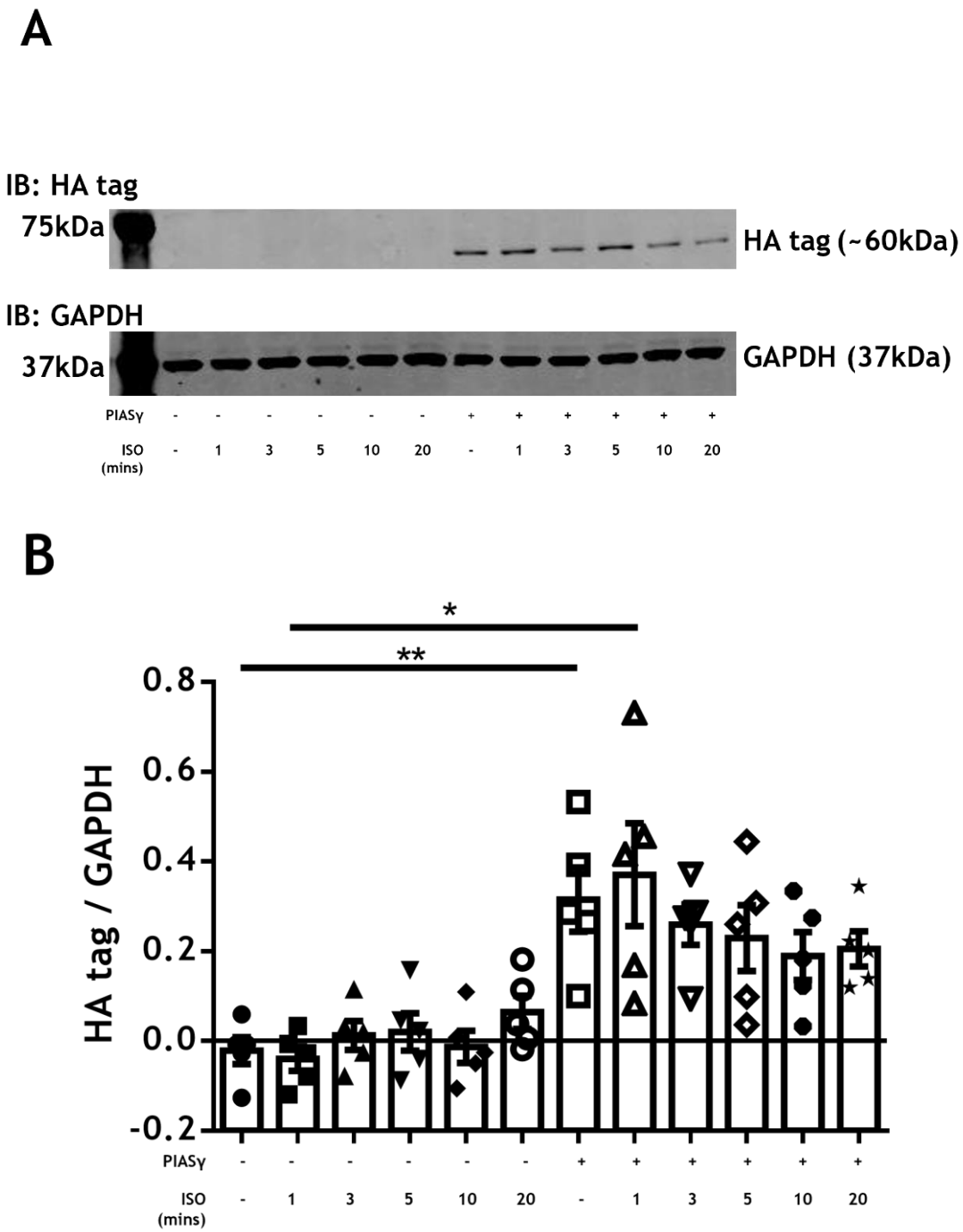

Figure 3.4 PIASγ plasmid DNA successfully transfected in HEKβ$_2$ cells. (A) PIASγ with HA tag was transfected in HEKβ$_2$ cells to promote β$_2$AR SUMOylation. Cells were treated with 10μM ISO for 0,1,3,5,10,20 minutes time course before harvsting. Primary concentration 1:1000, secondary concentration 1:5000. (A) Representative blots shown. (B) Data are displayed as mean ± SEM, (N=5) (*p<0.05, *p<0.01).

HEKβ_2 cells overexpressing PIASγ were treated with 10μM ISO for 0, 1, 3, 5, 10, 20 minutes to examine where adrenergic stimulation could influence the SUMOylation of β_2AR. Cell lysates were probed with the SUMO-β_2 antibody (**Figure 3.5A**). SUMOylation of the β_2AR under basal conditions could be detected but only when HA-PIASγ had been transfected. This data matched that seen in **Figure 3.4,** (**work that had been carried out previously by Dr. Lauren Wills**). The ISO time course resulted in a rapid diminution of the SUMO-βAR$_2$ band at 75KD (**Figure 3.5A, upper panel**) while the non-SUMOylated fraction remained constant (**Figure 3.5A**, **lower panel**). Analysis of the data from n=5 repeats confirmed that ISO treatment promotes the de-SUMOylation of the β_2AR (**Figure 3.5C)** whilst the total βAR$_2$ protein levels remained unchanged (**Figure 3.5D)**.

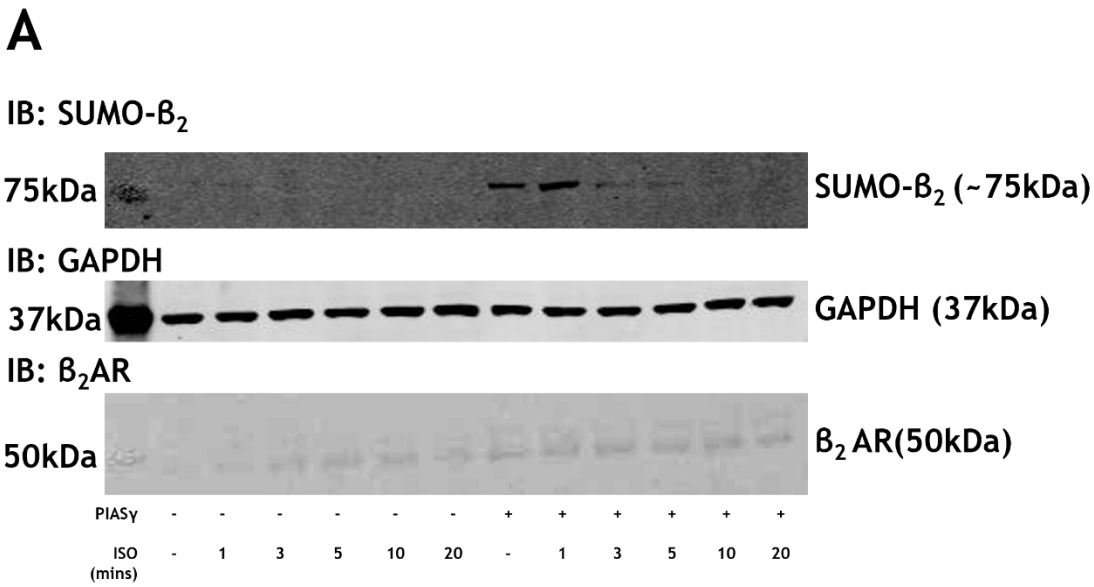
A
IB: SUMO-β2
75kDa
SUMO-β2 (~75kDa)
IB: GAPDH
37kDa
GAPDH (37kDa)
IB: β2AR
50kDa
β2 AR(50kDa)
PIASγ - - - - - - + + + + + +
ISO (mins) - 1 3 5 10 20 - 1 3 5 10 20

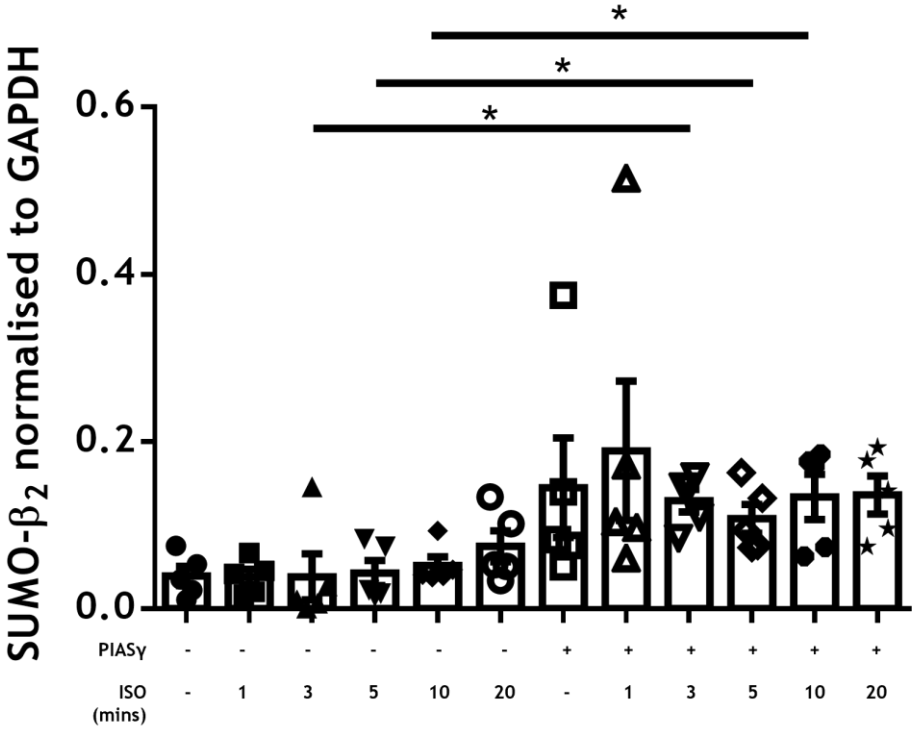
B
SUMO-β2 normalised to GAPDH
0.6
0.4
0.2
0.0
*
*
*
PIASγ - - - - - - + + + + + +
ISO (mins) - 1 3 5 10 20 - 1 3 5 10 20

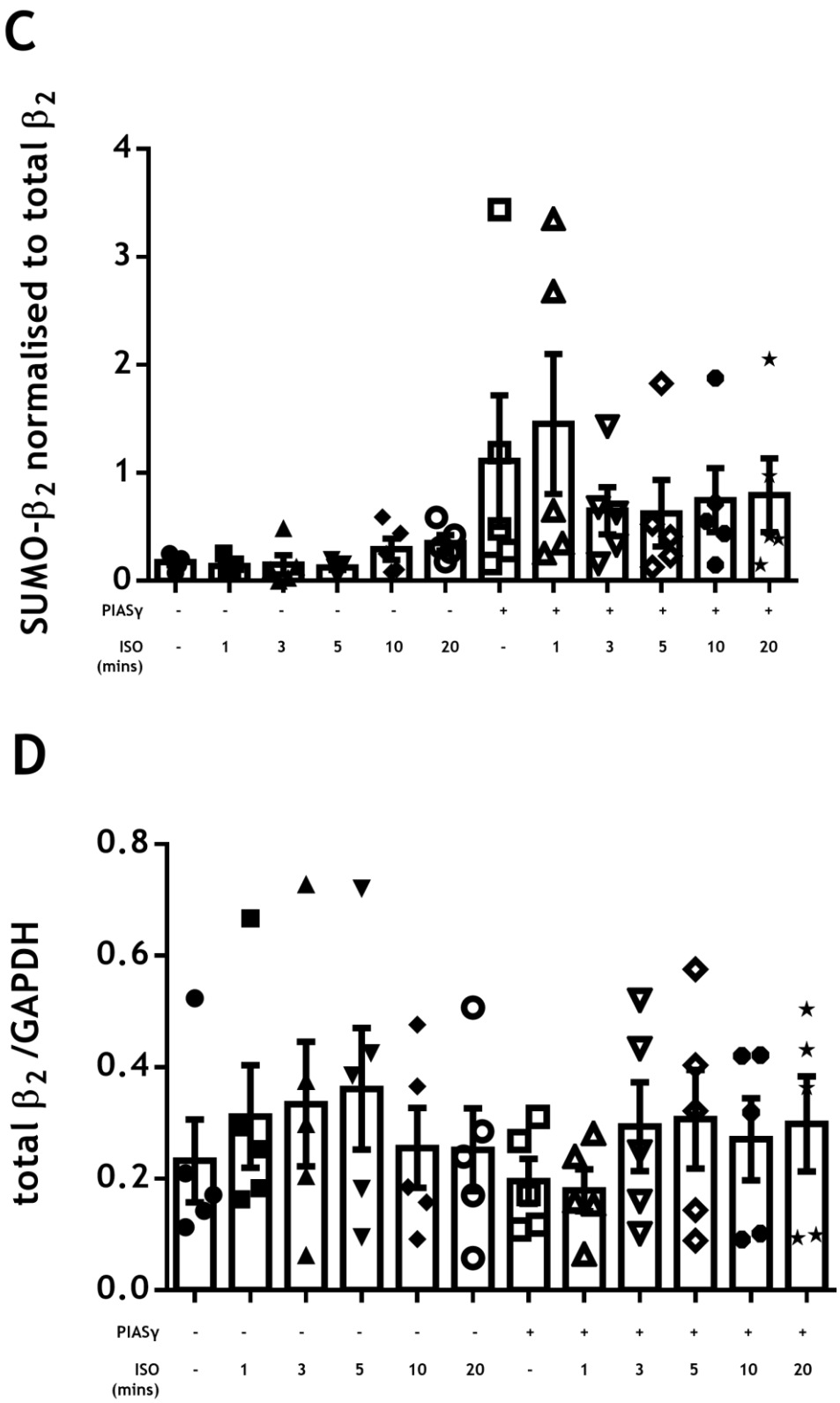

Figure 3.5 SUMOylation of the β_2AR in HEKβ_2 cells overexpressing PIASγ. Cells were treated with 10μM ISO for 0,1,3,5,10,20 minutes time course before harvsting. Primary concentration 1:1000, secondary concentration 1:5000. (A) Representative blots shown. (B) SUMO-β_2 normalised to GAPDH and Data are displayed as mean ± SEM. (C) SUMO-β_2 normalised to total β_2AR. (D) total β_2AR normalised to GAPDH (N=5) (*$p<0.05$).

To evaluate possible effects of the SUMOylation of the β_2AR on the downstream signalling events promoted by the receptor, I measured the general PKA substrate phosphorylation and ERK MAP kinase activation after ISO treatment (**Figure 3.6-Figure 3.7**). As expected, PKA phosphorylation of general PKA substrates were significantly enhanced following receptor activation irrespective of whether they overexpressed HA-PIASγ or not (N=5) (**p<0.01) (**Figure 3.6**). Expression of the SUMO E3 ligase did not have much effect on this aspect, suggesting that the amount of cAMP produced in both cases was equivalent. As previously published, ISO stimulation triggers ERK MAP kinase activation (Baillie et al., 2002). As with the data for the general PKA substrates, treatment stimulated significant ERK activation in both HEKβ_2 cells overexpressing PIASγ and mock transfected HEKβ_2 cells to an equal level (Figure 3.7) (N=5). These findings indicate that modification of the of the β_2AR induced by PIASγ expression (**Figure 3.5A, upper panel**) (Perry et al., 2002) didn't influence downstream signalling of β_2AR after ISO stimulation.

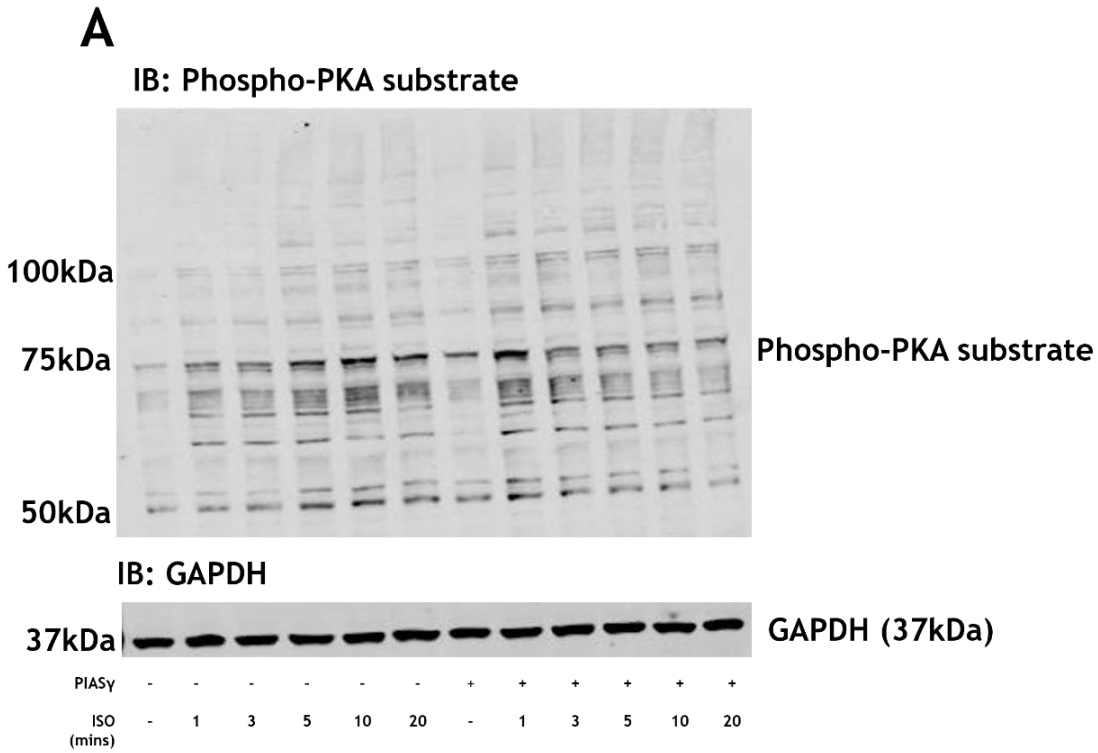

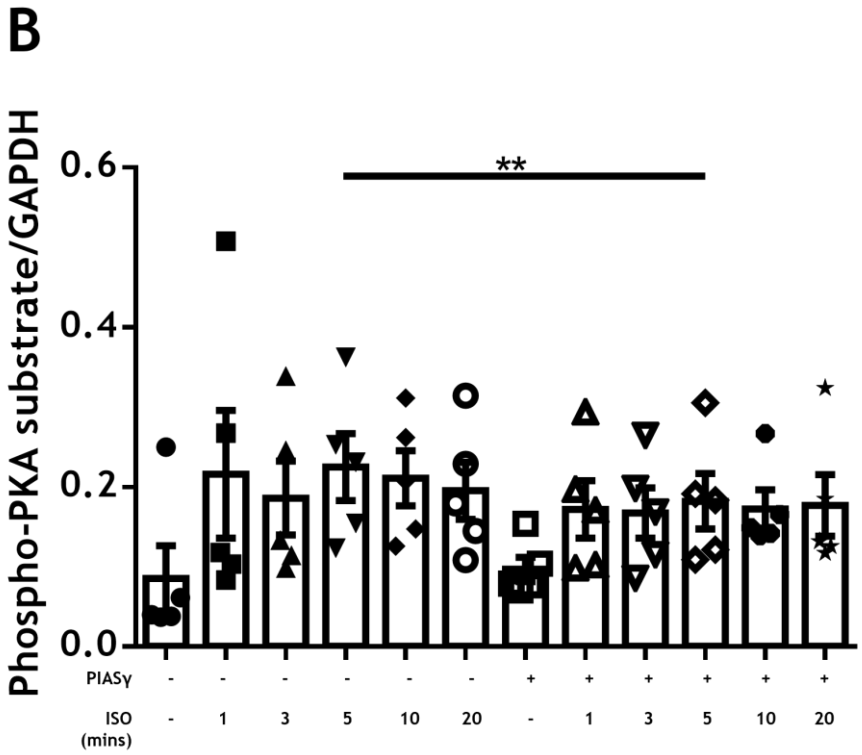

Figure 3.6 PIASγ had no effect on isoprenaline-mediated phosphorylated PKA substrate. Cells were treated with 10μM ISO for 0,1,3,5,10,20 minutes time course before harvesting. Primary concentration 1:1000, secondary concentration 1:5000. (A) Representative blots shown. (B) Quantification was displayed as a measurement of all the bands in the blots. Data are displayed as mean ± SEM, (N=5) (**$p<0.01$).

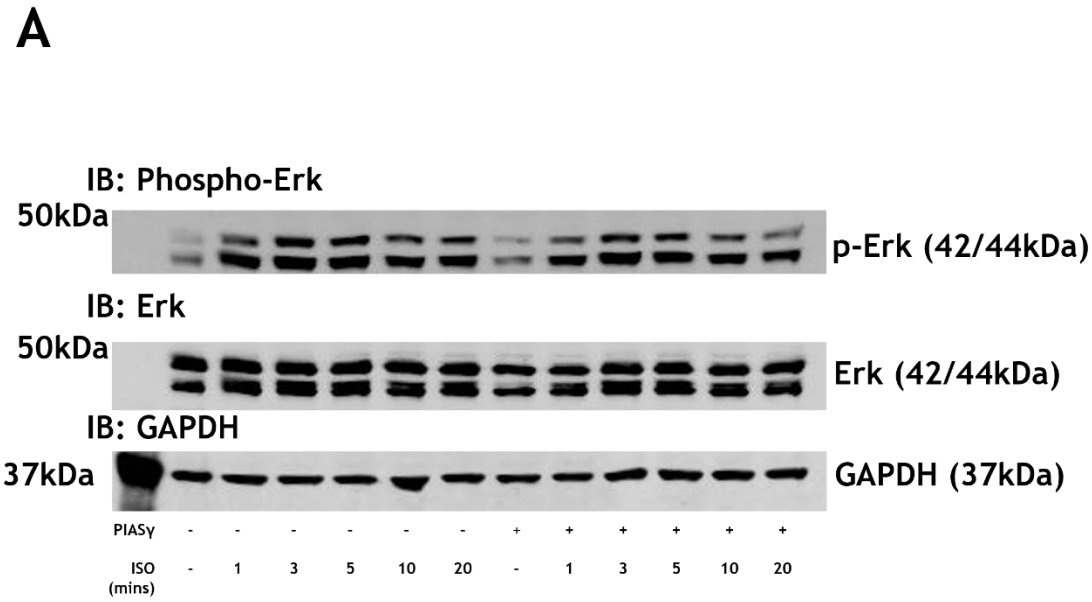

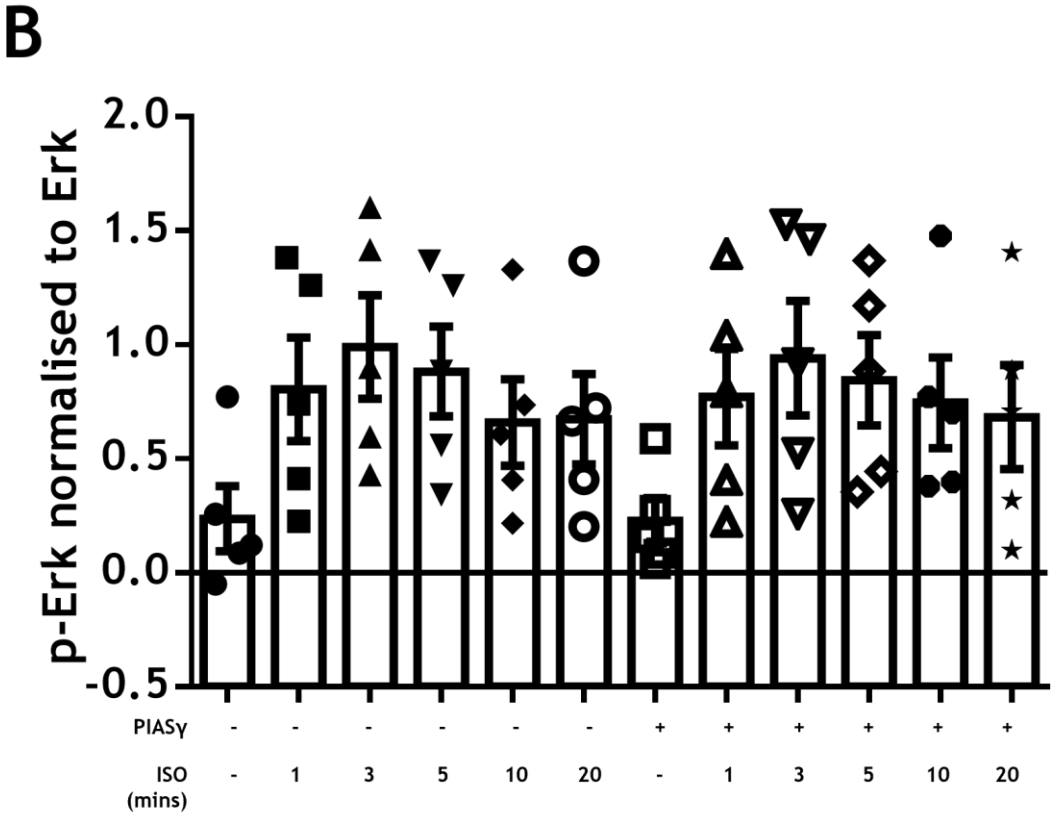

Figure 3.7 PIASγ did not significantly influence isoprenaline-mediated ERK activation of β_2AR. Cells were treated with 10μM ISO for 0,1,3,5,10,20 minutes time course before harvesting. Primary concentration 1:1000, secondary concentration 1:5000. (A) Representative blots shown. (B) Data are displayed as mean ± SEM, (N=5).

3.3.1.4 In vitro SUMOylation of β_2AR Peptide Array sequences.

The SUMO-β_2 antibody was tested on peptide array to see if it could recognize the SUMOylated epitope against which it was raised (**Figure 3.8**) (Wills, 2017). The antibody only bound to peptide sequences after they had been pre-SUMOylated using the SUMO assay mix (right panel). Peptide 4 (VFQEAKRQLQKIDKSEGRFHVQNLS) was strongly recognized by the antibody suggesting that the antibody picked up SUMOylation of the SUMO motif within this sequence. The epitope used to raise the antibody is shown in red. The antibody specificity for the SUMOylated motif was further tested using mutation analysis. Preliminary data from Baillie lab confirmed that the SUMO site on β_2AR is likely to be at lysine 235 and the SUMO site contains the 4 amino acid stretch 'KIDK'. Based on this data, I designed a peptide array to confirm this. The arrays were incubated with SUMO assay kit reaction mix and blotted for SUMO-1. Dark spots represent SUMOylated peptides. Motif shifting arrays (**Figure 3.9A**) where the KIDK motif was sequentially moved through the sequence did not prevent SUMOylation of the sequences. This result could be expected as the acceptor lysine is always present, but it shows that none of the other more remote amino acids were involved. No SUMOylation of peptides was evident in -ve controls where the SUMO assay mix was not included. As the potential SUMO motif has 2 lysines, I next mutated them singly or together (**Figure 3.9B**). Only peptides containing mutated (K-A) K235 nullified the SUMOylation of the sequence confirming that the antibody is specific for SUMOylated K235. Usually, mutation of the hydrophobic residue preceding the acceptor lysine also prevents SUMOylation, however in this instance the residue is aspartic acid (D234). I replaced it with alanine, a hydrophobic residue which had no effect. Nevertheless, this data shows that I have a site-specific SUMO antibody for K235 of the β_2AR which I will use in experiments in this thesis.

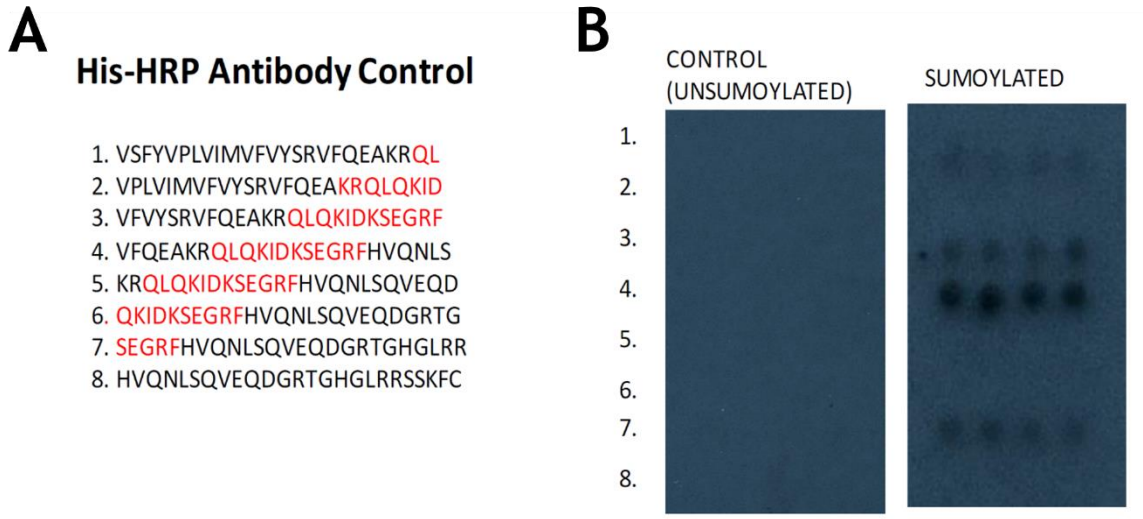

Figure 3.8 SUMO-ß$_2$ antibody tested with His-HRP antibody control. (A) Peptide array slides spotted with truncations of epitope highlighted in red. (B) Arrays were SUMOylated via ENZO in vitro SUMOylation kit. Control arrays didn't go through the SUMOylation kit and remains unSUMOylated. His-HRP antibody were incubated with the arrays overnight on both control and SUMOylated arrays. (n=3) Repressive images shown. Antibody concentration 1:5000. Representative peptide array spots shown. Amino acid abbreviations in appendix. (Wills, 2017).

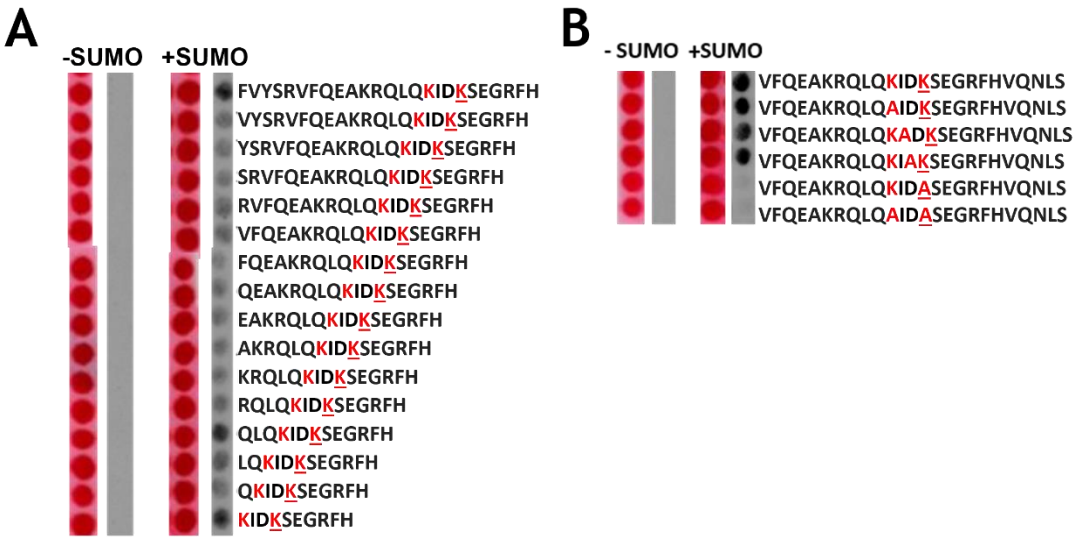

Figure 3.9 ß$_2$AR-SUMO interaction assessed by peptide array overlay. ß$_2$AR peptide array membrane incubated with SUMO kit for 4 hours with constant agitation, following the incubation with SUMO-1 antibody and ECL detection, the point of interaction was identified with black spots (N=1). Lysine 235 is indicated in red underlined. Ponceau stain was displayed on the left of each panel. Primary on the left side SUMO-1 antibody concentration 1:1000, secondary antibody concentration 1:5000. Amino acid abbreviations in appendix. (A) Truncation peptide array. (B) Alanine peptide array was designed, each of the amino acid were replaced with alanine in each spot.

3.3.1.5 Visualisation of SUMOylated β_2AR in HEK β_2 cell line

Next, to determine whether I could detect SUMOylated β_2AR in fixed cells, I used confocal microscopy to look at the colocalization of total β_2AR staining with SUMOylated β_2AR staining. When β_2AR is inactive and SUMOylation enzyme PIASγ was not introduced into the cells, the florescent signals of β_2AR remained low level as a starting point. Confocal microscopy showed that SUMOylated β_2AR is localized predominantly on the membrane of the HEKβ_2 cells, with some also in the cytoplasm that may reflect internalized receptor or non-specific labelling. Note that as in the case of western blotting, little SUMOylated β_2AR could be detected without PIASγ transfection (**Figure 3.5 & Figure 3.10A)**. Total β_2AR can clearly be seen at the membrane. To abrogate the possibility that the SUMOylated β_2AR staining represented predominantly non-specific interaction, analysis of the co-localization of epitope recognition for both antibodies was undertaken.

Pearson's coefficients evaluating the similarity of cellular locations recognized by both antibodies showed that PIASγ transfection significantly upregulated the amount of co-localization of both antibodies but that this was not affected by ISO treatment (**Figure 3.10B**). **Figure 3.10C** shown enlarged merge images of fluorescent signals for each condition, indicates protein location in the cell component and colocalization. When the receptors activated by ISO, co-localized SUMO-β_2 and β_2AR were observed in the cytoplasm. When the receptor activated and PIASγ overexpressed, there are more colocalized protein complex shown on the plasma membranes and endosome near the membranes. The latter observation may relate to the time used for ISO treatment, which was after 1 minute and it means that a large amount of de-SUMOylation had already taken place (**Figure 3.5**).

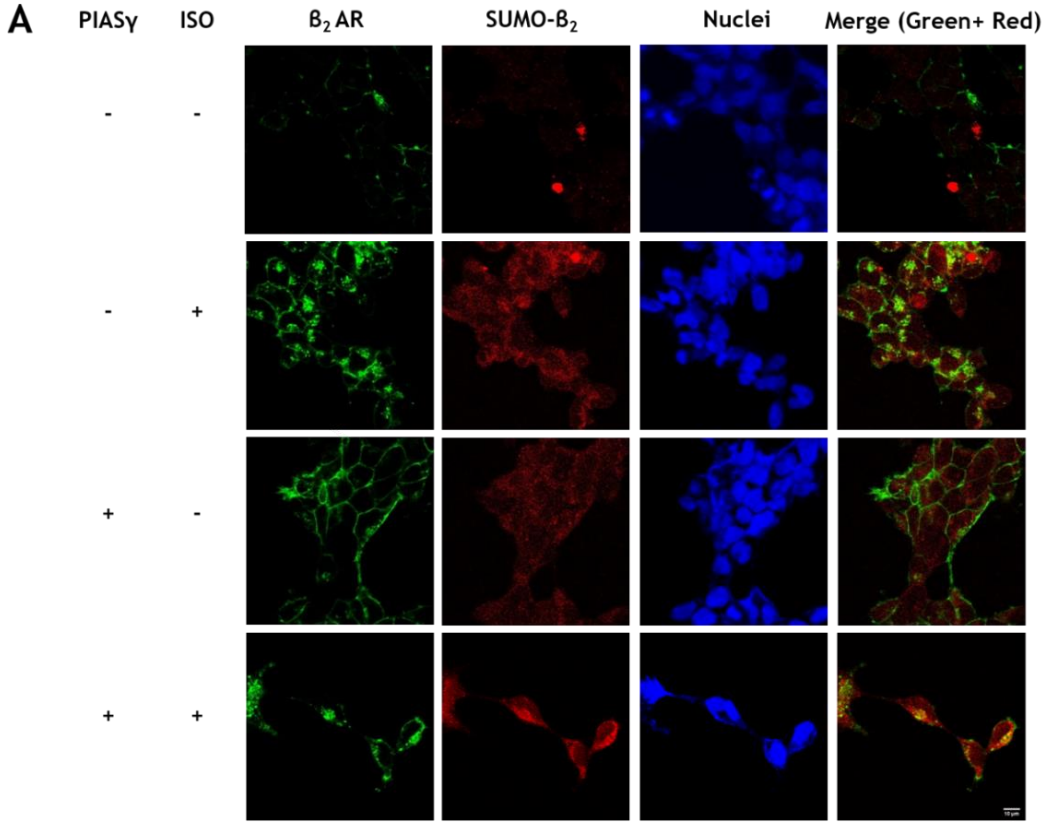
A
PIASγ
ISO
β2 AR
SUMO-β2
Nuclei
Merge (Green+ Red)
-
-
-
+
+
-
+
+

B

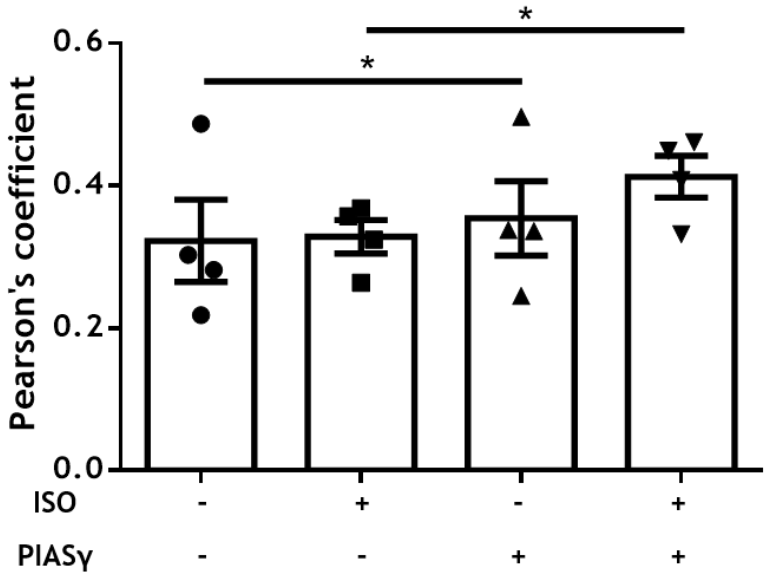
*
*
0.6
0.4
0.2
0.0
Pearson's coefficient
ISO - + - +
PIASγ - - + +

C

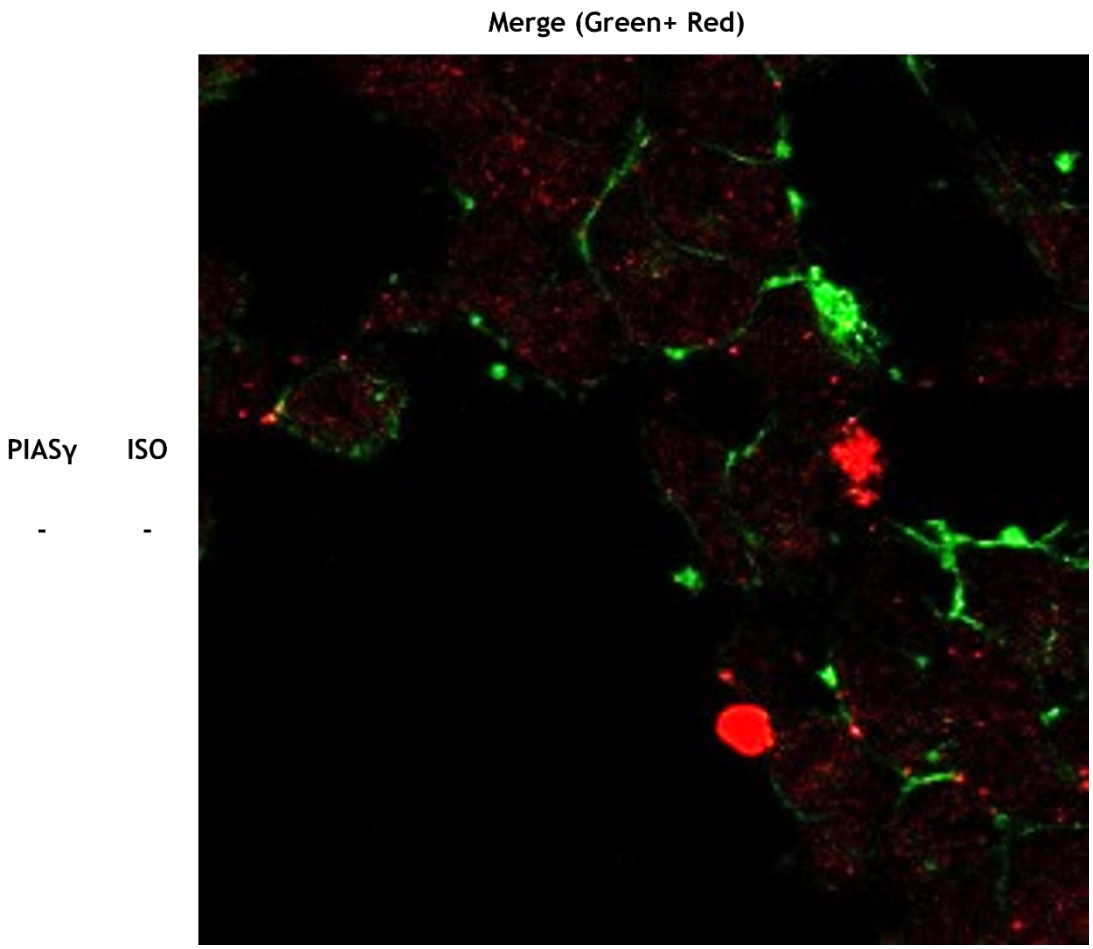
Merge (Green+ Red)
PIASγ ISO
- -

Merge (Green+ Red)

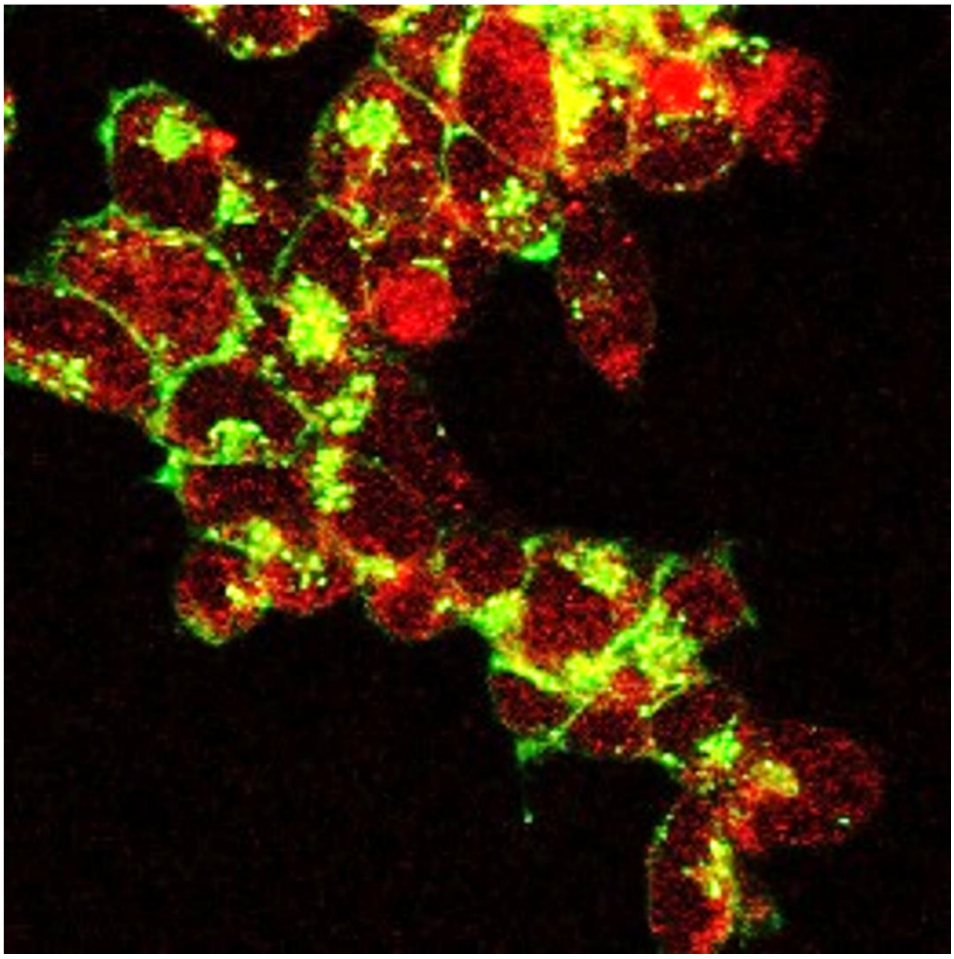

PIASγ ISO

- +

Merge (Green+ Red)

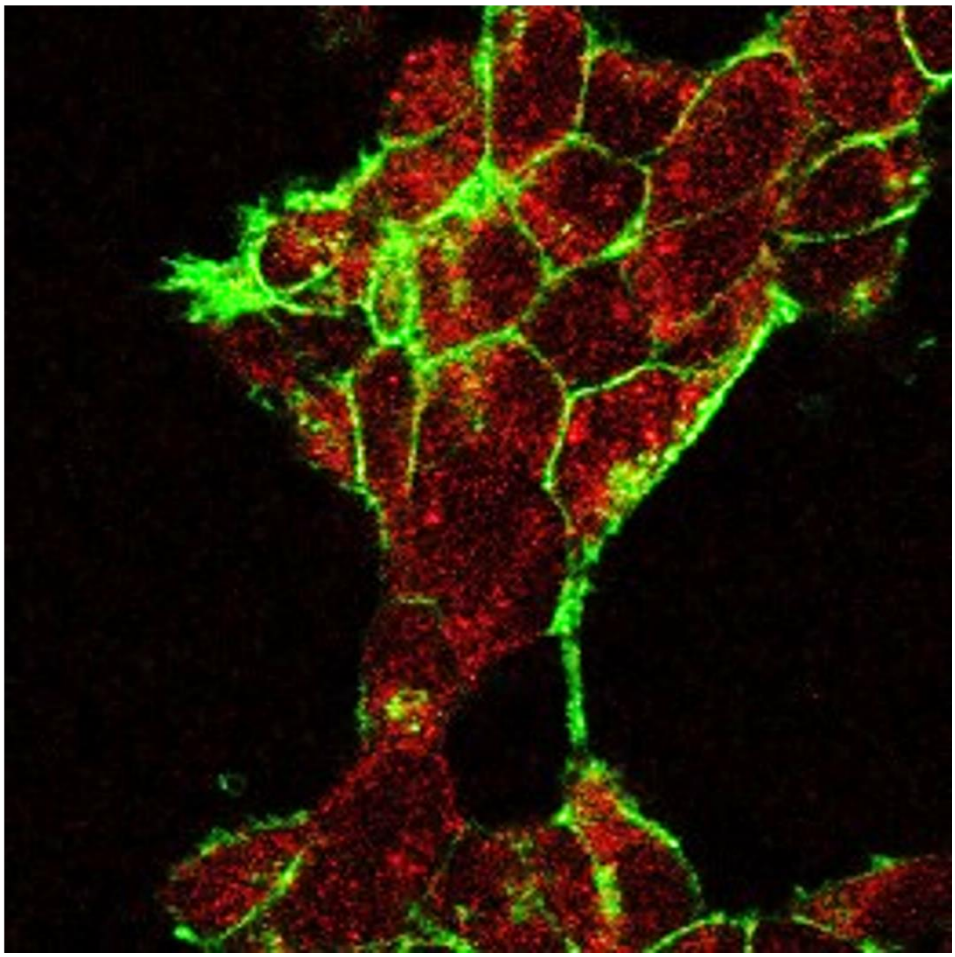

PIASγ	ISO
+	-

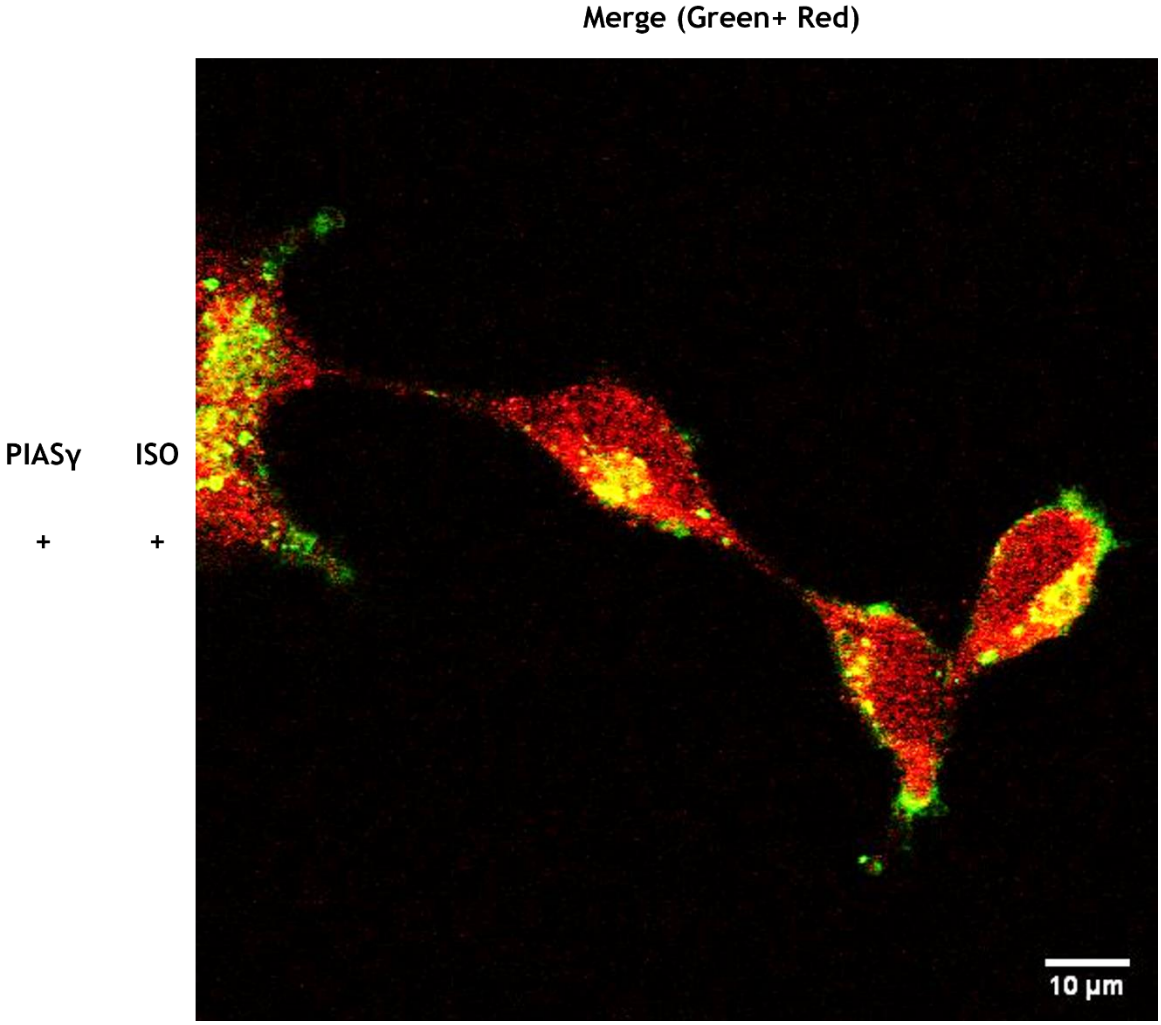

Figure 3.10 Confocal immunofluorescence imaging of SUMOylated $ß_2$AR in HEK$ß_2$ cell line. Confocal analysis in HEK293 cells stably expressing GFP-tagged wild type $ß_2$AR (green) and DAPI staining for nuclear (blue) under basal conditions. After ISO (10µM) stimulation and PIASγ transfection in HEK$ß_2$ cells, SUMOylated $ß_2$AR immunofluorescence signals (red) were observed and increased compared to the basal condition. (A) Representative confocal images for each condition. Representative immunofluorescence images of $ß_2$AR are shown in the table. (B) The Pearson's coefficient significantly increased after PIASγ present in HEK$ß_2$ to promote SUMOylation (n=4, *$p < 0.05$). (C) Enlarged Merged images of each condition are shown. ISO-Isoprenaline, GFP-Green fluorescence protein, DAPI-4′,6-diamidino-2-phenylindole.

3.3.2 Wild Type β_2AR and SUMO-null β_2AR Overexpression in HEK293 cells: analysis using PLA and RTCA

3.3.2.1 Interaction of SUMOylated β_2AR Reduction in SUMO Mutant β_2AR Overexpression HEK293 cells

PLA is a technique that measures the proximity of two distinct epitopes that are recognized by 2 separate antibodies (described in 2.10.2 DuolinkTM Proximity Ligation Assay (PLA)) and allows the position of the interaction to be visualized in fixed cells. In this case, each red PLA signal represents an event where antibodies recognizing the SUMOylated β_2AR interact with antibodies recognizing total β_2AR. This method safeguards against non-specific antibody interaction with random proteins. The different epitopes need to be less than 40nm apart before association is detected. In order to detect all PLA signals for the cells of interest, images were taken throughout the entire thickness of the cells using Z stacking. The red PLA signals were counted by Image J software. For each condition, images were taken from 50 cells and statistical analysis undertaken on the average of the total. Three independent experiments were conducted. Firstly, detection of red PLA spots confirms the data seen using traditional colocalization (**Figure 3.10**) microscopy that suggests that the total and SUMO- β_2AR recognize the same protein (when PIASγ was transfected). As before, signals could be seen at the membrane and in the cytoplasm suggesting SUMO- β_2AR may be in internalized vesicles. Next, we wanted to validate that the antibody picks up the SUMO motif containing K235 when it is SUMOylated. For this purpose, we used transient transfection of the β_2AR WT vs the K232R-K325R β_2AR mutant. Statistical analysis showed that there was a significant reduction of colocalization between total β_2AR and SUMO- β_2AR signals when the SUMO-null mutant is overexpressed in HEK293 cells (compared to WT β_2AR) (**Figure 3.11C**). This suggests that construction of the SUMO-null mutant was successful in reducing modification by SUMO and could be used to investigate possible functional outcomes association with β_2AR SUMOylation.

A

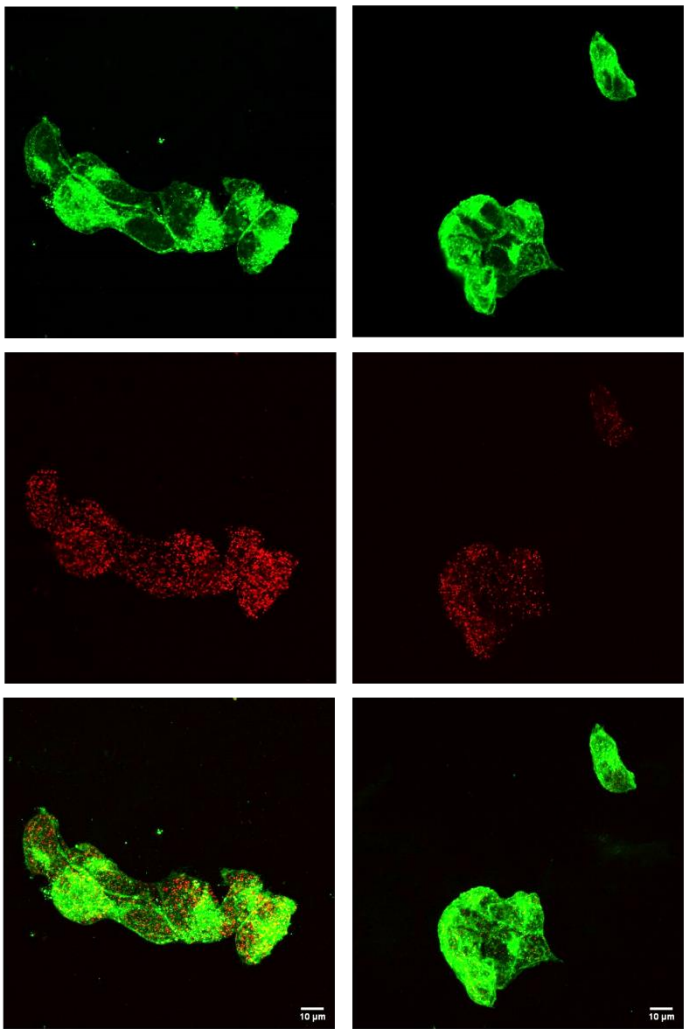

Wild type β_2AR	+	-
SUMO Mutant β_2AR	-	+
PIASγ	+	+
ISO (10µM)	+	+

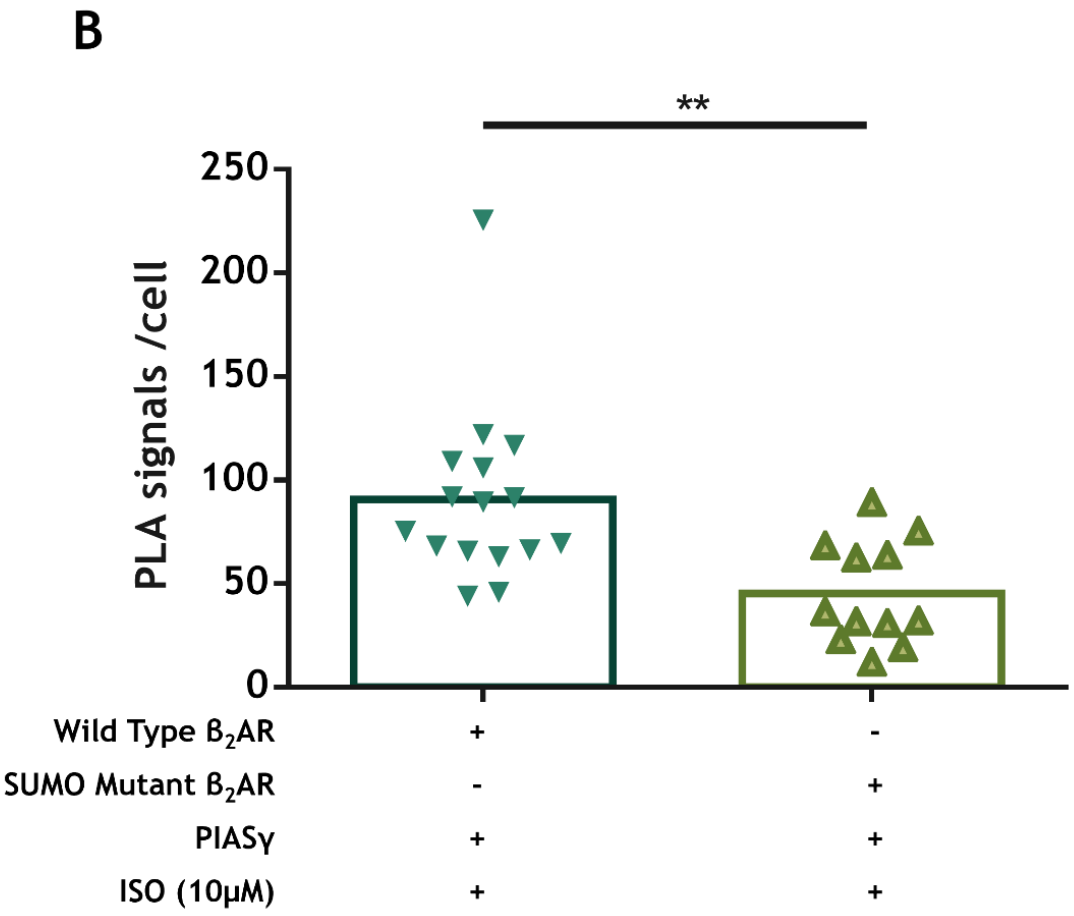

Figure 3.11 The effect of Isoproterenol (ISO) on SUMOylation of the β_2AR. PLA indicating colocalization of antibodies against SUMOylated β_2AR and total β_2AR are described in **2.10.2 DuolinkTM Proximity Ligation Assay (PLA)**. PLA signals (Red particles) indicate sites of a positive interaction. Cell membranes were stained with WGA to show the structure and location of the cells. Representative images shown. The statistic results (B) biological repeat n=3, average cells observed in each experimental condition = 113 (*p <0.05, **p <0.01, ***p <0.001).

3.3.2.2 Evaluation of SUMO-site mutation on receptor activation using xCELLigence Real-time Cell Assay (RTCA)

xCELLigence technology uses impedance to monitor cell growth or cell shape change in real time (Urcan et al., 2010). Short-term cell shape change can be used to measure the extent of receptor activation to different concentrations of any given agonist assuming the cell being tested expresses the correct receptor (Stallaert et al., 2012). HEK293 cells transiently expressing wild type β_2AR or SUMO mutant (K235R) β_2AR and untransfected HEK293 cells were seeded in a 96-well E-plate the day before treatment. To determine whether this technique could be used for monitoring the β_2AR, the cells were treated with a series of different concentrations of ISO. The stimulation of cells that expressed β_2AR led to a concentration-dependent, time-resolved impedance response within the first 10 minutes (**Figure 3.12**). Untransfected cells showed a dose-dependent transient increase in normalized cell index between 4 and 10 minutes (**Figure 3.12A**), followed by a static phase. This data may reflect endogenous expression of the receptor. Conversely, cells overexpressing the β_2AR exhibited an initial and rapid, dose-dependent fall in cell index followed by a slower recovery (between 4 and 10 minutes) and then a static phase (**Figure 3.12B**). Other researchers have successfully used such data to evaluate the kinetics and sensitivity to various GPRs to different agonist types (Roche, 2008).

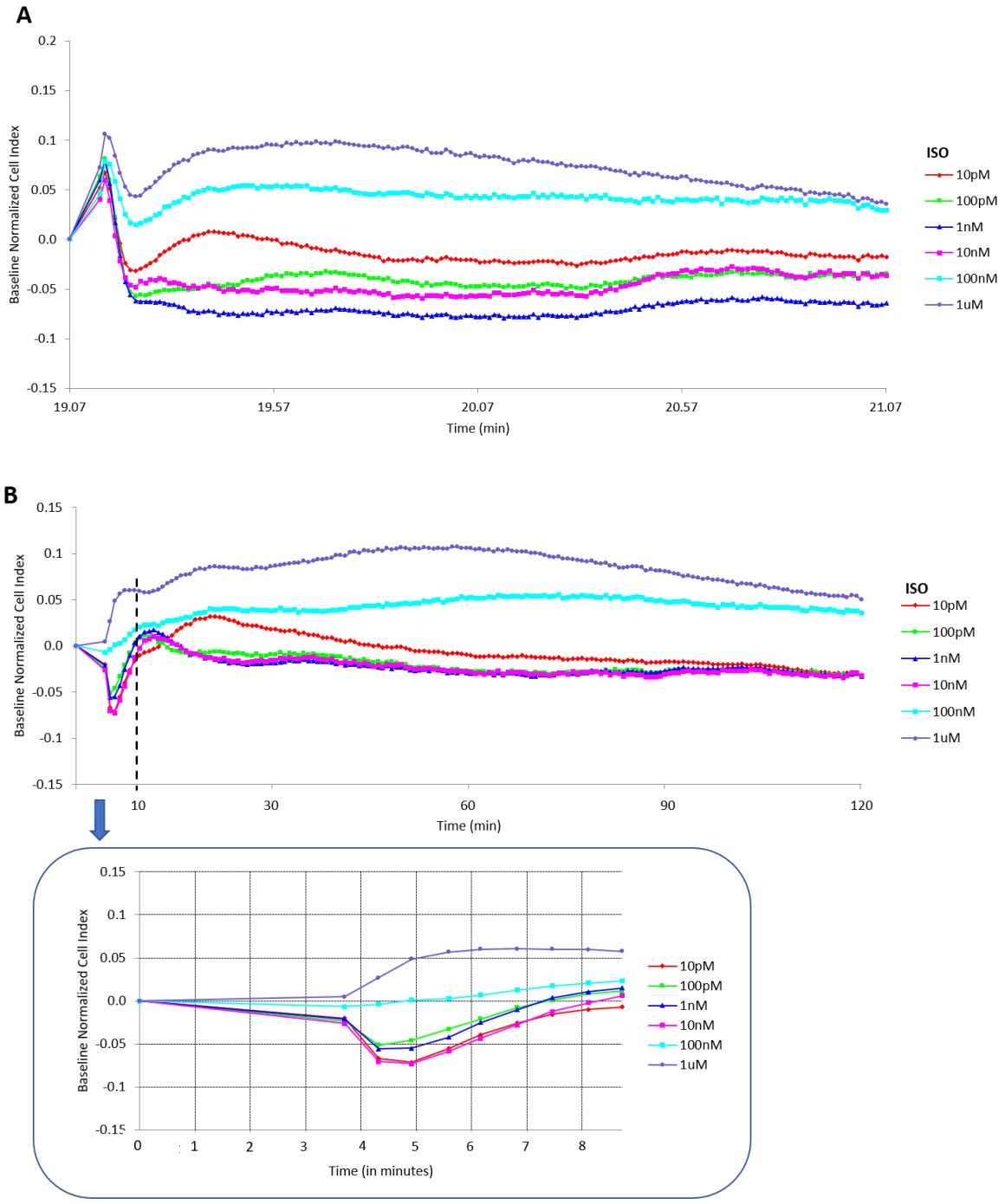
A
Baseline Normalized Cell Index
0.2
0.15
0.1
0.05
0.0
-0.05
-0.1
-0.15
19.07
19.57
20.07
20.57
21.07
Time (min)
ISO
10pM
100pM
1nM
10nM
100nM
1uM
B
Baseline Normalized Cell Index
0.15
0.1
0.05
0.0
-0.05
-0.1
-0.15
10
30
60
90
120
Time (min)
ISO
10pM
100pM
1nM
10nM
100nM
1uM
Baseline Normalized Cell Index
0.15
0.1
0.05
0.0
-0.05
-0.1
-0.15
0
1
2
3
4
5
6
7
8
Time (in minutes)
10pM
100pM
1nM
10nM
100nM
1uM

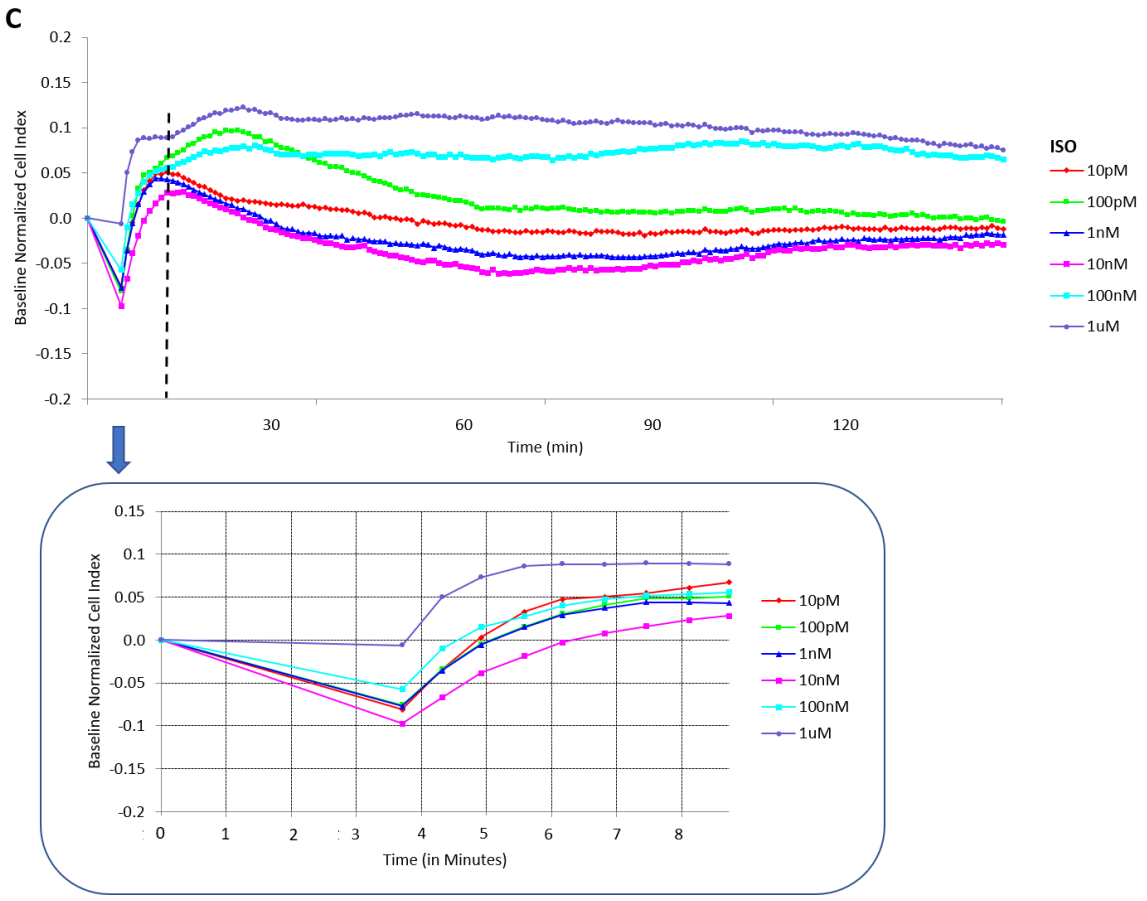

Figure 3.12 β_2AR activator treatment in impedance are multi-featured and concentration dependent. Impedance measurements were obtained in HEK293 cells untransfected or transiently expressed wild type β_2AR and SUMO mutant β_2AR following with isoprenaline (ISO) at the concentration indicated. Impendence responses (represented as changes in Cell index) were normalized by the timepoint of the stimulation of ISO and baseline-corrected by vehicle (DMSO alone) treated cell index. (A) Baseline normalized Cell index of untransfected HEK293 cells after 2 hours of ISO stimulation. (B) Baseline normalized Cell index of HEK293 cells transiently expressed wild type β_2AR after 2 hours of ISO stimulation, expanded figure to illustrate the first 10 minutes of treatment. (C) Baseline normalized Cell index of HEK293 cells transiently expressed SUMO mutant β_2AR after 2 hours of ISO stimulation, expanded figure to illustrate the first 10 minutes of treatment.

As untransfected cells gave a different profile to those transfected with β_2AR, I decided to compare responses from the WT β_2AR with the mutated (K235R) β_2AR. When baseline normalized cell index responses were compared with respect to Log ISO concentration, it was possible to compare WT and mutant receptor responses to ISO at each time point (**Figure 3.13A**). Generally, the slope (change in response per unit dose) of the curve changed from steep to flat over 30 minutes time course in cells that were overexpressing either mutant or WT β_2AR, suggesting that there was a degree of desensitization towards the end of the period (**Figure 3.13B**). **Figure 3.13B** displays the dose-response curves for all time points of WT and mutated receptors on respective graphs with longer time points generally exhibiting flatter curves that suggest a degree of receptor desensitization. There was no significant difference between WT and K235R receptor curves using this analysis suggesting that SUMOylation does not alter the temporal response of the β_2AR. Another way to analyses this data is to compare time after ISO treatment to reach maximum cell index (**Figure 3.14**). When I looked at the concentrations 10^{-4} and 10^{-5} there was a trend suggesting WT was faster to the peak compared to K235R β_2AR, however the changes were not significant suggesting that the receptor responses were being transduced at the same rate. Overall, this data suggests that mutation of the SUMO site on the β_2AR does not affect either sensitivity to agonist or response rate of the receptors to stimulation.

A

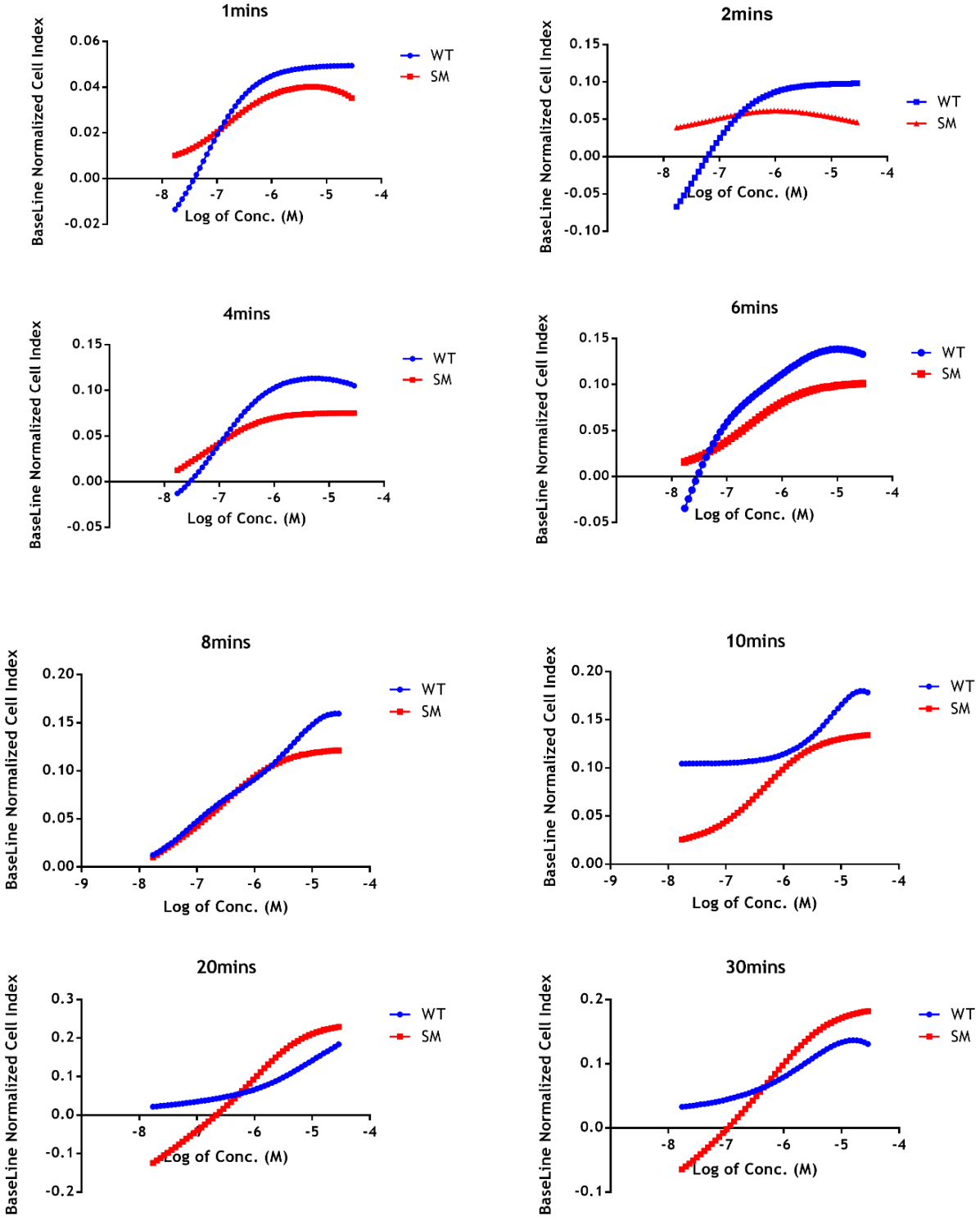
1mins
2mins
4mins
6mins
8mins
10mins
20mins
30mins
BaseLine Normalized Cell Index
Log of Conc. (M)
WT
SM

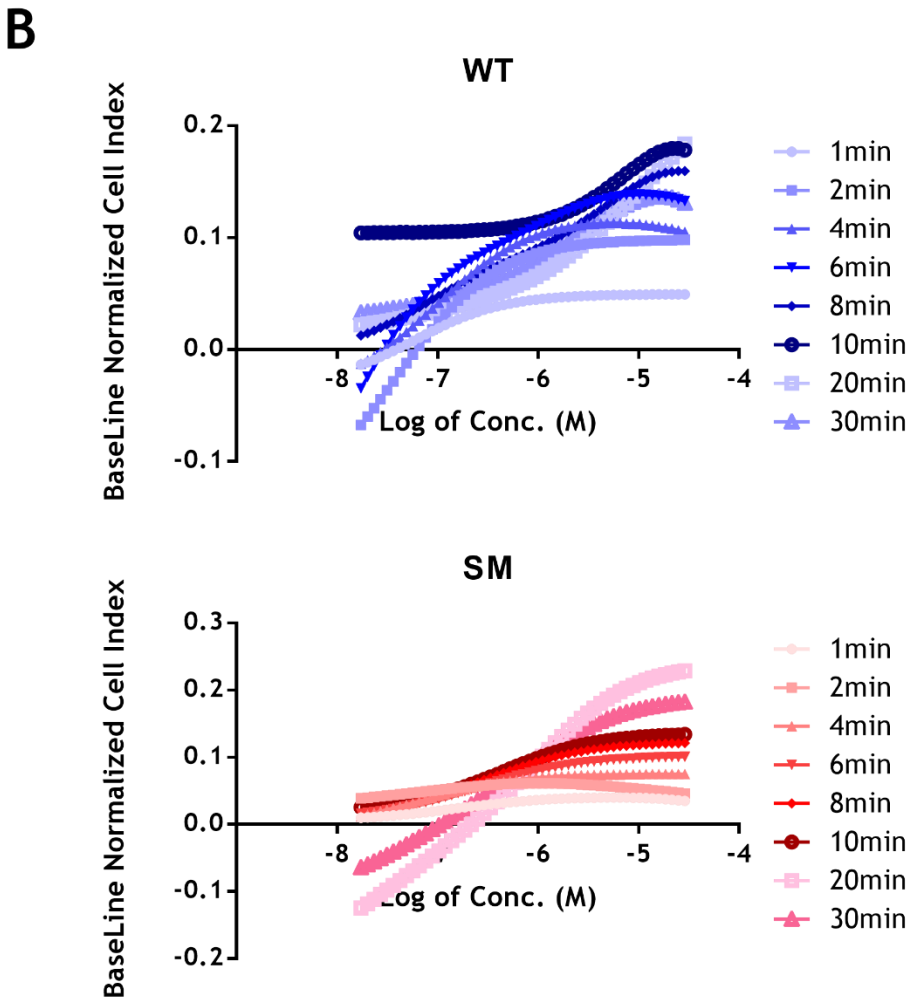

Figure 3.13 Concentration-response curves describing the baseline normalized cell index up to 30 minutes after the ISO treatment. Data represents means of at least three independent experiments. HEK represents HEK cells that were used as a control group. WT represents HEK cells that overexpress wild type β_2AR while SM represents HEK cells that overexpress SUMO mutant β_2AR. (A) Concentration-response curves described the baseline normalized cell index displaced as Log of concentration (B) Data are presented desperately based on the mock HEK cells, wild type β_2AR overexpressed cells and K232R-K235R mutant β_2AR overexpressed cells (n=5).

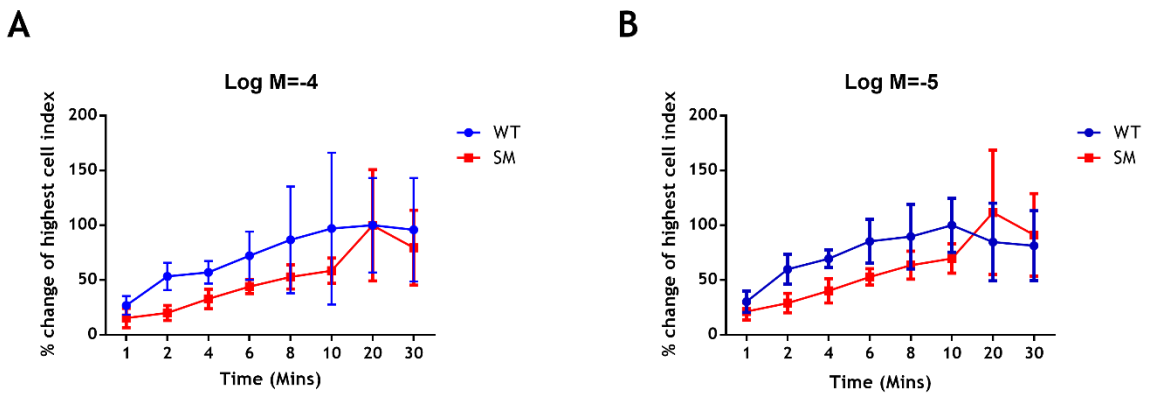

Figure 3.14 Percentage changes of the time to reach highest cell index at different concentration ISO stimulation (n=5). (A) Percentage changes for the cell to reach the highest CI at concentration Log M=-4. (B) Percentage changes for the cell to reach the highest CI at concentration Log M=-5.

3.3.3 SUMOylated β_2AR Protein Expression in different Animal Models and Human Tissues

3.3.3.1 PIASγ Overexpression in Healthy Adult Rabbit Cardiomyocytes

PIASγ over-expression has previously been shown to promote β_2AR SUMOylation (Wills, 2017). Adenoviral-mediated PIASγ gene transduction was carried out at a multiplicity of infection of 100 virus particles per well (vp/cell). This approach was successful in promoting expression of PIASγ within cardiomyocytes as it can be detected in the transduced adult rabbit cardiomyocytes via immunoblotting but not in control cells (**Figure 3.15**) which were not transduced with PIASγ adenovirus. Analysis was performed by student t-test resulted in data that indicated a significant increase in expression following adenoviral-mediated PIASγ gene transfection (**Figure 3.15B**).

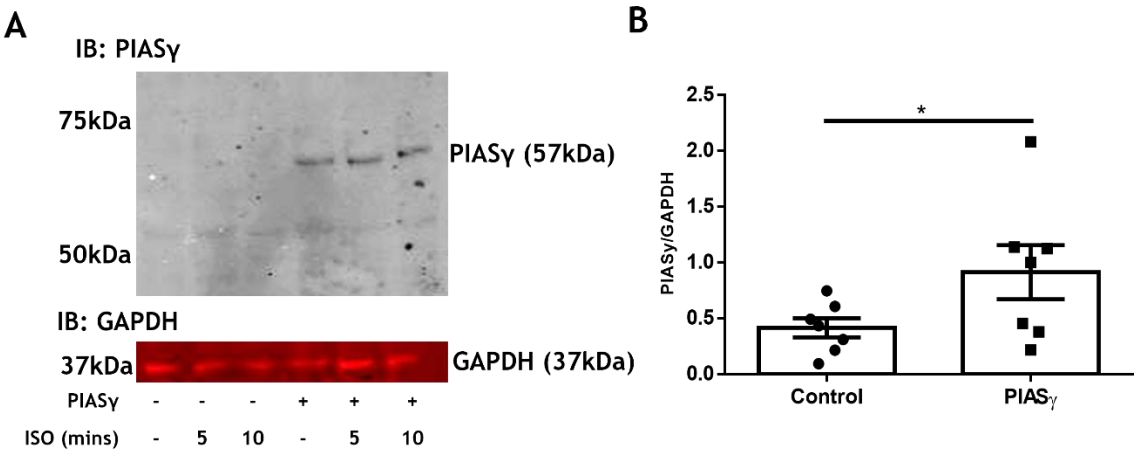

Figure 3.15 Adenoviral PIASγ was successfully transduced into adult rabbit cardiomyocytes. Cardiomyocytes overexpressing PIASγ via adenovirus transduction and mock transduction were stimulated with 10μM ISO for 5 and 10 minutes. Western blotting with an antibody against PIASγ detected bands at 57kDa showed which were PIASγ. (*p<0.05) (A) Representative blots shown. (B) Quantifications of bands in A are displayed as mean ± SEM, N=7, *p<0.05.

The PIASγ adenovirus was used to increase PIASγ expression in adult rabbit cardiomyocytes **Figure 3.15**. The effect of the increased levels of the SUMO-E3 ligase on β_2AR signalling was assessed. Cardiomyocytes were treated with 10μM isoprenaline for 5 or 10 minutes to activate the β_2AR signalling pathway. Downstream signals that had previously been shown to be correlates of β_2AR signalling were evaluated by western blotting. Stimulation of cardiomyocytes with isoprenaline had previously shown to result in an elevation of 1) PKA phospho-substrates ERK MAP Kinase activation, and 2) PKA cytosolic activity (Baillie et al., 2002). The effects of β_2AR SUMOylation of these downstream signals was evaluated (**Figure 3.16**&**Figure 3.17**). As with the HEKβ_2 cells above (**Figure 3.6**), ISO treatment caused an expected increase in PKA phospho-substrates in both control and PIASγ over-expressing cells (**Figure 3.16**)(N=5). There were no significant differences between the increases seen at 10 minutes for both sets of cells suggesting that SUMOylation does not alter cAMP production/PKA activation. When assessing the phospho-ERK signal following β_2AR activation, the first noticeable difference between the HEKβ_2 cells above was that ERK activation was high under basal conditions without ISO treatment (**Figure 3.17**). Presumably, this difference reflects the disparity between the model cell and the physiologically relevant cell which is actively beating. Unexpectedly, ISO caused a reduction in ERK phosphorylation in the ARVMs. The cardiomyocytes transduced with PIASγ and stimulated with 10μM isoprenaline for 10 minutes exhibited approximately 91% less activation in ERK compared to the PIASγ cardiomyocytes under basal conditions. (**Figure 3.17**) (N=7) (*$p<0.05$). This data is in contrast to that published for NRVMs that showed an increase in phosphor-ERK following ISO treatment attributed to Gs to Gi “switching” (Baillie et al., 2002).

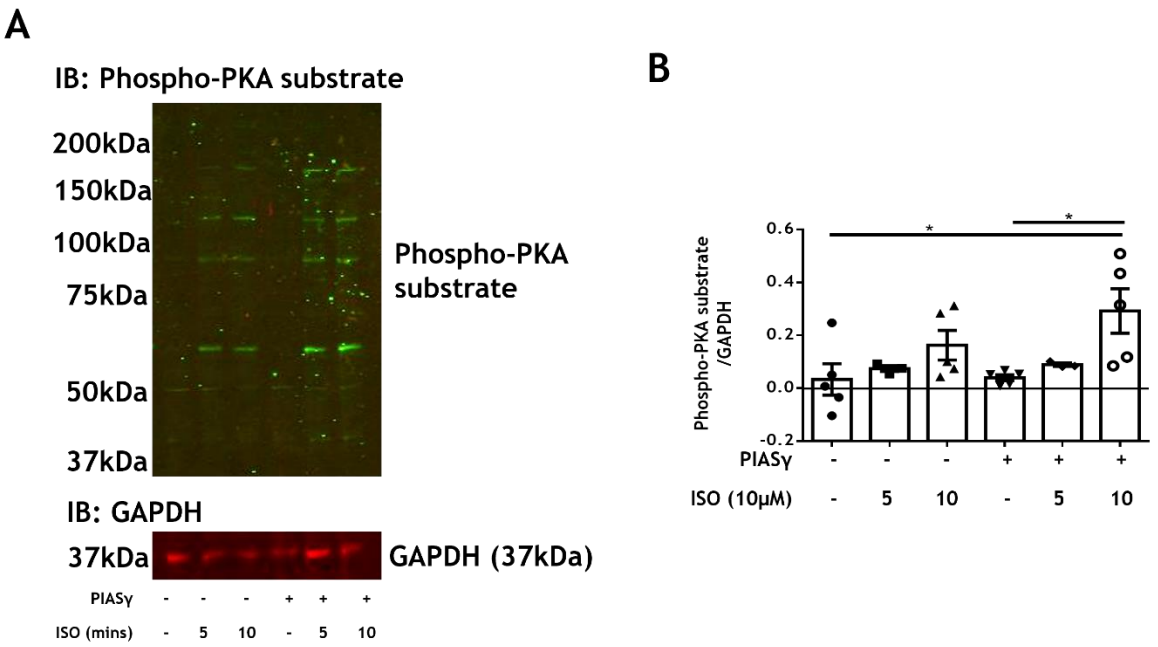

Figure 3.16 PIASγ Transduction increases isoprenaline-mediated PKA cytosolic activity. (A&B) Cardiomyocytes transduced with PIASγ to promote β_2AR SUMOylation and cardiomyocytes without transduction were stimulated with 10μM isoprenaline for 5 and 10 minutes. SUMOylation of the β_2AR caused a significant increase in PKA activity after 10 minutes stimulation of 10μM isoprenaline in comparison of cardiomyocytes without PIASγ transduction and 10μM isoprenaline treatment. Primary concentration 1:1000, secondary concentration 1:5000. (A) Representative blots shown. (B) Data are displayed as mean ± SEM, (N=5) (*p<0.05).

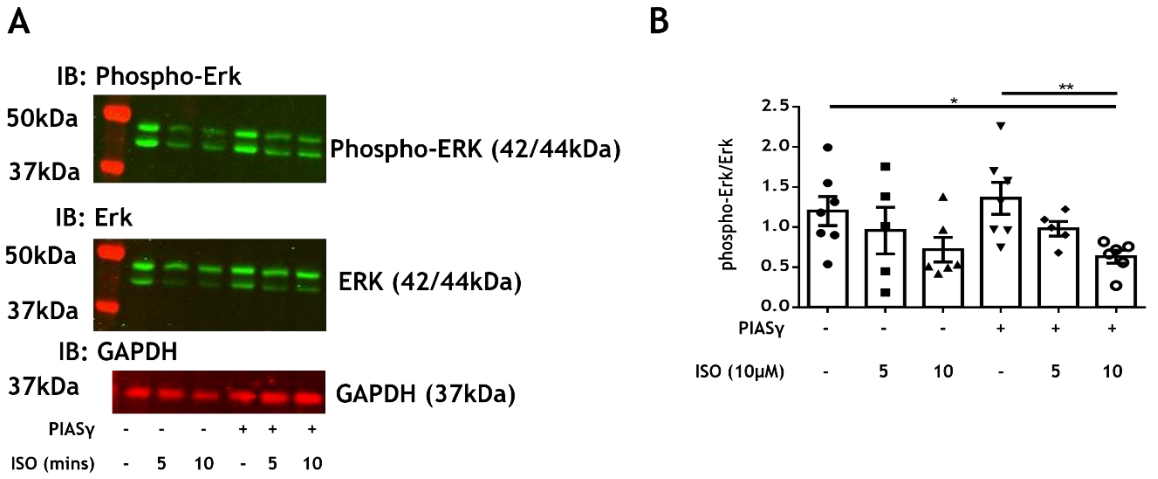

Figure 3.17 PIASγ Transduction decreases isoprenaline-mediated ERK activation. (A&B) Cardiomyocytes transduced with PIASγ to promote β_2AR SUMOylation and cardiomyocytes without transduction were stimulated with 10μM isoprenaline for 5 and 10 minutes. SUMOylation of the caused β_2AR a significant difference in phos-ERK expression at basal levels and after transduced with PIASγ and 10 minutes isoprenaline stimulation, and also compared to the basal level after transduced with PIASγ. Primary concentration 1:1000, secondary concentration 1:5000. (A) Representative blots shown. (B) Data are displayed as mean ± SEM, (N=7) (*p<0.05, *p<0.01).

3.3.3.2 Human Heart Tissue from Cardiac Diseases

As I have validated the SUMO-site specific (K235) antibody, this gave me the opportunity to look at SUMO modification of the β_2AR in healthy and diseased human heart samples. Samples were a kind gift from Dr. Ken Campbell, University of Kentucky. The epicardium is the outermost layer of the heart while the endocardium is the innermost layer of the heart (Road, 1980). The endocardium and epicardium tissues were both collected in this experiment and blotted with the antibody. All western blots were performed double blinded. The gel loading order is listed in **Table 3.1.** and the detailed patient information was recorded at the analysis stage and shown in **Table 3.2**. Samples were subjected to western blotting to determine whether any disease associated trends in β_2AR SUMOylation could be discovered.

Gel loading order:

No.	1	2	3	4	5	6	7	8	9	10	11	12	13
Sample	D61ZE LV	B23E 3 LV	2B487 LV	632FD LV	31331 LV	4B3FA LV	BC90C LV	CB8AS LV HT	3F6DC LV	4D931 LV	8E8D8 LV	92CDC LV3	632FD LV
Endo/ Epicardium	epi	epi	epi	endo	epi	endo	epi	epi	epi	endo	epi	Not specifi ed	epi

No.	14	15	16	17	18	19	20	21	22	23	24	25	26
Sample	BO64 4 LV	AF1FF LV	3F6D C LV	D61ZE LV	BC90 C LV	C3B57 LV	BO64 4 LV	31331 LV	5155DL V	C3B57 LV	D8822 LV	A7A62 LV	4B3FA LV
Endo/ Epicardium	epi	endo	endo	endo	endo	epi	endo	endo	epi	endo	endo	epi	epi

No.	27	28	29	30	31	32	33	34	35	36	37	38	39
Sample	8296A LV	97CD C LV1 HT	D0F54 LV	8296A LV	CB8A 5 LV HT	14C39 LV3	4D931 LV	AF1FF LV	D0F54 LV	8E8D8 LV	5155D LV	B8BE2 LV HT	2B487 LV
Endo/ Epicardium	epi	Not specif ied	epi	endo	endo	not specifi ed	epi	epi	endo	endo	endo	endo	endo

No.	40	41	42	43	44	45	46	47	48	49	50	51	52
Sample	EF5CB LV3 HT	B23E 3 LV	FE8E2 LV	DA820 LV	5845F LV	6DB85 LV	8CB30 LV	24713 LV	05FF7 LV	F8EE8 LV	7CE52 LV	FE8E2 LV	FC3CB LV
Endo/ Epicardium	Not specif ied	endo	endo	epi	epi	endo	endo	endo	endo	endo	endo	epi	endo

No.	53	54	55	56	57	58	59	60	61	62	63	64	65
Sample	DA820 LV	FC3C B LV	6DB85 LV	9D7E9 LV	F8EE8 LV	58545 F LV	046E1 LV	7CE52 LV	8CB30 LV	046E1 LV	24713 LV	05FF7 LV	9D7E9 LV
Endo/ Epicardium	endo	epi	epi	endo	epi	endo	endo	epi	epi	epi	epi	epi	epi

Table 3.1 Order of gel loading for human heart tissue. 15-well gels were used in this experiment, each table listed the loading order for one gel. Endo represents endocardium tissue. Epi represents epicardium tissue. The combination of letters and numbers are the samples code for each tissue sample.

A

Record ID	Case type	Heart failure type	Primary diagnosis
2B487 epi and endo	Organ donor		
3F6DC epi and endo	Heart transplant	Ischemic	Ischemic cardiomyopathy
4B3FA epi and endo	Organ donor		
4D931 epi and endo	Organ donor		
8E8D8 epi and endo	Heart transplant	Ischemic	Ischemic cardiomyopathy
14C39 Not specified	Heart transplant	Ischemic	Ischemic cardiomyopathy
97CDC Not specified	Heart transplant	Ischemic	Ischemic cardiomyopathy
632FD epi and endo	Organ donor		
5155D epi and endo	Organ donor		
8296A epi and endo	Heart transplant	Ischemic	Ischemic cardiomyopathy
31331 epi and endo	Organ donor		
A7A62 Epi	Heart transplant	Ischemic	Ischemic heart failure
AF1FF epi and endo	Heart transplant	Ischemic	Chronic systolic heart failure
B0644 epi and endo	Heart transplant	Ischemic	Ischemic cardiomyopathy
B8BE2 endo	Heart transplant	Ischemic	Ischemic heart failure
B23E3 epi and endo	Organ donor		
BC90C epi and endo	Organ donor		
C3B57 epi and endo	Heart transplant	Ischemic	Ischemic cardiomyopathy
CB8A5 epi and endo	Heart transplant	Ischemic	Ischemic cardiomyopathy
D0F54 epi and endo	Organ donor		
D612E epi and endo	Organ donor		
D8822 endo	Heart transplant	Ischemic	Ischemic heart failure and post-MI pericarditis
EF5CB Not specified		Ischemic	Ischemic heart failure
046E1 epi and endo	Heart transplant	Ischemic	Ischemic cardiomyopathy
05FF7 epi and endo	Heart transplant	Ischemic	Ischemic HFrEF
24713 epi and endo	Organ donor		
5845F epi and endo	Heart transplant	Ischemic	Ischemic Cardiomyopathy s/p MI
6DB85 epi and endo	Heart transplant	Ischemic	HFrEF from Ischemic cardiomyopathy
7CE52 epi and endo	Heart transplant	Ischemic	Ischemic heart failure
8CB30 epi and endo	Organ donor		
9D7E9 epi and endo	Heart transplant	Ischemic	Ischemic cardiomyopathy
DA820 epi and endo	Heart transplant	Ischemic	Ischemic cardiomyopathy
F8EE8 epi and endo	Heart transplant	Ischemic	Ischemic cardiomyopathy
FC3CB epi and endo	Organ donor		
FE8E2 epi and endo	Heart transplant	Ischemic	Chronic systolic HF

B

Case type (Primary diagnosis)	Patient Numbers	Sample Numbers
Health	13	26
Ischemic Cardiomyopathy	13	24
Ischemic heart failure	4	5
Chromic systolic heart failure	1	2
Ischemic heart failure and post-MI pericarditis	1	1
Ischemic HFrEF	1	2
HFrEF from Ischemic cardiomyopathy	1	2
Chronic systolic HF	1	2
Total	35	64

Table 3.2 Human heart tissue information. (A) List of case type, heart failure type and primary diagnosis of each patient that provides heart tissue. (B) Patient numbers and sample numbers count catalogued based on the primary diagnosis.

Firstly, there was no significant change in the ratio of SUMOylated β_2AR to total β_2AR when control and diseased myocardium samples were compared (**Figure 3.18B, D&F**). On the other hand, total β_2AR was significantly increased in diseased samples (**Figure 3.18C, E&G**). Expression of intermediates in the SUMO pathway SUMO E2 ligase UBC9, E3 ligase PIASγ, SUMO-1 and SUMO-2/3 remained constant, and no significant changes were identified when comparing disease to control tissue. (**Figure 3.19**-**Figure 3.22**). However, there was a change in -phospho-PKA substrate level which increased significantly in disease myocardium (**Figure 3.23**). Overall, the level of PKA phosphorylated β_2AR remained constant between the healthy group and disease group, but there was a difference in diseased patients that received beta-blocker treatment where the level of PKA phosphorylated β_2AR decreased compared to the patients without beta-blocker treatment and the healthy group (**Figure 3.23D**). Beta-blockers prevent the ligand from binding to the β_2AR by competing for the binding site. The level of phosphorylated β_2AR dropped dramatically if samples came from patients taking beta-blockers compared to those that haven't and the healthy group. Interestingly, the patients with heart disease but without beta-blockers had an increase of phosphorylated β_2AR over total β_2AR compared to healthy samples and significantly improved compared with beta-blocker treatment group (**Figure 3.24D**). Phosphorylated extracellular signal-regulated kinases (Erk) increased after heart failure while the total Erk on the other hand, is decreasing (**Figure 3.25**). After the beta-blocker treatment, the ratio of phosphorylated Erk over total Erk decreases largely compared to both diseased samples without treatment and the healthy group.

A

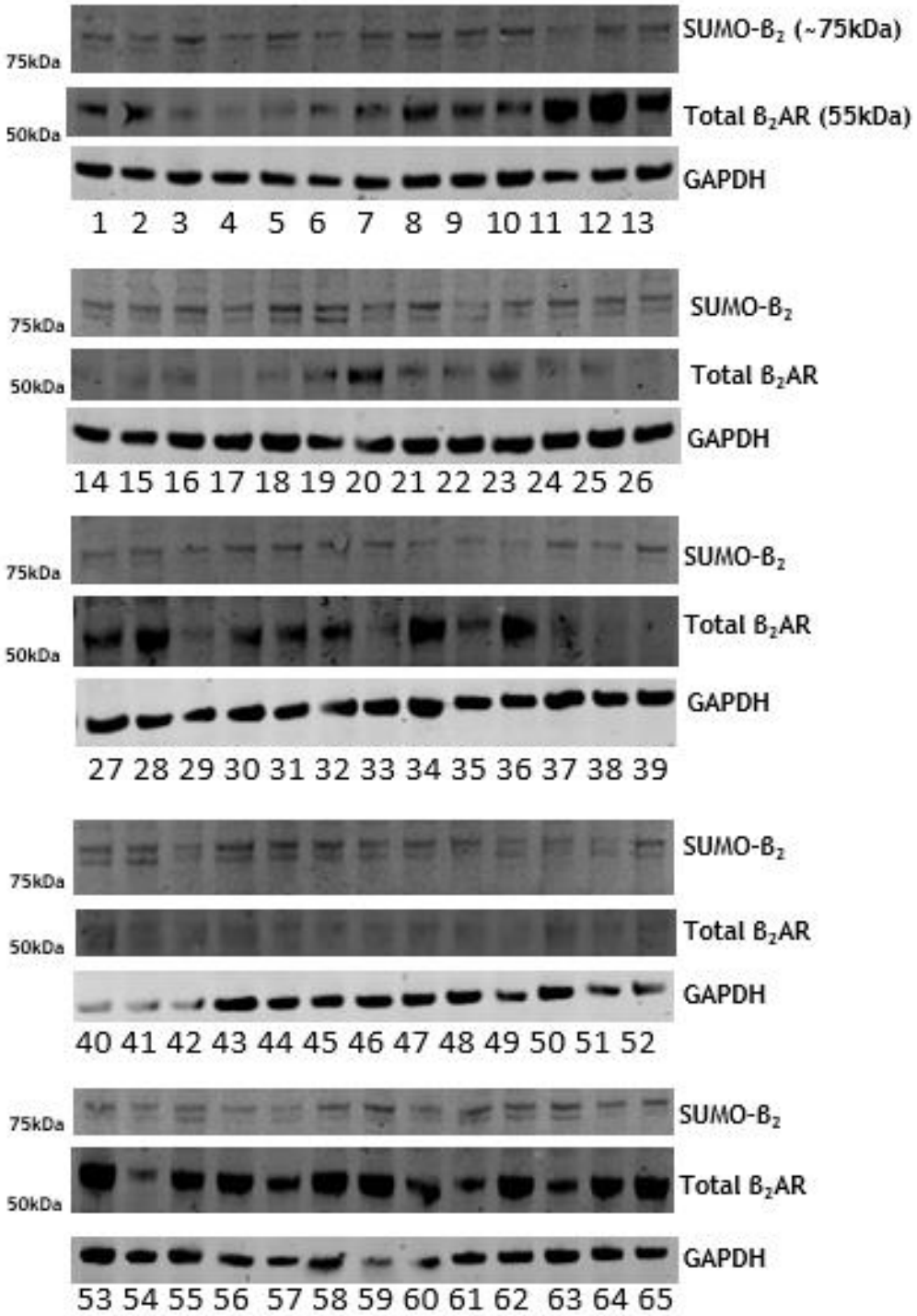
75kDa
50kDa
SUMO-β2 (~75kDa)
Total β2AR (55kDa)
GAPDH
1 2 3 4 5 6 7 8 9 10 11 12 13
SUMO-β2
Total β2AR
GAPDH
14 15 16 17 18 19 20 21 22 23 24 25 26
27 28 29 30 31 32 33 34 35 36 37 38 39
40 41 42 43 44 45 46 47 48 49 50 51 52
53 54 55 56 57 58 59 60 61 62 63 64 65

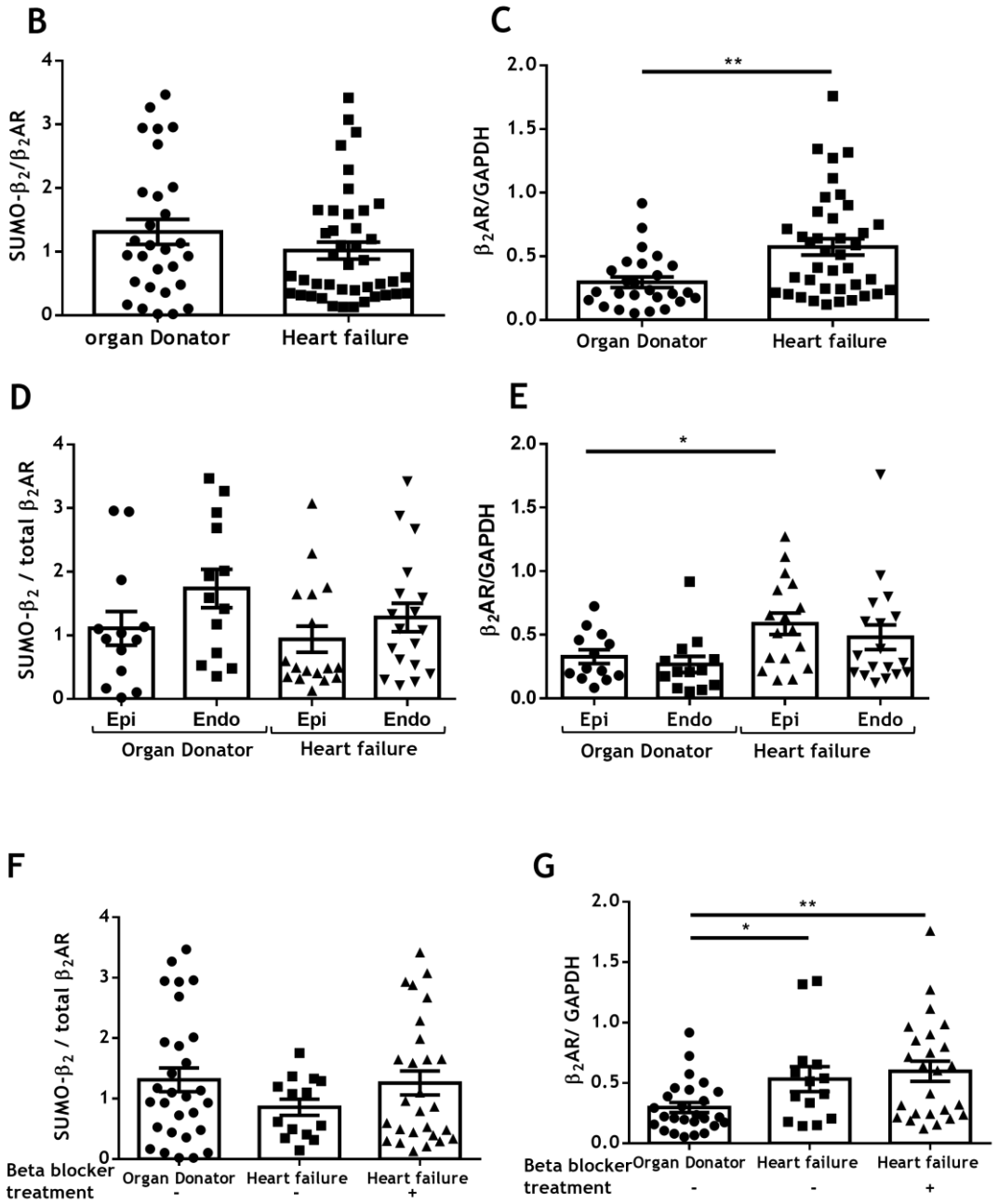

Figure 3.18 SUMO-ß$_2$ was reduced in human diseased myocardium while total ß$_2$ expression increased. (A) Human heart tissue samples were immunoblotted for SUMO-ß$_2$, total ß$_2$AR and GAPDH as a loading control. (B)-(G) Quantitative analysis revealed that the expression of SUMO-ß$_2$ (as a ratio of total ß$_2$AR) was reduced in diseased myocardium but reversed after receiving beta-blocker treatment in diseased patients. The expression of total ß$_2$AR was increased in diseased samples. Student *t*-test between every two groups were performed. Data are displayed as mean ± SEM, n=26 healthy, n=38 diseased.

A

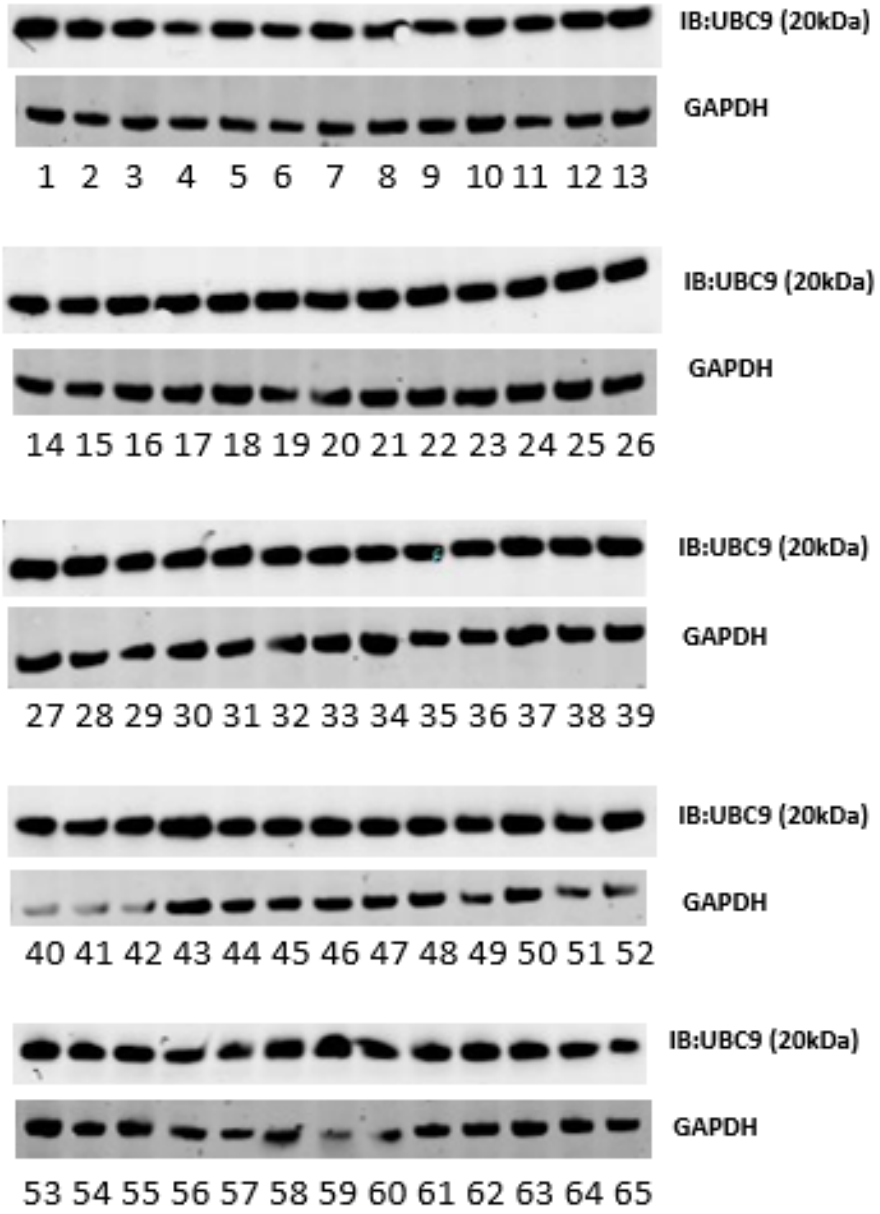
IB:UBC9 (20kDa)
GAPDH
1 2 3 4 5 6 7 8 9 10 11 12 13
IB:UBC9 (20kDa)
GAPDH
14 15 16 17 18 19 20 21 22 23 24 25 26
IB:UBC9 (20kDa)
GAPDH
27 28 29 30 31 32 33 34 35 36 37 38 39
IB:UBC9 (20kDa)
GAPDH
40 41 42 43 44 45 46 47 48 49 50 51 52
IB:UBC9 (20kDa)
GAPDH
53 54 55 56 57 58 59 60 61 62 63 64 65

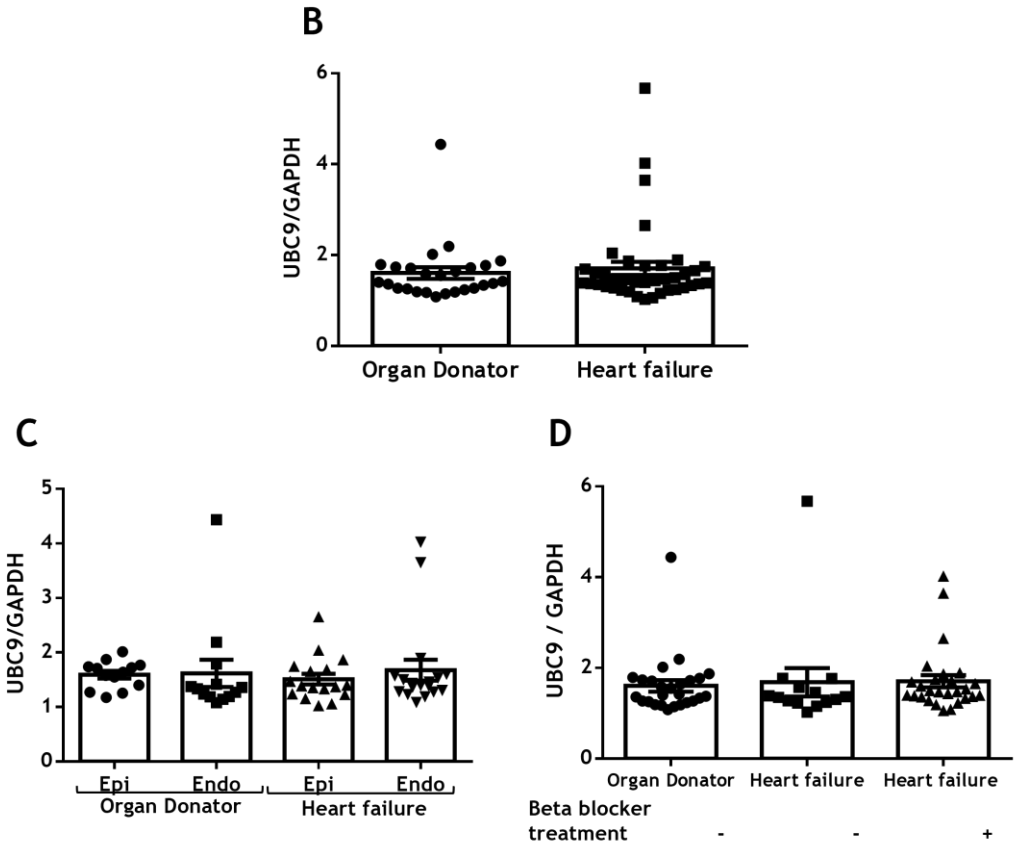

Figure 3.19 Expression of UBC9 was not affected by human heart disease. (A) Human heart tissue samples were immunoblotted for UBC9 and GAPDH as a loading control. Quantitative analysis revealed that the expression of UBC9 was not affected by the pathophysiological state of the myocardium. (B)-(D) Student *t*-test between every two groups were performed. Data are displayed as mean ± SEM, n=26 healthy, n=38 diseased.

A

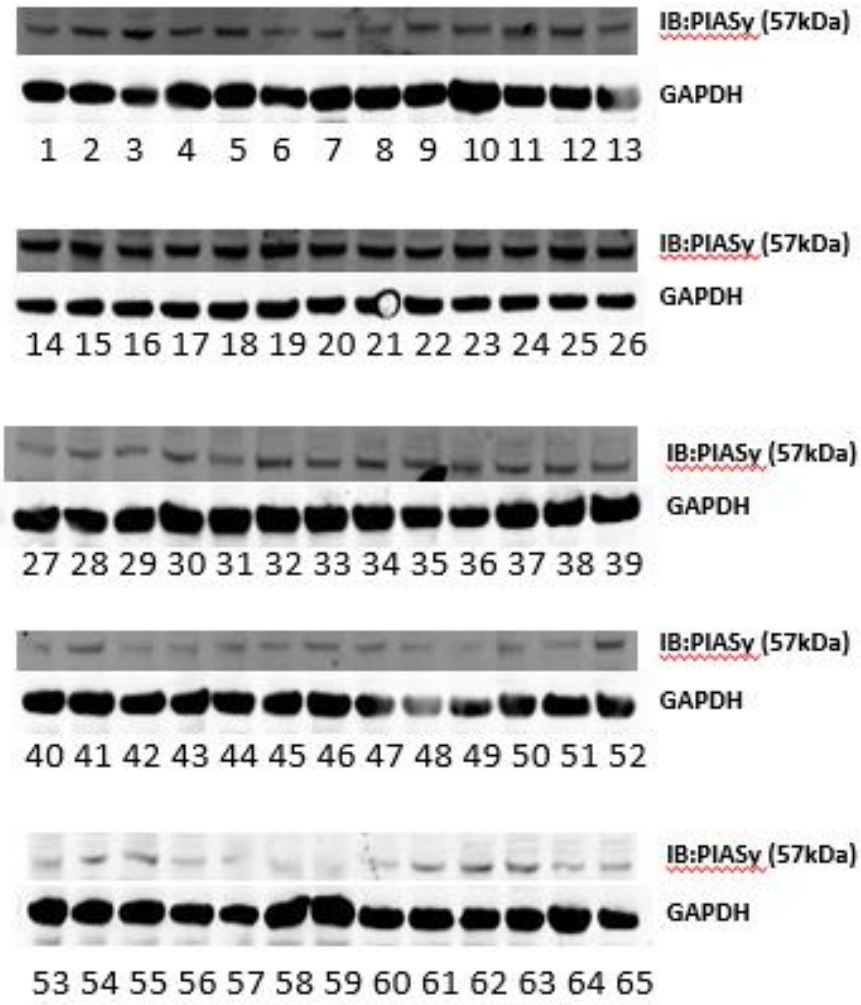
IB:PIASy (57kDa)
GAPDH
1 2 3 4 5 6 7 8 9 10 11 12 13
IB:PIASy (57kDa)
GAPDH
14 15 16 17 18 19 20 21 22 23 24 25 26
IB:PIASy (57kDa)
GAPDH
27 28 29 30 31 32 33 34 35 36 37 38 39
IB:PIASy (57kDa)
GAPDH
40 41 42 43 44 45 46 47 48 49 50 51 52
IB:PIASy (57kDa)
GAPDH
53 54 55 56 57 58 59 60 61 62 63 64 65

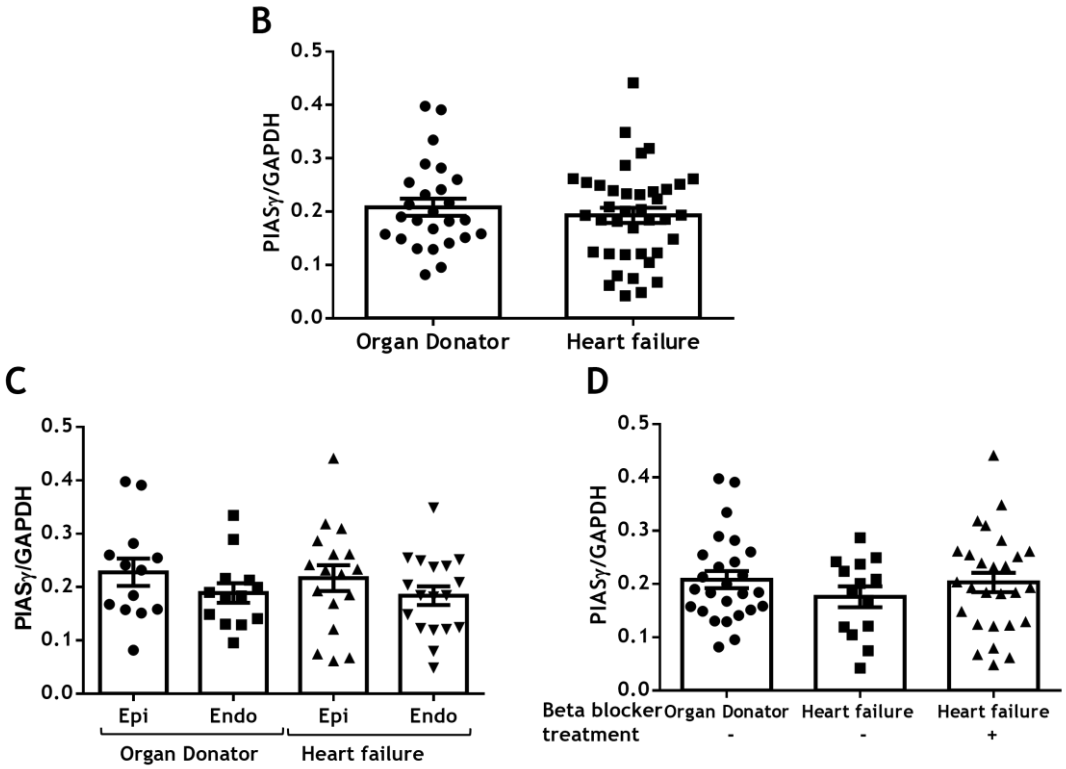

Figure 3.20 Expression of PIASγ was not affected by human heart disease. (A) Human heart tissue samples were immunoblotted for PIASγ and GAPDH as a loading control. Quantitative analysis revealed that the expression of SUMO was not affected by the pathophysiological state of the myocardium. (B) Student *t*-test between every two groups were performed. Data are displayed as mean ± SEM, n=26 healthy, n=38 diseased.

A

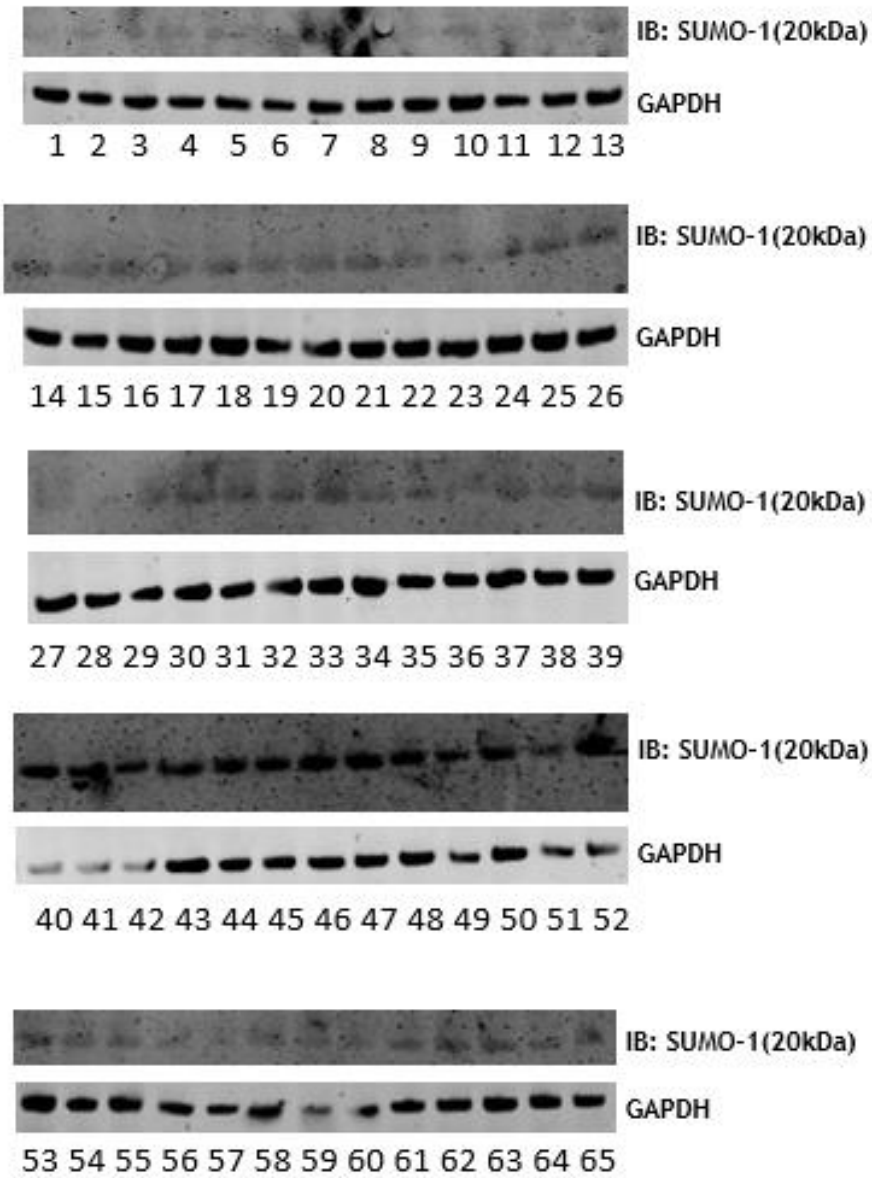
IB: SUMO-1(20kDa)
GAPDH
1 2 3 4 5 6 7 8 9 10 11 12 13
IB: SUMO-1(20kDa)
GAPDH
14 15 16 17 18 19 20 21 22 23 24 25 26
IB: SUMO-1(20kDa)
GAPDH
27 28 29 30 31 32 33 34 35 36 37 38 39
IB: SUMO-1(20kDa)
GAPDH
40 41 42 43 44 45 46 47 48 49 50 51 52
IB: SUMO-1(20kDa)
GAPDH
53 54 55 56 57 58 59 60 61 62 63 64 65

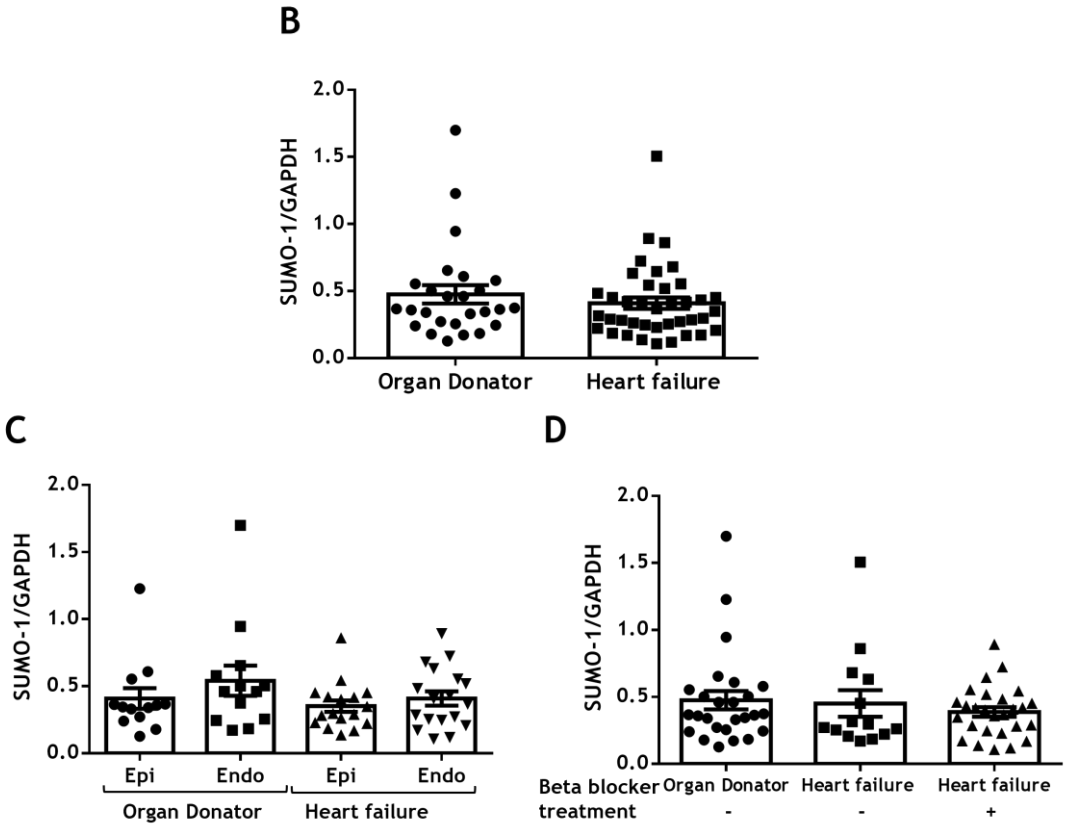

Figure 3.21 Expression of SUMO-1 was not affected by human heart disease. (A) Human heart tissue samples were immunoblotted for SUMO 1 and GAPDH as a loading control. Quantitative analysis revealed that the expression of SUMO 1 was not affected by the pathophysiological state of the myocardium. (B)-(D) Student *t*-test between every two groups were performed. Data are displayed as mean ± SEM, n=26 healthy, n=38 diseased.

A

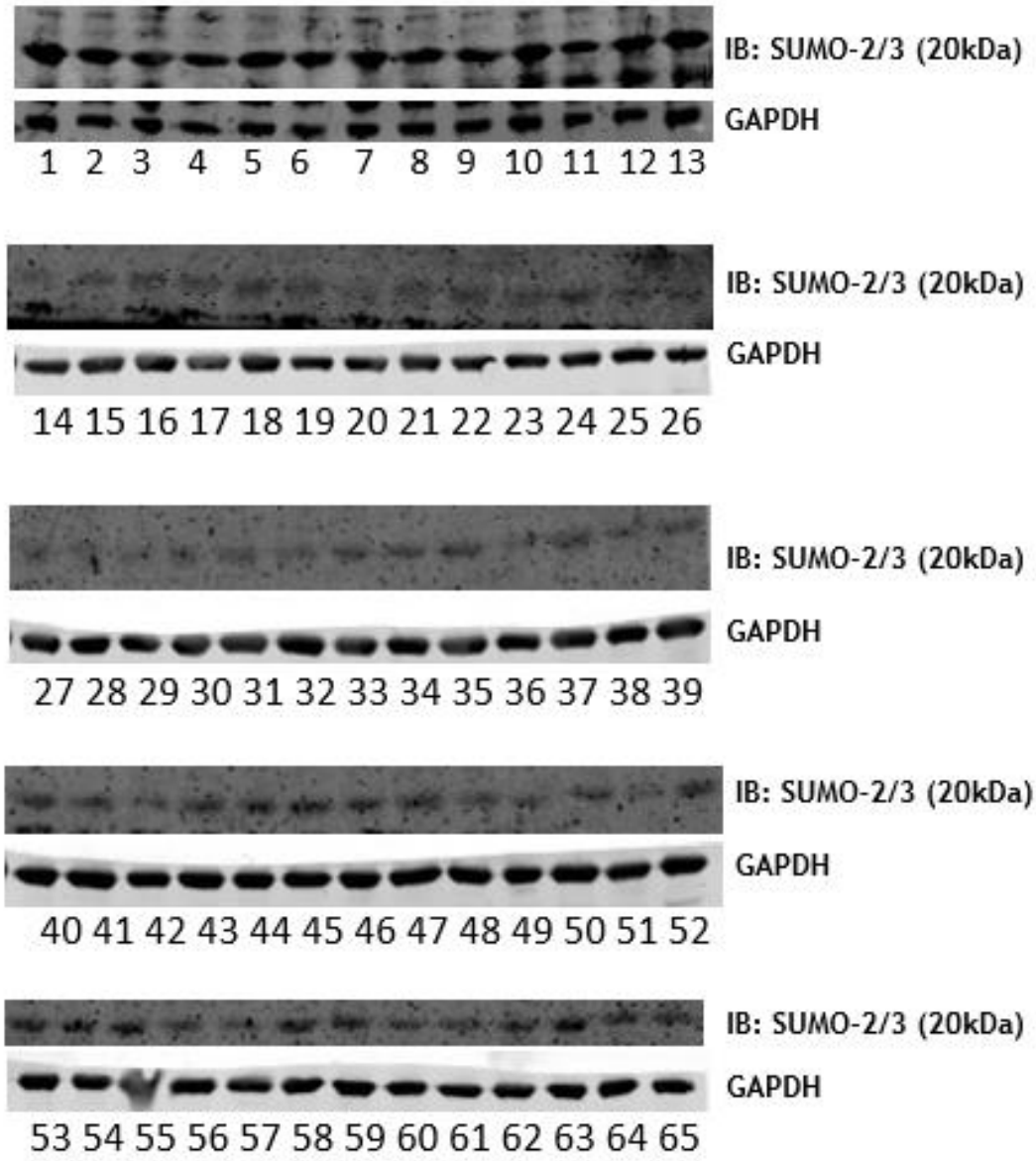
IB: SUMO-2/3 (20kDa)
GAPDH
1 2 3 4 5 6 7 8 9 10 11 12 13
IB: SUMO-2/3 (20kDa)
GAPDH
14 15 16 17 18 19 20 21 22 23 24 25 26
IB: SUMO-2/3 (20kDa)
GAPDH
27 28 29 30 31 32 33 34 35 36 37 38 39
IB: SUMO-2/3 (20kDa)
GAPDH
40 41 42 43 44 45 46 47 48 49 50 51 52
IB: SUMO-2/3 (20kDa)
GAPDH
53 54 55 56 57 58 59 60 61 62 63 64 65

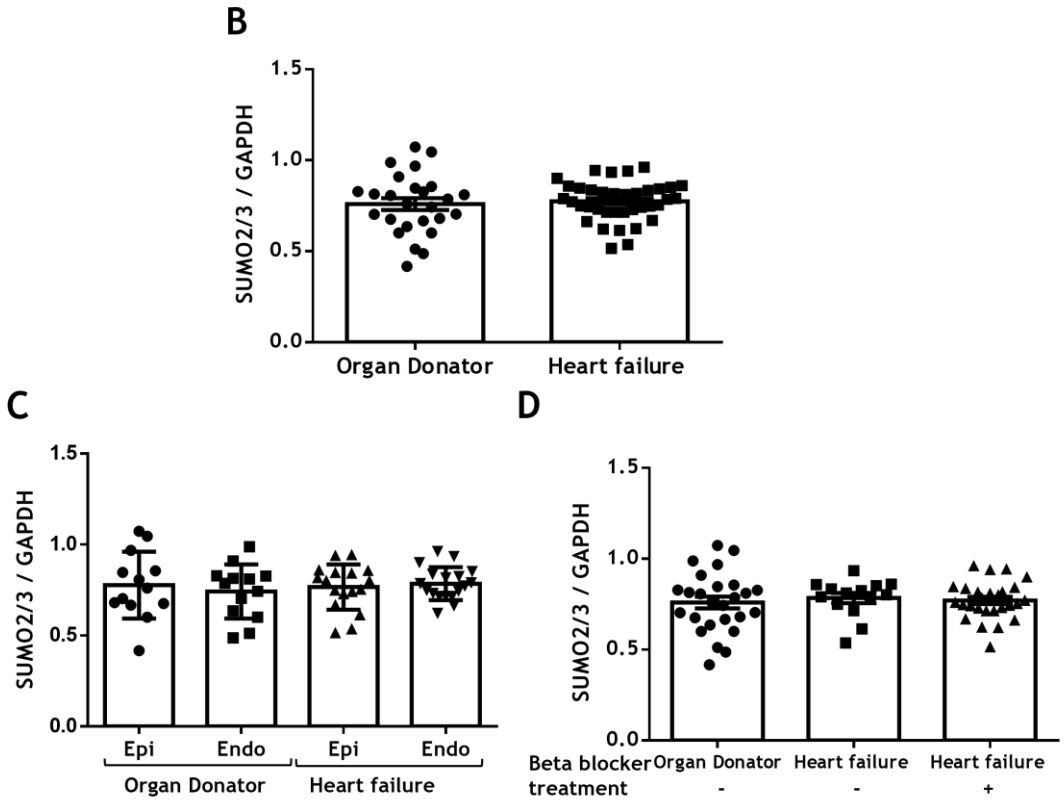

Figure 3.22 Expression of SUMO-2/3 was not affected by human heart disease. (A) Human heart tissue samples were immunoblotted for SUMO-2/3 and GAPDH as a loading control. Quantitative analysis revealed that the expression of SUMO-2/3 was not affected by the pathophysiological state of the myocardium. (B)-(D) Student *t*-test between every two groups were performed. Data are displayed as mean ± SEM, n=26 healthy, n=38 diseased.

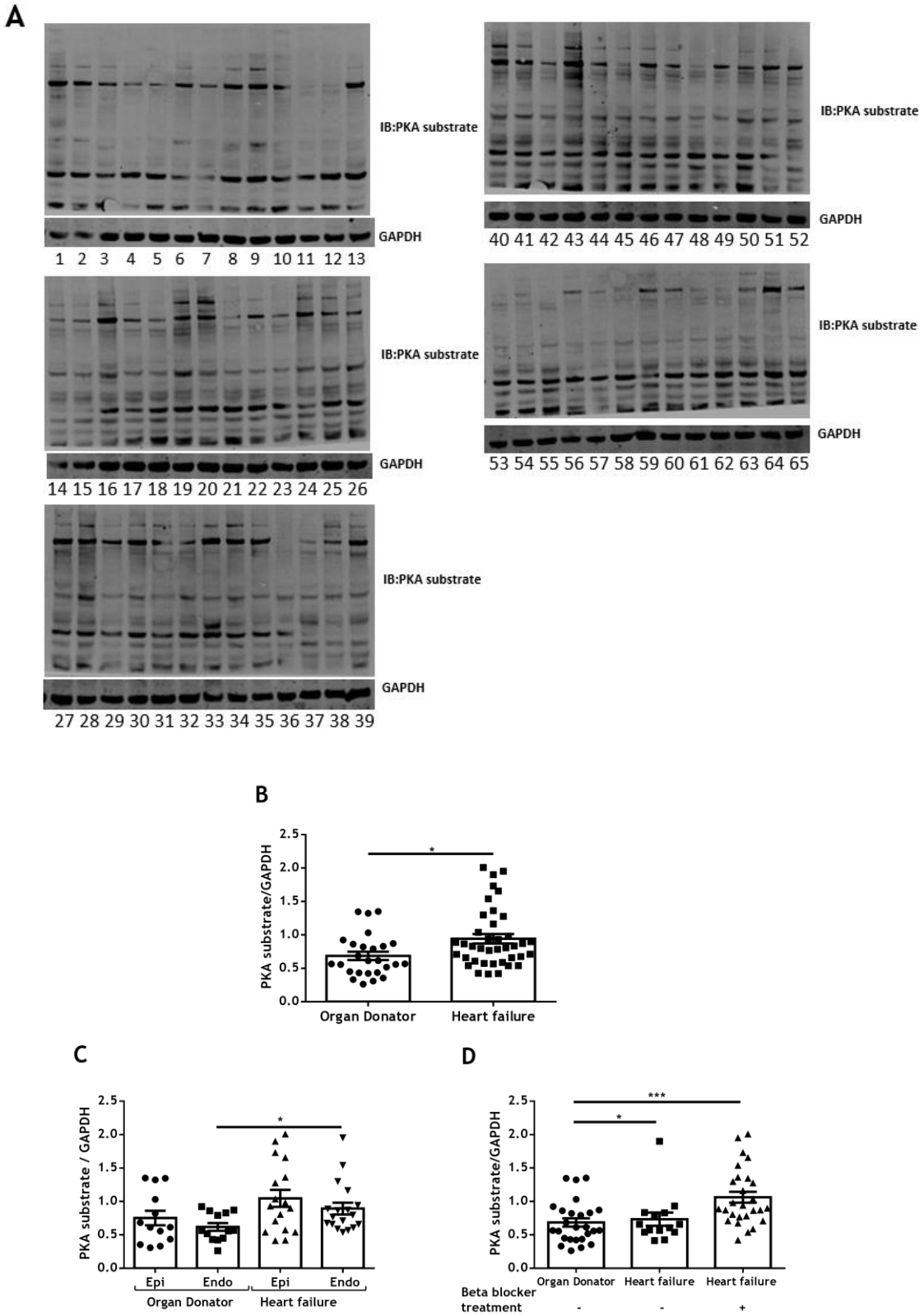

Figure 3.23 Expression of PKA substrate was increased in human heart diseases. (A) Human heart tissue samples were immunoblotted for PKA substrate and GAPDH as a loading control. Quantitative analysis revealed that the expression of PKA substrate was not increased by the pathophysiological state of the myocardium. (B)-(D) Student *t*-test between every two groups were performed. Data are displayed as mean ± SEM, n=26 healthy, n=38 diseased.

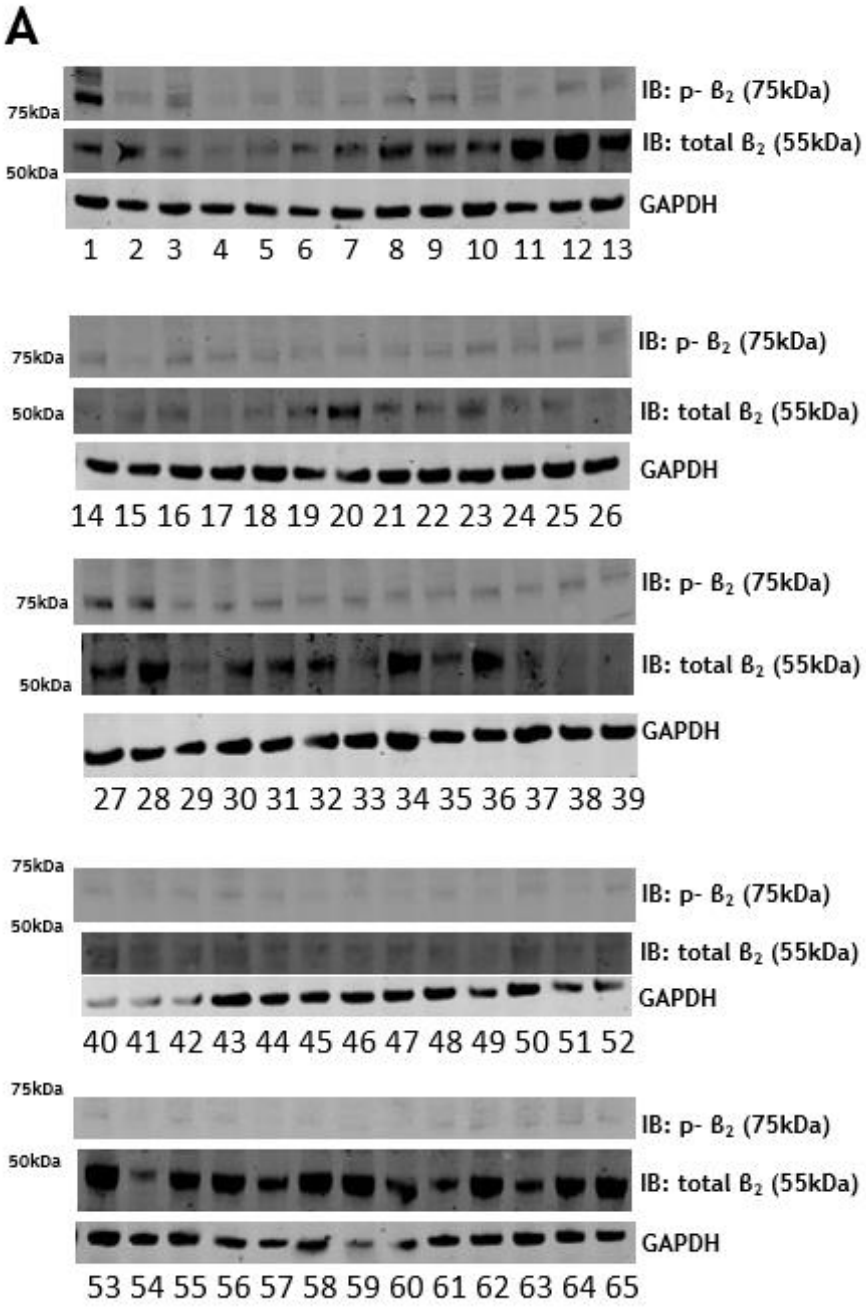
A
75kDa
50kDa
IB: p- β2 (75kDa)
IB: total β2 (55kDa)
GAPDH
1 2 3 4 5 6 7 8 9 10 11 12 13
14 15 16 17 18 19 20 21 22 23 24 25 26
27 28 29 30 31 32 33 34 35 36 37 38 39
40 41 42 43 44 45 46 47 48 49 50 51 52
53 54 55 56 57 58 59 60 61 62 63 64 65

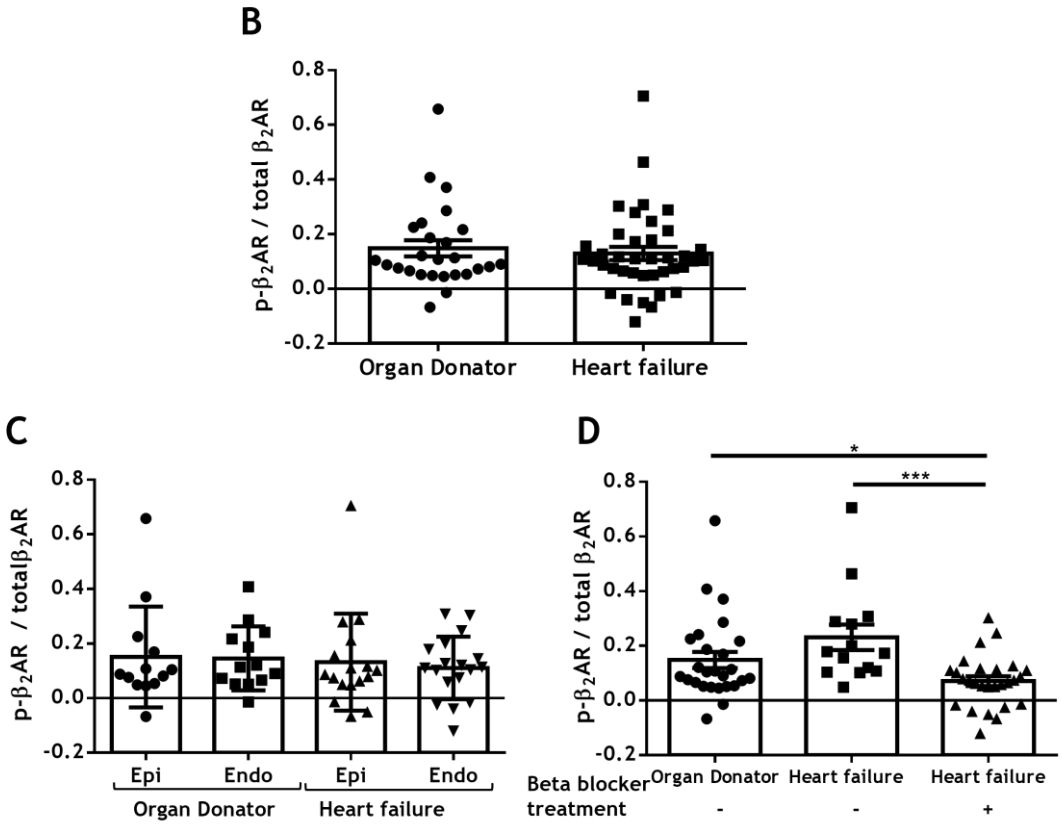

Figure 3.24 Expression of phosphorylated ß$_2$AR was decreased after receiving beta-blocker treatment in human heart disease patients. (A) Human heart tissue samples were immunoblotted for phosphorylated ß$_2$AR, total ß$_2$AR and GAPDH as a loading control. Quantitative analysis revealed that the expression of phosphorylated ß$_2$AR (as a ratio of total ß$_2$AR) was decreased after beta-blocker treatment in diseased patient. (B)-(D) Student *t*-test between every two groups were performed. Data are displayed as mean ± SEM, n=26 healthy, n=38 diseased.

A

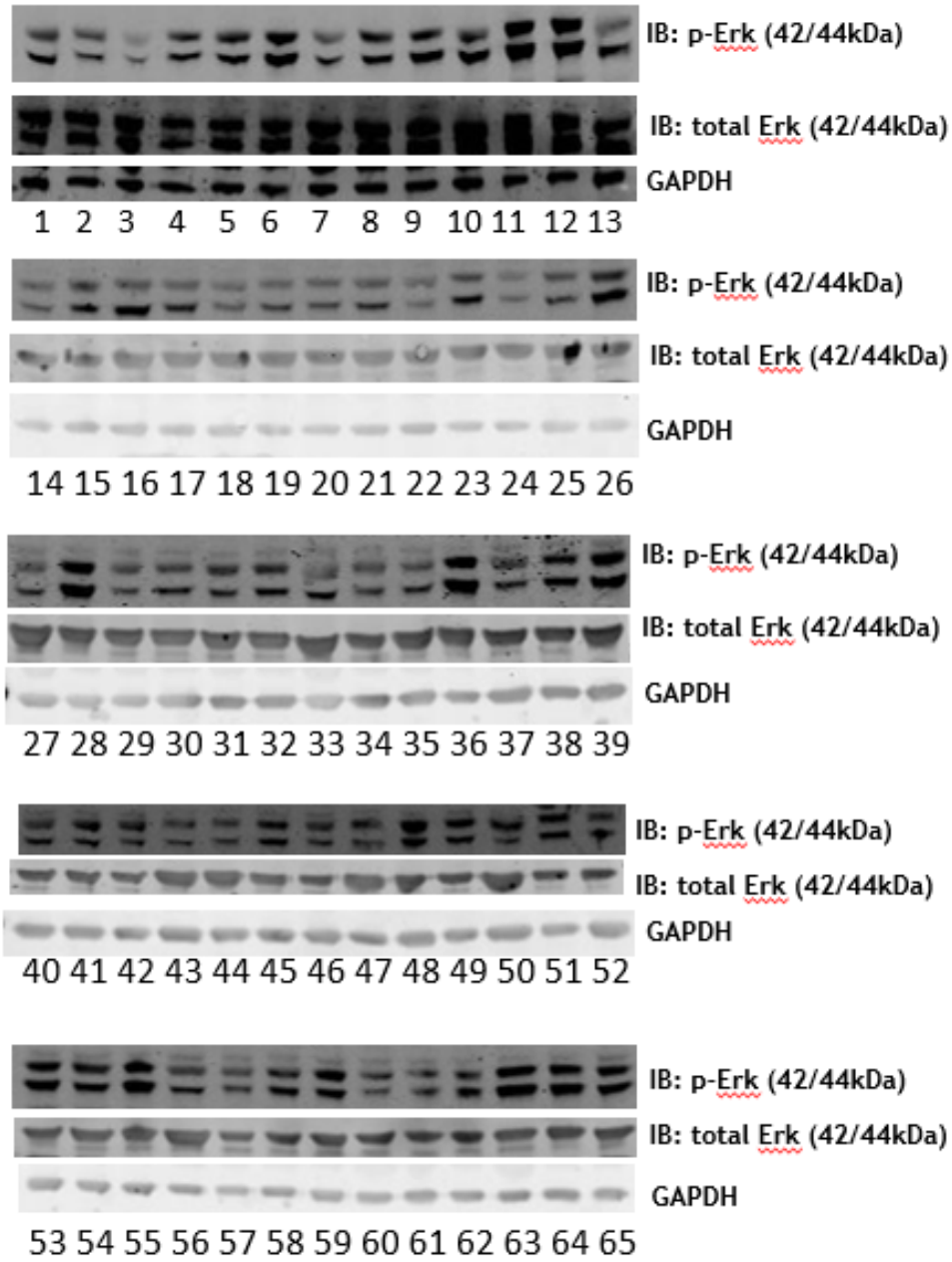
IB: p-Erk (42/44kDa)
IB: total Erk (42/44kDa)
GAPDH
1 2 3 4 5 6 7 8 9 10 11 12 13
IB: p-Erk (42/44kDa)
IB: total Erk (42/44kDa)
GAPDH
14 15 16 17 18 19 20 21 22 23 24 25 26
IB: p-Erk (42/44kDa)
IB: total Erk (42/44kDa)
GAPDH
27 28 29 30 31 32 33 34 35 36 37 38 39
IB: p-Erk (42/44kDa)
IB: total Erk (42/44kDa)
GAPDH
40 41 42 43 44 45 46 47 48 49 50 51 52
IB: p-Erk (42/44kDa)
IB: total Erk (42/44kDa)
GAPDH
53 54 55 56 57 58 59 60 61 62 63 64 65

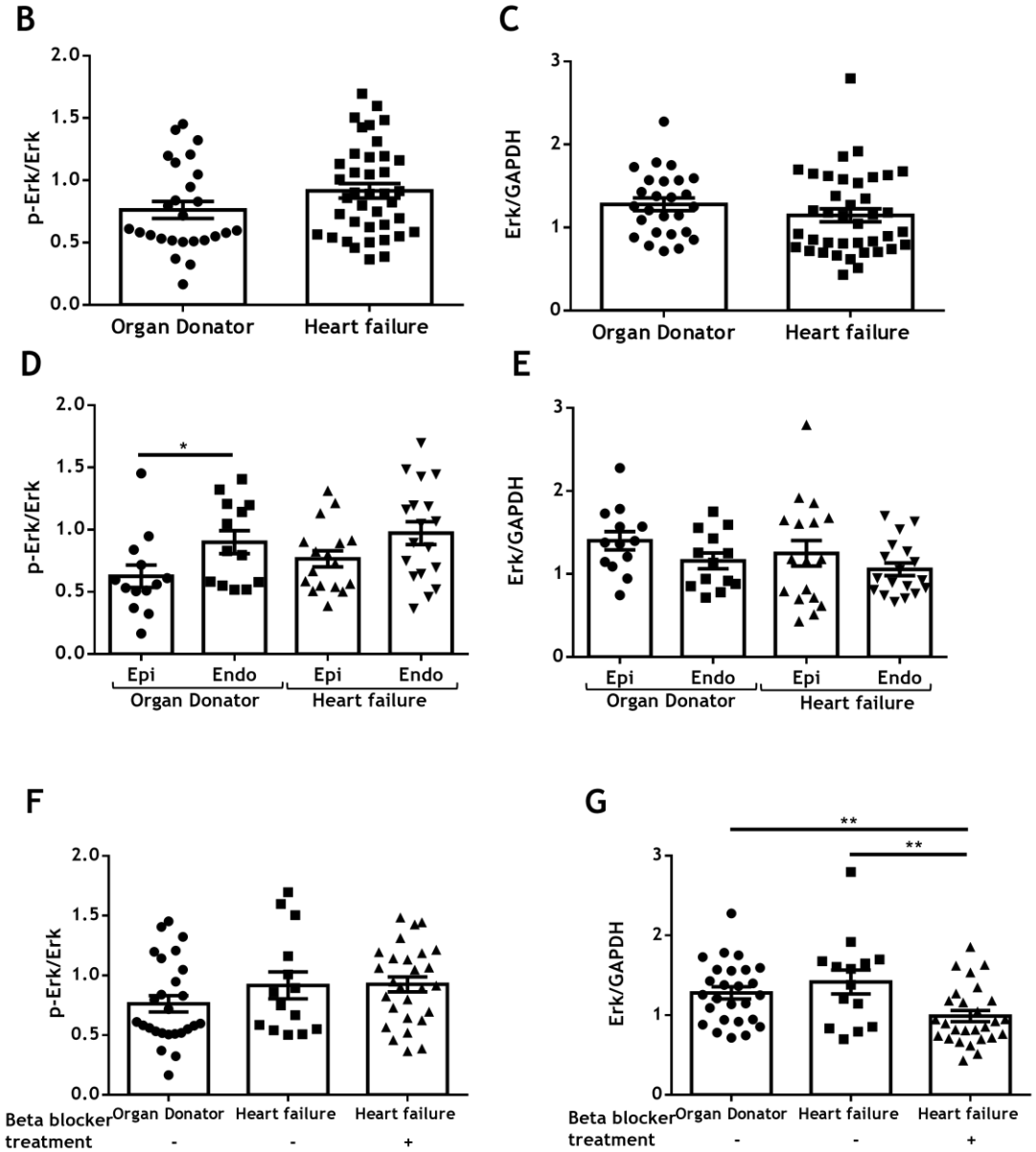

Figure 3.25 Expression of phosphorylated Erk was decreased after receiving beta-blocker treatment in human heart disease patients. (A) Human heart tissue samples were immunoblotted for phosphorylated Erk, total Erk and GAPDH as a loading control. Quantitative analysis revealed that the expression of phosphorylated Erk (as a ratio of total Erk) was decreased after receiving beta-blocker treatment in diseased patients. (B)-(G) Student *t*-test between every two groups were performed. Data are displayed as mean ± SEM, n=26 healthy, n=38 diseased.

3.4 Discussion

This study presents first evidence that β_2AR can be SUMOylated at 235K within the consensus motif KIDK 232-235. Initially, to detect the SUMOylated β_2AR, an *in vitro* SUMOylation assay was used in cell lysates to 'force' detectable SUMOylation. This assay was also used to allow the putative site to be identified using peptide arrays and in cell lysates with a bespoke SUMO-β_2 antibody. The data in this chapter shows that Baillie lab have developed a SUMO-site specific antibody that can detect SUMOylated β_2AR in cellular lysates, whole cells, and tissue. This is the first time to my knowledge that such an antibody has been produced.

Previously, the detection of SUMOylated substrate proteins has relied on detection of a band shift shown above the original band on western blots when probed for the substrate protein. For example, the UBC9 fusion-directed SUMOylation method has been used to drive SUMOylation of a variety of substrates where a slower migrating SUMOylated band can be detected. (Jakobs et al., 2007). On the other hand, immunoprecipitation of SUMO substrate protein products can be immunoblotted for SUMO paralogues (Kho et al., 2015b). None of these methods can directly detect SUMOylated β_2AR. Working with SUMOylation is difficult because only a small percentage of any substrate is SUMOylated at any time which presents a technical challenge. The development of the SUMO-β_2 antibody was developed to overcome this technical challenge. Direct detection has allowed me to characterize SUMO β_2AR in several ways including evaluation of clinical samples (shown in this chapter).

SUMOylation is an important post-translational modification that regulates GPCR signalling with more and more evidence in the recent decade. M1 muscarinic acetylcholine receptor (M1 mAChR) as a member of GPCR family has been recognized as a new substrate for SUMOylation (Xu et al., 2019). Xu and colleagues report that SUMOylation of the M1 mAChR increases the ligand-binding affinity for M1 mAChR, enhances down-stream signalling outputs and facilitates receptor endocytosis. My data suggests that these important receptor functions are not similarly changed in the case of β_2AR SUMOylation.

There are a group of non-GPCR type receptors that can be SUMOylated as well. These include nuclear receptor 4A (NR4A), thyroid hormone nuclear receptor (TR), T cell antigen receptor (TCR) and nuclear receptor, live receptor homolog 1 (LRH-1). In general, SUMOylation of these receptors influences protein stability, transcriptional activity, apoptosis, and protein-protein interaction (Zárraga-Granados et al., 2020) (Rytinki et al., 2012)(Stein et al., 2014) (Y. Y. Liu et al., 2015).

NR4A1 is a nuclear receptor that acts as a sensor of the cellular environment. It can regulate different processes such as metabolism, proliferation, and apoptosis. NR4A1 is a verified SUMO substrate and it's SUMOylation induces autophagic cell death. Lack of SUMOylation of NR4A1 increases transcriptional activity and alters the receptor's intracellular distribution (Zárraga-Granados et al., 2020).

The T cell antigen receptor (TCR) is another receptor that can be regulated by SUMOylation. Studies have shown that TCR activation depends on the SUMOylation cascade. In this case, it is not the receptor itself that gets modified but rather the SUMOylation of Phospholipase C-γ1 (PLC-γ1) that is important for receptor activation (Q. L. Wang et al., 2019). PLC-γ1 is tagged with SUMO-1 at K54 and K987 following TCR stimulation. SUMOylation at K54 is essential to promote PLC-γ1 binding to adaptor proteins, which in turn assembles PLC-γ1 micro clusters. This facilitates T cell activation and downstream NFAT activation and IL-2 production (Q. L. Wang et al., 2019). Interestingly, overexpression of PIAS constructs could enhance SUMOylation of PLC-γ1 and a K54R mutant effectively blocked downstream signalling of the TCR. This is in stark contrast to my data that showed little change in downstream signalling when the SUMO-site mutation of the $ß_2$AR was utilized. However, I have shown that the SUMOylation of $ß_2$AR is upregulated by E3 ligase PIASγ and that this modification is reversed following isoproterenol treatment although a signalling function has not been identified in my case.

B-arrestin is a well stablished protein regulator of GPCRs desensitization trafficking and signalling (Cabasso & Horowitz, 2015). B-arrestins can be SUMOylated and SUMOylation of B-arrestin2 promotes it's binding to GPCRs and

nuclear pore complexes (Nagi et al., 2020). SUMOylation of B-arrestin can also improve its association with the clathrin adaptor protein A2 and facilitate rapid β_2AR internalization (Sudha K. Shenoy & Lefkowitz, 2011). In the recent study of B-arrestin2 SUMOylation (Nagi et al., 2020), the Shenoy group used a B-arrestin2-SUMO-1 fusion protein which promoted the SUMOylation of B-arrestin2 to demonstrate that the intracellular trafficking of B-arrestin2 is regulated by this modification. Other functional changes that can occur on SUMOylation of arrestin proteins include inhibition of arrestin binding to the protein TRAF6 which results in enhanced TRAF6 mediated NFKB activation (N. Xiao et al., 2015a). Once again, in contrast to my data, SUMOylation of the major desensitizing protein for the β_2AR has well defined signalling consequences that I could not detect for SUMOylation of the β_2AR itself.

Antibodies designed to recognise post-translational modification (PTM) of the β_2AR only cover phosphorylation at different sites. The β_2AR can be phosphorylation by PKA and GRK as discussed previously, and commercially available antibodies have been designed against these sites. These reagents have facilitated study PTM of β_2AR by these kinases. The Shenoy group (2006) used the β_2AR phosphorylation antibodies from Santa Cruz Biotechnology to characterize PKA and GRK mediated β_2AR phosphorylation. The two antibodies they used are against 1) phospho-β_2AR at serines 345/346 by PKA; 2) phospho-β_2AR at serines 355/356 by GRK. Specifically, the Phospho-β_2AR 345/346 antibody was used to study the effects of various β_2AR mutations on PKA phosphorylation (Sudha K. Shenoy et al., 2006). Mutation of this PKA site on β_2AR made the receptor functionally uncoupled from Gs, resulting in a reduced cAMP increase after the receptor was stimulated by ISO. After testing the cell lysates via western blotting with the 345/346 antibody, it was confirmed that the mutated β_2AR was unable to be phosphorylated by PKA. The other phospho-β_2AR antibody (355/356) was also used in the study to test if the β_2AR could be phosphorylated in the presence of GRK5/6 but not GRK2. Data from the study suggested that β_2AR stimulation can activate the ERK MAPK signalling cascade in a β-arrestin-dependent manner, but independent from PKA-mediated Gs to Gi transition (Sudha K. Shenoy et al., 2006). I was unable to see any changes in PKA phosphorylation of the receptor or ERK signalling following overexpression of PIASγ to promote β_2AR SUMOylation.

In this chapter I have attempted to find a signalling function for β_2AR SUMOylation using a variety of techniques (signalling changes via western blotting, xCELLigence, analysis of human tissue), however no firm conclusions have been reached. It is clear that enhanced SUMOylation forced by PIASγ over-expression rapidly declines after ISO treatment suggesting that SUMOylation is involved in early signalling events however I can only speculate as to what the function is. Ubiquitination is another important PTM that plays a functional role in GPCR signalling. A mutation lacking in lysine residues of β_2AR has been used to study how ubiquitination may influence β_2AR signalling (Shenoy et al., 2001). The mutant β_2AR was not ubiquitinated, was internalized normally but was degraded ineffectively (Shenoy et al., 2001). The same group has shown that the ubiquitination of the β_2AR receptor happens on both the third intracellular loop and carboxyl tail of the β_2AR. It is important to identify the ubiquitination sites located in the third loop due to its role in receptor-G protein coupling or recruitment of B-arrestin to GRK mediated phosphorylation sites. Work on the crystal structure of β_2AR clearly illustrated the role of helix 3 and helix 6 in maintaining and switching the conformational balance from the inactive to the active state of the receptor after agonist-stimulation (Rasmussen et al., 2007)(Rosenbaum et al., 2002). One theory to explain this was that Lysine 263 in loop 3, in close proximity to Glu-268 in helix 6, might be essential for conformational change, Additionally, receptor activation may interrupt the “ionic lock” process facilitating agonist-mediated ubiquitination of the β_2AR (Sarker et al., 2011). These two domains are essential for definition of magnitude, extent and cellular destination of downstream signalling of the β_2AR mediated by both G protein and B-arrestin pathway (K. Xiao & Shenoy, 2011). The third intracellular loop is also where the SUMOylation site studied in this work is located. Lysine 235 is in the loop 3 is physically close to ubiquitination site. Ubiquitination and SUMOylation share quite some similarities and are both dependent on surface associated lysine residues. They also both play vital roles in signalling propagation, protein trafficking, protein stability and transcriptional regulation (Wei et al., 2012). The SUMOylation and ubiquitination pathways both coordinate the determination of protein fate. Studies in the cancer field have demonstrated that SUMOylation and ubiquitination can cause abnormal protein homeostasis that contributes to cancer development (Wei et al., 2012).

Successful detection of SUMO-β_2 antibody allowed the detection and comparison of SUMOylated β_2AR from healthy and diseased human heart myocardium. Our results suggesting that there was no significant change in the ratio of SUMOylated β_2AR to total β_2AR when control and diseased myocardium samples were compared, but at the same time the total β_2AR expression is largely elevated in diseased samples. From this data, I could not make conclusions about the functional role of SUMOylation of β_2AR in the heart failure disease process. Therefore, my next goal was to try and establish a role for β_2AR SUMOylation in more functional studies. The data is displayed in Chapter 5 of this work.

Although I have not observed disease relevance for SUMOylation of β_2AR, this has not been the case for other SUMO substrates in the heart. For example, SERCA2a SUMOylation was investigated in large and small animal models of disease by the Hajjar group. This group demonstrated that SUMOylation was protective because it stabilised SERCA's expression and function, which are both diminished in heart disease (Kho et al., 2011). Overexpression of SUMO-1 by gene therapy in large and small animal models of heart failure enhanced SERCA2a SUMOylation and therefore improved heart function (Lee et al., 2016). On the contrary, when the SERCA2a was absent, the protective effect of SUMO-1 expression was not realised, suggesting that SERCA was the primary target of this modification in heart (Lee et al., 2016). This may be the reason why I have struggled to see significant differences in the work described above, especially in the human samples.

Chapter4. Generation of Wild Type β_2AR and SUMO Site Null β_2AR via Adenoviral Vector

4.1 Introduction

Observing the effects of β_2AR SUMOylation in the HEK β_2 cell line has provided a few insights into the role of this modification but confirmation of any mechanistic effects would have to be verified in a more physiological context. A more appropriate cell type would be the cardiomyocyte which is a primary cell that expresses both β_1AR and β_2AR, at 70-80% and 20-25% respectively (Madamanchi, 2007) .

Liposomal transfection is a process by which DNA is processed into liposomes that fuse with cell membranes and release DNA into the cell interior by endocytosis (Felgner *et al.*, 1987). This method works in a highly efficient manner in non-cardiac cells, however when it is employed in neonatal cardiomyocytes, transfection rates of only up to 15% have been reported. Furthermore, adult cardiomyocytes are even more difficult to transfect than neonatal cardiomyocytes (Djurovic *et al.*, 2004). Compared to the liposomal transfection method, viral based techniques largely increase the transfection efficiency and stable gene transfer in cardiac cells (Louch, Sheehan and Wolska, 2011). Therefore, the full-length sequence of β_2AR and SUMO site mutant β_2AR have been designed with a YFP (Yellow fluorescent protein) tag in an adenoviral system.

4.1.1 The Structure and Biology of Adenovirus

The replication-deficient adenoviral vectors widely used currently for *in vivo* gene transfer are largely derived from adenovirus serotype 5(Ad5). Adenoviruses have a double stranded linear 36kb DNA genome with an icosahedral, unenveloped capsid. The unenveloped capsid is composed of three main proteins: penton base, hexon and fiber. The Hexon constitutes the majority of the capsid while there are extra 12 pentameric penton bases and from the penton base there are trimeric fiber protein protrusions at each of the 12 vertices of the capsid, which consist of shaft and knob (Alba, Baker and Nicklin, 2012)(**Figure 4.1**). The fiber knob can bind with coxsackievirus and adenovirus receptor (CAR) which is a surface receptor found in multiple cell types including cardiac cells (Tomko, Xu and Philipson, 1997).

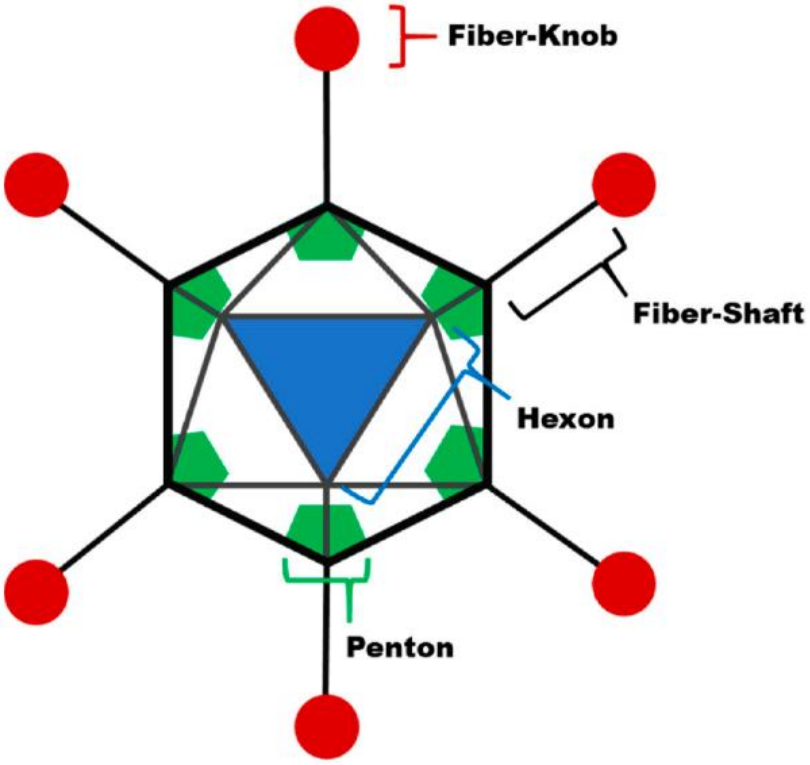

Figure 4.1 Schematic Diagram of Adenovirus Structure. Adenovirus consists of icosahedral, unenveloped capsid which is made of three main proteins: hexon, penton base, and fiber. The fiber consists of the shaft and globular knob (Alba, Baker and Nicklin, 2012).

Adenoviruses have been chosen as tools for gene transfer because of the exceptionally high frequency with which they are able to infect the target cells in comparison with plasmid-based techniques (Schneider and French, 1993). Adenovirus genomes can be manipulated with inserted foreign genes, and this is true even with genes of large DNA size which can achieve high levels of recombinant protein expression. Another advantage of adenovirus gene transfer is that adenoviruses can be grown to exceptionally high titers, exceeding $10^{10}mL^{-1}$, and can be effective in different mammalian cells, including cardiomyocytes cells (Alba, Baker and Nicklin, 2012).

4.1.2 Viral Based Gene Transfer System

Adenoviruses have been extensively developed for gene therapy because of the ease by which replication deficient adenoviral vectors can be made in HEK293 cell lines. The adenovirus used within this project utilized the Adeno-X adenoviral system. This is the first generation of the adenoviral vector, with a deletion of extensive portions of Early Regions 1 (E1) and 3 (E3) of wild type adenovirus, enabling the insertion of desired gene expression cassettes of up to 8kb of foreign DNA without affecting the efficiency of viral particle formation. The E1 region encodes for proteins necessary for the expression of the other early and late genes. The “early” genes include those which are involved in the adenovirus DNA replication, whereas “late” genes are those which are involved in virion assembly, therefore combined they are vital for the viral life cycle. Conceptually, replacement of the E1 region with an expression cassette in adenovirus results in the requirement of a producer cell line which will complement the missing region (Kovesdi and Hedley, 2010). Another advantage of adenoviral vectors for gene expression in adult cardiomyocytes is that adenoviral vectors readily infect adult cardiomyocytes and have a relatively fast onset of protein expression within 24 hours. Since adult cardiomyocytes begin to differentiate after 3-4 hours in culture (Louch, Sheehan and Wolska, 2011), this could help improve the protein expression. The human embryonic kidney (HEK) 293 cell line was developed as a producer cell line through an insertion of E1A and E1B sequence, to complement for the lacking region in the adenovirus, allowing viral replication(Graham *et al.*, 1977; Louis, Evelegh and Graham, 1997). The HEK293adherence (HEK293AD) cell line is derived from the parental 293 cell line, specifically selected for adenovirus applications. There are several advantages of HEK293AD cell line over the regular 293 cells. One advantage is that 293AD cells firmly attach to culture plates, which is ideal for amplification and titering of adenovirus. The flattened morphology and larger cell surface area also contributes to higher transfection and better yield of recombinant adenovirus.

4.1.3 Adenovirus and Adeno-associated Virus (AAVs) in Cardiovascular Gene Therapy

Gene therapy is a new potential treatment option for acquired and inherited cardiovascular diseases. Adenoviruses have been designed as vectors for gene therapy applications. Following a better understanding of the pathogenesis of heart failure, gene therapy clinical trials have been undertaken recently. The CUPID2 trial treated chronic systolic heart failure or non-ischemic cardiomyopathy patients with one dose of adeno-associated virus (AAV)1-sarcoplasmic reticulum calcium ATPase 2a (SERCA2a). Surprisingly the endpoints were negative although the previous smaller trial showed positive results (Greenberg et al., 2016). The best gene therapy vector for cardiovascular disease should have the minimized off-target sequestration, neutralizing antibody recognition and inflammatory activation after delivery, while retaining the capacity to transduce vascular cells with high efficiency (A. C. Bradshaw & Baker, 2013).

4.2 Aims

The aims of this chapter were twofold:

1) To generate wild type and SUMO mutant β_2AR recombinant adenoviral DNA.
2) To prepare a high-titer stock of wild type and SUMO mutant β_2AR recombinant adenoviral DNA to enable functional experimentation in primary cardiac cells.

4.3 Methods

The Adeno-X adenoviral system was used to generate the wild type β_2AR and SUMO mutant β_2AR recombinant viral DNA. Instead of traditional homologous recombination or direct ligation-based methods, in-fusion cloning techniques were used to clone the polymerase chain reaction (PCR) fragment of the β_2AR directly into the linearized adenoviral vector. The process is depicted by the workflow diagram (**Figure 4.2**). This system allows introduction of any cassette into an E1/E3-deleted replication-incompetent human adenoviral vector. To produce recombinant adenoviral vectors using In-Fusion technology, the PCR-generated

sequence of wild type β_2AR and SUMO mutant β_2AR with prelinearized pAdenoX vector DNA was efficiently and precisely constructed by recognizing a 15bp overlap at their respective ends. This 15bp overlap is engineered into the primers used for amplification of the desired sequence. pAdeno-CMV vector was used in this work (**Figure 4.3**).

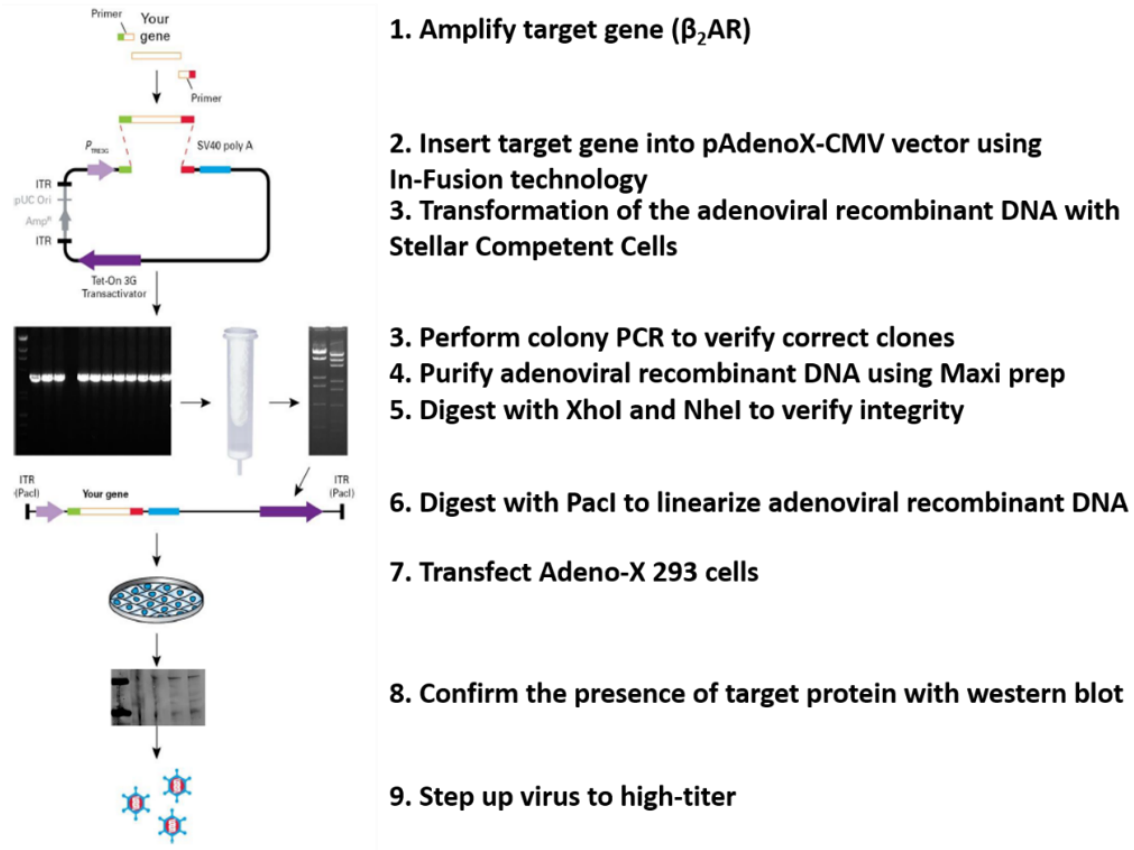

Figure 4.2 Constructing recombinant adenovirus with In-Fusion technology. Wild type and SUMO mutant β_2AR genes were amplified with 15bp extensions that are homologous to the ends of the linearized adenoviral vector. The PCR products were then purified and mixed with the linearized adenoviral vector in the In-Fusion reaction. Following the reaction, a portion of the mixture was transferred to E. coli (Stellar Competent cells) and screened. After PCR-positive clones have been identified, the recombinant pAdeno-X vector with receptors were subsequently linearized with the restriction enzyme PacI, then transfected into Adeno-X HEK293 cells for viral rescue and amplification.

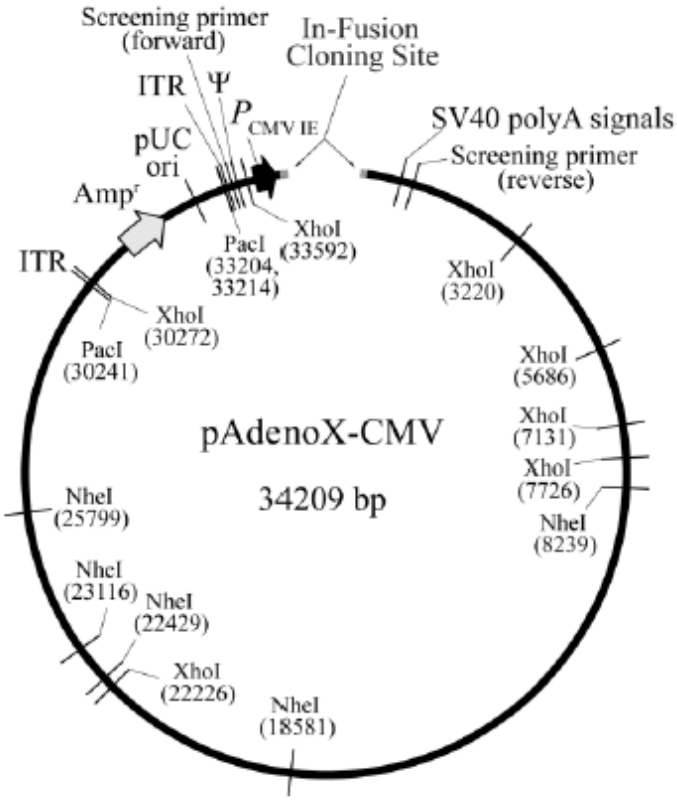

Figure 4.3 pAdenoX-CMV (Linear) Vector maps. (TakaRa® Adeno-XTM Adenoviral System 3 CMV user manual).

4.3.1 PCR Primer Design and Amplification of the β_2AR Gene with 15bp of Homology to pAdenoX

The PCR primers used to amplify the β_2AR gene were designed in a way that ensured each end of the PCR products shared 15bp of homology with one end of the linearized pAdenoX vector (**Figure 4.4**).

A Clone Amp HiFi Premix kit was used to amplify the sequence of β_2AR with a YFP tag following the manufacturer's instructions. After PCR amplification, PCR products were processed on an agarose gel to verify the positive results. PCR products then were purified using a PCR clean up kit.

Figure 4.4PCR primer design diagram. (A) In-Fusion PCR forward primer. (B) In-Fusion PCR reverse primer. The red box indicates the primers used for In-Fusion reaction.

4.3.2 In Fusion Cloning of Purified PCR Fragments

Purified PCR products were added into an In-Fusion reaction following manufacturer's instructions, the amount of insert DNA and vector was 1:2 in proportion. The reaction mixture was then incubated for 15 minutes at 50°C, following by placement on ice. The cloning reactions are stored at -20°C before further use.

4.3.3 Transformation of In-Fusion Reaction Mixture

2.5 µl of In-Fusion reaction mixture was added into 50 µl of competent cells and incubated on ice for 30 minutes. The competent cells then went through heat shock for 45 second at 42°C, then placed on ice for 2 minutes, 447.5 µl of SOC medium was added to reach a final volume to 500 µl. The mixture was incubated at 37°C for 1 hour shaking at 250 rpm. Different dilution (1:5, 1:20 and 3:4) of transformation mixture were spread onto LB agar plates containing 100 µl/ml ampicillin. The plates were incubated overnight at 37°C.

4.3.4 PCR Colony Screening of Clones

20 random single colonies of each construct were picked by sterile pipette tip and transferred into 40 µl of deionized H_2O. The colony was resuspended by gently pipetting up and down. 20 µl of the suspension was transferred into 5ml of liquid LB medium containing 100 µl/ml ampicillin and then incubated at 37°C for 8 hours with shaking at 220 rpm. 5µl of the suspension was prepared with a PCR master mix for the PCR colony screening reaction. The PCR colony screening of clones was performed as per manufacturer's instructions. The PCR reaction products were visualized by running on a 1.2% agarose gel.

4.3.5 Amplification and Purification of Recombinant Adenoviral DNA

After the positive clones were identified following the PCR reaction, they were amplified by inoculating 300ml of liquid 100 µl/ml of LB/Amp medium with 5ml of long phase culture prepared beforehand. The plasmids were purified using plasmid Maxi kit as per manufacturer's instruction, then concentrated in TE buffer. The recombinant Adeno-X plasmids were reconfirmed via individual digestions with XhoI and NheI since the adenoviral vector has the XhoI and NheI restriction sites. The products were visualized by loading an overnight 0.8-1% agarose gel in order to get the best resolution of bands. The plasmids were finally confirmed by sequence analysis.

4.3.6 Linearization of Recombinant pAdenoX DNA via Restriction Enzyme PacI and Ethanol Precipitation

The recombinant plasmids were digested with Pac I to expose inverted terminal repeats (ITRs) located at either end of the adenoviral genome and release the adenoviral genome from the plasmid backbone. Digestion reaction mixtures were prepared by following manufacturer's instructions. Briefly, mixtures were incubated at 37°C for 3 hours, the digestion products were analysed on a 1% agarose gel to confirm the completeness of Pac I digestion. The Pac I digestion products were then diluted 1 in 10 with sodium acetate. Two volumes of the sodium acetate and digestion products mixtures of 100% ethanol was added to precipitate the DNA plasmid, then the mixtures were incubated at -20°C overnight. The following day, mixtures were centrifuged at 14,000 rpm for 10 minutes, the supernatant was discarded, and the DNA pellet was washed with 500 µl 70% ethanol twice. After the last wash, the pellet was spun down at 14,000 rpm for 5 minutes and air dried for 15 minutes, before the pellets were resuspended in Elution Buffer. The concentration of recombinant adenoviral DNA was determined by nanodrop analysis.

4.3.7 Transfection of Linearized Recombinant pAdenoX DNA into Adeno-X HEK293 Cells and Amplification for High-titer Stock of Recombinant Adenovirus

The linearized recombinant pAdenoX DNA was transfected in HEKAD 293 cell lines to prepare high-titer stock of adenovirus by using Lipofectamine LTX transfection reagent. The transfection reaction was prepared following Lipofectamine LTX transfection manufacturer's instructions. The linearized adenovirus DNA mixtures were transfected in 60% confluent 10cm dishes of HEKAD 293 cells and incubated at 37°C in a humidified atmosphere maintained at 5% CO_2. The cytopathic effect (CPE) has been considered as an important signal for virus infection (Albrecht et al., 1996). Infected cells typically remain intact but round up and may detach from the surface, these changes are collectively referred to as the CPE. The cell cultures were harvested after observing a late CPE phenotype and the cell culture medium was collected and prepared for high-titer stock. After each amplification, high-titer virus was obtained by manually lysing cells with a series of freeze-thaw cycle. The cells and medium were transferred to a 50ml conical centrifuge tube without using trypsin, the remaining attached cells were dislodged into medium by gentle agitation and pipetting. The mixture was centrifuged at 1,500Xg at room temperature. The cell pellet was resuspended in a suitable volume of PBS. The cells were lysed by freezing in a dry ice/ethanol bath followed by thawing in a 37°C bath for 5 times. The cells were vortexed to mix each time after thawing. The second amplification of viruses was infected using the cell lysate from first amplification. The presence of recombinant adenoviral β_2AR was identified by western blotting.

4.3.8 Cesium Chloride (CsCl) Gradient Purification

Centrifugation on CsCl density gradients was used to concentrate and purify the wild type β_2AR adenovirus stock, isolating it from cell debris, empty particles (particles which lack the viral genome) and small media components. This was

essential for *in vivo* work because any component, in addition to the purified adenovirus would initiate an immune response greater than that expected to be caused by adenovirus alone.

Ultracentrifuge tubes were sterilised by rinsing with 70% ethanol followed by distilled H_2O. Then, 2.5 mL of 1.25 g/mL density CsCl was added to each tube with 2.5ml of 1.40g/ml density CsCl added below the first gradient. This was achieved by placing the pipette to the bottom of the tube and releasing fluid slowly under the already existent solution in the tube. Adenovirus solution to be purified was pipetted slowly drop by drop on top of the first gradient - 1.25 g/mL density CsCl – with care not to disturb the gradient. The remaining space in the tube was filled with PBS, before subjecting adenovirus solution on gradients to centrifugation in the SW40Ti rotor in the ultracentrifuge (Beckman Coulter) for 1.5 hours at 217,874×g. After centrifugation, the adenovirus presents as a discrete white layer between the two CsCl gradient layers. Using a 21-gauge needle and a 5-mL syringe, the side of the ultracentrifuge tube was pierced underneath the adenovirus band, and with a side-to-side sweeping motion the adenovirus was collected, without collecting excess solution. A further CsCl gradient was added to a fresh ultracentrifuge tube containing 5 mL of 1.34 g/mL density CsCl. The adenovirus was applied to the gradient as described above and centrifuged in the SW40Ti rotor for 18 hours (or overnight) at 217,874xg. The adenovirus band was then removed using needle and syringe as described above.

4.4 Results

4.4.1 Amplification of β_2AR Gene with 15bp of Homology to pAdenoX

Wild type β_2AR and the β_2AR SUMOylation site mutant lysine 232 and 235 to argenine) with a Yellow Fluorescence Protein (YFP) tag were amplified with CloneAmp HiFi Premix. The presence of correct PCR products was tested via agarose gel separation and visualization. Bands were detected at 2kb, and this indicated the present of β_2AR (**Figure 4.5A**). After PCR product purification, a clean band at 2kb was observed by running an agarose gel (**Figure 4.5B**).

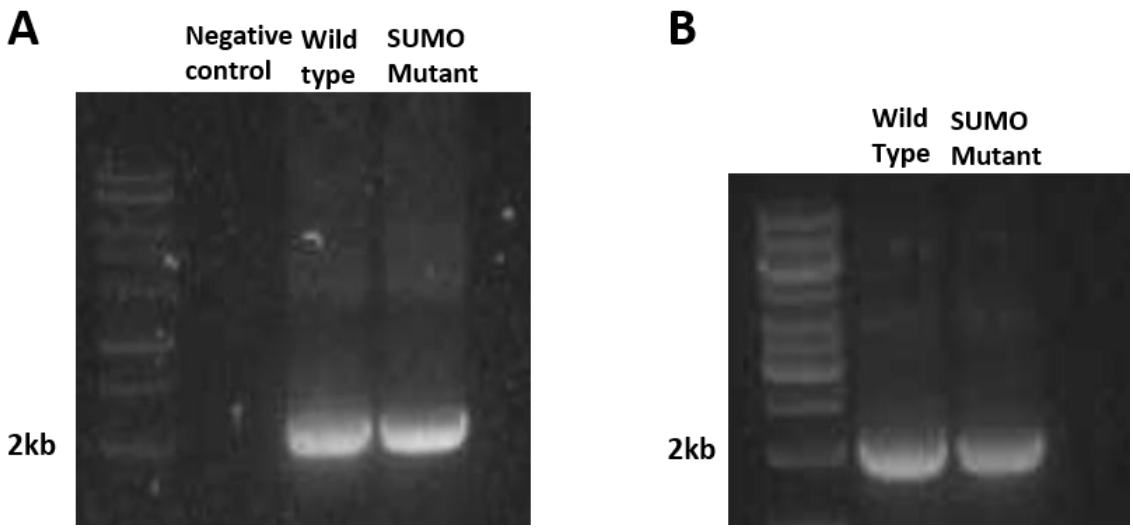

Figure 4.5 The presence of β_2AR gene after amplification. (A) A band shown at 2kb indicate that presence of β_2AR. (B) After PCR product purification, clean bands at 2kb were also observed.

4.4.2 PCR Screening of Clones and Recombinant Adenoviral DNA Confirmation by XhoI and NheI Digestion

20 randomly chosen colonies of the each adenoviral β_2AR fragment were subjected to PCR and visualized on a 1.2% agarose gel. The parental vector alone was also analysed as a negative control. Bands at 2kb was observed as the correct band size of β_2AR. 90% of adenoviral wild type β_2AR clones were positive (**Figure 4.6A**) while 85% of adenoviral SUMOylation mutant β_2AR clones were positive (**Figure 4.6B**). The identity of recombinant adeno-X plasmid DNA was reconfirmed by individual digestions with XhoI and NheI. The correct band sizes were calculated according to the vector map and restriction sites (**Figure 4.3**). For pAdenoX-CMV vector and β_2AR, the estimated band size is 18749bp for NheI and 5937bp for XhoI (**Figure 4.6C**).

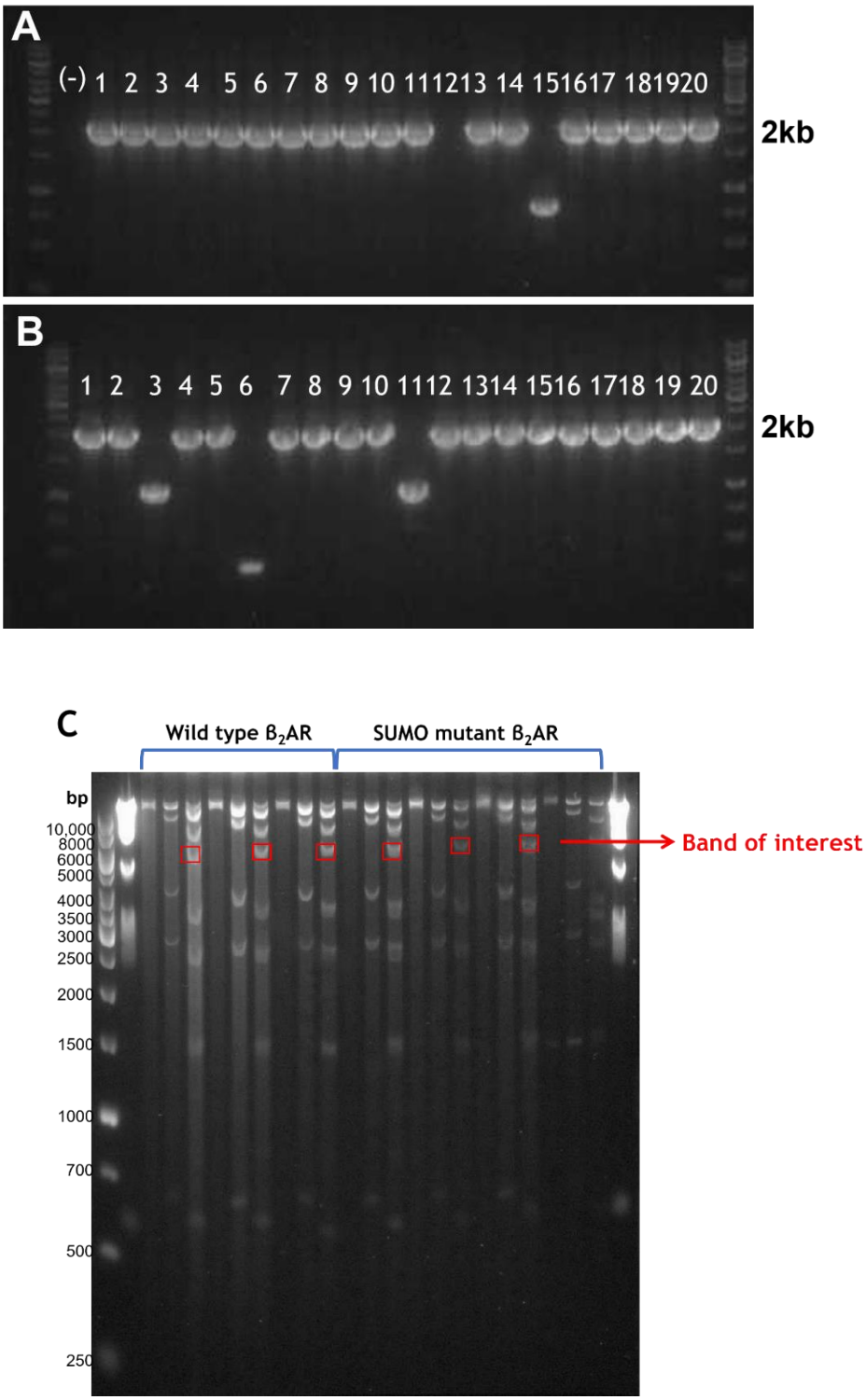

Figure 4.6 PCR screening of adenoviral clones and restriction analysis of pAdenoX DNA. The Adeno-X control Fragment was cloned into the pAdeno-X CMV vector and 20 randomly chosen colonies were subjected to PCR, PCR products then analysed on a 1.2% agarose gel. The size of 2kb bands indicates the positive clones. (A) 90% of adenoviral wild type β_2AR clones were positive. (B) 85% of adenoviral SUMOylation mutant β_2AR clones were positive. (C) To demonstrate correct restriction digestion and band intensity of the adenoviral DNA, positive clones were digested with the indicated restriction enzymes and then subsequently analysed on a 1.2% agarose gel. The red box indicates the correct size of extra band as evidence of β_2AR.

4.4.3 Linearization of Recombinant pAdenoX DNA via Restriction Enzyme PacI

Before pAdenoX DNA can be packaged, the recombinant plasmid DNA must be digested with PacI to expose the inverted terminal repeats (ITRs) located at either end of the adenoviral genome and release the adenoviral genome from the plasmid backbone. Bands at 3kb indicate that the PacI digestion has been completed since the plasmid portion of the recombinant pAdenoX vector migrate at 3kb (indicated by red box), while the adenoviral genome remains at the top of the lane (**Figure 4.7**).

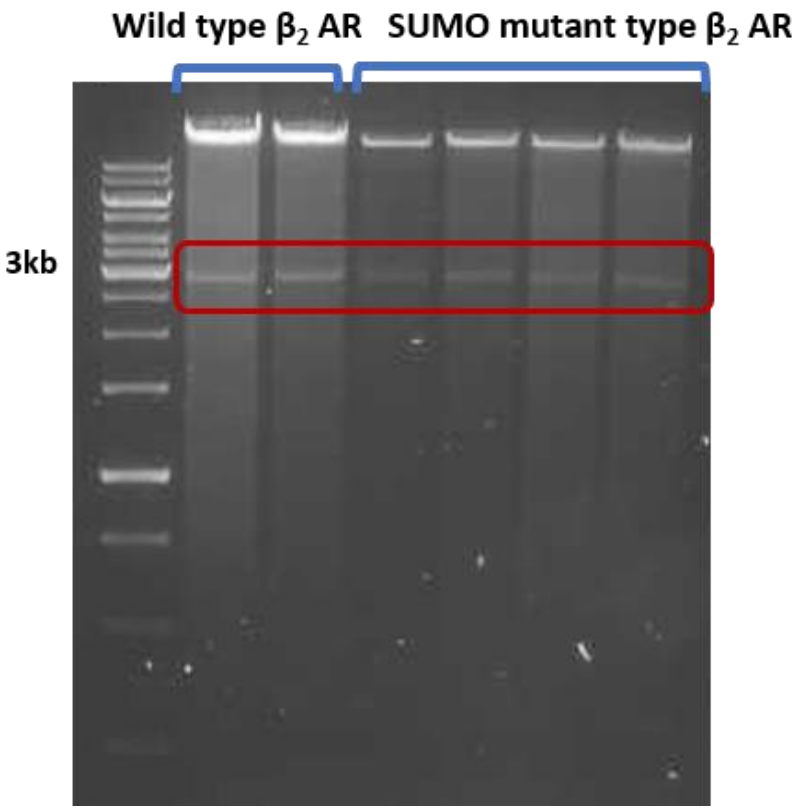

Figure 4.7 Linearization of recombinant adenoviral DNA via restriction enzyme PacI. Bands at 3kb indicate that the PacI digestion has been completed The red box indicates the recombinant pAdenoX vector at 3kb.

4.4.4 Observing the Cytopathic Effect when Culturing Adenovirus

The cytopathic effect (CPE) is a critical sign of adenovirus presence in cell monolayers, this reflects structural changes in host cells that are caused by viral invasion. Rounding of the infected HEK293 cells, fusion with adjacent cells to form syncytia and the appearance of nuclear or cytoplasmic inclusion bodies were observed in when CPE appeared after infection. CPE was observed 20 days after transfected in HEK293 AD cells for first amplification of adenoviral DNA in both type of β_2AR. From day 19, in both wild type and SUMO mutant β_2AR transfected cells, gaps between HEK293 cell clusters were clearly observed (shown with red arrows in **Figure 4.8**) which indicates that adenovirus has been transduced into cells successfully (**Figure 4.8**).

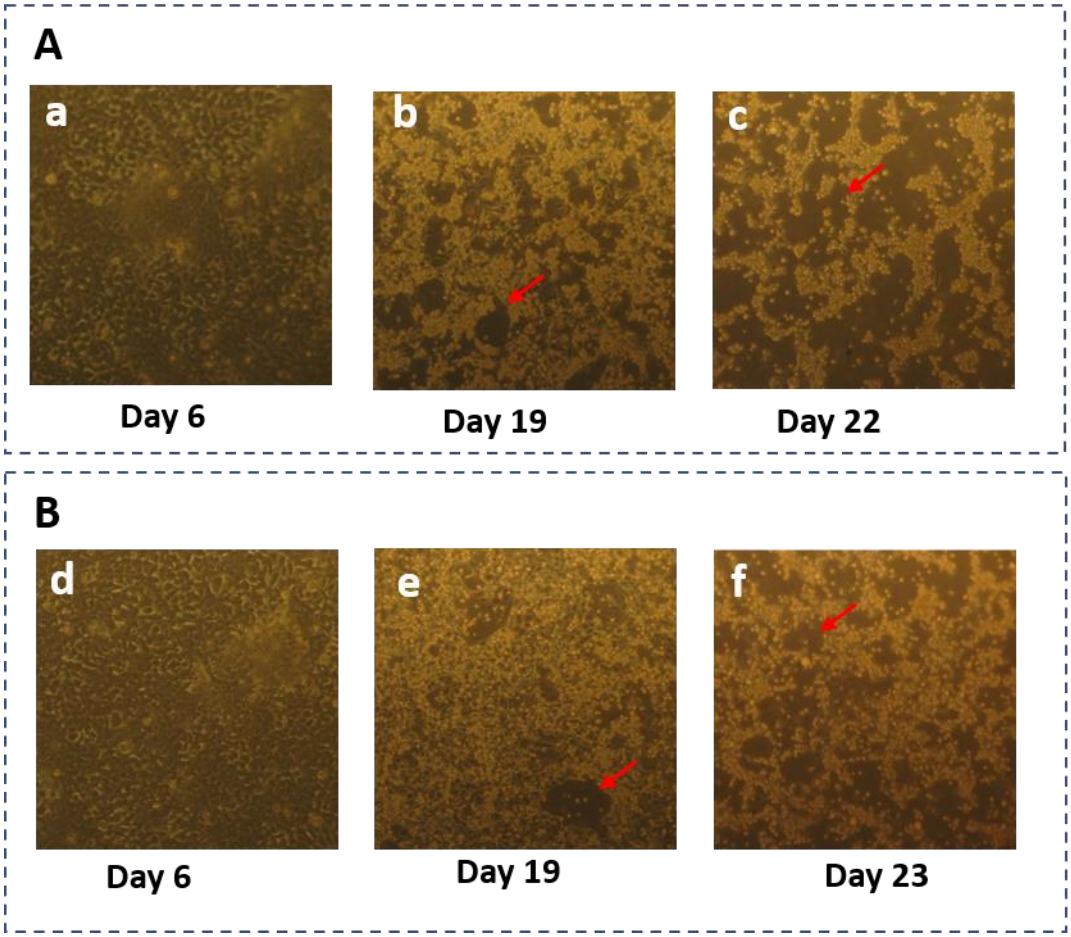

Figure 4.8 The cytopathic effect (CPE) of HEK293 AD cells. (A) CPE was observed from 19 days after transfection in HEK293 AD cells for first amplification of adenoviral DNA of wild type β_2AR. (B) CPE was observed from 19 days after transfection in HEK293 AD cells for first amplification of adenoviral DNA of SUMO mutant β_2AR. Gaps between cell clusters were observed in both wild type and SUMO mutant adenovirus overexpressed HEK293 AD cells as a successful sign of transduction (indicated by red arrows).

4.4.5 Confirmation of β_2AR Expression After First and Second Amplification of High-titer Recombinant Adenovirus

Recombinant adenoviral β_2AR expression was analysed by western blotting. The blots detected YFP and β_2AR to test the transfection efficiency. YFP-tagged β_2AR should be expressed and show up at approximately 75kDa after both first amplification (**Figure 4.9A**) and second amplification (**Figure 4.9B**). The YFP protein tag should be at 26kDa while β_2AR protein expressed at around 46kDa. Weak bands were observed at 75kDa in first amplification of wild type and SUMO mutant overexpressed HEK293 AD cells when probing with β_2AR antibody (**Figure 4.9A upper red box**). However, similar bands were not observed at the same molecular weight following the second amplification (**Figure 4.9B)** lower red box). This data suggests that the virus was not successfully replicated in the HEK cells following the second amplification. The cells transfected with β_2AR SUMO mutant adenoviral DNA started to detach from the cell culture flasks 3 days after transfection and appeared dead when the third amplification was generated.

In summary, although I was able to generate constructs of the correct sequence (WT β_2AR and mutant β_2AR), these were not successfully amplified in HEK293 AD cells. Unfortunately, this meant that I had to find an alternative means of obtaining these important reagents for the study of mechanistic changes in β_2AR function underpinned by SUMOylation.

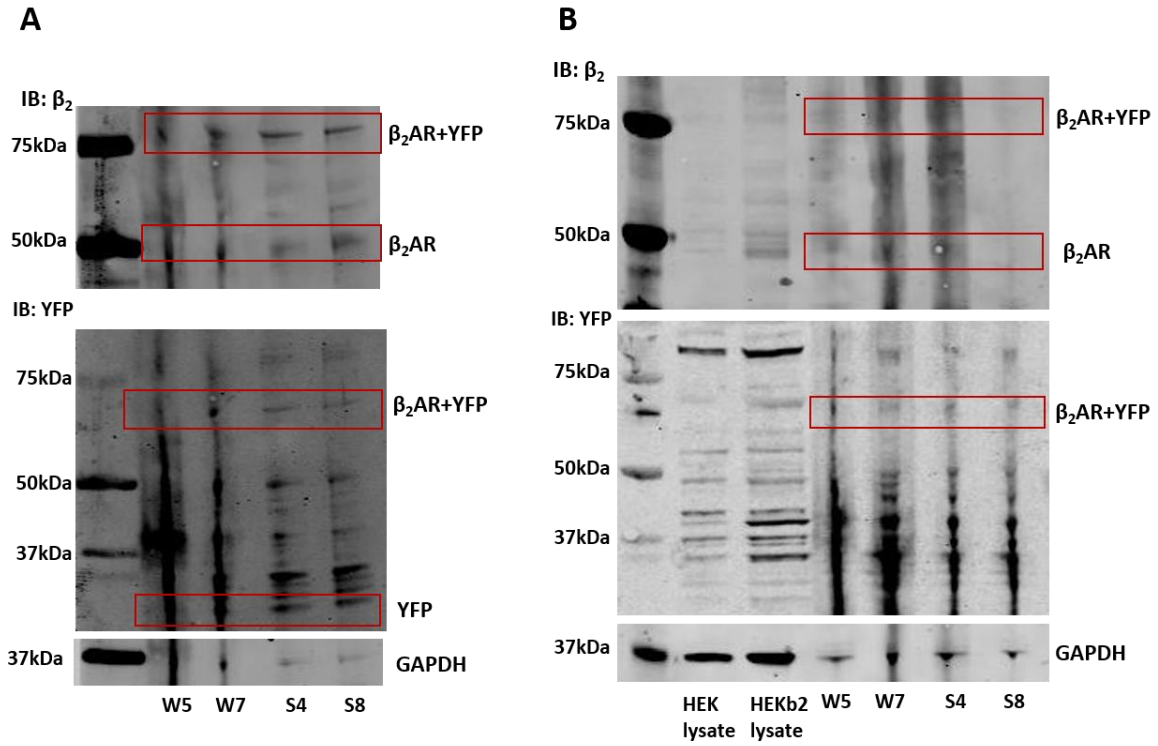

Figure 4.9 ß$_2$AR expression shown in after first and second amplification of high-titer recombinant adenovirus. (A) YFP-tagged ß$_2$AR was weakly detected at approximately 75kDa after first amplification while ß2AR alone expressed at 46kDa and YFP tag alone shown at 26kDa. (B) YFP-tagged ß2AR was not detected at approximately 75kDa after second amplification. W5- wild type ß$_2$AR colony 5, S4- SUMOylation site null ß$_2$AR colony 4.

4.5 Discussion

The work in Chapter 3 has examined the effects of SUMOylation of the β_2AR within the HEKβ_2 cell line. This is a cell line which is easily maintained and transfected, but since it is a human embryonic kidney (HEK) cell line in which the β_2AR is stably overexpressed, it does not have the similarity to cardiac cells function and physiology characteristic. Also, in chapter 3 I have used wild type β_2AR and K232R-K235R β_2AR overexpression in HEK293 cells to study the influence of SUMOylation on β_2AR signalling. However, these studies do not provide evidence on how the function of the β_2AR could be affected by SUMOylation in a physiologically relevant system. In this chapter I attempted to generate wild type and SUMO mutant β_2AR recombinant adenoviral DNA to introduce the genes of interest to primary cardiac cell lines.

New-born rat cardiomyocytes are a widely used cell model to study cardiovascular disease mechanisms and it was my plan to infect these cells with the constructs described above. Unfortunately, I could not achieve successful amplification and additionally, the SUMO mutant β_2AR stopped expressing in the HEK293 AD cells and caused cell death over time. The HEK cells transfected with SUMO mutant recombinant adenovirus grew well for the first 3 days after transfection, then the speed of growth started to slow down, the cells started to detach from the plates, and ultimately the cells died after being transfected for a week. A negative transfection control that only contained empty transfection reagent and no virus was always done at the same time and always grew well, suggesting that the host cell death is caused by the SUMO mutant adenovirus transfection. Studies have shown that successful adenovirus infection is associated with high toxicity and as a result viral titers must be balanced to achieve high infection with tolerable levels of toxicity (Gordon, 2002). One possible reason for the failure in amplification of the SUMO mutant β_2A in HEK293 AD cells is that there was high cell toxicity related to viral titer numbers. The virus concentration may have been too high for the HEK cells to survive associated virus toxicity. I tried to adjust the concentration of the virus when transfecting the cells, however I was not able to find a titer that gave detectable expression while allowing the host cells to live.

SUMOylation is a post-translational modification that is involved in controlling many cellular processes including regulation of protein function, stability and localization (Geiss-Friedlander & Melchior, 2007). In the process of adenovirus infection, E1A and E1B-55k as two proteins of the E1 region have been shown to be linked to the SUMOylation machinery (Wimmer et al., 2013). E1B-55k is a multifunctional regulatory protein that can regulate a variety of different molecular activities during infection and transformation of primary mammalian cells (Wimmer et al., 2013). Wimmer et al. provided evidence E1B-55K PTMs facilitated exploitation of the host cell SUMOylation machinery. In other words, studies have shown that adenoviral proteins can mediate the SUMOylation cascade of host cell. During the process of adenovirus infection, research shows that both the host cell proteins and viral proteins undergo SUMOylation.

Ad early proteins can become a targets for SUMOylation and interact with the SUMO machinery (S. Y. Sohn & Hearing, 2016). The AdE4-ORF3 protein induces the SUMOylation of cellular proteins, many of which are involved in a DNA damage response and, in some cases, subsequent proteasomal degradation (S. Y. Sohn & Hearing, 2016). Adenovirus was shown to interfere with host SUMOylation. A vital aspect of the interplay between viruses and SUMOylation is the potential for viruses to interact with or target host SUMOylated cellular proteins, and further regulates their activities (Everett et al., 2013). Therefore, one of the reasons that the amplification failed may be due to the fact that I was using adenoviral genomic DNA containing SUMOylation site mutations. Since the SUMOylation motif on the β_2AR has been mutated, the regular cellular process of the host HEK293 cells could have been disturbed by irregular SUMOylation. There is precedence for this in the literature where research indicated that replacing the SUMOylation lysine residues K7, K23, K24 and K162 by arginine residues reduced accumulation of a core protein V at the host nucleoli, while the wild type remained at that location. At the same time, these four mutations increased virus replication and progeny yield (Freudenberger et al., 2017). In my study, the opposite case could be true i.e., virus replication was hampered in some way by mutant β_2AR expression.

Finally, increasing virus replication that results in cytotoxicity of the host cells could be plausible reason why the host HEK293 cells starts to detach and die. Due

to the unsuccessful generation of SUMO site null β_2AR adenovirus, we decided to purchase commercially made adenovirus with high titer potential that contained either wild type or SUMO mutant β_2AR from Welgen, Inc. The validation of viral overexpression of β_2AR-YFP proteins and functional studies of relative cell lines will be described and discussed in the chapter 5.

Chapter5. Investigating the physiological effects of β_2AR SUMOylation

5.1 Introduction

Data from other chapters in this thesis have shown that K235 on the β_2AR can be SUMOylated in cells and my next task was to try and determine the functional relevance of this post translational modification of β_2AR. SUMOylation is known to influence many cellular functions via alterations of molecular interactions including regulation of protein-protein interactions, DNA binding activity, nucleocytoplasmic trans localization and protein stability (Schwartz & Yeh, 2012). In addition, post-translational modification of the β_2AR can influence downstream signalling and receptor directed physiological change so I have hypothesised that SUMOylation may have a measurable influence on cardiac myocyte contraction.

5.1.1 Physiological Effects of β_2AR

The β_2AR has been shown to transduce signals designed to alter many cardiovascular, pulmonary, and skeletal muscle physiological processes. In skeletal muscle, β_2AR-mediated hypertrophy and contractility are regulated by β-arrestin 1-dependent processes (J. Kim et al., 2018). It is also known that β_2AR stimulation can increase lean mass and alter metabolic properties of skeletal muscle (Lemminger et al., 2019). In the cardiovascular system, β_2AR-signalling has a key role in the regulation of contractility of cardiomyocytes and mice with cardiac-specific overexpression of β_2AR exhibit enhanced basal contractility (Madamanchi, 2007). Clinical trials have also proved that patients with diabetes show a blunted cardiac inotropic response to β-adrenergic stimulation despite normal cardiac contractile reserve (Fu et al., 2017). Additionally, the stimulation of the β-AR signalling pathway with the non-selective β-AR agonist ISO can significantly decrease the proliferation of mid gestation ventricular cells (Feridooni et al., 2017). So, from the above evidence, it is easy to reach the conclusion that maintenance of the fidelity of β_2AR-driven signalling is an important matter for cells of the cardiovascular system.

5.1.2 SUMOylation in Cardiac Functions

Studies have shown that SUMOylation plays a critical role in protection against heart disease. Research suggests that SUMO-1 and SENP2 are key regulators of early cardiac morphogenesis (E. Y. Kim et al., 2013). SUMOylation has also been identified as a potential target to treat cardiac disease. For example, it has been shown that UBC9-mediated SUMOylation enhancement, may be a novel strategy for improving autophagic flux and ameliorating morbidity in proteotoxic cardiac disease (Gupta et al., 2017). More on the protective actions of SUMOylation is detailed in introductory Chapter 1.

5.1.3 Upregulation of SUMOylation with N106

SUMOylation is often difficult to study as only small amounts of cellular proteins get modified at any one time. Recently, it has been shown that a small molecule called N106, whose full name is (N-(4-methoxybenzo[d]thiazol-2-yl)-5-(4-methoxyphenyl)-1,3,4-oxadiazol-2-amine) can activate the SUMOylation cascade, promoting SUMOylation of multiple substrate concomitantly (Kho et al., 2015a). Work has confirmed that N106 increases SERCA2a SUMOylation, resulting in enhanced contractility in both *in vitro* and *in vivo* situations (**Figure 5.1**).

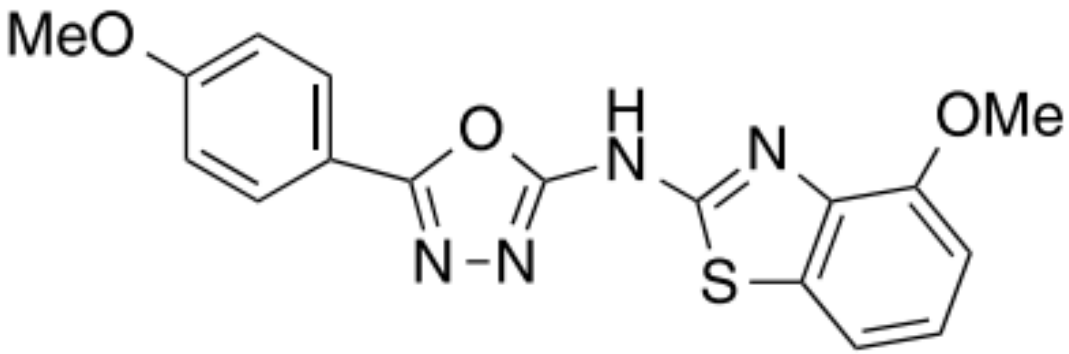

Figure 5.1 Chemical structure of a small molecule activator of SUMOylation, N106. (Kho et al., 2015a).

N106 specifically targets SUMO E1 enzymes to activate the rest of the SUMO cascade leading to a general upregulation of SUMOylated substrates. Treatment with N106 increased the contractility of isolated adult rat cardiac myocytes and haemodynamic improvements in a mouse model of HF (Kho et al., 2015a). This data illustrates the protective effects that SUMOylation can have in a cardiovascular setting.

5.2 Hypothesis and Aims

The functional effects of β_2AR SUMOylation have not yet been determined. Adenoviral overexpression of mutant β_2AR protein lacking the SUMOylation site K232-K235 (β_2AR-YFP MUT) or wild type β_2AR (β_2AR-YFP WT) was used to determine whether the ablation of β_2AR SUMOylation resulted in any physiological effects. It was hypothesised that SUMOylated forms of β_2AR would function differently within the myofilament of cardiac myocytes when compared with the β_2AR that could not be SUMOylated. The aims of the experimental work in this chapter were as follows:

1. To confirm the expression of viral β_2AR proteins in NRVM using western blotting and immunofluorescence.
2. To determine whether ablation of the β_2AR SUMO site resulted in any β_2AR changes in downstream signalling events.
3. To determine whether ablation of β_2AR SUMO site resulted in any functional effects on NRVM contractility using live cell contractility imaging.

5.3 Methods

The methods described in this section were used to collect the data displayed within this chapter. Experiments utilising cell culture and biochemical methods are described previously in Chapter2 of this thesis.

5.3.1 Contractility Imaging with CellOPTIQ®

5.3.1.1 NRVM Preparation for CellOPTIQ®

For acquiring contractile activity data, NRVM were seeded in monolayers for the recording of contraction videos. Following isolation, cells were counted and seeded in 96-well plates with 1% (w/v) bovine gelatin coated at a density of 7×10^4 cells per well in a final volume of 200µl of medium. 24 hours after seeding, NRVM were virally transfected to overexpress with MOI 100 $ß_2$AR-YFP proteins (WT and SUMO site mutant). Following a 24hour incubation with virus, NRVM were imaged.

5.3.1.2 Contractility Measurements

CellOPTIQ® (Clyde Biosciences Ltd; Glasgow, UK) was used for the collection of high-speed images of contracting cell monolayers. This *in vitro* system allows measurement of contractility, voltage, and calcium in live cells, but for the purpose of this project, only contractility was analysed. For each field, an 8 second recording at 100 frames per second was acquired using a 40× objective lens and contractility tool software. A baseline recording was taken before any treatments. 50µl of the medium was replaced with 0.08% PBS or 40µM ISO to make a final 0.02% PBS or 10µM ISO in 200µl medium in each condition. The recordings were taken 1, 2, 3, 4, 5, 6, 7, 8, 9, 10, 15, 20, 25, 30 minutes after the treatments.

5.3.1.3 Analysis

Contractility recordings were analysed using an ImageJ Macro named MUSCLEMOTION (Sala et al., 2018a). This software allows the determination of

dynamic changes in pixel intensity between image frames and transforms the output as a relative measure of movement during muscle contraction and relaxation. A raw acquired image and an analysed image presenting moving pixels are shown in **Figure 5.2**. The measure of movement was shown as a trace of contraction over time. For each contraction, a variety of parameters could be measured and compared between conditions. The following parameters were recorded: Interval, i.e., the time between contractions; UP90, a measure of the time from baseline to 90% of the contraction peak; similarly, DN90, a measure of the time from 90% of the peak to baseline; finally, CD50, a measure as the time between 50% of the upstroke to 50% of the downstroke were determined and compared in this study. The data was present by calculating the relative change in each parameter compared to baseline (the recording before the ISO or PBS treatment) and then was corrected by expressing the change relative to the time control, as expressed by the formula:

%delta delta Y = 100*deltaY/(100+(deltaYPBS*100))

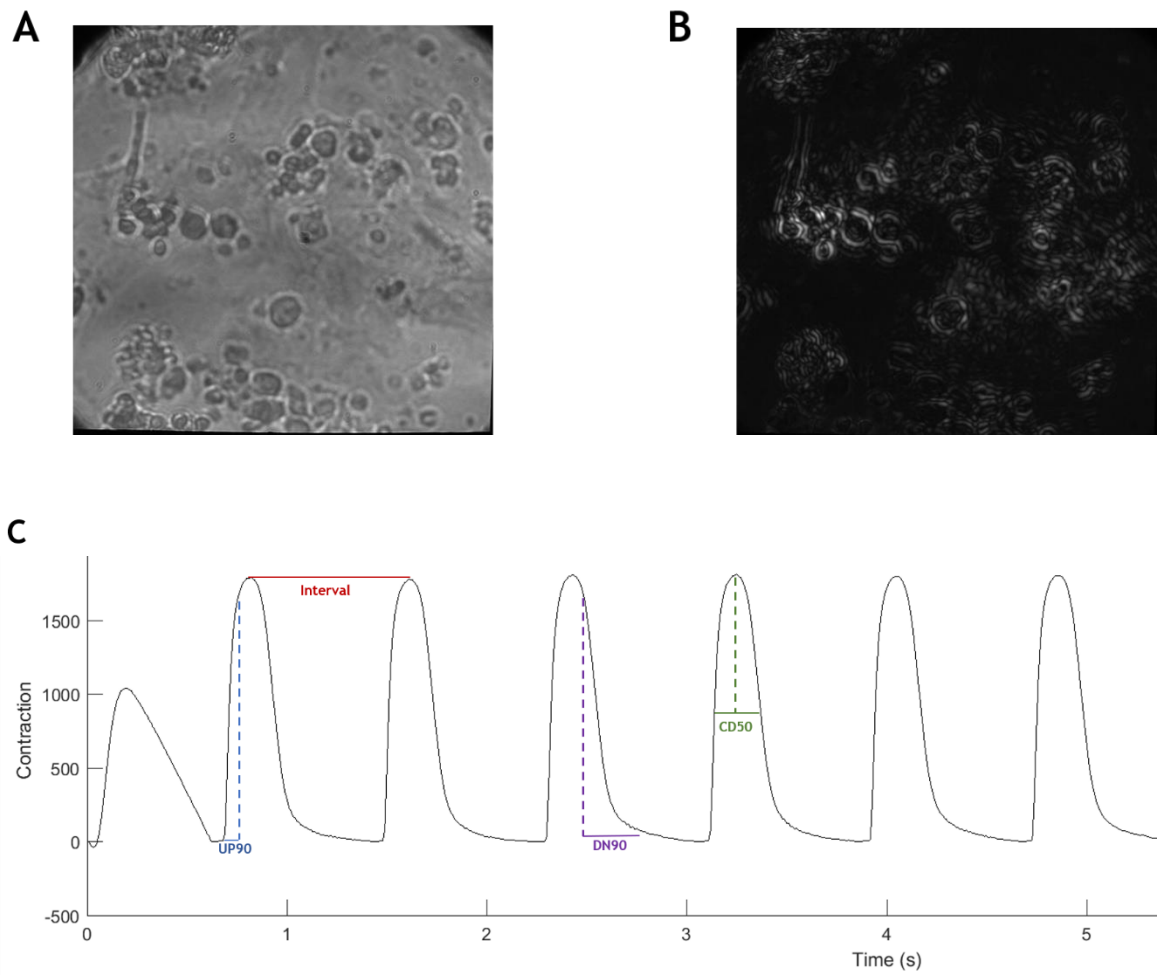

Figure 5.2 Representative example of images acquired by CellOPTIQ® and schematic representation of measurement parameters. A. Brightfield image of NRVM monolayer was taken at 60× magnification. B. To analyse the contractility, the moving pixels of the monolayer contraction were converted into white dots on a black background, then the amount of the white pixels was converted into a contraction trace. C. Contraction trace were conducted by MUSCLEMOTION software can be used to measure numerous parameters. Four of these were used in this project. Interval, also known as the time between contractions was measured to compare the frequency of the contractions between WT β_2AR-YFP and MUT β_2AR -YFP overexpressed NRVM. UP90 is a measurement of the time to contract and was calculated as the time from baseline to 90% of the peak. DN90 (Down90) is a measurement of the time to relax and was calculated as the time from 90% peak to baseline. CD50 (contraction duration at 50%) was measured as the time between 50% of the contraction and 50% of the relaxation.

5.4 Results

5.4.1 Confirmation of Viral Overexpression of β_2AR-YFP Proteins and PIASγ-HA Proteins

Adenoviruses containing β_2AR-YFP WT and β_2AR-YFP MUT for mammalian overexpression were purchased commercially from Welgen, Inc (USA). It was important to confirm the viruses overexpressed the β_2AR-YFP proteins in NRVM before any functional study could proceed. β_2AR-YFP proteins were detected with a robust expression level in NRVM after incubation with 10-500 MOI of virus for 24 hours (**Figure 5.3**). Increased intensity bands shown at 75kDa in **Figure 5.3A red box** indicates the β_2AR-YFP expression. However, similar pattern of bands only shown at 27kDa in **Figure 5.3B** indicates free form of YFP tag instead of β_2AR-YFP fusion protein are shown in the cell lysates. The possible reason of the disassociation between YFP tag and β_2AR is that proteolysis of protein may happened during protein lysate preparation. In addition, there was no significant difference between the expression of β_2AR-YFP of the MUT and WT proteins at the same dose, indicating that cells treated with the same dose of the two viruses would show comparable β_2AR. expression that would allow direct comparison.

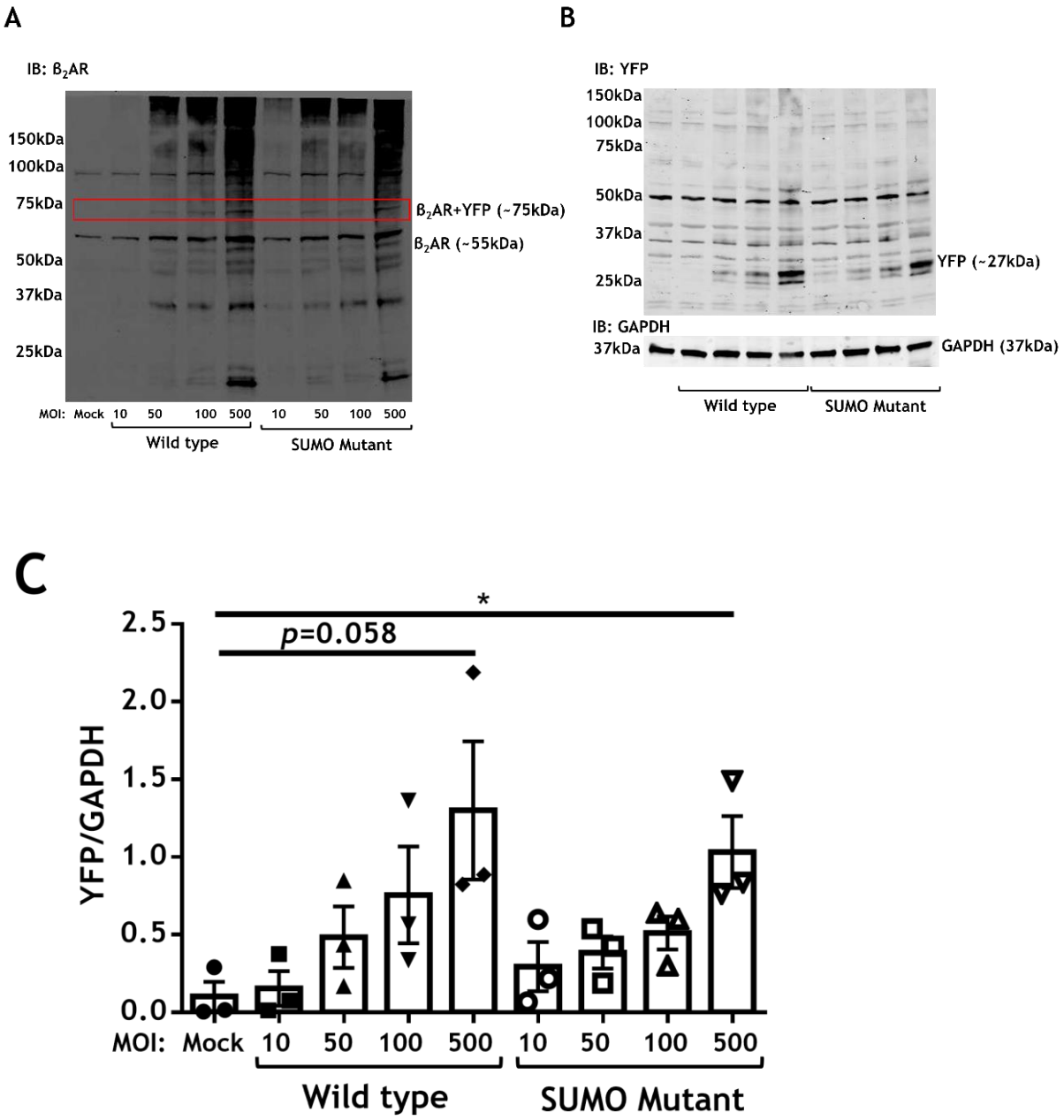

Figure 5.3 Confirmation of viral overexpression of β_2AR-YFP in NRVM. NRVM were infected with viruses in doses increasing from 10-500 MOI for 24 hours prior to harvesting the cell lysates and analysis via immunoblotting. A. Representative example blots. B. Results represented as mean ± SEM, n=3. *p<0.05. Statistical differences were determined using the student's t-test.

The appropriate membrane localised expression of β_2AR-YFP is shown in **Figure 5.4** using immunocytochemistry with the YFP tag in red signals. The red staining of YFP confirmed that the viral proteins express in the NRVM cells. It also indicates that the NRVM cells do not express a high level of endogenous β_2AR compared with viral overexpression.

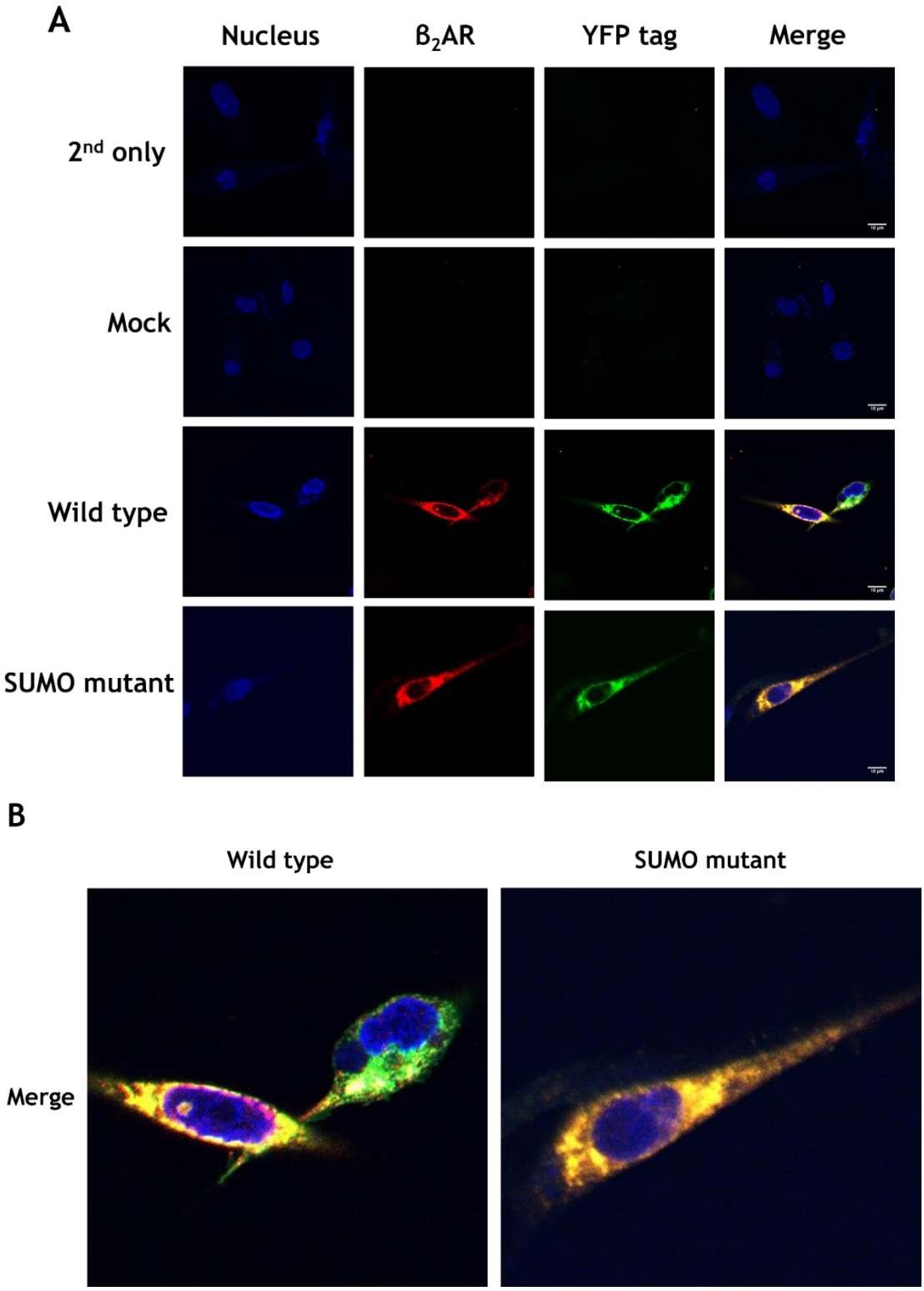

Figure 5.4 Immunocytochemical visualisation of ß$_2$AR-YFP protein localisation. NRVM were seeded in laminin coated coverslips then infected with ß2AR-YFP WT or ß$_2$AR -YFP MUT viruses for 24 hours at MOI 500. The cells were then fixed, permeabilised and immunolabelled with primary antibodies against ß$_2$AR and YFP tag, then were fluorescently labelled with goat anti-rabbit AlexaFluor® 555 (A21428) and goat anti-mouse AlexaFluor® 488 (A21131). Lastly, the cells were mounted with ProLongTM GOLD Antifade Moutant (P36986) nucleus staining. (B) Enlarged merge images of wild type and SUMO mutant ß$_2$AR virus.

5.4.2 Analysis of Half-Life of β_2AR-YFP Proteins

To investigate whether the mutation of the β_2AR SUMOylation motif results in changes in protein turnover of the receptor, β_2AR-YFP proteins were virally overexpressed in NRVM cells treated with protein synthesis inhibitor, cycloheximide (CHX) over an 8-hour time course. Cells were then harvested and the expression of β_2AR-YFP proteins analysed via immunoblotting. The data suggests that both β_2AR-YFP constructs (WT and MUT) were stable over the time course tested (8 hours). As there was little degradation, half-life could not be estimated for either protein (**Figure 5.5**). There were no differences in stability between WT and mutant receptor.

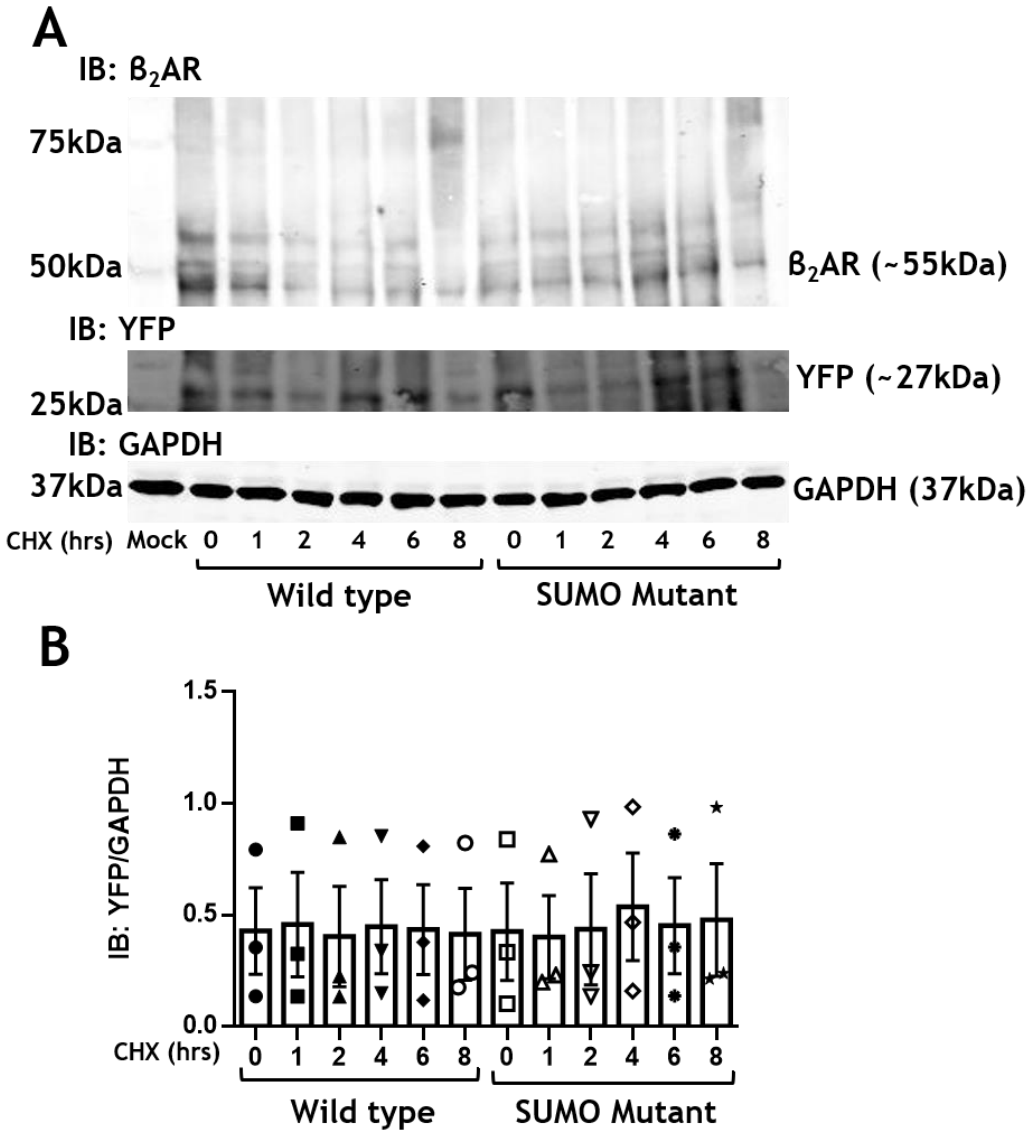

Figure 5.5 Investigation of ectopically expressed ß$_2$AR-YFP half-life in NRVM. NRVM cells overexpressing ß$_2$AR -YFP WT or MUT were treated with 50µg/ml CHX to inhibit protein synthesis. Expression levels following treatments were determined by immunoblotting lysates for YFP tag. A. Representative western blots. B. Results represented as mean ± SEM, n=3. Statistical differences were determined using the student's t-test.

NRVM cells overexpressing β_2AR-YFP WT or MUT proteins were also treated with the proteasome inhibitor MG-132, to determine whether SUMOylation affects proteasomal degradation of β_2AR. Inhibition of proteasome did not significantly affect the expression of β_2AR-YFP protein expression (WT and MUT) in NRVM (**Figure 5.6**). This agrees with the notion that the β_2AR protein is relatively stable (**Figure 5.6**) when it is not bound to ligand. For both β_2AR-YFP WT and SUMO mutant, the expression stayed at the same level.

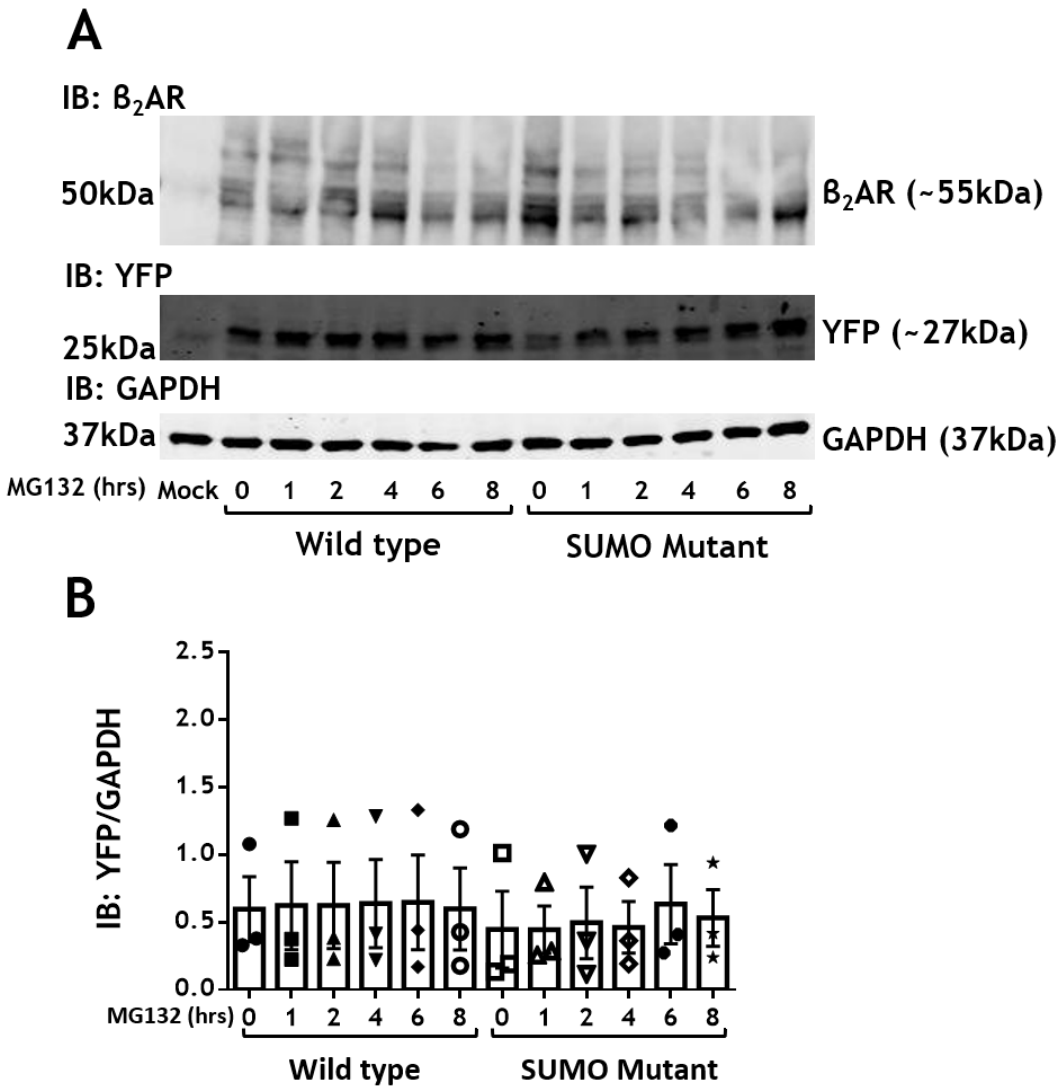

Figure 5.6 Analysis of β_2AR-YFP proteasomal degradation in NRVM. NRVM cells overexpressing β_2AR -YFP WT or MUT were treated with 20μM MG-132 to inhibit the proteasome. Expression levels following treatments were determined by immunoblotting lysates for YFP tag. A. Representative western blots. B. Results represented as mean ± SEM, n=4. Statistical differences were determined using the Student's t-test.

5.4.3 Detecting SUMOylated β_2AR-YFP PLA

PIASγ is a SUMO E3 ligase enzyme that promotes SUMOylation. An adenovirus that overexpresses PIASγ-HA has been generated with the help of Dr. Lauren Wills and Professor Stu Nicklin's group. NRVM cells infected with WT or MUT β_2AR-YFP underwent infection with the E3 ligase PIASγ virus or mock infection. Bands shown at 57kDa indicated that PIASγ has been successfully expressed in NRVM cells (**Figure 5.7**).

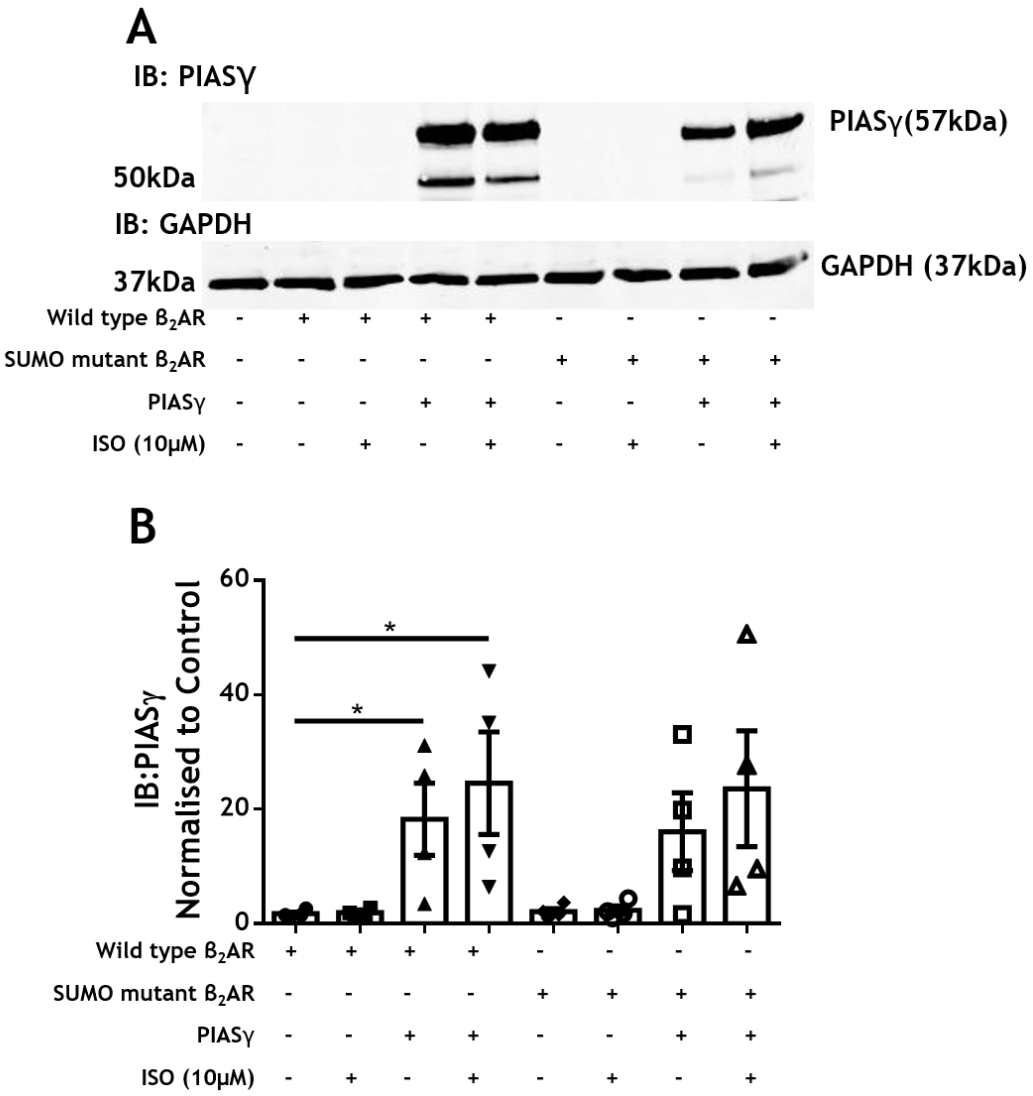

Figure 5.7 Confirmation of PIASγ-HA overexpression in NRVM. NRVM were infected with PIASγ-HA viruses MOI 100 for 24 hours prior to harvesting the cell lysates and analysis via immunoblotting. A. Representative example blots. B. Results represented as mean ± SEM, n=6. *$p<0.05$. Statistical differences were determined using the Student's t-test.

Previous data **Figure 3.11** in Chapter 3 from this thesis have shown that PLA signals resulting from the co-localisation of antibodies against β_2AR and SUMO-β_2AR decreases when the SUMOylation site of β_2AR is mutated in HEK293 cells overexpressing β_2AR-YFP. PLA assay was also performed in β_2AR-YFP WT or MUT overexpressing NRVM and PLA signals could be detected suggesting that SUMOylation of the β_2AR also happens in primary cell lines. Adenovirus overexpressing PIASγ-HA NRVM cells were subjected to PLA assay techniques as described before in Chapter 3. Under basal conditions, as in Chapter 3, I observed less PLA signals with the SUMO mutant compared to WT β_2AR (**Bar 1 vs 5, Figure 5.8B**), although the difference was not significant. The PLA signals for WT β_2AR-YFP overexpressing NRVM were enriched after 1 minute of 10μM ISO and PIASγ overexpression (**Figure 5.8A**) and this seemed to be the optimal condition producing the largest number of PLA complexes (**Figure 5.8B)**. There was less PLA detected when the mutant β_2AR was transfected under optimal conditions (with ISO+PIASγ) however, there was lack of significant differences between the treatments due to the high variability of the data (**Figure 5.8B**).

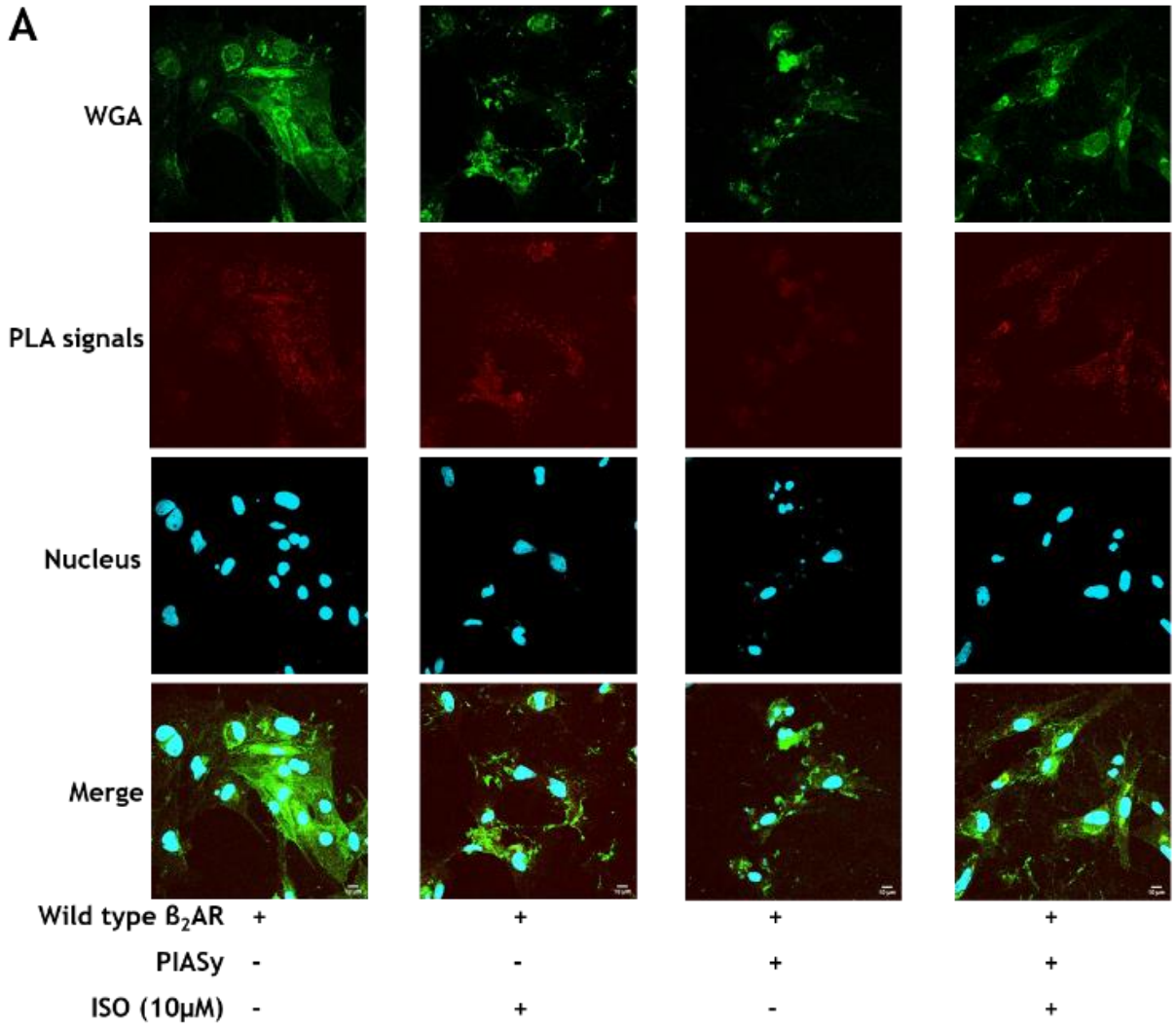
A
WGA
PLA signals
Nucleus
Merge
Wild type β2AR + + + +
PIASy - - + +
ISO (10μM) - + - +

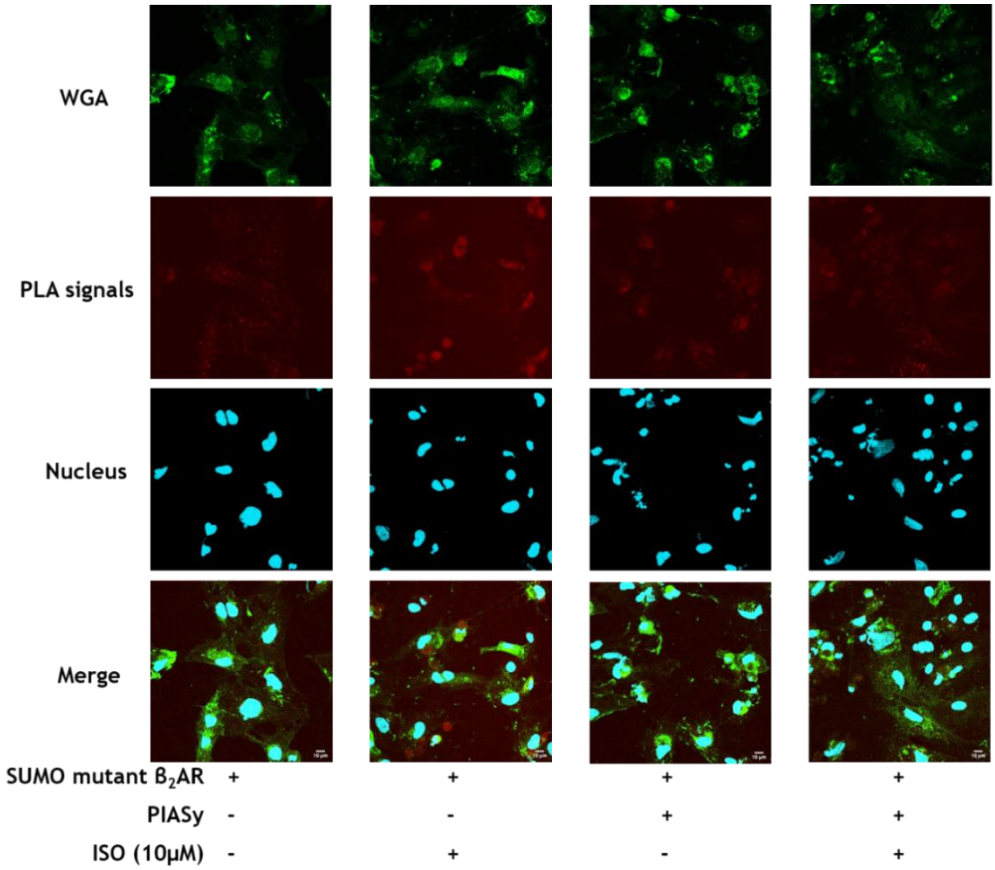

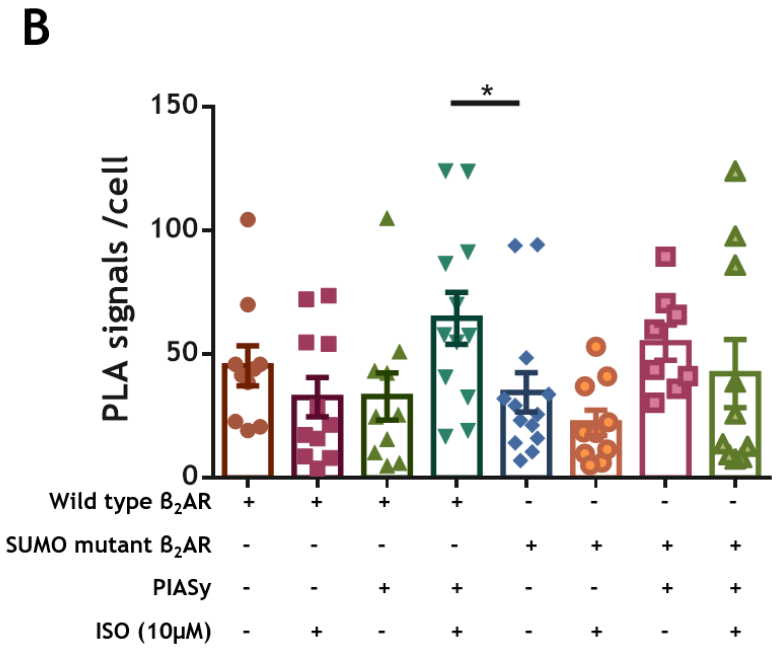

Figure 5.8 PLA assay on MUT or WT ß$_2$AR-YFP overexpressing NRVM. SUMOylated ß$_2$AR-complexes were recognised with PLA as red dots. PLA signals are only shown in cases where ß$_2$AR and SUMO-ß$_2$ antibodies were in close proximity. NRVM were counterstained with WGA to show the membranes. ProLongTM GOLD antifade moutant with SYTOXTM DEEP RED was used to mark nuclei. A. representative images. B. Results represented as mean ± SEM, n=4. Statistical differences were determined using the Student's t-test.

5.4.4 The Effect of β_2AR SUMOylation on β_2AR Signalling in NRVM.

NRVM cells were infected with MUT or WT β_2AR-YFP and PIASγ-HA virus prior to treatment. When infected NRVM cells were stimulated with 10μM isoprenaline for 1-minute, little increase in PKA-mediated phosphorylation of β_2AR by PKA was detected for any of the groups (**Figure 5.9**) (n=4). Total PKA phosphorylation of global substrates was also measured using a phospho-PKA consensus motif antibody and this also was not increased by ISO treatment in any of the groups (**Figure 5.10**). Surprisingly, isoprenaline stimulation also failed to promote the phosphorylation of ERK MAP kinase (**Figure 5.11**). No differences were detected between the PKA phosphorylation of WT and MUT β_2AR-YFP overexpressed in NRVM cells. All of the data were inconclusive as I failed to observe the classical PKA phosphorylation of the β_2AR and associated ERK activation previously seen in cardiac myocytes following ISO treatment (Baillie et al., 2002).

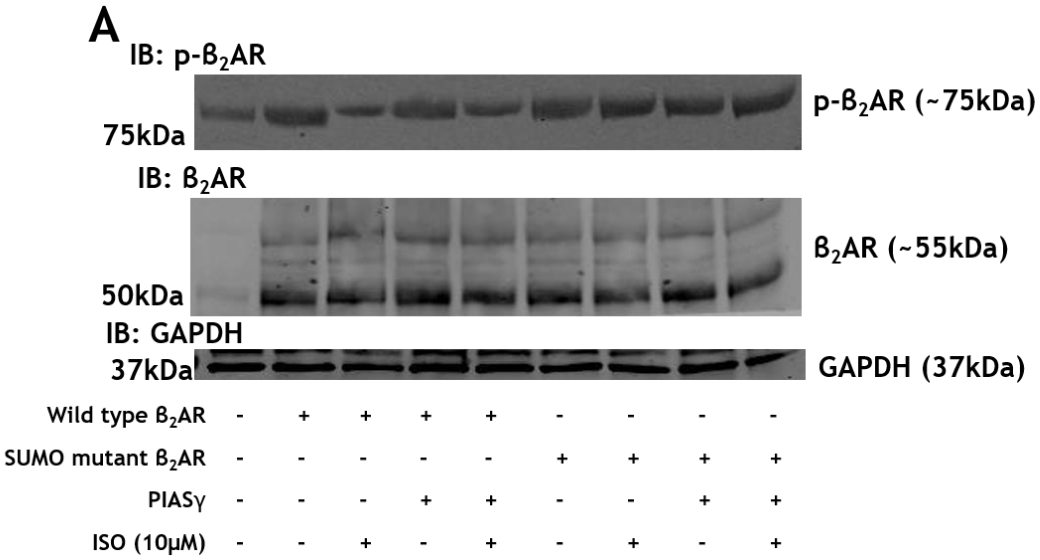

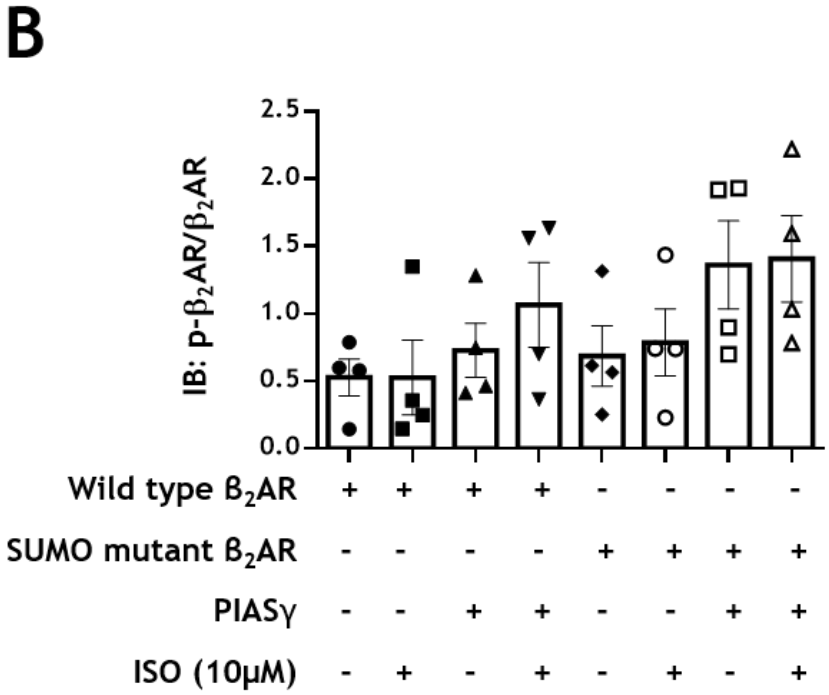

Figure 5.9 Influence of β2AR SUMOylation on PKA phosphorylation of β2AR mediated by isoprenaline. NRVM infected with MUT or WT β2AR -YFP virus MOI 500, and PIASγ-HA viruses MOI 100 for 24 hours were stimulated with 10μM ISO for 1 minute prior to harvesting the cell lysates and analysis via immunoblotting. A. Representative example blots. B. Results represented as mean ± SEM, n=4. *p<0.05, **p<0.01, ***p<0.001. Statistical differences were determined using the Student's t-test.

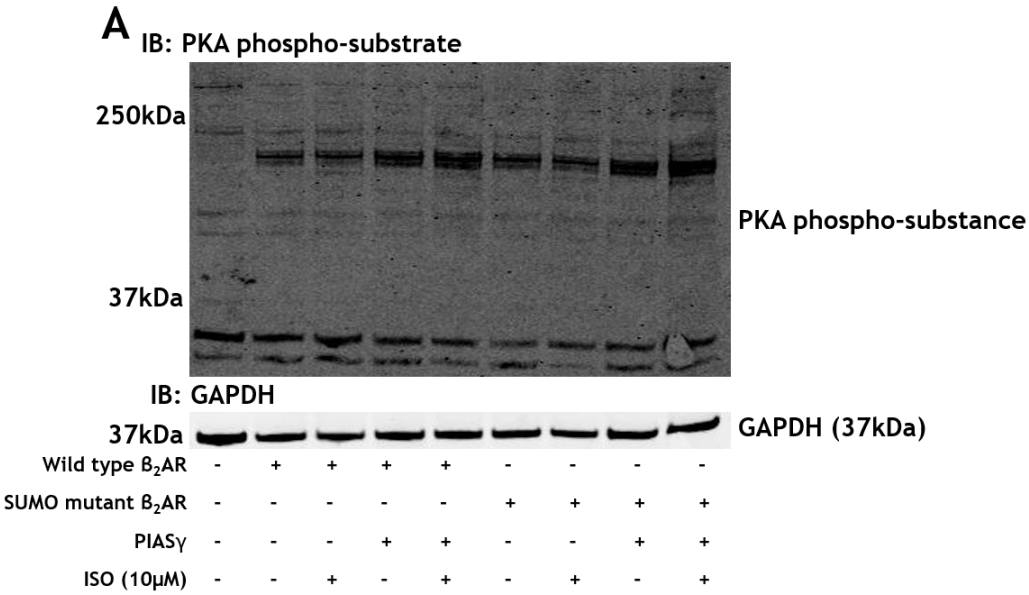

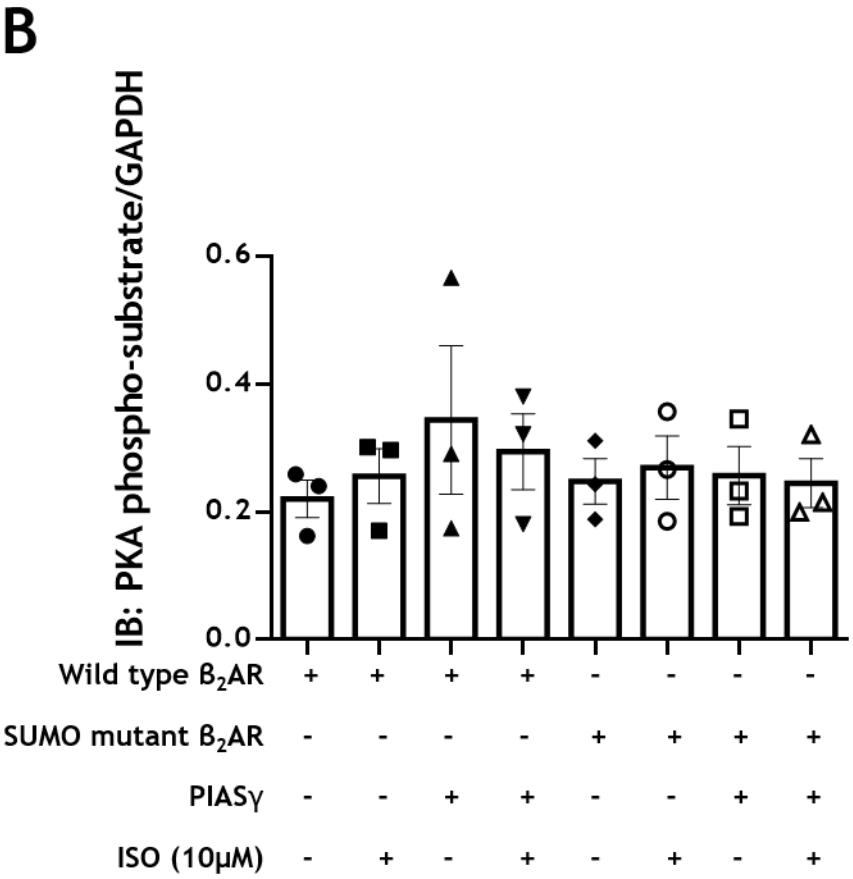

Figure 5.10 Analysis of PKA-mediated global substrate phosphorylation by isoprenaline. NRVM infected with MUT or WT β_2AR -YFP virus MOI 500, and PIASγ-HA viruses MOI 100 for 24 hours were stimulated with 10μM ISO for 1 minute prior to harvesting the cell lysates and analysis via immunoblotting. A. Representative example blots. B. Results represented as mean ± SEM, n=3. *$p<0.05$. Statistical differences were determined using the Student's t-test.

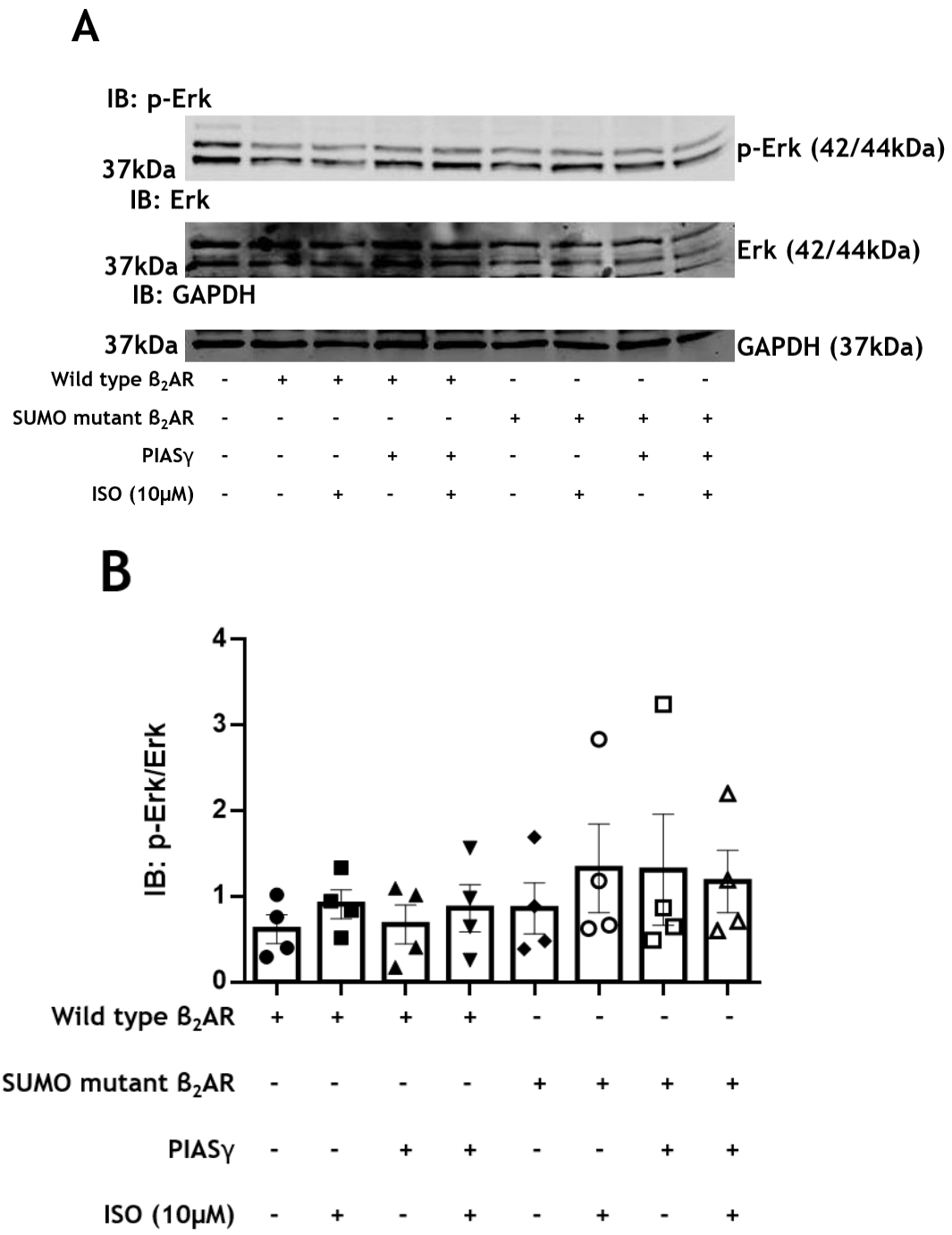

Figure 5.11 Evaluation of ERK activation mediated by isoprenaline. NRVM infected with MUT or WT β_2AR -YFP virus MOI 500, and PIASγ-HA viruses MOI 100 for 24 hours were stimulated with 10μM ISO for 1 minute prior to harvesting the cell lysates and analysis via immunoblotting. A. Representative example blots. B. Results represented as mean ± SEM, n=4. Statistical differences were determined using the Student's t-test.

The expression of proteins involved in the SUMOylation cascade was also investigated. The E2 enzyme conjugates SUMO to the consensus motif of a target substrate protein, and there is only one known E2 enzyme, UBC9. It is therefore possible that the level of UBC9 in the cells may influence the level of protein SUMOylation in the cells. However, I found no difference in endogenous UBC9 expression between WT and MUT β_2AR-YFP cells or combination with PIASγ-HA protein overexpression (**Figure 5.12**).

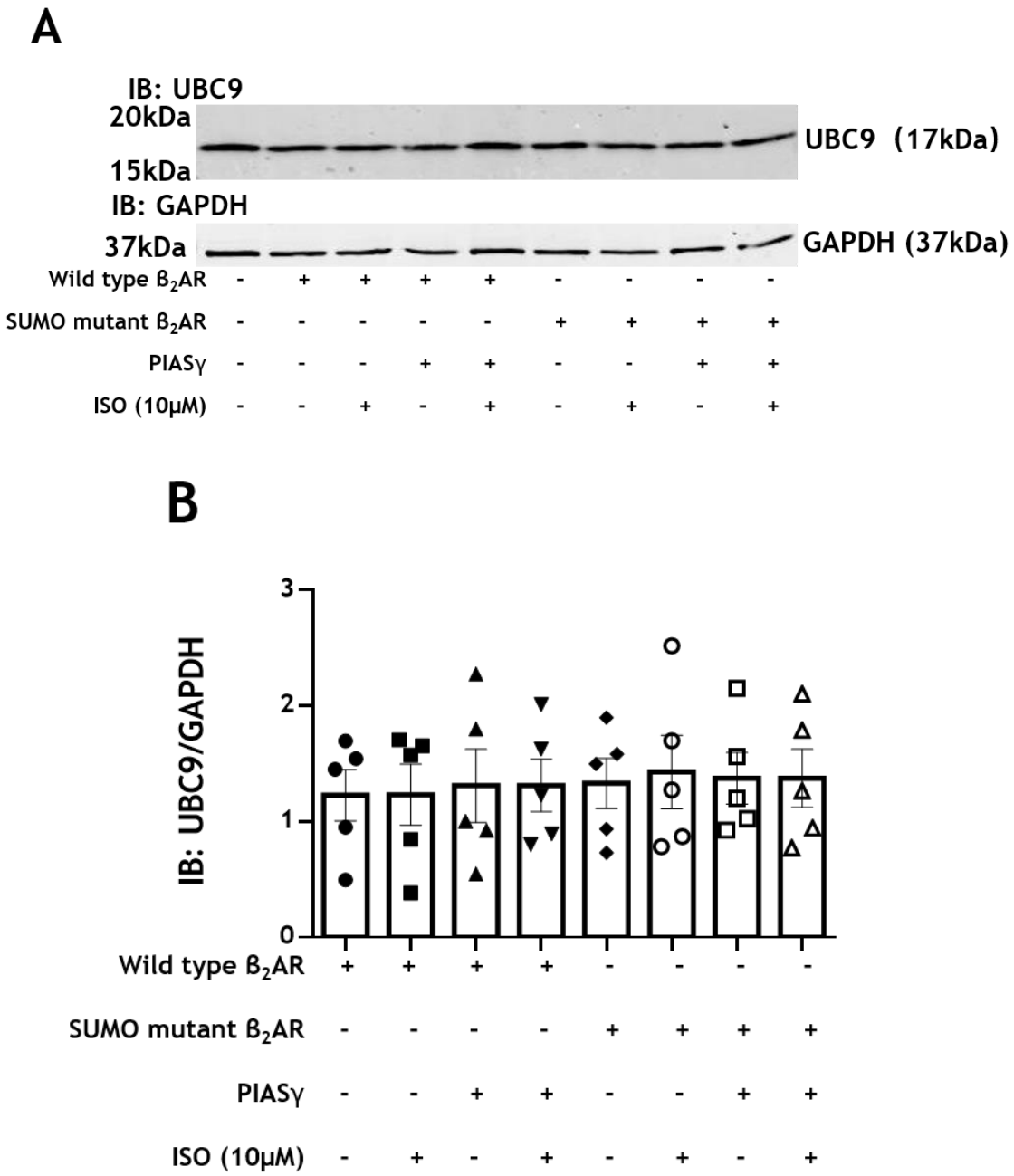

Figure 5.12 Influence of β_2AR on endogenous UBC9 expression. NRVM infected with MUT or WT β_2AR -YFP virus MOI 500, and PIASγ-HA viruses MOI 100 for 24 hours were stimulated with 10μM ISO for 1 minute prior to harvesting the cell lysates and analysis via immunoblotting. A. Representative example blots. B. Results represented as mean ± SEM, n=5. Statistical differences were determined using the Student's t-test.

5.4.5 Measuring possible activation of SUMOylation in cardiomyocytes following N106 treatment.

N106 is a small molecule that can enhance SERCA2a SUMOylation (Kho et al., 2015c). A putative mechanism has been offered by the Hajjar group and involves the compound binding directly to the SUMO E1 ligase to activate the enzyme. We used N106 to conduct a series of experiment in β_2AR-MUT and β_2AR-WT overexpressing NRVM cells. **Figure 5.13** shows that there was no significant increase in the SUMOylation of the proteome of NRVMs following treatment of increasing doses of N106. Different time courses of N106 treatment also resulted in no significant increase on general SUMOylation of substrates in NRVM (**Figure 5.14**). Unfortunately, it seems that N106 does not act to increase the SUMOylation in NRVM cells, hence it was impossible to draw any conclusions from these experiments.

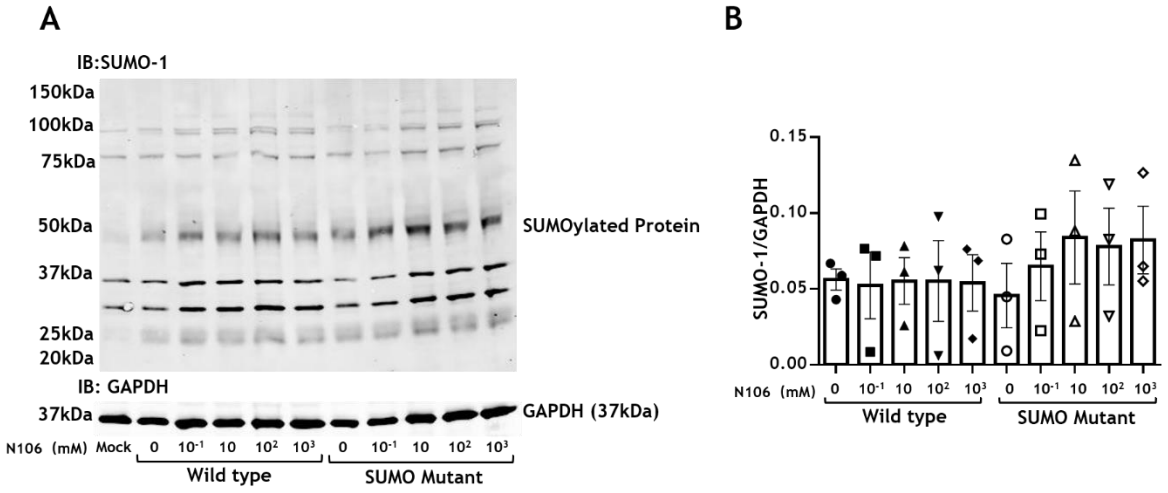

Figure 5.13 N106 treatment has no effect on global SUMOylation in cardiomyocytes. NRVM infected with MUT, or WT β_2AR -YFP virus MOI 500 for 24 hours were treated with a series concentration of N106 for 1hour prior to harvesting the cell lysates and analysis via immunoblotting. A. Representative example blots. B. Results represented as mean ± SEM, n=4. Statistical differences were determined using the Student's t-test.

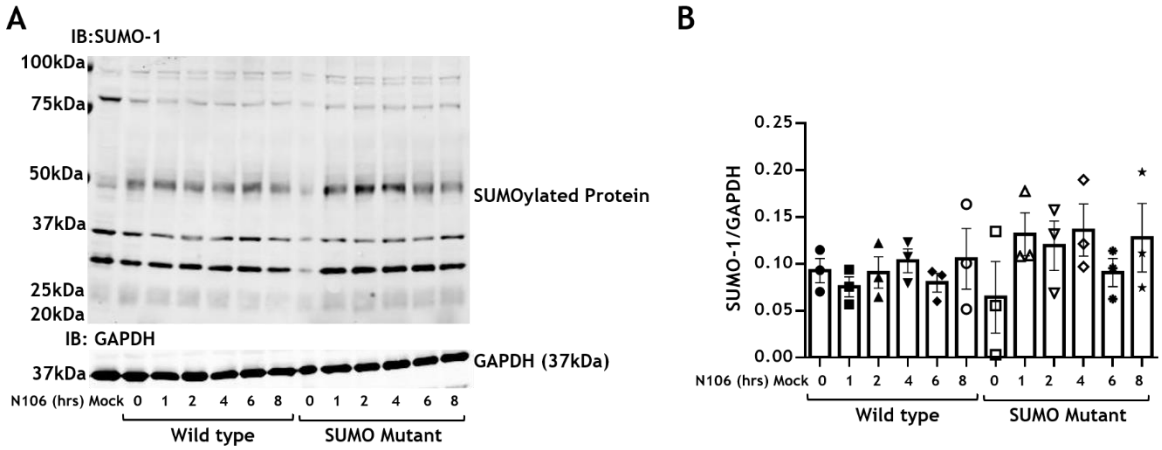

Figure 5.14 Treatment time of N106 has no effect on global SUMOylation in cardiomyocytes. NRVM infected with MUT, or WT β_2AR -YFP virus MOI 500 for 24 hours were treated of 10uM N106 for a series of time length prior to harvesting the cell lysates and analysis via immunoblotting. A. Representative example blots. B. Results represented as mean ± SEM, n=4. Statistical differences were determined using the Student's t-test.

5.4.6 The Effect of β_2AR SUMOylation on Cardiac Myocyte Contractility

To determine whether SUMOylation of the β_2AR affected the contraction dynamics of cardiac myocytes, NRVM monolayers were infected with recombinant adenoviruses to overexpress β_2AR-YFP MUT and β_2AR-YFP WT. The experiments were undertaken in cells treated with 10μM ISO stimulation or PBS as control. Baseline values were recorded before the stimulation, and for every minute during the first 10 minutes after ISO stimulation and thereafter every 5 minutes until 30 minutes. As described in **Figure 5.2**, image stacks of contracting NRVM monolayers were converted into contraction traces using MUSCLEMOTION software (Sala et al., 2018b). The traces were used to compare contractile parameters between the β_2AR MUT and β_2AR WT following ISO stimulation including interval, UP90, DN90 and CD50. All the data recorded were normalised to baseline recordings. Data were then converted into frequency delta and normalised to PBS control delta, finally, the data were displayed as double delta frequency in **Figure 5.15**-**Figure 5.18** with interval, UP90, DN90 and CD50 respectively.

Firstly, interval, also known as the time between contractions was measured, which provides information on the frequency of contraction (**Figure 5.15A).** Untransfected myocytes (labelled mock cells) showed a rapid response to ISO stimulation in the first minute reaching almost 150% of PBS response. After this the receptor response seemed to be desensitized, falling back to basal levels at 3 minutes (**Figure 5.15B)**. Surprisingly, this response was not observed in NRVMs over-expressing the β_2AR-WT and β_2AR-MUT, as in both these groups ISO treatment seemed to cause a small reduction in the rate of contraction to -25% over the first 3 minutes, followed by a slow and incomplete recovery over 30 minutes (**Figure 5.15C&D)**.

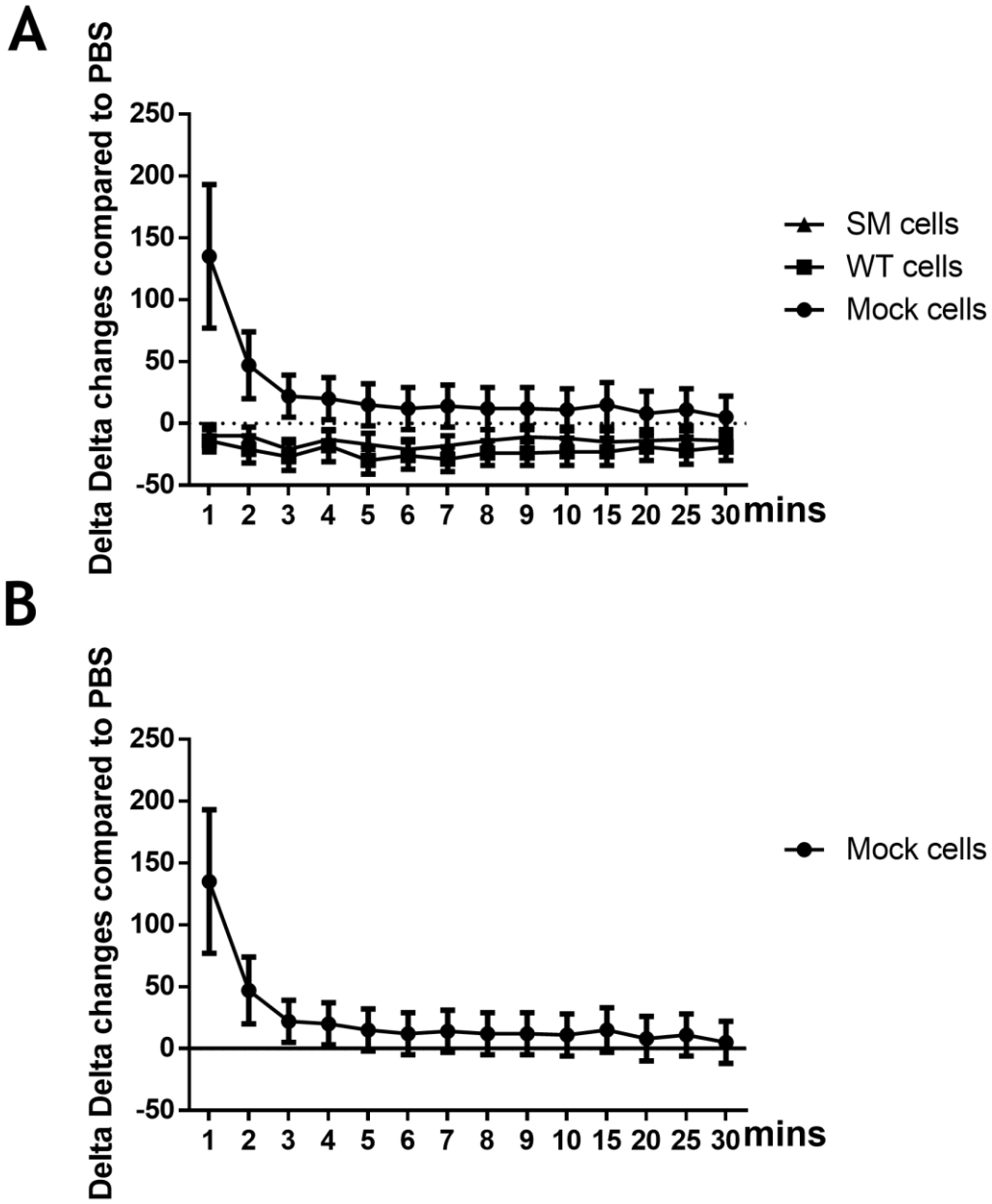
A
Delta Delta changes compared to PBS
250
200
150
100
50
0
-50
1 2 3 4 5 6 7 8 9 10 15 20 25 30 mins
SM cells
WT cells
Mock cells
B
Delta Delta changes compared to PBS
250
200
150
100
50
0
-50
1 2 3 4 5 6 7 8 9 10 15 20 25 30 mins
Mock cells

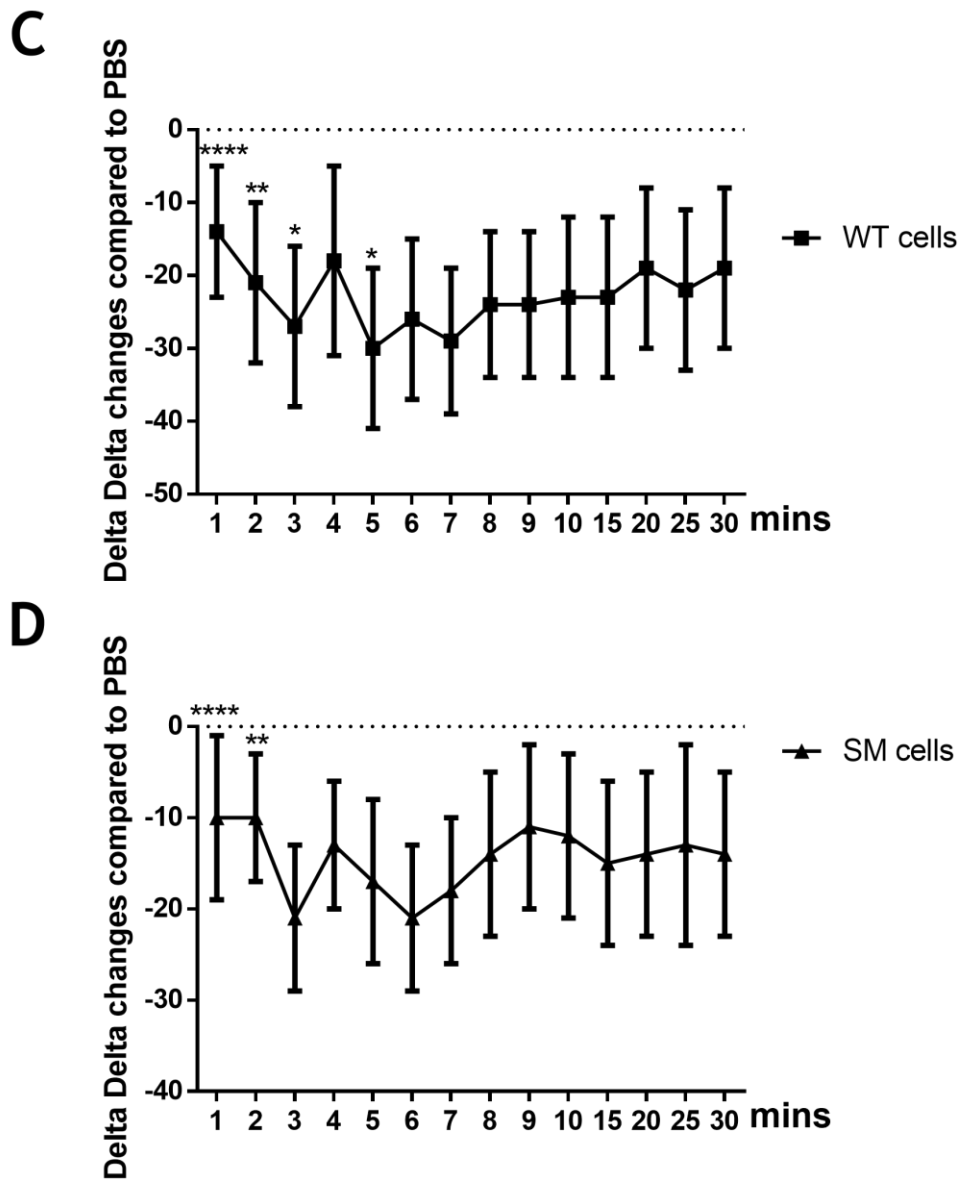

Figure 5.15 Analysis of NRVM contraction interval. Using CELLOPTIQ®, NRVM monolayer were imaged at a rate of 100 frames per second for eight seconds. Each microscope area was measured at baseline and every minute in first 10 minutes after treatment and every 5 minutes until 30 minutes after PBS or 10μM isoproterenol (ISO) stimulation. The image stacks were analysed using the ImageJ plug-in, MUSCLEMOTION, to create contractility traces. Interval was analysed to show the time between each contraction. A. Data were displayed the cells with mock, wild type β_2AR and mutant β_2AR overexpressed in double delta frequency change of interval contractility. B. Data were shown of contraction interval changes with the mock cells with 10 μM ISO treatment for double delta frequency change. C. Data were shown of contraction interval changes with the overexpressed wild type β_2AR NRVM cells with 10 μM ISO treatment for double delta frequency change. *$p<0.05$ β_2AR -WT vs. Mock, **$p<0.01$ β_2AR -WT vs. Mock, ****$p<0.0001$ β_2AR -WT vs. Mock. D. Data were shown of contraction interval changes with the overexpressed K232R-K235R β_2AR NRVM cells with 10 μM ISO treatment for double delta frequency change. **$p<0.01$ β_2AR -MUT vs. Mock, ****$p<0.0001$ β_2AR - MUT vs. Mock. Each data point is representative mean of 3 different microscope area from 4 different individual experimental days. N=4. Two-way-ANOVA with multiple comparisons test.

Secondly, UP90 was analysed as the time from baseline to 90% of the peak contraction (**Figure 5.16A**). This parameter is an estimation of the time it takes NRVM cells to contract. The untransfected NRVM cells (mock cells) had a rapid response to ISO stimulation, showing an increased contraction over the first 2 minutes and maintaining that rate for the duration of the 30-minute course (**Figure 5.16B**). The MUT β_2AR transfected NRVM cells also showed an ISO-induced increase in UP90 which means slowing down the contraction. These cells showed a similar response to untransfected cells (**Figure 5.16D**), but it took longer to reach a plateau and the UP90 was not significantly different from control after 30mins. The wild type β_2AR overexpressing NRVM, however, exhibited a surprising response with an initial (1 min) decrease in UP90 followed by an increase at 2 minutes followed by a sustained decline to approximately -20% of UP90 between 3 and 30 minutes (**Figure 5.16C**). There were statistically different responses between the WT and MUT β_2AR expressing cells at 6, 15, 20, 25 and 30minutes following ISO treatment suggesting that the mutation had an effect on this parameter (**Figure 5.16A**).

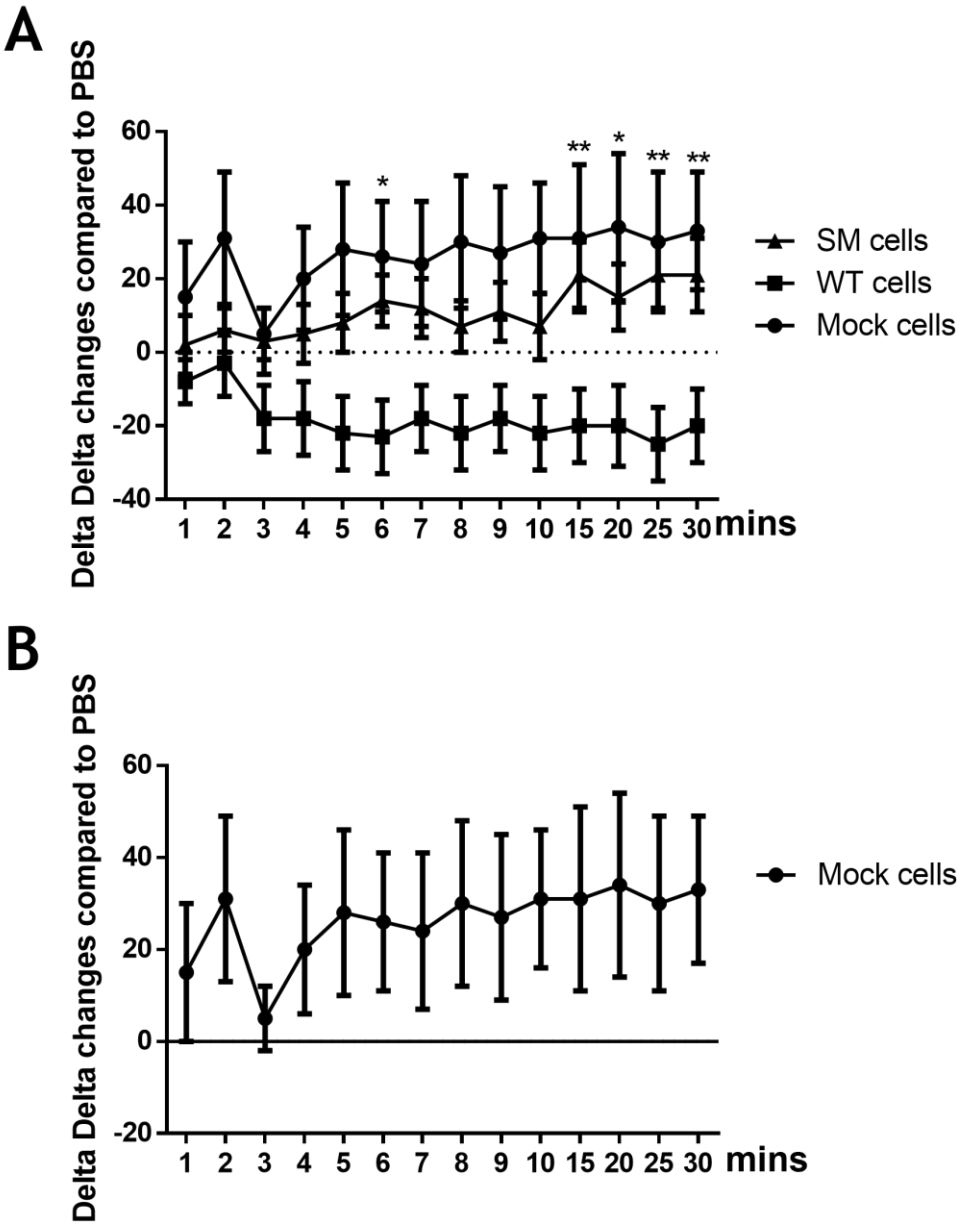
A
Delta Delta changes compared to PBS
60
40
20
0
-20
-40
1 2 3 4 5 6 7 8 9 10 15 20 25 30 mins
*
**
*
**
**
SM cells
WT cells
Mock cells
B
Delta Delta changes compared to PBS
60
40
20
0
-20
1 2 3 4 5 6 7 8 9 10 15 20 25 30 mins
Mock cells

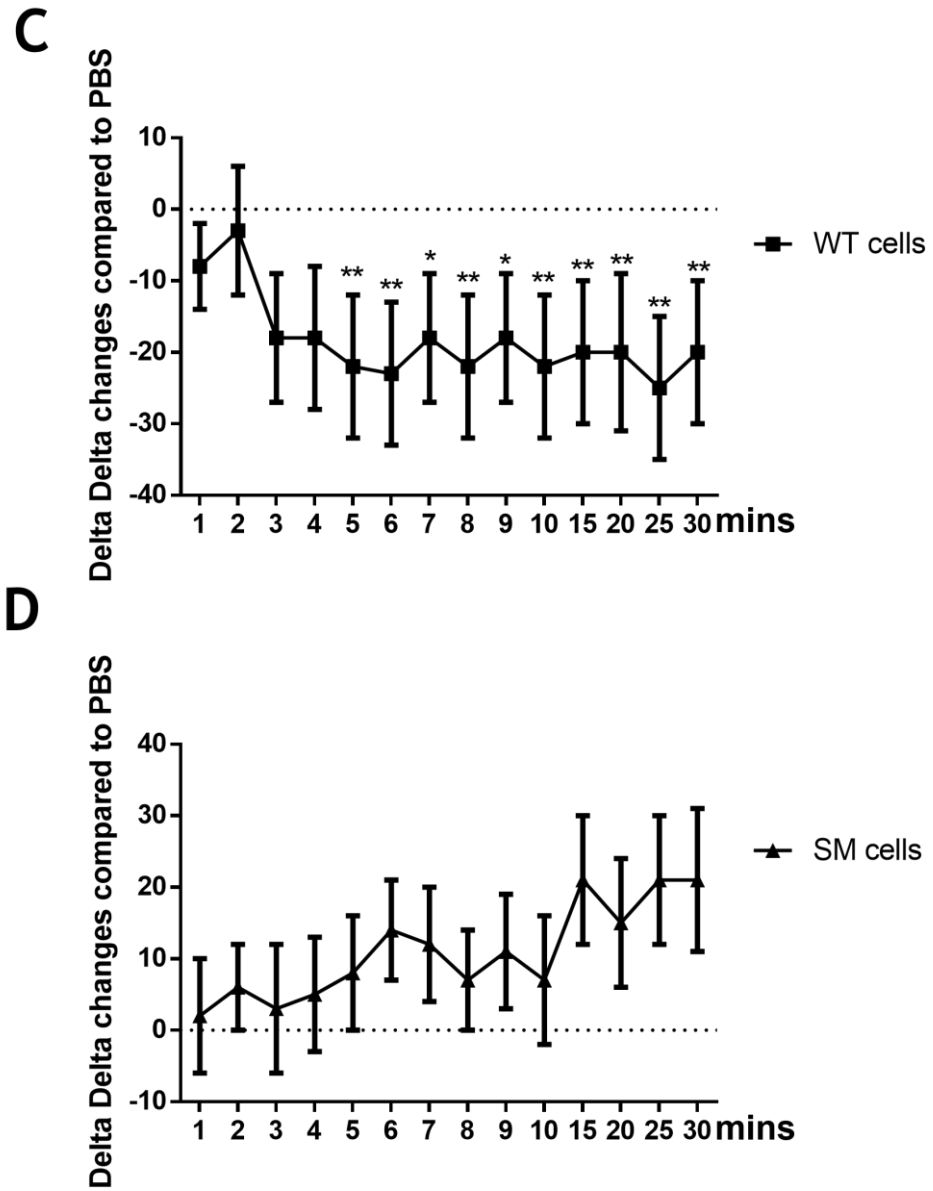

Figure 5.16 Analysis of NRVM contraction UP90. Using CELLOPTIQ®, NRVM monolayer were imaged at a rate of 100 frames per second for eight seconds. Each microscope area was measured at baseline and every minute in first 10 minutes after treatment and every 5 minutes until 30 minutes after PBS or 10μM isoproterenol stimulation. The image stacks were analysed using the ImageJ plug-in, MUSCLEMOTION, to create contractility traces. UP90 was analysed the time from baseline to 90% of peak upstroke and there are no significant differences among untransfected, β_2AR-MUT and β_2AR-WT NRVM. A. Data were displayed the cells with mock, wild type β_2AR and mutant β_2AR overexpressed in double delta frequency change of contraction time. *$p<0.05$ β_2AR -WT vs. β_2AR -MUT, **$p<0.01$ β_2AR -WT vs. β_2AR -MUT. B. Data were shown of contraction changes with the mock cells with 10 μM ISO treatment for double delta frequency change. C. Data were shown of contraction with the overexpressed wild type β_2AR NRVM cells with 10 μM ISO treatment for double delta frequency change. *$p<0.05$ β_2AR -WT vs. Mock, **$p<0.01$ β_2AR -WT vs. Mock. D. Data were shown of contraction changes with the overexpressed K232R-K235R β_2AR NRVM cells with 10 μM ISO treatment for double delta frequency change. Each data point is representative mean of 3 different microscope areas from 4 different individual experimental days. N=4. Two-way-ANOVA with multiple comparisons test.

Thirdly, DN90 was analysed to evaluate the time for myocytes to relax from contraction (**Figure 5.17A**). Mock cells exhibited a rapid increase in relaxation time after 1 minute ISO treatment but with a very high variability, and then the relaxation time dropped to basal levels at 3 minutes and was steady to 30 minutes (**Figure 5.17B**). A similar trend was recorded for the β_2AR MUT overexpressing cardiomyocytes, although the increase was not as dramatic, and the recovery was to a steady state slightly below the basal level (**Figure 5.17D**). Conversely, β_2AR-WT expressing NRVMs responded with a rapid decrease in DN90 following ISO stimulation in the first 2 minutes with a recovery to basal levels at 3 minutes and thereafter within the 30-minute time course (**Figure 5.17C**). The responses of the two transfected β_2AR types (WT vs MUT) were significantly different in the first 2 minutes.

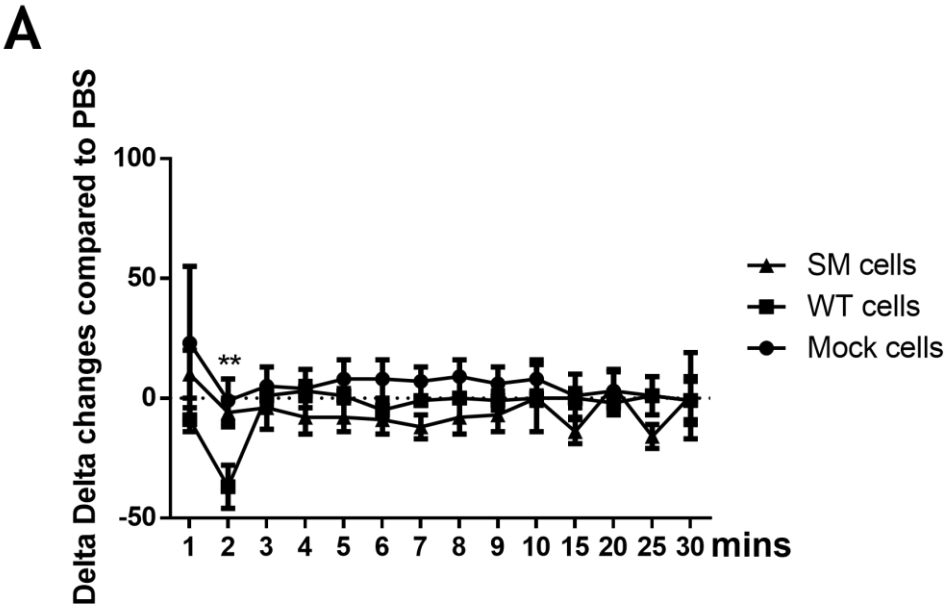
A
Delta Delta changes compared to PBS
100
50
0
-50
**
1 2 3 4 5 6 7 8 9 10 15 20 25 30 mins
SM cells
WT cells
Mock cells

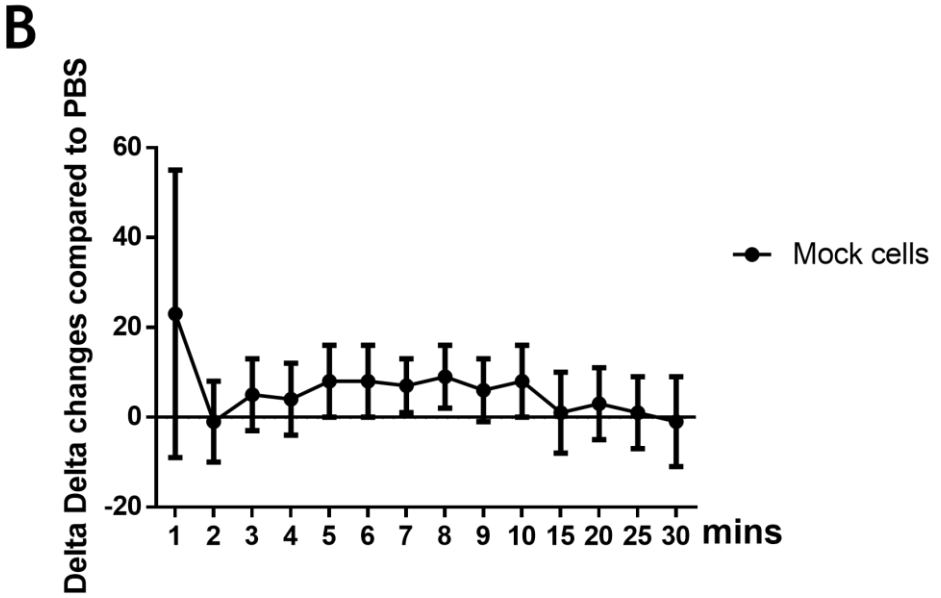
B
Delta Delta changes compared to PBS
60
40
20
0
-20
1 2 3 4 5 6 7 8 9 10 15 20 25 30 mins
Mock cells

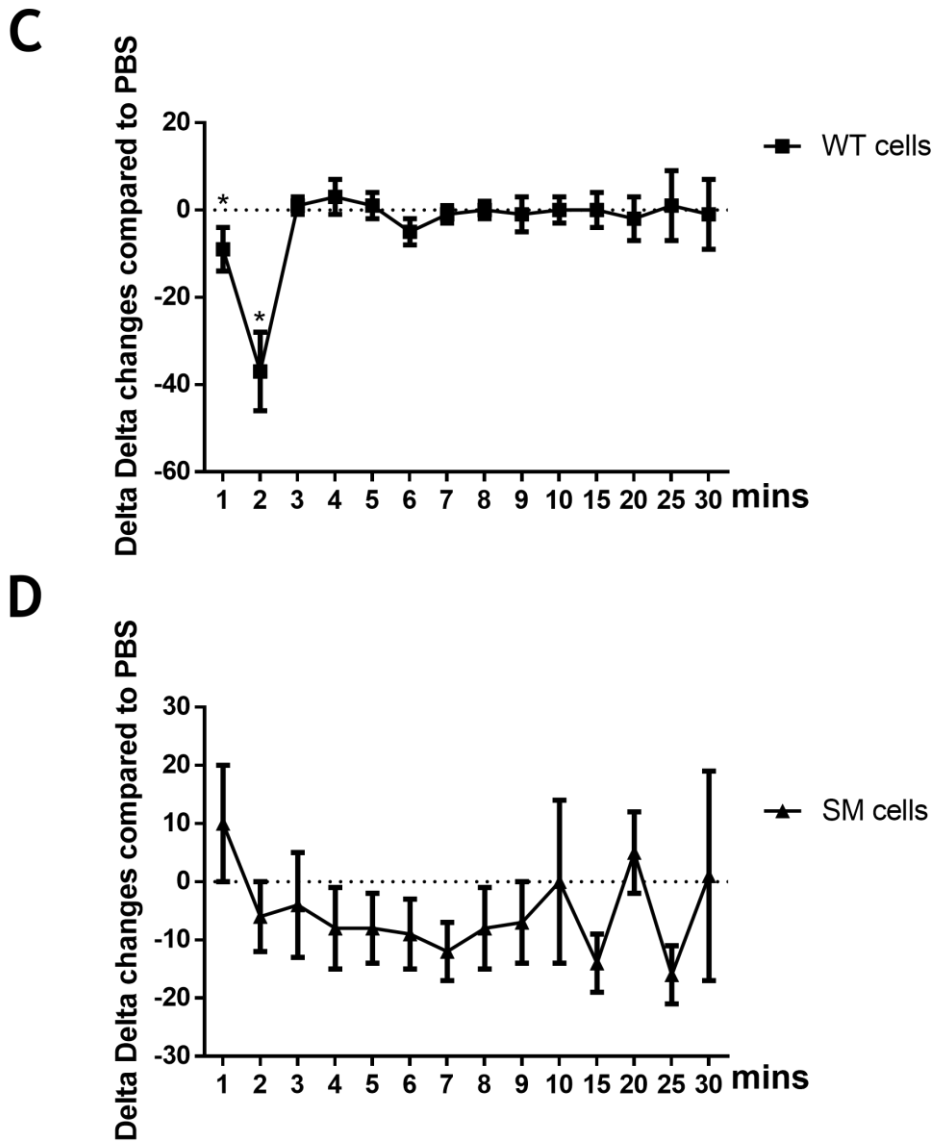

Figure 5.17 Analysis of NRVM contraction relaxation time (DN90). CELLOPTIQ®, NRVM monolayer were imaged at a rate of 100 frames per second for eight seconds. Each microscope area was measured at baseline and every minute in first 10 minutes after treatment and every 5 minutes until 30 minutes after PBS or 10μM isoproterenol stimulation. The image stacks were analysed using the ImageJ plug-in, MUSCLEMOTION, to create contractility traces. DN90 was analysed the time from 90% contraction after the peak back to the baseline. After 10 μM ISO stimulation, the DN90 which indicates the relaxation time of the contraction is longer in β_2AR-MUT overexpression NRVM cells compared to Mock cells. A. Data were displayed the cells with mock, wild type β_2AR and mutant β_2AR overexpressed in double delta frequency change of relaxation. B. Data were shown of relaxation changes with the mock cells with 10 μM ISO treatment for double delta frequency change. C. Data were shown of relaxation changes with the overexpressed wild type β_2AR NRVM cells with 10 μM ISO treatment for double delta frequency change. *$p<0.05$ β_2AR -WT vs. Mock. D. Data were shown of relaxation changes with the overexpressed K232R-K235R β2AR NRVM cells with 10 μM ISO treatment for double delta frequency change. Each data point is representative mean of 3 different microscope areas from 4 different individual experimental days. N=4. Two-way-ANOVA with multiple comparisons test.

Lastly, I evaluated contraction duration 50 (CD50) which is a measure of the time from 50% upstroke to 50% downstroke, taking both contraction and relaxation into account (**Figure 5.18A**). Mock cells exhibited a rapid decrease in CD50 in the first 3 minutes after ISO stimulation, followed by a recovery to a steady state (**Figure 5.18B**) along similar time course to the change in spontaneous frequency rate. This trend was mimicked by the MUT receptor which also observed a decrease till 3 minutes followed by slower recovery (**Figure 5.18D)** WT β_2AR once again was different from the other two groups by showing a fast increase in CD50 (i.e., a slower contraction time) in CD50 over the first 3 minutes followed by a steady decrease towards baseline. Due to the variation in the responses, no significant differences between the mock cells, WT or MUT β_2AR were measured (**Figure 5.18A**).

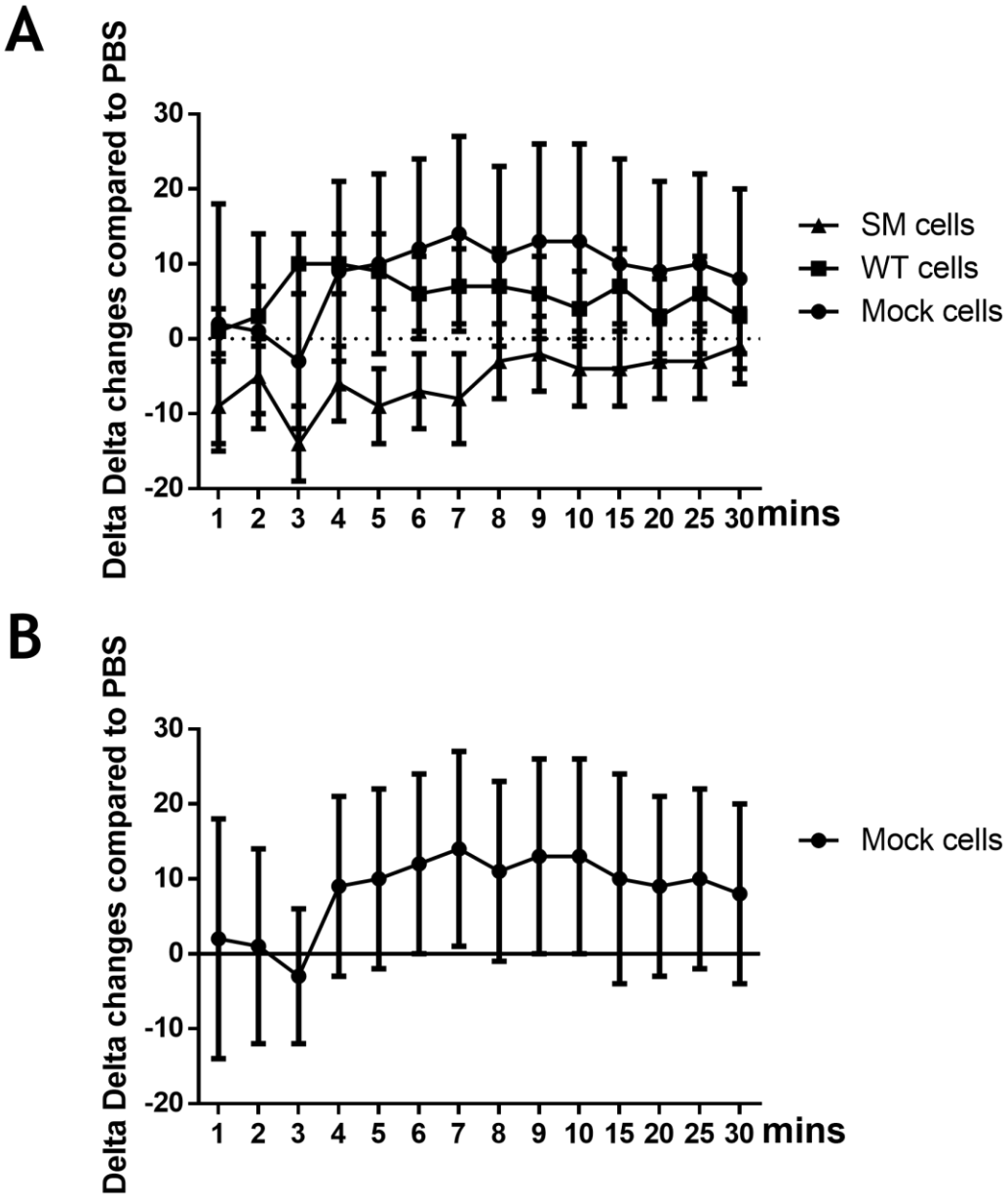
A
Delta Delta changes compared to PBS
30
20
10
0
-10
-20
1 2 3 4 5 6 7 8 9 10 15 20 25 30 mins
SM cells
WT cells
Mock cells
B
Delta Delta changes compared to PBS
30
20
10
0
-10
-20
1 2 3 4 5 6 7 8 9 10 15 20 25 30 mins
Mock cells

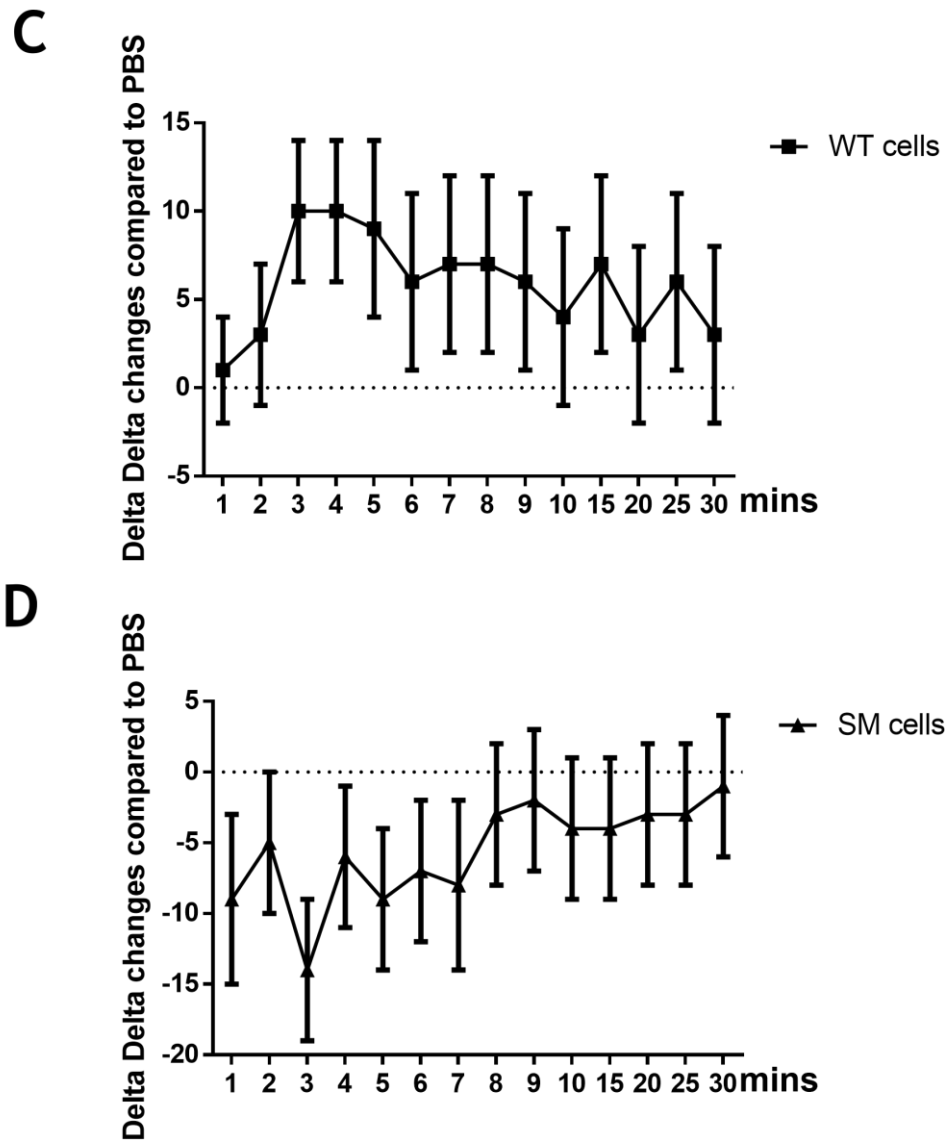

Figure 5.18 Ablation of ß$_2$AR SUMOylation does not affect NRVM contraction CD50. Using CELLOPTIQ®, NRVM monolayer were imaged at a rate of 100 frames per second for eight seconds. Each microscope area was measured at baseline and every minute in first 10 minutes after treatment and every 5 minutes until 30 minutes after PBS or 10μM isoproterenol stimulation. The image stacks were analysed using the ImageJ plug-in, MUSCLEMOTION, to create contractility traces. CD50 was measured the time from 50% upstroke to 50% downstroke and takes both contraction and relaxation changes. Both ß$_2$AR-MUT and ß$_2$AR-WT overexpressed NRVM have longer CD50 time compared to untransfected NRVM. A. Data were displayed the cells with mock, wild type ß$_2$AR and mutant ß$_2$AR overexpressed in double delta frequency change of contraction duration. B. Data were shown of CD50 changes with the mock cells with 10 μM ISO treatment for double delta frequency change. C. Data were shown of CD50 changes with the overexpressed wild type ß$_2$AR NRVM cells with 10 μM ISO treatment for double delta frequency change. D. Data were shown of CD50 changes with the overexpressed K232R-K235R ß$_2$AR NRVM cells with 10 μM ISO treatment for double delta frequency change. Each data point is representative mean of 3 different microscope areas from 4 different individual experimental days. N=4. Two-way-ANOVA with multiple comparisons test.

5.5 Discussion

In this chapter, I used the adenovirus to overexpress wild type or SUMO-null mutant K232R-K235R β_2AR in NRVM cells to study the physiological function of SUMOylation on β_2AR signalling. Firstly, I tested the expression efficiency of recombinant adenovirus overexpression in NRVM cells via western blotting and immunostaining. My data (**Figure 5.3**) indicates that best expression was achieved when MOI=500 of recombinant virus of either WT or MUT β_2AR were introduced into NRVM. Importantly, the WT and MUT in CD50 expressed at the same level meaning that I could directly compare the signalling and physiological data from the WT to the mutant. It is also worth noting that the levels of overexpression were large compared with endogenously expressed β_2AR as I could see little signal when mock transfected cells were probed under the microscope for β_2AR but very strong signals when either the WT or MUT receptor were expressed using the virus (**Figure 5.4**).

The half-life of the receptor protein was measured with cycloheximide (CHX) to study whether the ablation of β_2AR SUMOylation motif results in changes in protein turnover. The results indicated that the SUMO-site mutation had no effect on β_2AR protein turnover. Both WT β_2AR-YFP and MUT β_2AR proteins were stable over the drug time course treatment. This result was expected since the receptors were not activated by ISO in this experiment. β_2AR stability is known to be affected by receptor activation as it promotes receptor ubiquitination (Sudha K. Shenoy et al., 2008)(S. K. Shenoy et al., 2001) and one function of SUMOylation is to block protein degradation by competing for acceptor lysine residues (Ulrich, 2005). Hence, if I were repeating this experiment in the future, I would treat with agonist to see if the WT and MUT receptors were downregulated and ubiquitinated equally.

N106 is a small molecule that has been reported by Kho et al. that can increase SUMOylation of SERCA2a (Kho et al., 2015b). The group has identified that N106 can directly bind to SUMO-activating enzyme, E1 ligase and activate intrinsic SUMOylation of SERCA2a. N106 treatment in their study improved contractile properties of cultured rat cardiomyocytes therefore increased ventricular function

in failing hearts. SERCA2a is an important pump that controls intracellular calcium handling and contractility in cardiac cells. Heart failure can be characterized by impaired Ca^{2+} reuptake as a result of decreased expression and activity of SERCA2a. The same group had shown previously that SERCA2a is one of the substrates of SUMOylation, and in HF, SUMO-1 gene transfer resulted in the restoration of SERCA2a levels. This improved the haemodynamic situation and decreased mortality in a pressure overloaded HF murine model (Kho et al., 2011).

In this chapter, I also aimed to use N106 to increase the possible SUMOylation of the β_2AR as it had been previously been shown to be a substrate (Wills, 2017). Traditionally, it has always been difficult to "force" SUMOylation of substrates in cells and methods such as SUMO E3 ligase overexpression (Li et al., 2010), SUMO overexpression (Kho et al., 2011) and conjugation of proteins to UBC9 have been previously used (Gupta et al., 2014). A pharmacological tool (N106) to enhance SUMOylation represents an advance as it does not involve transfection of cells, instead working on the endogenous SUMO cascade. Unfortunately, the compound did not upregulate global SUMOylation in NRVM cells (**Figure 5.13&Figure 5.14**). This contradiction may be due to different experimental systems since Kho et al used mice aged 8-10 weeks or rats aged 3 months, whereas I used cell cultures of new-born rat cardiomyocytes. The age difference of the rats between the Kho group and cells used here might be a possible reason that the N106 has different outcome on SUMOylation in these studies. SUMOylation is highly implicated in cardiac gene expression during development of the heart (Mendler et al., 2016b). Hence it is unlikely that immature cardiac myocytes lack the available SUMOylation machinery and that was backed up in the data I present here where I show presence of SUMO and UBC9 (**Figure 5.12**). In hindsight, I should have shown that the SUMO E1 enzyme was present, as that is the enzyme on which N106 works. Since the discovery of N106, other work has shown that increases in SUMOylation triggered by the drug can enhance the nuclear translocation of pro-caspase1 to the nucleus (Lu et al., 2021). It is possible that the batch of N106 that I purchased was defective in some way as I used it at similar concentrations and protocol as to what has been previously published.

In an attempt to discover a physiological difference between responses evoked by the WT vs MUT, I used CellOPTIQ® and NRVM cells. Responses in the untransfected cells were largely as expected with quick, transient responses to ISO (compared with PBS control) in terms of an increased spontaneous frequency (**Figure 5.15**) enhanced contraction (**Figure 5.16**) and relaxation times (**Figure 5.17**) but quickly returned to basal following what appeared to be a rapid desensitisation. Overexpression of the β_2AR (WT and MUT) was expected to enhance these effects, however this was not the case for MUT β_2AR which, showed similar but less pronounced effects to mock transfected cells in all parameters except frequency (**Figure 5.15-Figure 5.18**), where the frequency was decreased marginally (Interval went up). Additionally, overexpression of the WT β_2AR produced a series of unexpected counter-intuitive data sets in all the parameters that are challenging to explain (**Figure 5.15C-Figure 5.18C**).

Contractility of cardiomyocytes have been thought as one of the important factors for heart function (Bazan et al., 2012). With respect to the response to isoprenaline, overexpression of both WT and MUT seemed to transiently decrease contraction rate over first few minutes followed by a slow desensitization over the following 27 minutes (**Figure 5.15**). Previous work has shown that gene transfer of the β_2AR into the heart enhances responses to ISO when low (x4) overexpression is achieved (Kawahira et al, 1999). It is possible that the unexpected results shown here relate to the level of overexpression of the exogenous receptors. I was unable to detect much β_2AR in the mock cells but saw very large overexpression in transfected cells (**Figure 5.4**). Liggett et al. have studied the potential relationship between the level of β_2AR overexpression and biochemical, molecular, and physiological functions. They found out that a 60-fold enhancement of β_2AR boosted basal cardiac function without increasing mortality whereas a 100-fold overexpression in mouse heart resulted in poorer output and the development of fibrotic cardiomyopathy and heart failure (Liggett et al., 2000). This study suggests that massive overexpression of the β_2AR may be detrimental to cardiac cell physiology, and this may partly explain why I see the opposite effect to what was expected and to what was seen in cells expressing endogenous levels of the β_2AR. Similarly, previous work using overexpression of the β_1AR in heart has recorded reduced contractility in response to ISO when the

WT β_1AR was transfected (Kawahira et al, 1999). This effect was linked to decreased adenylate cyclase activity caused by excess linking to the inhibitory G_i protein (Akhter et al., 1997). Another factor that significantly depressed contractile function in β_1AR overexpressing heart cells via desensitization was enhanced GRK (Beta-adrenergic receptor kinase) activity, which was upregulated in the cells overexpressing the receptor. These observations match well with the signalling data I present (**Figure 5.11**) where I could detect little evidence of cAMP activation of PKA. In hindsight, I should have evaluated expression and activity of GRK2 and adenylate cyclase in my cells. Treatment of pertussis toxin to block Gi signalling may also have restored the response to ISO in β_2AR (WT and MUT) overexpressing cells. There are also reports of spontaneous conformational changes in overexpressed β_2AR that lead to intrinsic activation and subsequent desensitization prior to agonist challenge (Zhou et al., 1999). This may have been happening in my case leading to a blunted response.

Previous work using systems to genetically enhance cardiac β_2AR expression have reported increased contractility above levels seen in control animals (Milano et al., 1994)(Bittner et al., 1996). In my work, I observed increases in contraction (UP90) in endogenous systems (**Figure 5.16B**) and MUT β_2AR overexpressing cells (**Figure 5.16D**) following ISO treatment. Enhanced WT receptor expression, however seemed to cause a decrease in contraction rates. It is known that spontaneous activation of the β_2AR can happen at very high expression levels (Liggett et al., 2000) and it may be that the receptors were in the desensitization phase already before ISO was administered. This parameter (UP90) showed the largest significant difference over time when compared with β_2AR MUT and it could be that a SUMO-deficient β_2AR mutant is less likely to spontaneously activate and be more susceptible to ISO enhanced contractile responses. Additionally, as the SUMO site on the β_2AR is unavailable in the MUT construct, an indirect effect caused by sequestration of the SUMO machinery by overexpression of the WT construct may not apply to the MUT construct. For example, it is known that SUMOylation is essential for sarcomeric coordination (Nayak & Amrute-Nayak, 2020) and sequestration of UBC9 by overexpressed WT β_2AR may be detrimental to the mechanism of the myofilaments causing changes in contraction. Sarcomere consists of filaments that are organized in an intricate structure and a

fundamental contractile unit of striated skeletal and cardiac muscle, which hosts a fine assembly of macromolecular protein complex (Nayak & Amrute-Nayak, 2020) Indeed, there are multiple reports of loss of muscle contractile capacity when the SUMO signalling system is perturbed (Mendler et al., 2016a)(Heras et al., 2019) (Nayak et al., 2019).

Studies have shown that perfused hearts from β_2AR overexpressing mice show an increased rate of relaxation compared with control hearts (Cross et al., 1999). Interestingly, in this chapter **Figure 5.17**, I observed a transient reduction in the relaxation response in β_2AR-WT overexpressing NRVM cells. This response was not seen for mock transfected cells or cells overexpressing β_2AR MUT. As the responses in WT vs MUT were different, again it could be possible that sequestration of proteins such as UBC9 to service β_2AR-WT in the overexpressed system could be of detriment to other essential SUMOylation events in the myocyte. The Baillie lab has found that both filament protein Troponin I (TNI) (Fertig, 2019) and Myosin Binding Protein C (MBPC) (unpublished data in Baillie group) can be SUMOylated and that in the case of TNI, abrogation of SUMOylation of TNI indirectly leads to changes in the force of contraction in response to calcium. Investigations into the SUMOylation of TNI and MBPC following transfection of β_2AR WT and β_2AR Mut may be able to identify a difference in the susceptibility of the filament proteins to be SUMOylated when the β_2AR-WT is overexpressed.

In conclusion, overexpression of β_2AR WT has not enhanced the contractility, frequency, or relaxation of NRVMs as I expected. I have provided tentative explanations that centre around the very high level of overexpression achieved. This however does not explain the contrast to the β_2AR MUT data, which may be more similar to that of the mock cells as both should not sequester large amounts of SUMOylation cascade proteins. All of the theories I have proposed will require robust testing before being regarded as factual. Future work should seek to find a level of overexpression that does not lead to unphysiological consequences.

Chapter6. General Discussion

6.1 β_2AR SUMOylation

The β_2AR is probably the best characterised G-protein coupled receptor (GPCR) as a substrate for various different post-translational modifications (PTM). As mentioned in Chapter 1, β_2AR has been identified as a substrate for phosphorylation, palmitoylation, ubiquitination and glycosylation (Grisan et al., 2020)(R. Liu et al., 2012)(S. K. Shenoy et al., 2001)(Mialet-Perez et al., 2004). As much recent evidence has been shown on the protective effects of SUMOylation on cardiac signalling proteins (Kho et al., 2011), my hypothesis was that the β_2AR may also be a substrate for SUMOylation. To my knowledge, this is the first time that the possibility of β_2AR SUMOylation had been considered.

In chapter 3, I used different methods to test the likelihood of the β_2AR being a SUMO substrate. Firstly, an *in vitro* SUMOylation assay was used in conjunction with a novel antibody. The SUMO-β_2 antibody is a custom designed anti-serum designed to recognise only SUMOylated forms of β_2AR at a SUMOylation site (**Figure 3.2**). The antibody was designed and made by Dr Lauren Wills (Wills, 2017). The data showed that the SUMO-β_2 antibody successfully recognized the SUMOylated β_2AR when cell lysates were incubated with SUMOylation assay mix. Secondly, I used peptide array to identify the SUMOylation site of β_2AR (**Figure 3.9**). In the SUMO motif, I replaced the lysine at 232 or/and 235 with arginine and this identified K235 as the acceptor lysine for SUMO. Lastly, immunofluorescence staining was used to detect the co-localization of SUMOylated β_2AR and total β_2AR protein (**Figure 3.10**). The SUMO-β_2 antibody labelled the SUMOylated β_2AR and the Pearson's coefficient indicated that overexpression of the SUMO E3 ligase, PIASγ, significantly promoted the SUMOylation of β_2AR. In conclusion, I provide strong evidence that β_2AR is a substrate of SUMOylation and the SUMOylation of β_2AR can be promoted by E3 ligase PIASγ. However, lysine 235 may not be the only lysine within the β_2AR that can be covalently bonded to SUMO-1. Future work should seek to sequentially substitute each lysine in the cytoplasmic parts of the β_2AR to see which ones affect SUMOylation. SUMO-proteomic techniques have also emerged and confirmation of the SUMO-site at Lysine 235 (and other sites) using "omics" techniques should be done (Matic et al., 2010)(Sharma et al., 2019).

As mentioned in chapter 1, the initial SUMO site sequencing analysis of β_2AR was completed back in 2010 (Wills, 2017). The software at that time was based on detecting amino acid that formed the traditional consensus motif ψKxE/D (Hay, 2005) (Hilgarth & Sarge, 2005), phosphorylation-dependent SUMO motifs (Hietakangas et al., 2003)(Yang et al., 2003), and negatively charged amino acid-dependent SUMO motifs (Yang et al., 2006). Several different methods have been developed in the last decade to predict the SUMO conjugation motif on substrates. A system called SUMOgo was developed that considered the influence of PTM information for other sites within the same protein on the accuracy of prediction results to predict SUMOylation sites on the substrate lysines (Chang et al., 2018). The team used Random Forest machine learning methods, motif screening models and chemical features of the potential substrate protein in developing the tool. SUMOgo has largely increased the accuracy of predicting SUMO sites. Another powerful tool called JASSA was invented to predict SUMOylation sites using a scoring system based on a Position Frequency Matrix descended from the alignment of experimental SUMO-interacting motifs (Impens et al., 2014). The advantage of JASSA is that the tool includes database identification, which matches the query sequence and representation of candidate sites within the secondary structural elements. The prediction analysis of β_2AR should be run on these more developed tools to identify novel motifs of β_2AR for SUMOylation.

Following the original discovery of SERCA2a SUMOylation, Kho et al (2011) further investigated SUMOylation on lysines 480 and 585 of SERCA2a by generating mutants of SERCA2a where the lysines were substituted with arginines. This mutation construct helped the researchers to confirm that these lysines were responsible for decreasing the ATPase activity of SERCA2a and preventing ubiquitination of SERCA2a (Kho et al., 2011). A similar approach was attempted in this work. We used a K232R-K235R mutant β_2AR plasmid DNA to study the influence of ablating SUMOylation of the β_2AR on receptor signalling. However, as I focused on only two SUMOylation sites, it is possible that there are other potential SUMOylation sites on the protein. This may limit the extent of SUMOylation attenuation of the β_2AR. In fact, I showed by PLA in chapter 3 (**Figure 3.11**) that PLA signals were still evident in cells expressing the K232R-K235R mutant. The PLA signals may indicate that there are other potential SUMOylation sites on the β_2AR.

xCELLigence results also showed that the K232R-K235R substitutions did not have a significant effect on receptor sensitivity to the agonist or on receptor response rate. Perhaps if I had substituted every possible SUMOylation site on β_2AR, I may have expected to see significant differences.

6.2 The Influence of β_2AR SUMOylation on Receptor signalling

In this thesis, I used PIASγ recombinant adenovirus to study the overexpression of the E3 ligase on β_2AR SUMOylation in adult rabbit cardiac myocytes. I found out when PIASγ was overexpressed, ISO stimulation resulted in a reduction of the β_2AR downstream signalling that concluded with activated ERK MAP Kinase. This is in contrast to previous data that was published on NRVMs where an increase in phosphorylated ERK was observed after ISO treatment (Baillie et al., 2002). Dr Lauren Wills, showed in her thesis that the overexpression of PIASγ in HEKβ_2 stable cell lines lead to a reduction of β_2AR mediated activation of PKA and downstream signalling. She also showed that PIASγ overexpression in HEKβ_2 cells inhibited β_2AR ubiquitination and degradation, and delayed β_2AR internalisation (Wills, 2017). A possible reason for the reduction in β_2AR mediated activation of PKA and ERK activation following PIASγ overexpression is that the changes mediated by SUMO covalently binding to the lysines 232 and 235 located in the third intracellular loop, could result in impedance of helical movements in the third loop which is essential for receptor activation (Ballesteros et al., 2001) (X. Yao et al., 2006). To further confirm this theory, the crystal structure of the SUMOylated β_2AR should be studied for the future direction of this project.

β_2AR is a G protein coupled receptor that can internalise and desensitise after agonist binding (Ali et al., 2020). Previous research has shown that β_2AR SUMOylation can delay internalisation of the receptor (Wills, 2017). In this thesis, xCELLigence results in HEK 293 cells that overexpress WT β_2AR or the K232R-K235R mutant displayed a trend suggesting that the mutation of the receptor may cause prolongation of the desensitization. Caveolin-3 (Cav-3) can be post-translationally modified by SUMO and Cav-3 SUMOylation is considered as a novel regulatory

mechanism for agonist-induced desensitization of β_2AR (Fuhs & Insel, 2011). The Insel group used site-directed mutagenesis to generate a SUMO site null Cav-3 construct and found out that the Cav-3 mutant may promote agonist-stimulated desensitization of β_2AR (Fuhs & Insel, 2011). Although the mechanism of how SUMOylation of Cav-3 affects β_2AR desensitization is not clear, similar results have been observed in my work, which suggesting that both β_2AR and Cav-3 SUMOylation may go through a similar mechanism to affect receptor desensitization. β-arrestin links the receptor internalisation and desensitization by binding and uncoupling the receptor from the G protein, facilitating desensitization and facilitates clathrin-mediated endocytosis (Nobles et al., 2011). Previous work has shown that the interaction between β-arrestin and β_2AR was not changed by SUMOylation of the receptor (Wills, 2017), however β-arrestin itself has been shown as a substrate of SUMOylation (N. Xiao et al., 2015b).

6.3 SUMOylation of β_2AR in Cardiac Myocyte Contractility

Contractility is one of the most studied functions that can be readily assessed in cardio myocytes at all stages of cardiac function development (Bazan et al., 2012). I attempted to use adenoviral gene transfer to overexpress WT and K232R-K235R SUMO mutant β_2AR to study the influence of β_2AR SUMOylation on contractility in new-born rat cardiac myocytes. However, I was not able to detect many differences in contractility parameters between the WT and SUMO mutant transfected cells. A possible reason has been discussed in chapter 5, i.e., the dramatic increase of β_2AR expression in the myocytes altered the receptor response to agonist. β_2AR activation has been recognized as a primary control factor for regulation of heart rate and myocardial contractility (Wachter & Gilbert, 2012). Previous research has shown that once β_2ARs are activated, receptors coupled to Gαs, which leads to increased contractility via a cAMP dependent mechanism (Najafi et al., 2016). Signalling by the β_2AR has a regulatory function on contractility and it is considered to be a new target for HF treatment. SUMOylation as a PTM is also considered to be involved in regulating contractility. SERCA2a is one of the cardiac proteins that has been reported to be SUMOylated and this action on SERCA2a has a cardiac protective effect and improves the ventricular function in HF (Lee et al., 2014)(Kho et al., 2011)(Tilemann et al.,

2013)(Kho et al., 2015c). Unfortunately, I was not able to make any robust conclusions about whether SUMOylation of the β_2AR was a protective or regulatory mechanism in NRVMs.

6.4 SUMOylation of β_2AR in Heart Failure

The essential cardiac protein SERCA2a has been shown to be a substrate for SUMOylation and it's activity regulated by SUMO-1 (Kho et al., 2011). It is also noteworthy that the SUMOylation of SERCA2a is decreased in the development of HF. The Hajjar group proved that the overexpression of SUMO-1 via adenoviral gene transfer improved cardiac function and maintained heart weight to body weight ratio during disease (Tilemann et al., 2013). Since the β_2AR is also involved in regulating cardiac function, the concept of SERCA2a SUMOylation inspired me to investigate whether β_2AR SUMOylation may also be changed in the HF progression.

In chapter 3, I had the privilege to access a batch of human heart tissue from healthy and different stages of heart failure patients. I used the specific SUMO-β_2 antibody on the heart tissue, but unfortunately there was no significant differences observed for SUMOylated β_2AR comparing healthy and disease heart. In a previous study by Dr Lauren Wills, the SUMO-β_2 antibody was used to screen tissue from a transverse aortic constriction (TAC) pressure overload HF model in mice. Similar results were obtained, i.e., no differences were observed. These findings contradict our hypothesis that β_2AR SUMOylation is modified during the progression of HF.

The role that SUMOylation of β_2AR plays in HF progress remains unclear to date. In this thesis, I attempted to use WT and K232R-K235R β_2AR adenoviral gene transfer in healthy NRVMs to measure contractility. Dramatic overexpression of β_2AR in the myocytes, completely altered the way the receptor responded to agonist binding. To circumvent this in the future, the role of β_2AR SUMOylation in HF should be studied in a HF animal model when SUMOylation is enhanced or SUMOylation is completely blocked. Depending on the role that β_2AR SUMOylation plays either cardiac protective or toxic on heart function, the extent of β_2AR

SUMOylation could be regulated by small molecule. This may lead to a new potential therapeutic strategy for HF treatment.

6.4 Final Conclusion

In conclusion, I report the novel finding that the β_2AR is a substrate of SUMOylation. A first-in-class SUMO-β_2 antibody was used to test SUMOylation of β_2AR in different cells and tissues confirming that the modification is ubiquitous. However, using a variety of different model systems and techniques I was unable to definitively characterise the function of this modification.

Appendix

Amino acid	abbreviation
Alanine	A
Arginine	R
Asparagine	N
Aspartic acid	D
Cysteine	C
Glutamic acid	E
Glutamine	Q
Glycine	G
Histidine	H
Isoleucine	I

Leucine	L
Lysine	K
Methionine	M
Phenylalanine	F
Proline	P
Serine	S
Threonine	T
Tryptophan	W
Tyrosine	Y
Valine	V

List of References

Akhter, S. A., Milano, C. A., Shotwell, K. F., Cho, M. C., Rockman, H. A., Lefkowitz, R. J., & Koch, W. J. (1997). Transgenic mice with cardiac overexpression of α(1B)-adrenergic receptors. In vivo α1-adrenergic receptor-mediated regulation of β- adrenergic signaling. *Journal of Biological Chemistry*, *272*(34), 21253–21259. https://doi.org/10.1074/jbc.272.34.21253

AHA heart failure. Causes of heart failure. http://www.heart.org/HEARTORG/Conditions/HeartFailure/CausesAndRisksForHeartFailure/Causes-and-Risks-for-HeartFailure_UCM_002046_Article.jsp#.WN1wtul1q02.

Albrecht T, Fons M, Boldogh I, et al. Effects on Cells. In: Baron S, editor. Medical Microbiology. 4th edition. Galveston (TX): University of Texas Medical Branch at Galveston; 1996. Chapter 44. Available from: https://www.ncbi.nlm b.nih.gov/books/NBK7979/

Ali, D. C., Naveed, M., Gordon, A., Majeed, F., Saeed, M., Ogbuke, M. I., Atif, M., Zubair, H. M., & Changxing, L. (2020). β-Adrenergic receptor, an essential target in cardiovascular diseases. *Heart Failure Reviews*, *25*(2), 343–354. https://doi.org/10.1007/s10741-019-09825-x

Baillie, G. S., Sood, A., Mcphee, I., Gall, I., Perry, S. J., Lefkowitz, R. J., & Houslay, M. D. (2002). *Arrestin-mediated PDE4 cAMP phosphodiesterase recruitment regulates-adrenoceptor switching from G s to G i*. www.pnas.orgcgidoi10.1073pnas.262787199

Ballesteros, J. A., Jensen, A. D., Liapakis, G., Rasmussen, S. G. F., Shi, L., Gether, U., & Javitch, J. A. (2001). Activation of the β2-Adrenergic Receptor Involves Disruption of an Ionic Lock between the Cytoplasmic Ends of Transmembrane Segments 3 and 6. *Journal of Biological Chemistry*, *276*(31), 29171–29177. https://doi.org/10.1074/jbc.M103747200

Bazan, C., Barba, D. T., Hawkins, T., Nguyen, H., Anderson, S., Vazquez-Hidalgo,

E., Lemus, R., Moore, J., Mitchell, J., Martinez, J., Moore, D., Larsen, J., & Paolini, P. (2012). Contractility assessment in enzymatically isolated cardiomyocytes. In *Biophysical Reviews* (Vol. 4, Issue 3, pp. 231–243). https://doi.org/10.1007/s12551-012-0082-y

Benovic, J. L. (2002). Novel β2-adrenergic receptor signaling pathways. *Journal of Allergy and Clinical Immunology*, *110*(6 SUPPL.), 229–235. https://doi.org/10.1067/mai.2002.129370

Benya, R. V., Kusui, T., Katsuno, T., Tsuda, T., Mantey, S. A., Battey, J. F., & Jensen, R. T. (2000). Glycosylation of the gastrin-releasing peptide receptor and its effect on expression, G protein coupling, and receptor modulatory processes. *Molecular Pharmacology*, *58*(6), 1490–1501. https://doi.org/10.1124/mol.58.6.1490

Bittner, H. B., Chen, E. P., Peterseim, D. S., & Van Trigt, P. (1996). A work-performing heart preparation for myocardial performance analysis in murine hearts. *Journal of Surgical Research*, *64*(1), 57–62. https://doi.org/10.1006/jsre.1996.0306

Bodor, G.S., Oakeley, A.E., Allen, P.D., Crimmins, D.L., Ladensons, J.H., and Anderson, P.A.W. (1997) 'Troponin I phosphorylation in the normal and failing adult human heart', Circulation, 96, pp. 1495-1500

Bohm, M., Gierschik, P., Jakobs, K. H., Pieske, B., Schnabel, P., Ungerer, M., & Erdmann, E. (1990). Increase of G(iα) in human hearts with dilated but no ischemic cardiomyopathy. *Circulation*. https://doi.org/10.1161/01.CIR.82.4.1249

Bolger, G. B., Baillie, G. S., Li, X., Lynch, M. J., Herzyk, P., Mohamed, A., High Mitchell, L., McCahill, A., Hundsrucker, C., Klussmann, E., Adams, D. R., & Houslay, M. D. (2006). Scanning peptide array analyses identify overlapping binding sites for the signalling scaffold proteins, β-arrestin and RACK1, in cAMP-specific phosphodiesterase PDE4D5. *Biochemical Journal*, *398*(1), 23–36. https://doi.org/10.1042/BJ20060423

Bolger, G. B., McCahill, A., Huston, E., Cheung, Y. F., McSorley, T., Baillie, G. S., & Houslay, M. D. (2003). The unique amino-terminal region of the PDE4D5 cAMP phosphodiesterase isoform confers preferential interaction with beta-arrestins. *The Journal of Biological Chemistry*. https://doi.org/10.1074/jbc.M303772200

Bradshaw, A. C., & Baker, A. H. (2013). Gene therapy for cardiovascular disease: Perspectives and potential. *Vascular Pharmacology*, *58*(3), 174–181. https://doi.org/10.1016/j.vph.2012.10.008

Bradshaw, R. A., Medzihradszky, K. F., & Chalkley, R. J. (2010). Protein PTMs: Post-translational modifications or pesky trouble makers? *Journal of Mass Spectrometry*, *45*(10), 1095–1097. https://doi.org/10.1002/jms.1786

Cabasso O., Pekar O. & Horowitz, M. (2015). SUMOylation of EHD3 Modulates Tubulation of the Endocytic Recycling Compartment. https://doi.org/10.1371/journal.pone.0134053

Cao, Y. (2019). Advances in Membrane Proteins. In *Advances in Membrane Proteins*. https://doi.org/10.1007/978-981-13-9077-7

Carr, R., Schilling, J., Song, J., Carter, R. L., Du, Y., Yoo, S. M., Traynham, C. J., Koch, W. J., Cheung, J. Y., Tilley, D. G., & Benovic, J. L. (2016). B-Arrestin-Biased Signaling Through the B2-Adrenergic Receptor Promotes Cardiomyocyte Contraction. *Proceedings of the National Academy of Sciences of the United States of America*, *113*(28), E4107–E4116. https://doi.org/10.1073/pnas.1606267113

Chang, C. C., Tung, C. H., Chen, C. W., Tu, C. H., & Chu, Y. W. (2018). SUMOgo: Prediction of sumoylation sites on lysines by motif screening models and the effects of various post-translational modifications. *Scientific Reports*, *8*(1), 1–10. https://doi.org/10.1038/s41598-018-33951-5

Chen, J., Luo, Y., Wang, S., Zhu, H., & Li, D. (2019). Roles and mechanisms of SUMOylation on key proteins in myocardial ischemia/reperfusion injury.

Journal of Molecular and Cellular Cardiology, *134*(July), 154–164. https://doi.org/10.1016/j.yjmcc.2019.07.009

Cross, H. R., Steenbergen, C., Lefkowitz, R. J., Koch, W. J., & Murphy, E. (1999). *Inhibitor Both Increase Myocardial Contractility but Have Differential Effects on Susceptibility to Ischemic Injury*. *1*.

Dohlman, H. G., Thorner, J., Caron, M. G., & Lefkowitz, R. J. (1991). Model systems for the study of seven-transmembrane-segment receptors. *Annual Review of Biochemistry*, *60*, 653–688. https://doi.org/10.1146/annurev.bi.60.070191.003253

Dong, C., Li, Y., Niu, Q., Fang, H., Bai, J., Yan, Y., Gu, C., & Xiao, N. (2020). SUMOylation involves in ß-arrestin-2-dependent metabolic regulation in breast cancer cell. *Biochemical and Biophysical Research Communications*, *529*(4), 950–956. https://doi.org/10.1016/j.bbrc.2020.06.033

Everett, R. D., Boutell, C., & Hale, B. G. (2013). Interplay between viruses and host sumoylation pathways. *Nature Reviews Microbiology*, *11*(6), 400–411. https://doi.org/10.1038/nrmicro3015

Fabjato, A., & Fabjato, F. (1975). 469 With 2 plate8 and I11 text-ftgure8 CONTRACTIONS INDUCED BY A CALCIUM-TRIGGERED RELEASE OF CALCIUM FROM THE SARCOPLASMIC RETICULUM OF SINGLE SKINNED CARDIAC CELLS. In *J. Phy.~iol* (Vol. 249).

Feldman, A. M., Cates, A. E., Veazey, W. B., Hershberger, R. E., Bristow, M. R., Baughman, K. L., Baumgartner, W. A., & Van Dop, C. (1988). Increase of the 40,000-mol wt pertussis toxin substrate (G protein) in the failing human heart. *Journal of Clinical Investigation*. https://doi.org/10.1172/JCI113569

Feridooni, T., Hotchkiss, A., Baguma-Nibasheka, M., Zhang, F., Allen, B., Chinni, S., & Pasumarthi, K. B. S. (2017). Effects of ßadrenergic receptor drugs on embryonic ventricular cell proliferation and differentiation and their impact on donor cell transplantation. *American Journal of Physiology - Heart and*

Circulatory Physiology, *312*(5), H919–H931. https://doi.org/10.1152/ajpheart.00425.2016

Fertig, B. A. (2019). *Characterising the phosphorylation and SUMOylation of cardiac troponin I in heart failure*. *September*, 1–213.

Fisher, G. W., Adler, S. A., Fuhrman, M. H., Waggoner, A. S., Bruchez, M. P., & Jarvik, J. W. (2010). Detection and quantification of ß2AR internalization in living cells using FAP-based biosensor technology. *Journal of Biomolecular Screening*, *15*(6), 703–709. https://doi.org/10.1177/1087057110370892

Frank, R. (2002). The SPOT-synthesis technique: Synthetic peptide arrays on membrane supports—principles and applications. *Journal of Immunological Methods*, *267*(1), 13–26. https://doi.org/10.1016/S0022-1759(02)00137-0

Freedman, N. J., & Lefkowitz, R. J. (2004). *Anti-ß 1-adrenergic receptor antibodies and heart failure: causation, not just correlation*. https://doi.org/10.1172/JCI200421748

Freudenberger, N., Meyer, T., Groitl, P., Dobner, T., & Schreiner, S. (2017). HAdV protein V core protein is targeted by the host SUMOylation machinery to limit essential viral functions. *Journal of Virology*, *92*(4), JVI.01451-17. https://doi.org/10.1128/jvi.01451-17

Fu, Q., Hu, Y., Wang, Q., Liu, Y., Li, N., Xu, B., Kim, S., Chiamvimonvat, N., & Xiang, Y. K. (2017). High-fat diet induces protein kinase A and G-protein receptor kinase phosphorylation of ß2-adrenergic receptor and impairs cardiac adrenergic reserve in animal hearts. *Journal of Physiology*, *595*(6), 1973–1986. https://doi.org/10.1113/JP273314

Fuhs, S. R., & Insel, P. A. (2011). Caveolin-3 undergoes SUMOylation by the SUMO E3 ligase PIASy: SUMOylation affects G-protein-coupled receptor desensitization. *Journal of Biological Chemistry*, *286*(17), 14830–14841. https://doi.org/10.1074/jbc.M110.214270

Gareau, J. R., & Lima, C. D. (2010). The SUMO pathway: Emerging mechanisms that shape specificity, conjugation and recognition. *Nature Reviews Molecular Cell Biology*, *11*(12), 861–871. https://doi.org/10.1038/nrm3011

Geiss-Friedlander, R., & Melchior, F. (2007). Concepts in sumoylation: A decade on. *Nature Reviews Molecular Cell Biology*, *8*(12), 947–956. https://doi.org/10.1038/nrm2293

Golden, H. B., Gollapudi, D., Gerilechaogetu, F., Li, J., Cristales, R. J., Peng, X., & Dostal, D. E. (2012). Isolation of Cardiac Myocytes and Fibroblasts from Neonatal Rat Pups. In X. Peng & M. Antonyak (Eds.), *Cardiovascular Development: Methods and Protocols* (pp. 205–214). Humana Press. https://doi.org/10.1007/978-1-61779-523-7_20

Goodman, O., Krupnick, J. G., Santini, F., Gurevich, V. V, Penn, R. B., Gagnon, A. W., Keen, J. H., & Benovic, J. L. (1996). *P-Arrestin acts as a clathrin*. *383*(October), 447–450.

Gordon, J. W. (2002). High toxicity, low receptor density, and low integration frequency severely impede the use of adenovirus vectors for production of transgenic mice. *Biology of Reproduction*, *67*(4), 1172–1179. https://doi.org/10.1095/biolreprod67.4.1172

Granger, A., Abdullah, I., Huebner, F., Stout, A., Wang, T., Huebner, T., Epstein, J. A., & Gruber, P. J. (2008). Histone deacetylase inhibition reduces myocardial ischemia-reperfusion injury in mice. *The FASEB Journal*, *22*(10), 3549–3560. https://doi.org/10.1096/fj.08-108548

Greenberg, B., Butler, J., Felker, G. M., Ponikowski, P., Voors, A. A., Desai, A. S., Barnard, D., Bouchard, A., Jaski, B., Lyon, A. R., Pogoda, J. M., Rudy, J. J., & Zsebo, K. M. (2016). *Calcium upregulation by percutaneous administration of gene therapy in patients with cardiac disease (CUPID 2): a randomised , multinational , double-blind , placebo-controlled , phase 2b trial*. *387*(Cupid 2). https://doi.org/10.1016/S0140-6736(16)00082-9

Grisan, F., Burdyga, A., Iannucci, L. F., Surdo, N. C., Pozzan, T., Di Benedetto, G., & Lefkimmiatis, K. (2020). Studying β1 and β2 adrenergic receptor signals in cardiac cells using FRET-based sensors. *Progress in Biophysics and Molecular Biology*, *154*, 30–38. https://doi.org/10.1016/j.pbiomolbio.2019.06.001

Gupta, M. K., Gulick, J., Liu, R., Wang, X., Molkentin, J. D., & Robbins, J. (2014). Sumo E2 enzyme UBC9 is required for efficient protein quality control in cardiomyocytes. *Circulation Research*, *115*(8), 721–729. https://doi.org/10.1161/CIRCRESAHA.115.304760

Gupta, M. K., Mclendon, P. M., Gulick, J., James, J., & Khalili, K. (2017). *Function in Compromised Hearts*. *118*(12), 1894–1905. https://doi.org/10.1161/CIRCRESAHA.115.308268.UBC9-Mediated

Han, S. O., Kommaddi, R. P., & Shenoy, S. K. (2013). Distinct roles for β-arrestin2 and arrestin-domain-containing proteins in β2 adrenergic receptor trafficking. *EMBO Reports*, *14*(2), 164–171. https://doi.org/10.1038/embor.2012.187

Hay, R. T. (2005). SUMO: A history of modification. *Molecular Cell*, *18*(1), 1–12. https://doi.org/10.1016/j.molcel.2005.03.012

Hay, R. T. (2013). Decoding the SUMO signal. *Biochemical Society Transactions*, *41*(2), 463–473. https://doi.org/10.1042/BST20130015

Heras, G., Namuduri, A. V., Traini, L., Shevchenko, G., Falk, A., Bergström Lind, S., Jia, M., Tian, G., & Gastaldello, S. (2019). Muscle RING-finger protein-1 (MuRF1) functions and cellular localization are regulated by SUMO1 post-translational modification. *Journal of Molecular Cell Biology*, *11*(5), 356–370. https://doi.org/10.1093/jmcb/mjy036

Herring, Neil, and David J. Paterson. Levick's Introduction to Cardiovascular Physiology, Taylor & Francis Group, 2018. ProQuest Ebook Central, http://ebookcentral.proquest.com/lib/gla/detail.action?docID=5352247.

Hietakangas, V., Ahlskog, J. K., Jakobsson, A. M., Hellesuo, M., Sahlberg, N. M., Holmberg, C. I., Mikhailov, A., Palvimo, J. J., Pirkkala, L., & Sistonen, L. (2003). Phosphorylation of Serine 303 Is a Prerequisite for the Stress-Inducible SUMO Modification of Heat Shock Factor 1. *Molecular and Cellular Biology*, *23*(8), 2953–2968. https://doi.org/10.1128/mcb.23.8.2953-2968.2003

Hilgarth, R. S., & Sarge, K. D. (2005). Detection of Sumoylated Proteins. In C. Patterson & D. M. Cyr (Eds.), *Ubiquitin-Proteasome Protocols* (pp. 329–337). Humana Press. https://doi.org/10.1385/1-59259-895-1:329

Hilger, D. (2021). The role of structural dynamics in GPCR-mediated signaling. *FEBS Journal*, *288*(8), 2461–2489. https://doi.org/10.1111/febs.15841

Impens, F., Radoshevich, L., Cossart, P., & Ribet, D. (2014). Mapping of SUMO sites and analysis of SUMOylation changes induced by external stimuli. *Proceedings of the National Academy of Sciences of the United States of America*, *111*(34), 12432–12437. https://doi.org/10.1073/pnas.1413825111

Jakobs, A., Himstedt, F., Funk, M., Korn, B., Gaestel, M., & Niedenthal, R. (2007). Ubc9 fusion-directed SUMOylation identifies constitutive and inducible SUMOylation. *Nucleic Acids Research*, *35*(17), 1–8. https://doi.org/10.1093/nar/gkm617

Jes´, J., Banales, J. M., Masyuk, T. V, Gradilone, S. A., Masyuk, A. I., Medina, J. F., & Larusso, N. F. (2009). The cAMP Effectors Epac and Protein Kinase A (PKA) Are Involved in the Hepatic Cystogenesis of an Animal Model of Autosomal Recessive Polycystic Kidney Disease (ARPKD). *HEPATOLOGY*, *49*, 160–174. https://doi.org/10.1002/hep.22636

Junqueira, S. C., Centeno, E. G. Z., Wilkinson, K. A., & Cimarosti, H. (2019). Post-translational modifications of Parkinson's disease-related proteins: Phosphorylation, SUMOylation and Ubiquitination. *Biochimica et Biophysica Acta - Molecular Basis of Disease*, *1865*(8), 2001–2007. https://doi.org/10.1016/j.bbadis.2018.10.025

Kallal, L., Gagnon, A. W., Penn, R. B., & Benovic, J. L. (1998). Visualization of agonist-induced sequestration and down-regulation of a green fluorescent protein-tagged β2-adrenergic receptor. *Journal of Biological Chemistry*, *273*(1), 322–328. https://doi.org/10.1074/jbc.273.1.322

Kaumann, A., Bartel, S., Molenaar, P., Sanders, L., Burrell, K., Vetter, D., Hempel, P., Karczewski, P., & Krause, E. (1999). Mediates Phosphorylation of Phospholamban, Troponin I, and C-Protein in Ventricular Myocardium From Patients With Terminal Heart Failure. *Online*.

Kawahira Y, Sawa Y, Nishimura M, Sakakida S, Ueda H, Kaneda Y, Matsuda H. In vivo transfer of a beta 2-adrenergic receptor gene into the pressure-overloaded rat heart enhances cardiac response to beta-adrenergic agonist. Circulation. 1998 Nov 10;98(19 Suppl):II262-7; discussion II267-8. PMID: 9852912.

Kawahira Y, Sawa Y, Nishimura M, Sakakida S, Ueda H, Kaneda Y, Matsuda H. Gene transfection of beta 2- adrenergic receptor into the normal rat heart enhances cardiac response to beta-adrenergic agonist.The Journal of Thoracic and Cardiovascular Surgery. 1999 (118) No.3, 446-451.

Kho, C., Lee, A., Jeong, D., Oh, J. G., Chaanine, A. H., Kizana, E., Park, W. J., & Hajjar, R. J. (2011). SUMO1-dependent modulation of SERCA2a in heart failure. *Nature*. https://doi.org/10.1038/nature10407

Kho, C., Lee, A., Jeong, D., Oh, J. G., Gorski, P. A., Fish, K., Sanchez, R., Devita, R. J., Christensen, G., Dahl, R., & Hajjar, R. J. (2015a). Small-molecule activation of SERCA2a SUMOylation for the treatment of heart failure. *Nature Communications*, *6*, 1–11. https://doi.org/10.1038/ncomms8229

Kho, C., Lee, A., Jeong, D., Oh, J. G., Gorski, P. A., Fish, K., Sanchez, R., Devita, R. J., Christensen, G., Dahl, R., & Hajjar, R. J. (2015b). Small-molecule activation of SERCA2a SUMOylation for the treatment of heart failure. *Nature Communications*. https://doi.org/10.1038/ncomms8229

Kho, C., Lee, A., Jeong, D., Oh, J. G., Gorski, P. A., Fish, K., Sanchez, R., Devita, R. J., Christensen, G., Dahl, R., & Hajjar, R. J. (2015c). Small-molecule activation of SERCA2a SUMOylation for the treatment of heart failure. *Nature Communications*, *6*, 1–11. https://doi.org/10.1038/ncomms8229

Kim, E. Y., Chen, L., Ma, Y., Yu, W., Chang, J., Moskowitz, I. P., & Wang, J. (2013). *dysfunction*. *52*(3), 638–649. https://doi.org/10.1016/j.yjmcc.2011.11.011.Enhanced

Kim, E. Y., Zhang, Y., Ye, B., Segura, A. M., Beketaev, I., Xi, Y., Yu, W., Chang, J., Li, F., & Wang, J. (2015). Involvement of activated SUMO-2 conjugation in cardiomyopathy. *Biochimica et Biophysica Acta - Molecular Basis of Disease*, *1852*(7), 1388–1399. https://doi.org/10.1016/j.bbadis.2015.03.013

Kim, J., Grotegut, C. A., Wisler, J. W., Li, T., Mao, L., Chen, M., Chen, W., Rosenberg, P. B., Rockman, H. A., & Lefkowitz, R. J. (2018). B-Arrestin 1 Regulates B2-Adrenergic Receptor-Mediated Skeletal Muscle Hypertrophy and Contractility. *Skeletal Muscle*, *8*(1), 1–13. https://doi.org/10.1186/s13395-018-0184-8

Laporte, S. A., Oakley, R. H., Holt, J. A., Barak, L. S., & Caron, M. G. (2000). The interaction of ß-arrestin with the AP-2 adaptor is required for the clustering of ß2-adrenergic receptor into clathrin-coated pits. *Journal of Biological Chemistry*, *275*(30), 23120–23126. https://doi.org/10.1074/jbc.M002581200

Le, N. T., Martin, J. F., Fujiwara, K., & Abe, J. ichi. (2017a). Sub-cellular localization specific SUMOylation in the heart. *Biochimica et Biophysica Acta - Molecular Basis of Disease*, *1863*(8), 2041–2055. https://doi.org/10.1016/j.bbadis.2017.01.018

Le, N. T., Martin, J. F., Fujiwara, K., & Abe, J. ichi. (2017b). Sub-cellular localization specific SUMOylation in the heart. *Biochimica et Biophysica Acta - Molecular Basis of Disease*, *1863*(8), 2041–2055. https://doi.org/10.1016/j.bbadis.2017.01.018

Lee, A., Jeong, D., Mitsuyama, S., Oh, J. G., Liang, L., Ikeda, Y., Sadoshima, J., Hajjar, R. J., & Kho, C. (2014). The role of SUMO-1 in cardiac oxidative stress and hypertrophy. *Antioxidants and Redox Signaling*, *21*(14), 1986–2001. https://doi.org/10.1089/ars.2014.5983

Lee, A., Oh, J. G., Gorski, P. A., Hajjar, R. J., & Kho, C. (2016). Post-translational Modifications in Heart Failure: Small Changes, Big Impact. *Heart Lung and Circulation*, *25*(4), 319–324. https://doi.org/10.1016/j.hlc.2015.11.008

Lemminger, A. K., Jessen, S., Habib, S., Onslev, J., Xu, S. F. S., Backer, V., Bangsbo, J., & Hostrup, M. (2019). Effect of beta2-adrenergic agonist and resistance training on maximal oxygen uptake and muscle oxidative enzymes in men. *Scandinavian Journal of Medicine and Science in Sports*, *29*(12), 1881–1891. https://doi.org/10.1111/sms.13544

Li, X., Vadrevu, S., Dunlop, A., Day, J., Advant, N., Troeger, J., Klussmann, E., Jaffrey, E., Hay, R. T., Adams, D. R., Houslay, M. D., & Baillie, G. S. (2010). Selective SUMO modification of cAMP-specific phosphodiesterase-4D5 (PDE4D5) regulates the functional consequences of phosphorylation by PKA and ERK. *Biochemical Journal*. https://doi.org/10.1042/BJ20091672

Liberati, A., Altman, D., Tetzlaff, J., Mulrow, C., Gotzsche, P., Loannidis, J., Clarke, M., Devereaux, P., Kleijnen, J., & Moher, D. (2018). Enhanced Reader.pdf. In *Nature* (Vol. 388, pp. 539–547).

Liggett, S. B., Tepe, N. M., Lorenz, J. N., Canning, A. M., Jantz, T. D., Mitarai, S., Yatani, A., & Ii, G. W. D. (2000). *Overexpression in Mouse Hearts Critical Role for Expression Level*. 1707–1714.

Liu, R., Wang, D., Shi, Q., Fu, Q., Hizon, S., & Xiang, Y. K. (2012). *Palmitoylation Regulates Intracellular Trafficking of b 2 Adrenergic Receptor/Arrestin/Phosphodiesterase 4D Complexes in Cardiomyocytes*. https://doi.org/10.1371/journal.pone.0042658

Liu, Y. Y., Ayers, S., Milanesi, A., Teng, X., Rabi, S., Akiba, Y., & Brent, G. A.

(2015). Thyroid hormone receptor sumoylation is required for preadipocyte differentiation and proliferation. *Journal of Biological Chemistry*, *290*(12), 7402–7415. https://doi.org/10.1074/jbc.M114.600312

Lu, Y., Nanayakkara, G., Sun, Y., Liu, L., Xu, K., Drummer, C., Shao, Y., Saaoud, F., Choi, E. T., Jiang, X., Wang, H., & Yang, X. (2021). Procaspase-1 patrolled to the nucleus of proatherogenic lipid LPC-activated human aortic endothelial cells induces ROS promoter CYP1B1 and strong inflammation. *Redox Biology*, *47*, 102142. https://doi.org/10.1016/j.redox.2021.102142

Lynch, J. R., & Wang, J. Y. (2016). *Molecular Sciences G Protein-Coupled Receptor Signaling in Stem Cells and Cancer*. https://doi.org/10.3390/ijms17050707

MacLannan, D.H., and Kranias, E.G. (2003) 'Phospholamban: a crucial regulator of cardiac contractility', Nature, 4, pp. 565-577

Madamanchi, A. (2007). ß-adrenergic receptor signaling in cardiac function and heart failure. In *McGill Journal of Medicine*.

Maeda, S., & Schertler, G. F. X. (2013). Production of GPCR and GPCR complexes for structure determination. *Current Opinion in Structural Biology*, *23*(3), 381–392. https://doi.org/10.1016/j.sbi.2013.04.006

Markovic, D., & Grammatopoulos, D. K. (2009). Focus on the splicing of Secretin GPCRs transmembrane-domain 7. *Trends in Biochemical Sciences*, *34*(9), 443–452. https://doi.org/10.1016/j.tibs.2009.06.002

Matic, I., Schimmel, J., Hendriks, I. A., van Santen, M. A., van de Rijke, F., van Dam, H., Gnad, F., Mann, M., & Vertegaal, A. C. O. (2010). Site-Specific Identification of SUMO-2 Targets in Cells Reveals an Inverted SUMOylation Motif and a Hydrophobic Cluster SUMOylation Motif. *Molecular Cell*, *39*(4), 641–652. https://doi.org/10.1016/j.molcel.2010.07.026

McGraw, D. W., & Liggett, S. B. (2005). Molecular mechanisms of ß2-adrenergic receptor function and regulation. *Proceedings of the American Thoracic*

Society, *2*(4), 292–296. https://doi.org/10.1513/pats.200504-027SR

McLean, A. J., & Milligan, G. (2000). Ligand regulation of green fluorescent protein-tagged forms of the human ß1- and ß2-adrenoceptors; comparisons with the unmodified receptors. *British Journal of Pharmacology*, *130*(8), 1825–1832. https://doi.org/10.1038/sj.bjp.0703506

Mendler, L., Braun, T., & Müller, S. (2016a). The Ubiquitin-Like SUMO System and Heart Function: From Development to Disease. *Circulation Research*, *118*(1), 132–144. https://doi.org/10.1161/CIRCRESAHA.115.307730

Mendler, L., Braun, T., & Müller, S. (2016b). The Ubiquitin-Like SUMO System and Heart Function. In *Circulation Research* (Vol. 118, Issue 1, pp. 132–144). https://doi.org/10.1161/circresaha.115.307730

Mialet-Perez, J., Green, S. A., Miller, W. E., & Liggett, S. B. (2004). A primate-dominant third glycosylation site of the ß2- adrenergic receptor routes receptors to degradation during agonist regulation. *Journal of Biological Chemistry*, *279*(37), 38603–38607. https://doi.org/10.1074/jbc.M403708200

Milano, C. A., Allen, L. F., Rockman, H. A., Dolber, P. C., McMinn, T. R., Chien, K. R., Johnson, T. D., Bond, R. A., & Lefkowitz, R. J. (1994). Enhanced myocardial function in transgenic mice overexpressing the ß2-adrenergic receptor. *Science*, *264*(5158), 582–586. https://doi.org/10.1126/science.8160017

Morrison, K. J., Moore, R. H., Carsrud, N. D. V., Trial, J., Millman, E. E., Tuvim, M., Clark, R. B., Barber, R., Dickey, B. F., & Knoll, B. J. (1996). Repetitive endocytosis and recycling of the ß2-adrenergic receptor during agonist-induced steady state redistribution. *Molecular Pharmacology*, *50*(3), 692–699.

Nagi, K., Kaur, S., Bai, Y., & Shenoy, S. K. (2020). In-frame fusion of SUMO1 enhances ßarrestin2's association with activated GPCRs as well as with nuclear pore complexes. *Cellular Signalling*, *75*(April), 109759. https://doi.org/10.1016/j.cellsig.2020.109759

Najafi, A., Sequeira, V., Kuster, D. W. D., & van der Velden, J. (2016). B-Adrenergic Receptor Signalling and Its Functional Consequences in the Diseased Heart. *European Journal of Clinical Investigation*, *46*(4), 362–374. https://doi.org/10.1111/eci.12598

Nayak, A., & Amrute-Nayak, M. (2020). SUMO system – a key regulator in sarcomere organization. In *FEBS Journal* (Vol. 287, Issue 11, pp. 2176–2190). https://doi.org/10.1111/febs.15263

Nayak, A., Lopez-Davila, A. J., Kefalakes, E., Holler, T., Kraft, T., & Amrute-Nayak, M. (2019). Regulation of SETD7 Methyltransferase by SENP3 Is Crucial for Sarcomere Organization and Cachexia. *Cell Reports*, *27*(9), 2725-2736.e4. https://doi.org/10.1016/j.celrep.2019.04.107

Neumann, J., Scholz, H., Döring, V., Schmitz, W., Meyerinck, L. Von, & Kalmár, P. (1988). INCREASE IN MYOCARDIAL Gi-PROTEINS IN HEART FAILURE. *The Lancet*. https://doi.org/10.1016/S0140-6736(88)92601-3

New York Heart Association. The Criteria Committee of the New York Heart Association, Functional Capacity and Objective Assessment. Nomenclature and Criteria for Diagnosis of Diseases of the Heart and Great Vessels. Boston, MA: Little Brown and Company; 1994:253–255.

Noble, H., & Smith, J. (2015). untitled _ Enhanced Reader.pdf. In *Clinical Infectious Diseases*.

Nobles, K. N., Xiao, K., Ahn, S., Shukla, A. K., Lam, C. M., Rajagopal, S., Strachan, R. T., Huang, T. Y., Bressler, E. A., Hara, M. R., Shenoy, S. K., Gygi, S. P., & Lefkowitz, R. J. (2011). Distinct phosphorylation sites on the ß 2-adrenergic receptor establish a barcode that encodes differential functions of ß-arrestin. *Science Signaling*, *4*(185), 1–11. https://doi.org/10.1126/scisignal.2001707

Ovchinnikov, Y. A., Abdulaev, N. G., & Bogachuk, A. S. (n.d.). *Two adjacent cysteine residues in the C-terminal cytoplasmic fragment of bovine rhodopsin are palmitylated* (Vol. 230, Issue 1).

Pagan, J., Seto, T., Pagano, M., & Cittadini, A. (2013). Role of the ubiquitin proteasome system in the heart. *Circulation Research*, *112*(7), 1046–1058. https://doi.org/10.1161/CIRCRESAHA.112.300521

Palczewski, K., Kumasaka, T., Hori, T., Behnke, C. A., Motoshima, H., Fox, B. A., Le Trong, I., Teller, D. C., Okada, T., Stenkamp, R. E., Yamamoto, M., & Miyano, M. (n.d.). *Crystal Structure of Rhodopsin: A G Protein-Coupled Receptor*. www.sciencemag.org

Parmar, V. K., Grinde, E., Mazurkiewicz, J. E., & Herrick-Davis, K. (2017). Beta2-adrenergic receptor homodimers: Role of transmembrane domain 1 and helix 8 in dimerization and cell surface expression. *Biochimica et Biophysica Acta - Biomembranes*, *1859*(9), 1445–1455. https://doi.org/10.1016/j.bbamem.2016.12.007

Perry, S. J., Baillie, G. S., Kohout, T. A., McPhee, I., Magiera, M. M., Ang, K. L., Miller, W. E., McLean, A. J., Conti, M., Houslay, M. D., & Lefkowitz, R. J. (2002). Targeting of cyclic $\uppercase{AMP}$ degradation to beta 2-adrenergic receptors by beta-arrestins. *Science*.

Rands E, Candelore MR, Cheung AH, Hill WS, Strader CD, Dixon RA. Mutational analysis of beta-adrenergic receptor glycosylation. J Biol Chem. 1990 Jun 25;265(18):10759-64. PMID: 2162359.

Rasmussen, S. G. F., Choi, H. J., Rosenbaum, D. M., Kobilka, T. S., Thian, F. S., Edwards, P. C., Burghammer, M., Ratnala, V. R. P., Sanishvili, R., Fischetti, R. F., Schertler, G. F. X., Weis, W. I., & Kobilka, B. K. (2007). Crystal structure of the human β2 adrenergic G-protein-coupled receptor. *Nature*, *450*(7168), 383–387. https://doi.org/10.1038/nature06325

Road, C. (1980). Anatomy, and. *Group*, *37*(January), 129–198.

Roche. (2008). Dynamic Monitoring of Receptor Tyrosine Kinase Activation in Living Cells Dynamic Monitoring of Receptor Tyrosine Kinase Activation in Living Cells. *Culture*, *4*.

Rosenbaum, D. M., Cherezov, V., Hanson, M. A., F Rasmussen, S. G., Sun Thian, F., Sun Kobilka, T., Choi, H.-J., Yao, X.-J., Weis, W. I., Stevens, R. C., & Kobilka, B. K. (2002). GPCR Engineering Yields High-Resolution Structural Insights into b 2-Adrenergic Receptor Function. *Nat. Rev. Mol. Cell Biol*, *3*, 2021. https://doi.org/10.1126/science.1150577

Rytinki, M. M., Kaikkonen, S., Sutinen, P., & Palvimo, J. J. (n.d.). *Analysis of Androgen Receptor SUMOylation*. https://doi.org/10.1007/978-1-61779-243-4_12

Sadeghi, H., & Birnbaumer, M. (1999). O-Glycosylation of the V2 vasopressin receptor. In *Glycobiology* (Vol. 9, Issue 7). https://academic.oup.com/glycob/article/9/7/731/674991

Sala, L., Van Meer, B. J., Tertoolen, L. G. J., Bakkers, J., Bellin, M., Davis, R. P., Denning, C., Dieben, M. A. E., Eschenhagen, T., Giacomelli, E., Grandela, C., Hansen, A., Holman, E. R., Jongbloed, M. R. M., Kamel, S. M., Koopman, C. D., Lachaud, Q., Mannhardt, I., Mol, M. P. H., … Mummery, C. L. (2018a). Musclemotion: A versatile open software tool to quantify cardiomyocyte and cardiac muscle contraction in vitro and in vivo. *Circulation Research*. https://doi.org/10.1161/CIRCRESAHA.117.312067

Sala, L., Van Meer, B. J., Tertoolen, L. G. J., Bakkers, J., Bellin, M., Davis, R. P., Denning, C., Dieben, M. A. E., Eschenhagen, T., Giacomelli, E., Grandela, C., Hansen, A., Holman, E. R., Jongbloed, M. R. M., Kamel, S. M., Koopman, C. D., Lachaud, Q., Mannhardt, I., Mol, M. P. H., … Mummery, C. L. (2018b). Musclemotion: A versatile open software tool to quantify cardiomyocyte and cardiac muscle contraction in vitro and in vivo. *Circulation Research*, *122*(3), e5–e16. https://doi.org/10.1161/CIRCRESAHA.117.312067

Sampson, D. A., Wang, M., & Matunis, M. J. (2001). The Small Ubiquitin-like Modifier-1 (SUMO-1) Consensus Sequence Mediates Ubc9 Binding and is Essential for SUMO-1 Modification. In *Journal of Biological Chemistry* (Vol. 276, Issue 24, pp. 21664–21669). https://doi.org/10.1074/jbc.M100006200

Sarker, S., Xiao, K., & Shenoy, S. K. (2011). *Communicative & Integrative Biology A Tale of Two Sites-How ubiquitination of a G protein-coupled receptor is coupled to its lysosomal trafficking from distinct receptor domains How ubiquitination of a G protein-coupled receptor is coupled to its lysosoma*. https://doi.org/10.4161/cib.16458

Schlüter, K. D. (2016). Cardiomyocytes - active players in cardiac disease. In *Cardiomyocytes - Active Players in Cardiac Disease*. https://doi.org/10.1007/978-3-319-31251-4

Schwartz, R. J., & Yeh, E. T. H. (2012). Weighing in on heart failure: The role of SERCA2a SUMOylation. *Circulation Research*, *110*(2), 198–199. https://doi.org/10.1161/RES.0b013e318246f187

Sharma, A., Lysenko, A., López, Y., Dehzangi, A., Sharma, R., Reddy, H., Sattar, A., & Tsunoda, T. (2019). HseSUMO: Sumoylation site prediction using half-sphere exposures of amino acids residues. *BMC Genomics*, *19*(Suppl 9), 1–7. https://doi.org/10.1186/s12864-018-5206-8

Shenoy, S. K., McDonald, P. H., Kohout, T. A., & Lefkowitz, R. J. (2001). Regulation of receptor fate by ubiquitination of activated β2-adrenergic receptor and β-arrestin. *Science*, *294*(5545), 1307–1313. https://doi.org/10.1126/science.1063866

Shenoy, Sudha K., Barak, L. S., Xiao, K., Ahn, S., Berthouze, M., Shukla, A. K., Luttrell, L. M., & Lefkowitz, R. J. (2007). Ubiquitination of β-arrestin links seven-transmembrane receptor endocytosis and ERK activation. *Journal of Biological Chemistry*, *282*(40), 29549–29562. https://doi.org/10.1074/jbc.M700852200

Shenoy, Sudha K., Drake, M. T., Nelson, C. D., Houtz, D. A., Xiao, K., Madabushi, S., Reiter, E., Premont, R. T., Lichtarge, O., & Lefkowitz, R. J. (2006). β-arrestin-dependent, G protein-independent ERK1/2 activation by the β2 adrenergic receptor. *Journal of Biological Chemistry*, *281*(2), 1261–1273. https://doi.org/10.1074/jbc.M506576200

Shenoy, Sudha K., & Lefkowitz, R. J. (2011). B-Arrestin-Mediated Receptor Trafficking and Signal Transduction. *Trends in Pharmacological Sciences*, *32*(9), 521–533. https://doi.org/10.1016/j.tips.2011.05.002

Shenoy, Sudha K., Xiao, K., Venkataramanan, V., Snyder, P. M., Freedman, N. J., & Weissman, A. M. (2008). Nedd4 mediates agonist-dependent ubiquitination, lysosomal targeting, and degradation of the β2-adrenergic receptor. *Journal of Biological Chemistry*, *283*(32), 22166–22176. https://doi.org/10.1074/jbc.M709668200

Shenoy, Sudha K, Mcdonald, P. H., Kohout, T. A., & Lefkowitz, R. J. (n.d.). *Regulation of Receptor Fate by Ubiquitination of Activated 2-Adrenergic Receptor and-Arrestin*. http://science.sciencemag.org/

Shetty, P. M. V., Rangrez, A. Y., & Frey, N. (2020). SUMO proteins in the cardiovascular system: friend or foe? *Journal of Biomedical Science*, *27*(1), 1–14. https://doi.org/10.1186/s12929-020-00689-0

Shiels, H. A. (2011). DESIGN AND PHYSIOLOGY OF THE HEART | Cardiac Excitation–Contraction Coupling: Routes of Cellular Calcium Flux. *Encyclopedia of Fish Physiology*, *2*, 1045–1053. https://doi.org/10.1016/B978-0-12-374553-8.00175-1

Sohn, S.-Y., & Hearing, P. (2012). *Adenovirus Regulates Sumoylation of Mre11-Rad50-Nbs1 Components through a Paralog-Specific Mechanism*. *86*, 9656–9665. https://doi.org/10.1128/JVI.01273-12

Sohn, S. Y., & Hearing, P. (2016). Adenovirus early proteins and host sumoylation. *MBio*, *7*(5), 1–7. https://doi.org/10.1128/mBio.01154-16

Squire, J. M. (2016). Muscle contraction: Sliding filament history, sarcomere dynamics and the two Huxleys. *Global Cardiology Science and Practice*, *2016*(2). https://doi.org/10.21542/gcsp.2016.11

Stallaert, W., Dorn, J. F., van der Westhuizen, E., Audet, M., & Bouvier, M. (2012).

Impedance responses reveal β 2-adrenergic receptor signaling pluridimensionality and allow classification of ligands with distinct signaling profiles. *PLoS ONE*, *7*(1). https://doi.org/10.1371/journal.pone.0029420

Stein, S., Oosterveer, M. H., Mataki, C., Xu, P., Lemos, V., Havinga, R., Dittner, C., Ryu, D., Menzies, K. J., Wang, X., Perino, A., Houten, S. M., Melchior, F., & Schoonjans, K. (2014). SUMOylation-dependent LRH-1/PROX1 interaction promotes atherosclerosis by decreasing hepatic reverse cholesterol transport. *Cell Metabolism*, *20*(4), 603–613. https://doi.org/10.1016/j.cmet.2014.07.023

Sun, H., Lu, L., Zuo, Y., Wang, Y., Jiao, Y., Zeng, W. Z., Huang, C., Zhu, M. X., Zamponi, G. W., Zhou, T., Xu, T. Le, Cheng, J., & Li, Y. (2014). Kainate receptor activation induces glycine receptor endocytosis through PKC deSUMOylation. *Nature Communications*, *5*, 1–17. https://doi.org/10.1038/ncomms5980

Talke, I. N., Blaudez, D., Maathuis, F. J. M., & Sanders, D. (2003). CNGCs: Prime targets of plant cyclic nucleotide signalling? *Trends in Plant Science*, *8*(6), 286–293. https://doi.org/10.1016/S1360-1385(03)00099-2

Thermo fisher Scientific. (2017, April 10). HA Tag Antibodies. Retrieved April 10,2017, from www.thermofisher.com: https://www.thermofisher.com/uk/en/home/lifescience/antibodies/primary-antibodies/epitope-tag-antibodies/ha-tagantibodies.html#

Tiberi M. (2014). G Protein Coupled Receptor Signaling. https://doi.org/10.1038/nprot.2014.017

Tilemann, L., Lee, A., Ishikawa, K., Aguero, J., Rapti, K., Santos-Gallego, C., Kohlbrenner, E., Fish, K. M., Kho, C., & Hajjar, R. J. (2013). SUMO-1 gene transfer improves cardiac function in a large-animal model of heart failure. *Science Translational Medicine*, *5*(211). https://doi.org/10.1126/scitranslmed.3006487

Tota, M. R., & Strader, C. D. (1990). Characterization of the binding domain of the ß-adrenergic receptor with the fluorescent antagonist carazolol: Evidence for a buried ligand binding site. *Journal of Biological Chemistry*, *265*(28), 16891–16897. https://doi.org/10.1016/s0021-9258(17)44846-0

Ulrich, H.D. (2005). Mutual interactions between the SUMO and ubiquitin systems: a plea of no contest. Trends Cell Biol 15, 525-532.

Urcan, E., Haertel, U., Styllou, M., Hickel, R., Scherthan, H., & Reichl, F. X. (2010). Real-time xCELLigence impedance analysis of the cytotoxicity of dental composite components on human gingival fibroblasts. *Dental Materials*, *26*(1), 51–58. https://doi.org/10.1016/j.dental.2009.08.007

Voigt, & Antje. (2014). *(No Title)*. https://doi.org/10.1161/CIRCULATIONAHA.114.009847

Wachter, S. B., & Gilbert, E. M. (2012). Beta-adrenergic receptors, from their discovery and characterization through their manipulation to beneficial clinical application. *Cardiology (Switzerland)*, *122*(2), 104–112. https://doi.org/10.1159/000339271

Wang, J., Gareri, C., & Rockman, H. A. (2018). G-protein-coupled receptors in heart disease. *Circulation Research*, *123*(6), 716–735. https://doi.org/10.1161/CIRCRESAHA.118.311403

Wang, Q. L., Liang, J. Q., Gong, B. N., Xie, J. J., Yi, Y. T., Lan, X., & Li, Y. (2019). T cell recreptor (TCR) Induced PLCλ1 sumouylation via PIAS×ß and PIAS3 SUMO E3 ligases regulates the microcluster assembly and physiological function of PLC-λ1. *Frontiers in Immunology*, *10*(FEB). https://doi.org/10.3389/fimmu.2019.00314

Watts, F. Z. (2013). Starting and stopping SUMOylation: What regulates the regulator? In *Chromosoma*. https://doi.org/10.1007/s00412-013-0422-0

Wei, W., Lin, H.-K., & Galluzzi, L. (2012). *The key role of ubiquitination and*

sumoylation in signaling and cancer: a research topic. https://doi.org/10.3389/fonc.2012.00187

Wilkinson, K. A., & Henley, J. M. (2010). Mechanisms, regulation and consequences of protein SUMOylation. *Biochemical Journal*, *428*(2), 133–145. https://doi.org/10.1042/BJ20100158

Wills, L. (2017). *SUMOylation of the β 2 AR Influences Receptor Internalisation , Desensitisation and Downstream Signalling*. *September*.

Wimmer, P., Blanchette, P., Schreiner, S., Ching, W., Groitl, P., Berscheminski, J., Branton, P. E., Will, H., & Dobner, T. (2013). Cross-talk between phosphorylation and SUMOylation regulates transforming activities of an adenoviral oncoprotein. *Oncogene*, *32*(13), 1626–1637. https://doi.org/10.1038/onc.2012.187

Xiao, K., & Shenoy, S. K. (2011). B2-Adrenergic Receptor Lysosomal Trafficking Is Regulated By Ubiquitination of Lysyl Residues in Two Distinct Receptor Domains. *Journal of Biological Chemistry*, *286*(14), 12785–12795. https://doi.org/10.1074/jbc.M110.203091

Xiao, N., Li, H., Mei, W., & Cheng, J. (2015a). SUMOylation attenuates human ß-arrestin 2 inhibition of IL-1R/TRAF6 signaling. *Journal of Biological Chemistry*, *290*(4), 1927–1935. https://doi.org/10.1074/jbc.M114.608703

Xiao, N., Li, H., Mei, W., & Cheng, J. (2015b). SUMOylation attenuates human ß-arrestin 2 inhibition of IL-1R/TRAF6 signaling. *Journal of Biological Chemistry*, *290*(4), 1927–1935. https://doi.org/10.1074/jbc.M114.608703

Xu, J., Tan, P., Li, H., Cui, Y., Qiu, Y., Wang, H., Zhang, X., Li, J., Zhu, L., Zhou, W., Chen, H., & Direct, H. (n.d.). *Direct SUMOylation of M1 muscarinic acetylcholine receptor increases its ligand-binding affinity and signal transduction*. https://doi.org/10.1096/fj.201800936R

Yang, S. H., Galanis, A., Witty, J., & Sharrocks, A. D. (2006). An extended

consensus motif enhances the specificity of substrate modification by SUMO. *EMBO Journal*, *25*(21), 5083–5093. https://doi.org/10.1038/sj.emboj.7601383

Yang, S. H., Jaffray, E., Hay, R. T., & Sharrocks, A. D. (2003). Dynamic interplay of the SUMO and ERK pathways in regulating Elk-1 transcriptional activity. *Molecular Cell*, *12*(1), 63–74. https://doi.org/10.1016/S1097-2765(03)00265-X

Yao, Q., Liu, B. Q., Li, H., McGarrigle, D., Xing, B. W., Zhou, M. T., Wang, Z., Zhang, J. J., Huang, X. Y., & Guo, L. (2014). C-terminal src kinase (CSK)-mediated phosphorylation of eukaryotic elongation factor 2 (EEF2) promotes proteolytic cleavage and nuclear translocation of EEF2. In *Journal of Biological Chemistry* (Vol. 289, Issue 18, pp. 12666–12678). https://doi.org/10.1074/jbc.M113.546481

Yao, X., Parnot, C., Deupi, X., Ratnala, V. R. P., Swaminath, G., Farrens, D., & Kobilka, B. (2006). Coupling ligand structure to specific conformational switches in the β2-adrenoceptor. *Nature Chemical Biology*, *2*(8), 417–422. https://doi.org/10.1038/nchembio801

Zárraga-Granados, G., Muciño-Hernández, G., Sánchez-Carbente, M. R., Villamizar-Gálvez, W., Peñas-Rincón, A., Arredondo, C., Andrés, M. E., Wood, C., Covarrubias, L., & Castro-Obregón, S. (2020). The nuclear receptor NR4A1 is regulated by SUMO modification to induce autophagic cell death. *PLoS ONE*, *15*(3). https://doi.org/10.1371/journal.pone.0222072

Zhou, Y. Y., Cheng, H., Song, L. S., Wang, D., Lakatta, E. G., & Xiao, R. P. (1999). Spontaneous β2-adrenergic signaling fails to modulate L-type Ca2+ current in mouse ventricular myocytes. *Molecular Pharmacology*, *56*(3), 485–493. https://doi.org/10.1124/mol.56.3.485